Stony Brook University

Mechanotransduction of Low Intensity Vibration in Human Bone Marrow Mesenchymal Stem Cells and Macrophages

A Dissertation Presented

by

Suphannee Pongkitwitoon

to

The Graduate School

in Partial Fulfillment of the

Requirements

for the Degree of

Doctor of Philosophy

in

Biomedical Engineering

Stony Brook University

May 2015

Stony Brook University

The Graduate School

Suphannee Pongkitwitoon

We, the dissertation committee for the above candidate for the

Doctor of Philosophy degree, hereby recommend acceptance of this dissertation.

Stefan Judex, Ph.D.
Dissertation Advisor
Professor, Department of Biomedical Engineering, Stony Brook University

Clinton T. Rubin, Ph.D.
Chairperson of Defense
Distinguished Professor and Chair, Department of Biomedical Engineering
Director, Center for Biotechnology

Yizhi Meng, Ph.D.
Assistant Professor
Chemical and Molecular Engineering Program
Department of Materials Science and Engineering, Stony Brook University

Timothy Koh, Ph.D.
Professor, Kinesiology and Nutrition
Department of Bioengineering, University of Illinois at Chicago

This dissertation is accepted by the Graduate School

Charles Taber
Dean of the Graduate School

Abstract of the Dissertation

Mechanotransduction of Low Intensity Vibration in Human Bone Marrow Mesenchymal Stem Cells and Macrophages

by

Suphannee Pongkitwitoon

Doctor of Philosophy

in

Biomedical Engineering

Stony Brook University

2015

Human bone marrow mesenchymal stem cells in bone marrow niches are sensitive to the low intensity vibration. The question of what specific mechanical signals (i.e. fluid shear, frequency, or acceleration) cells sense requires the understanding of the underlying pathways. The cellular and molecular responses to LIV in vivo require fundamental investigation of human MSCs and macrophages in bone marrow niches. We aim to elucidate mechanotransduction pathways of LIV in hBMSCs including macrophages and their functions in bone marrow niches. Understanding mechanotransduction pathways can provide the successful use of LIV in controls of regulatory bone pathways in vivo.

We first hypothesized that the physical interaction of cellular and nuclear structures could involve in the mechanotransduction. To test the physical structures based mechanotransduction, we vibrated hBMSC cells under horizontal and vertical directions. Signal combinations of LIV

(reflecting a range of fluid shear, i.e. the highest fluid shear at 30Hz-1g and the lowest fluid shear at 100Hz-0.15g by horizontal LIV) were used during cell proliferation and differentiation. The standard assay of MTS monitored cell proliferation and the alizarin red s including oil red o assays were used to monitor cell osteoblastogenic- and adipogenic- differentiations. Flow cytometric analysis of the %gated positive cells confirmed the data from these assays and the gene expression. Gene expression levels (in fold changes) with the GAPDH housekeeping gene were analyzed by the real-time PCR. The cluster and enrichment analysis validated the relation of gene expressions in the proposed mechanotransduction pathway. Based on cellular structures, the mechanosensitive system could derive from the outermost cell membrane (n-cadherins), inside cells (cytoskeletal f-actins) and the nucleoskeletons (NuAnCE-LiNC) anchoring throughout the nuclear envelope (nesprins) across the inner nuclear membrane (sun proteins) to the inner nuclear basement membranes (laminins and chromatins). The mechanotransduction of the physical connections between cellular and nuclear structures provided the potential pathway from the outermost cell membrane to inside cells across the nuclear double membranes as n-cadherins – cytoskeletal f-actins – nesprins.

We identified the mechanical signals that hBMSCs could sense. The frequency of LIV influenced the proliferation while the direction had strong effects on the osteoblastogenic differentiation of hBMSCs. Gene profiles showed that the physical interactions of cellular and nuclear structures involved in the mechanotransduction. During LIV, cells and their neighboring cells were physical interacting with one another and formed mature adherent junctions (CDH11). The connections of the mature adherent junctions with cytoskeletons were dynamic. The dynamic changes in the cytoskeletal orientations (ACTn1) potentially maintained cellular

integrity. The cytoskeletal orientation was then anchoring the nuclear skeleton nesprins (Syne2). The CDH11-ACTn1-Syne2 pathway was the mechanotransduction of LIV in hBMSCs.

Secondly, we hypothesized that LIV could change cytoskeletal orientations and that the structural changes could affect the cellular mechanics. We used two-photon confocal microscopy to visualize cytoskeletal f-actins and validated specific physical interactions of cellular structures based mechanotransduction pathway. Atomic force microscope (with liquid mode) estimated the relative mechanical modulus that changed with the structural changes and remodeling. If cellular mechanical properties were different in LIV protocols, the relative cellular mechanics could provide information on the mechanical sensing mechanisms.

From two-photon images, we found that the cytoskeletal orientation anchoring nucleoskeletons. The changes in cytoskeletal structures driven changes in the mechanical modulus were measured by atomic force microscopy. We found that the cytoskeletal orientation of horizontal LIV was better than that of the vertical LIV. Correspondingly, the mechanical modulus of hLIV was higher than the moduli of vLIV. The cytoskeletal knockdown provided a confirmation of the CDH11-ACTn1-Syne2 mechanotransduction pathway. Without cytoskeletons, we found that the ACTn1-Syne2 was depleted, which confirmed the existing CDH11-ACTn1-Syne2 pathway.

The third hypothesis was to understand biological and molecular functions of LIV driven cytoskeletal orientation. We hypothesized that the cytoskeletal orientation could control differentiation fates of human stem cells. The osteoblastogenic and adipogenic differentiations of hBMSCs and hAMSCs under LIV were investigated with and without an induction of the differentiation media.

Our data supported that the cytoskeletal orientation promoted the osteoblastogenic differentiation but suppressed the adipogenic differentiation of both multilineage human bone marrow and adipose-derived MSCs. These data for the first time showed the LIV mechanisms in controlling the differentiation fates. Understanding LIV promoting the osteoblastogenesis and suppressing the adipogenesis provided strategies towards non-pharmacological programming multipotent stem cells towards preferential lineages.

The fourth hypothesis was to understand dynamic bone homeostasis and healing starting in the bone marrow niche. To understand biological mechanisms of LIV on bone marrow niches' cells, we investigated the effect of hLIV on macrophages. Understanding what drives macrophages toward the pro-healing phenotypes and linking pro-healing expression with hBMSCs could suggest the bone-healing mechanisms in vivo. Perhaps, LIV induced bone formation in balancing with bone resorption via IL-10 during bone homeostasis. We hypothesized that hLIV induced pro-healing macrophages and upregulated VEGF angiogenesis. The upregulated VEGF increased the osteoblastogenic differentiation of hBMSCs and bone survivals. The relation of pro-healing macrophages and hBMSCs provided fundamental understandings of bone homeostasis and healing in bone marrow niches.

We found that macrophages switched their phenotypes from the inflammatory to pro-healing phenotypes by hLIV. The anti-inflammatory cytokine interleukin-10 (IL-10) was increased as if the hLIV induced pro-healing macrophages. Activated IL-10 in the pro-healing macrophages promoted upregulated VEGF and TGFβ. The VEGF expression levels of hLIV were upregulated, supporting angiogenesis potentials of macrophages under hLIV. The upregulated TGFβ was maintained in all hLIV conditions as if macrophages maintained the ability of bone homeostasis. The relation of upregulated VEGF in macrophages with increasing

hBMSC-driven osteoblastogenesis has confirmed the bone regeneration starting in the bone marrow niches.

Dedication Page

To my parents who devote their lives to support my endeavors!

Frontispiece I

Physical Structures Based Mechanotransduction in Human Bone Marrow Mesenchymal Stem Cells: Cellular and Nuclear Structures

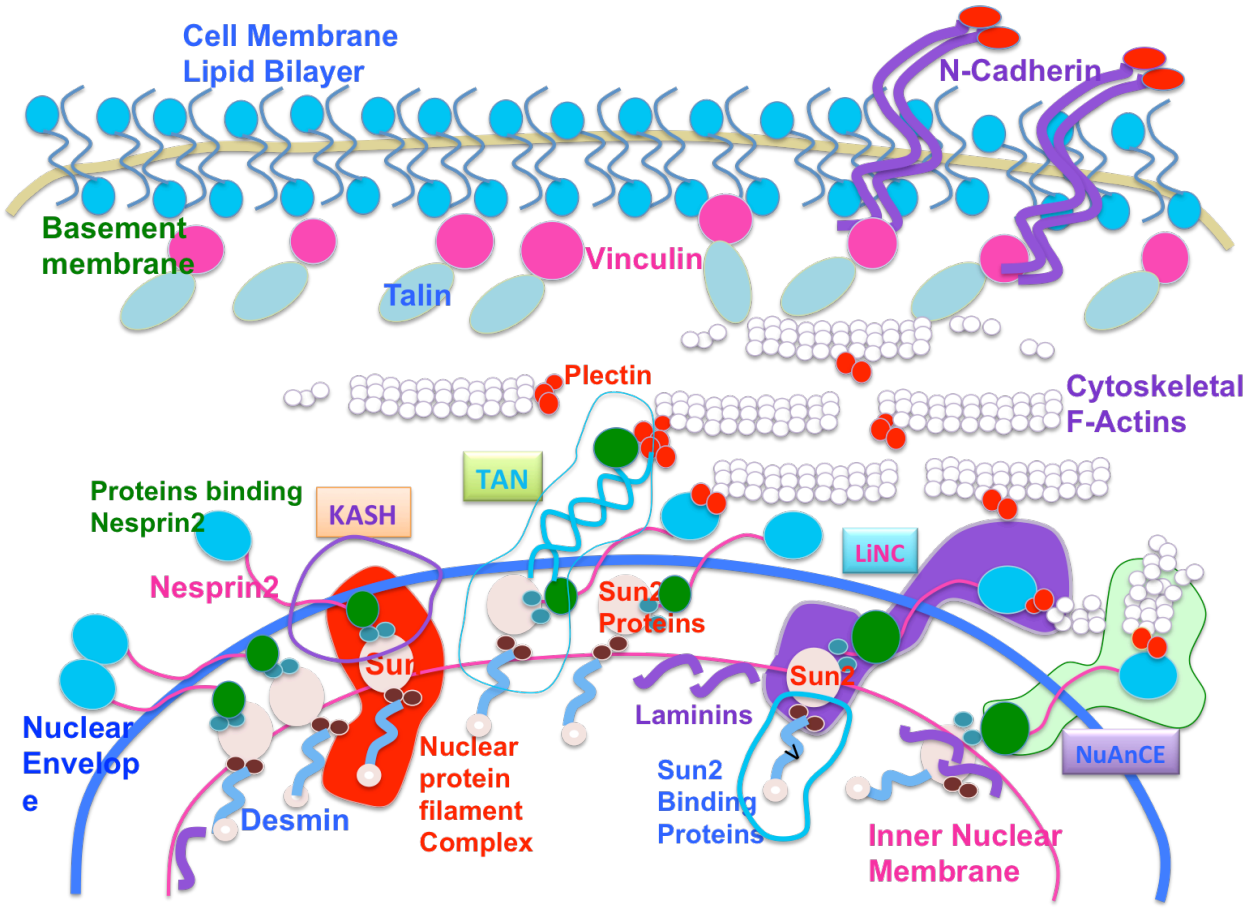

Table of Contents

List of Illustrations

Frontispiece: Physical Structures Based Mechanotransduction in Human Bone Marrow Mesenchymal Stem Cells: Cellular and Nuclear Structures

The proposed mechanotransduction is based on the physical interactions of cellular and nuclear structures. During the low intensity vibration (LIV), the hBMSCs would interact with their neighboring cells. The dynamic adherent junctions could form mature junction interfaces with cytoskeletons. The dynamic cytoskeletal orientation could anchor the nucleoskeletons from the outer nuclear envelope at nesprins towards inside the nuclear membrane at Sun-Kash complex to complete the mechanotransduction pathway.

Note: This picture was pieced together from the data found in several references such as: Rothball et al. 2013, Taply et al. 2012, Zhen et al. 2012.

List of Tables

List of Figures

Figure 1.3: The nuclear complex structure of the NuAnCE-LiNC is composed of the Nesprin nuclear fibers (Nesprin1, 2, 3 and 4), the inner nuclear Suns molecules (Sun1, 2, 3, and 4), Kash filament-protein domains, and Tan giant molecules connecting Kash to cytoskeleton and laminins at the nuclear basement membrane [Rothballer et al. 2013, Taply et al. 2012, Zhen et al. 2002].

Figure 1.4: Our modified horizontal LIV device connects a voice coil linear actuator (NCM15-15-032-2LB, H2W Technologies, Inc.) to a function generator (DS335, Stanford Research Systems) and a frictionless base (NK2-110B, Schneeberger) in the horizontal direction. The frequency and acceleration can be adjusted, which provides a well-defined mechanical signal.

Figure 1.5: The vertical vibration device connected the sound amplifier to the vibration base vertically with 4 coils at the base to maintain the amplitude of the base moving up and down without bouncing effects.

Figure 2.1: The schematic of the horizontal vibration device connects the function generator (that controls the frequency and acceleration) to the amplifier and the frictionless base. The plate holder attaches to the frictionless base and moves along the x axis. The accelerometer monitors the horizontal acceleration, which displays on the computer monitor by the LabView.

Figure 2.2: The vertical vibration device schematically connects to the speaker with a built-in AC amplifier. The plate holder is connected to the metal base with 4 coils and 4 shock absorbers to support the plate during the oscillatory acceleration without wobbling.

Figure 2.3: The mechanism of RNA interference knocks down the gene of interests by post silencing [Agrawal et al. 2003, Hannon 2002, Shan 2010]. After the transcription, the siRNA can interfere the miRNA transferring causing no translation DNA.

Figure 2.4: The RNA transfection silences the gene expression by compromising the DNA in the cytoplasm [Scheer et al. 2003, 2007]. During miRNA polymerization, the small molecule of siRNA can interfere the double strands causing the defect DNA.

Throughout **Chapter 3**, the control group (non-LIV) was represented by gray color. The dark and light colors were horizontal and vertical LIV, respectively. Blue was for 30Hz-0.15g groups, green was 30Hz-1g groups, purple was 100Hz-01.5g groups, and red was 100Hz-1g groups. The statistic significance of LIV conditions for the control group was referred to * ($p<0.05$) and ** ($p<0.01$), respectively.

Figures 3.1a and b: Fluorescent images of double staining living cells with Calcein AM (green) and Ethidium Homodimer (red), showed viable cells of non-LIV (a), and horizontal LIV at 100Hz-0.15g (b).

Figures 3.1c: Normalization of the averaged cell density [δ] in each group over 3days was presented. [δ] of all LIV conditions was increased and ~1.2-2.2x higher than the control.

Figure 3.2a: Normalization of the averaged alkaline phosphatase activity [ALP] on Day1 and Day7 in each LIV was presented. [ALP] of all LIV conditions was ~1.2-1.8x more than the control.

Figure 3.2b: Normalization of the averaged calcification [Ca^{2+}] of all conditions was ~1.2-3x higher than the control, for Day1, Day7, and Day14. (The fluorescent images of alizarin red assay were presented in A2 and A3.)

Figure 3.3a and b: (a) The average gene expression (n=6) in fold changes ($2^{-\Delta\Delta Ct}$) of ALPL and Runx2 on Day1 showed expression of LIV conditions were ~1.7-3.7x more than the control, with respect to GAPDH housekeeping. (The ALP protein expression can be confirmed by western blot in A1.)

(b) The average gene expression level of Runx2 for all LIV conditions on Day1 was ~1.2-2.7x folds higher than the control with respect to GAPDH housekeeping genes.

Figures 3.4a and b: (a) Gene expression levels of cytoskeletal remodeling (WHAMM) from pooled data on Day1, Day7 and Day14 showed that horizontal and vertical LIV at 100Hz-0.15g and 30Hz-1g were ~1.5-5 folds upregulated higher than the control.

(b) Gene expression levels of cytoskeletal f-actins protein (ACTn1) from pooled data on Day1, Day7 and Day14 were ~2-6 folds upregulated in horizontal and vertical LIV at 100Hz-0.15g and 30Hz-1g.

Figures 3.5a and b: (a) Gene expression levels of structure related genes of adherent junction (CDH11), cytoskeletal f-actins binding protein (ACTn1) and NuAnCE-LiNC (Syne2-Sun2) of horizontal 100Hz-0.15g vs the control were observed on Day1, Day7 and Day14. The expression levels of LIV were 2-6 folds upregulated from the control.

(b) Flow cytometric analysis of the normalization of the averaged %population positive to the hBMSCs conjugated CDH11, ACTn1 and Syne2 primary antibodies coupling with AlexaFlou488 and secondary IgG antibody (n=6) on Day1 showed ~1.2-1.6x more than the %P of the control.

Figure 3.6: Pooled data of extracellular matrix (ECM1) and focal adhesion kinase (FAK) were ~1.2-1.6 folds upregulated**.**

Throughout **Chapter 4**, the wild type hBMSCs under non-LIV (control group) represented by gray color. The dark and light purple was horizontal and vertical LIV at 100Hz-0.15g, respectively. The green and orange were for knockdown and silencing ACTn1 under non-LIV. The statistic significance of LIV conditions for the control group was referred to * ($p<0.05$) and ** ($p<0.01$), respectively.

Figures 4.1a and b: Two-photon confocal microscope of cytoskeletal f-actins immunofluorescent staining with Phalloidin AlexaFlor594 was imaged for non-LIV (a), and horizontal LIV at 100Hz-0.15g (b)

Figures 4.2: Normalized % Fiber orientations of cytoskeletal f-actins and nucleoskeleton from two-photon images of horizontal and vertical LIV at 100Ha-0.15g were calculated by MatLab programming.

Figure 4.3a: Averaged gene expression levels in fold changes ($2^{-\Delta\Delta Ct}$) of CDH11, ACTn1 and Syne2 (n=6) showed that upregulation of CDH11, ACTn1 and Syne2 in hLIV was higher than in vLIV.

Figure 4.3 b: Normalization of the averaged % Population of CDH11, ACTn1 and Syne2 of horizontal and vertical LIV at 100Ha-0.15g by flow cytometric analysis confirmed the relation of these genes with the mechanotransduction.

Figures 4.4a and b: (a) Force (pN) – displacement (μm) by liquid mode AFM provided a straight portion for calculation of the averaged relative modulus (unit-less).

(b) The averaged relative modulus was normalized to that of the control. The hLIV provided the highest normalized averaged relative modulus.

Figure 4.5a: We tested the effectiveness of the knockdown biogene technique by flow cytometric monitoring of %ACTn1 of hBMSCs; (i) wild-type had no any gene depletion, but stayed in knockdown conditions (in 1%DMSO at 37°C for Day1, Day2 and Day3) without LIV, (ii) knockdown cytoskeleton without LIV, (iii) knockdown cytoskeleton with hLIV, and (iv) knockdown cytoskeleton with vLIV. We found that all of the groups of the knockdown depolarized cytoskeleton had depleted ACTn1.

Figure 4.5b: Normalized averaged %population of CDH11, ACTn1 and Syne2 in knockdown cytoskeleton groups with and without LIV comparable with wild-type hBMSCs. The data demonstrated that all knockdown groups had depleted ACTn1 and %ACTn1 below 1 of the wild type, non-LIV. Without cytoskeleton (i.e. diminutive %ACTn1 <0.07), there was synchronously minuscule %Syne2 (<0.08) as if cytoskeleton regulating nucleoskeleton.

Figure 4.5c: Normalizaed averaged %population positive to CDH11, ACTn1 and Syne2 in transfection conditions vs wild-type hBMSCs. Transfection of hBMSCs in lipofectamine Opti MEM silencing cytoskeletons exhibited minute cytoskeleton (<0.3) and nuclear fibers (<0.4) in LIV groups.

Throughout **Chapter 5**, the control group (non-LIV) was represented by dot line. The dark and light purple was hBMSCs under hLIV at 100Hz-0.15g with and without induction, respectively. The dark and light red was hAMSCs under hLIV-100Hz-0.15g with and without induction, respectively. The statistic significance of LIV conditions for the control group was referred to * ($p<0.05$) and ** ($p<0.01$), respectively.

Figure 5.1a: Normalized averaged calcification of hBMSCs and hAMSCs with vs without osteoblastogenic induction. (The non-LIV was presented in a straight line.) The calcification of hBMSCs was >1.1x higher than of hAMSCs. The calcification of hBMSCs and hAMSCs with osteoblastogenic media was ~1.1x and ~1.2 without OS, respectively.

Figures 5.1b: Flow cytometric analysis of the normalization of the averaged %population positive to alizarin red (%calcification) of hBMSCs and hAMSCs with and without OS induction. hBMSCs exhibited >1.3x higher calcification than hAMSCs during osteoblastogenesis.

Figure 5.2a: The lipoprotein content by oil red of hBMSCs with adipogenic media was similar to the amount without AD. Lipoproteins accumulating in hBMSCs was >1.5x less than in hAMSCs.

Figure 5.2b: Flow cytometric analysis of %population positive to oil red (%Lipoprotein) was normalized with respect to the population of the non-LIV. The hAMSCs had >1.2-1.5x higher %Lipoprotein than that of hBMSCs.

Figure 5.3a: The averaged Runx2 gene expression levels of hBMSCs were >1.2-1.5x higher than of hAMSCs. Runx2 expression levels of hBMSCs and hAMSCs with OS were >1.3x and >1.1x folds higher than the expression w/o OS, respectively. The data suggested that hLIV improved osteoblastogenesis of human stem cells.

Figure 5.3b: Averaged PPARg expression levels of hBMSCs were down regulated and similar in both groups with and without adipogenic media. Down regulated PPARg in hLIV suggested suppression of adipogenesis by hLIV. The hAMSCs exhibited 1.5x higher PPARg folds than the hBMSCs.

Figure 5.4a: Flow cytometric analysis of %population positive to ACTn1 (%cytoskeletal orientation) was normalized with respect to the population of the non-LIV. During osteoblastogenic differentiation, hBMSCs with OS showed >1.4x better cytoskeletal orientation than hAMSCs, confirming improvement of the osteoblastogenesis with the cytoskeletal orientation.

The hAMSCs had >1.2-1.5x higher %Lipoprotein than that of hBMSCs. The %cytoskeletal orientation of hBMSCs was >1.4x higher than that of hAMSCs during adipogenic differentiation, supporting suppression of adipogenesis.

Figure 5.4b: Cytoskeletal orientation was plotted against the progress of osteoblastogenesis and adipogenesis. With re-plotted raw data of 4a and adding trend line, the relation of the cytoskeletal orientation with differentiation fates demonstrated that hLIV supported osteoblastogenesis but suppressed adipogenesis.

Throughout **Chapter 6**, the control group (non-LIV) was represented by gray color. The blue was for hLIV 30Hz-0.15g groups, green for 30Hz-1g groups, purple for 100Hz-01.5g groups, and red for 100Hz-1g groups. The statistic significance of LIV conditions for the control group was referred to * ($p<0.05$) and ** ($p<0.01$), respectively.

Figures 6.1a and b: Fluorescent images of double staining living cells with Calcein AM (green) and Ethidium Homodimer (red), showed viable cells of non-LIV (a), and horizontal LIV at 100Hz-0.15g (b) during macrophage proliferation.

Figure 6.2: Normalization of the averaged cell density, [δ] of macrophages during the proliferation under hLIV and non-LIV over 3days. The hLIV signals were 30Hz-0.15g, 30Hz-1g, 100Hz-0.15g and 100Hz-1g. The [δ] of all hLIV was >1.3-2.5x more than that of non-LIV across 3days. hLIV at 100Hz-0.15g provided the highest [δ] for all 3days. hLIV at 30Hz-0.15g and 100Hz-1g had similar [δ].

Figure 6.3: Flow cytometric analysis of normalized average %gm-CSF was divided by normalized average %m-CSF. The ratio of the m-CSF to the gm-CSF demonstrated the ratio of pro-healing to inflammatory macrophages under hLIV vs non-LIV during proliferation. The hLIV showed higher M2 more than M1 macrophages (1.9-2.5x) as the hLIV promoted pro-healing macrophages.

Figure 6.4: The inflammatory markers of IL-6, IFN-γ, and TNFα were observed in the non-LIV and LIV at 100Hz-0.15g on Day1 and Day3. All of the inflammatory markers were down regulated (>1-1.2x on Day1, and >1.8-2.2x on Day3). These data suggested that

the pro-inflammatory phenotype macrophages were suppressed by the LIV. And the suppressive effectiveness was more efficient over time.

Figure 6.5: After 2 days of the first inoculation, the macrophages were induced M2-macrophage polymerization. The normalized average %IL-10 of hLIV and non-LIV was reported. The amount of IL-10 in hLIV was >1.2-1.8x higher than the IL-10 in non-LIV as if the IL-10 is an M2 marker [Deng et al. 2012].

Figure 6.6a: The averaged VEGF expression levels (n=6) of hLIV were upregulated >1.6-2.5x folds higher than the expression level of the non-LIV. The 100Hz groups provided higher VEGF expression folds (>1.2-1.6x) than the 30Hz groups. The 30Hz-1g had ~1.2folds higher than VEGF of 30Hz-0.15g. The 100Hz-0.15g had ~1.3folds higher than VEGF of 100Hz-1g.

Figure 6.6b: The averaged TGF-β expression levels (n=6) of hLIV were upregulated >1.4-1.5x folds higher than that of the non-LIV. Though the upregulated TGF-β levels of the hLIV were very similar in all groups, indicating the hLIV sustained TGF-β.

List of Abbreviations and Terminology

Acceleration – strength or signal intensity of LIV

ACTn1 – cytoskeleton protein alpha actinin subunit 1 provides mechanical strength to cells and links transmembrane to cytoplasm. The ACTn1 is responsible to the cytoskeletal organization and bundles by its binding domain cross-linking the actin filaments into bundles.

ACTb – cytoskeletal actin beta is plenty in human cells and generally used as the house keeping gene in the PCR analysis.

Adipogenesis – cells become adipocytes

Adipogenic differentiation – differentiate cells into adipocytes with or without induction of adipogenic media

AFM – atomic force microscope used an atomic tip to scan across the hard or soft surface and monitor the surface torpography.

AKT1 – Akt murine thymoma viral oncogene homolog 1

Alizarin Red S assay – colorimetric measurement of dye (1,2-hydroxyanthraquinone) binding membraneous calcium deposit in cells or organisms

ALP – alkaline phosphatase activity can indicate the activity of the stem cell differentiation

ALPl – gene symbol for the alkaline phosphatase (plenty in liver, bone, kidney)

ANXa5 – annexin A5 protein can detect the cellular apoptotic cells and dead cells

ANPEP – alanyl membrane aminopeptidase (APN)

AP2α1 – adaptor-related protein complex 2, alpha 1 subunit

ARHGEF2 – Rho/Rac guanine nucleotide exchange factor GEF-2 (GEF-H1)

ATF4 – activating transcription factor 4 is a DNA-binding protein that can bind a tax-responsive enhancer element in the LTR of HTLV-1 and can be characterized as characterized as the cAMP-response element binding protein 2 (CREB-2).

BMP2 – bone morphogenic protein 2

BMP4 – bone morphogenic protein 4

BMPR2 – bone morphogenic protein receptor type II (serine / theonin kinase)

BMP7 – bone morphogenic protein 7 (OP-1)

BGLAP – bone gamma-carboxyglutamate, gla-protein

BMPR1A – bone morphogenic protein receptor type IA

CACNA1Hb – calcium channel, voltage dependent, T type, alpha 1H subunit

CACNA1C – calcium channel, voltage dependent, L type, alpha 1C subunit

CACNA2d1 – calcium channel, voltage dependent, alpha 2 delta subunit 1

Calcification – calcium deposition

CD44 – surface CD44 molecules

CDC42 – cell division cycle 42, GTP binding protein (25kDa)

CDH11 – cadherin 11 type 2, osteoblast-cadherin

Cell population – numbers of cells or cell density (i.e. cells/cm^2 or cells/ml)

Col1α1 – collagen type I, alpha 1

Confocal microscope – imaging technique uses point illumination with spatial pinholes to increase optical resolution and eliminate out of focus noise.

CREB1 – CAMP responsive element binding protein 1

CREBBP – CREB binding protein

CSF-1 – colony stimulating factor 1

CTNNB1 – beta catenin 1 (cadherin associated protein, 88 kDa)

Differentiation – multipotent stem cells become specific cell types

ECM1 – extracellular matrix protein 1

FGFR1 – fibroblast growth factor receptor 1

FGF2 – fibroblast growth factor 2

Flow cytometric analysis – analysis of %positive immunostaining population in the gated area (generally use FlowJo program analysis)

Fluid shear stress – shear stress of fluid moving along solid boundaries

FN1 – fibronectin 1

Fold change – gene expression calculated from $2^{-\Delta(\Delta C_t)}$ with respect to control and housekeeping gene

FOXO1 – forkhead box O1

Frequency – number of vibration in a second or speed of LIV

FRZB – frizzled related protein

FZD1 – frizzled family receptor 1

GAPDH – glyceraldehyde-3-phosphate dehydrogenase

Gated area – area compared to standard positive and negative population in flow cytometry

GJA1 – gap junction protein alpha 1 (43 kDa)

GDF10 – growth differentiation factor 10

Gene expression – transcription RNA converted to cDNA and amplified DNA

HAS1 – hyaluronan synthase 1

hAMSCs – human adipose derived mesenchymal stem cells

hBMSCs – human bone marrow derived mesenchymal stem cells

IBSP – integrin binding sialoprotein

ICAM1 – intercellular adhesion molecule 1

IGF1 – insulin like growth factor 1 (somatomedin C)

IGF1R – insulin like growth factor 1 receptor

IHH – Indian hedgehog

Immunostaining – color coated cellular structures using specific antibody

ITGA1 – integrin alpha 1

LAMA1 – laminin alpha 1

LIV – low intensity vibration

LRP5 – low-density lipoprotein receptor related protein 5

hLIV – horizontal LIV is the LIV parallel to cellular attachment

vLIV – vertical LIV is the LIV perpendicular to cellular attachment

M1 – pro-inflammatory macrophage phenotypes

M2 – pro-healing macrophage phenotypes

MAPK1 – mitogen activated protein kinase 1

MAP3K1 – mitogen activated protein kinase kinase kinase 1

Mechanotransduction pathway – transduction of mechanical signals

MKNK1 – MAP kinase interacting serine/theronin kinase 1

MTS assay – colorimetric assay assessing cell viability and numbers using XXT reagents

MYLK – myosin light chain kinase

MYH10 – myosin heavy chain 10, non-muscle

NET1 – neuroepithelial cell transforming 1

NFKB1 – nuclear factor kappa light polypeptide gene enhancer in B-cell 1

NFATC1 – nuclear factor of activated T-cells, cytoplasmic calcineurin dependent 1

NOTCH1 – notch1 is a protein-coding gene that could associate with aortic valve disease.

NOX1 – NADPH oxidase 1

Osteoblastogenesis – cells differentiate into osteoblasts

Osteoblastogenic differentiation – differentiate cells into osteoblasts with or without induction of osteoblastogenic induction media

OTX2 – orthodenticle homerobox 2

PAK1 – P21 protein CDC42/Rac-activated kinase 1

PCR – polymerase chain reaction to clone, sequence and amplify pieces of DNA as gene expression

PDGFA – platelet derived growth factor alpha polypeptide

PIK3CA – phosphoinositide-3-kinase catalytic alpha polypeptide

PPARD – peroxisome proliferator-activated receptor delta

PPARγ – peroxisome proliferator-activated receptor gamma

PTEN – phosphatase and tensin homolog

PTGS2 – prostaglandin-endoperoxide synthase 2 and cyclooxygenase (COX2)

PTK2 – PTK2 protein tyrosine kinase 2 (FAK)

Rac1 – Ras-related C3 botulinum toxin substrate 1 (Rho family small GTP binding protein Rac1)

RhoA – Ras homolog gene family member A

RNAi – RNA interference is a technique to knock down the biogenes in vitro

ROCK1 – Rho associated coil-coil containing protein kinase 1

Runx2 – Runt related transcription factor 2

SERPINH1 – serpin peptidase inhibitor clasde H member 1 (heat shock protein 47 collagen binding protein 1)

Signal combinations – mechanical signal combinations of frequency and acceleration generate fluid shear stress

shRNA – small or short RNA sequences targeting specific gene depletion in iRNA

siRNA – silencing RNA during transcription

SMAD1 – SMAD family member 1

SMAD4 – SMAD family member 4

SOX9 – sex determining region Y (SRY) – box 9

SP7 – SP7 transcription factor (Osterix)

SPP1 – secreted phosphoprotein 1 (Osteopontin; OPN)

STAT3 – signal transducer and activator of transcription 3 (acute pahse response factor)

Sun1 – Sad1 and UNC84 domain containing 1

Sun2 – Sad1 and UNC84 domain containing 2

Syne1 – Spectrin repeat containing nuclear envelope 1

Syne 2 – Spectrin repeat containing nuclear envelope 2 (Nesprin2)

TGFβ1 – transforming growth factor beta 1

TLN1 – Talin 1

TM7SF2 – transmembrane 7, superfamily membrane 2 (Ang1)

TNF – tumor necrosis factor

TNFSF11 – tumor necrosis factor ligand superfamily, member 11 (RANKL)

TRAF3IP2 – Traf3 interacting protein 2 (ACT1)

TRAF6 – TNF receptor associated factor 6

Transfection – silence RNA by siRNA in vitro

TUBB3 – Tubulin beta 3

Twist1 – Twist homolog 1

Two photon confocal microscope – imaging technique uses low energy two photons to excite fluorophore in one quantum event

VAV1 – VAV1 guanine nucleotide exchange factor

VEGFA – vascular endothelial growth factor A

VCL – Vinculin

Western blot – electrophoresis to separate proteins and colorimetric measurement of immunostaing proteins

WHAMM – WAS protein homolog associated with actin, Golgi membrane, and microtubules

WNT1 – Wingless type MMTV integration site family member 1

WNT10A- Wingless type MMTV integration site family member 10A

WNT3 – Wingless type MMTV integration site family member 3

XXT reagent – tetrazolium salts specific to living and growing cells

Acknowledgement

I would like to take this time to express my deepest appreciation and special thanks to my advisor, Professor Dr. Stefan J., especially for his tirelessly editing to improve my manuscripts. I would like to thank you for your excellent advice and tremendous mentor. Thank you for encouraging my research and allowing me to grow as a research scientist. Your magnificent advice on both writing scientific manuscripts as well as on my next potential career has been exceptionally valuable. Thanks for your appreciation of my hard work and your support of my relentless persistence and passion in science.

I would like to thank my committee members for serving as my committee members and for their support throughout the course. I would also like to thank you all for your brilliant comments and suggestions. I would like to especially thank Professor Dr. Clint R. for his care and support. Your care for our well being has brightened and warmed our hearts. Your support has made our strenuous work incredibly at ease. I would like to thank professor Dr. Yizhi M. for her support and care even in hardship. Your consistent consideration and support of my motivation has a great positive impact on me. I would also like to thank Professor Dr. Tim K. for his brilliant suggestions on macrophages. Your help with an overnight shipment has been appreciated. Thank you all for your cares and supports and for allowing my defense to be a happy moment.

I would like to especially thank Dr. Wei Y. for her help in an access to the flow cytometer. Your support and help with recommendation have been always appreciated. Your

views on many topics have been excellent and provided me wider perspectives. I would also like to thank Professor Dr. Yi-Xing Q. for his support and recommendation. Thank you for your appreciation and invariably recognition of my hard work. Thank you, Professor Dr. Kanokporn R. for her recommendation and support. Your cares have encouraged me to follow through my entire plan. Thank you, Dr. Anne S., for your help with acquiring the specific antibodies and biochemicals. Your support and knowledge on the antibody selection have brought perfection to my results. Thank you, Dr. Barbara R. and Dr. Ben A. for their support and always taking the time to discuss any topics in science and the world at large.

I would like to express my deepest appreciation to my friends, Patti and Bill W., Dr. Andrew and Linda R., Jesse and Margarett Y., Dr. Heather K., Carol and Dr. Bob L., Virginia H. and Leslie and Dr. David J. for always being my biggest supporters throughout even hardship. Thanks for your support and always care for my well being. I would like to thank Professor Ahmed H. and Masume A. for your support and help with everything.

I would like to give my special thanks to my parents. Their unwavering and strong belief in me has furthered me beyond my own limits. Thank mom and dad for always allowing me to be myself and to go after my goal all the way, even when seemingly challenging at the time. Thanks for your unconditional love and indestructible support of my endless endeavors. I am also grateful for my family, my brothers and sisters, mothers-in-law and fathers-in-law for all of their calls and their prayers for me. Thanks for all your support and all oversea cards and calls to me.

I would like to express my most and special appreciation to my fiancé Dr. Jesse H. for his devoted tenderness and perpetual patience. Your overwhelming appreciation of my perseverance has supported me in pursuing my ambition. Your understanding of my passion in research has encouraged me to accomplish my goal. Your support and compassion have always reinforced my strength and helped me strive towards my achievement. Your selfless sacrifices have sustained my success and me thus far.

Chapter 1

Introduction

(Pending publication and/or patent)

1.1 Introduction

1.1.1 Bone Functions and Morphology

Bone is a dynamic, highly vascularized organ that includes nervous, epithelial, and connective tissues. To adapt to the daily forces, bone constantly undergoes remodeling and change in its morphology and structures [Skerry 2008]. There are approximately 206 bones in the human skeletal system (, where generally includes bones, cartilage, and bone lining membranes).

Bone functions (i) as a supportive framework for the attachment of the skeletal muscles and tissues [Benjamin et al. 2006, DiGirolamo et al. 2013], and (ii) to protect internal organs [Grabowski 2009]. For examples, human cranial bone protects the human brain [Richtsmeier et al. 214], the vertebral column protects the human spinal cord [Kroeker et al. 2013, Swartz et al. 2005], and the thoracic vertebrae protect the human heart and lungs [Clemens et al. 2011]. Bone enables body movements by acting as levers and points of attachment for muscles [Cianferotti et al. 2014]. Bones serve as a reservoir for mineral storage of calcium phosphates [Nakamura et al. 2012] that are essential for various cellular activities and provide physiological strength and hardness [Copp et al. 1963]. Moreover, bone stores crucial nutrients, minerals, and lipids such as adipocytes in the medullary cavity containing yellow marrow to serve as energy storage [Devlin 2011]. Furthermore, human bone produces erythrocytes (i.e. red blood cells) and leukocytes (i.e. white blood cells) during hematopoiesis in bone marrow [Orkin et al. 2002]. Leukocytes are produced to protect the body against the infection during inflammatory and healing processes

[Wagner et al. 2014]. Human bone marrow (active red marrow) is found in the cavities of the femur and trabecular bones (during childhood), including the vertebral column, thoracic vertebrae, and sternum (in adulthood) [Sambuceti et al. 2012]. During adolescences (i.e. 19 years old and younger in human), the red bone marrow in femur and tibia mainly produces erythrocytes [Travlos. 2006]. Erythrocytes nourish the body by providing nutrients and oxygen. With advancing age, these hematopoietic cells are gradually replaced by adipose tissue (yellow or fatty marrow) [Malkiewicz et al. 2012]. Approximately one-half of the hematopoietic cells in the tibia and femur are replaced by fatty marrow. In adults, active bone marrow is found mostly in the vertebral column (spine) and pelvis (hip bone), including cavea thoracis (rib cage), clavicles (collarbone), sternum (chest bone), scapulae (shoulder blades), and calvaria (skull) [Ricci et al. 1990].

Bone tissue can be defined into cortical bone (or compact bone) and cancellous bone tissues (or trabecular bone) [Clarke 2008, Müller 2009]. Cortical bones form the diaphyseal shaft of long bones and consist of a very hard, solid mass of bone tissue arranged in concentric layers [Rose et al. 1984]. The cortical bone microscopically contains osteons riddled with Haversian canals, which are passageways of, and served as conduits for nerves, blood vessels, and lymphatic vessels [Qiu et al. 2003]. In each osteon, osteocytes in lacunar canaliculi form lamellae by laying down collagen fibers intermeshing with adjacent lamellae with different directions [Palmer et al. 2008]. These collagen lamellae provide a strong tissue structure that can withstand twisting and mechanical stress. Trabecular bone locates beneath the cortical bone and consists of a spongy meshwork of the irregularly arranged collagen lamellae and osteocytes

interconnecting with canaliculi and bone marrow cavities [Hipp et al. 1996, Wang et al. 2011]. Trabecular bone gives supporting strength to the ends of the weight-bearing bone.

1.1.2 Cells in Bone and Bone Marrow Niches

1.1.2.1 Osteoblast, Osteocyte, and Osteoclast Bone Cells

Bone cells (osteoblasts, osteocytes, and osteoclasts) reside in bone.

Osteoblasts are derived from bone marrow mesenchymal stem cells [Birmingham et al. 2012, Heino et al. 2008] and periosteum fibroblasts [Marie et al. 2006, Salmon 2015]. After osteoblastogenesis, the osteoblast lays down the osteoid and collagen in the bone matrix before transforming into the osteocytes [Dallas et al. 2010, Nijweide et al. 1988]. Molecular functions of osteoblasts are not only capable of differentiation into osteocytes [Franz-Odendaal et al. 2006], but also functioning as bone lining cells to support bone niches [Krishnan et al. 2010].

Osteocytes are derived from osteoblasts and can calcify in the bone matrix in the lacunar canalicular system [Thi et al. 2013]. After osteocytogenesis, the osteocytes are then embedded in the calcified bone matrix during the bone formation [Kato et al. 1997, Mattinzoli et al. 2012]. The mature osteocyte expresses the protein sclerostin, negatively regulating bone mass [Compton et al. 2014].

Osteoclasts are derived from macrophages and the peripheral blood monocyte lineage in the bone marrow. During the bone remodeling, osteoclasts resorb bone cells [Martin et al. 2007, Nakahama 2010] and matrix to initiate bone homeostasis [Boyce et al. 2009]. The increasing

bone resorption causes an imbalance in the bone homeostasis, which mediates the pathological bone loss [Abdelmagid et al. 2015].

Bone niches (so called osteoblast niches) involve osteoblasts, osteocytes, osteoclasts and macrophages, including hematopoietic stem cells [Long et al. 2012]. To maintain bone homeostasis, the osteoblasts in bone niches are differentiated to be osteocytes calcifying in the bone matrix [Mattinzoli et al. 2012] in balancing the osteoclast bone resorption. Though the initiation mechanism is unclear, the aged bone [Henrikson et al. 2007], however, has been thought to initiate multinucleated osteoclasts to resorb bone during the osteoclastogenesis [Groessner-Schreiber et al. 1991, Zaidi et al. 2003].

1.1.2.2 Human Bone Marrow Mesenchymal Stem Cells

Human bone marrow mesenchymal stem cells (hBMSCs) can differentiate into several bone lineages [Charbord et al. 2011] via osteoblastogenesis, osteochondrogenesis, etc. The best source for bone formation is the hBMSC differentiation through the osteochondrogenesis and osteoblastogenesis [Ehninger et al. 2011].

The hBMSCs reside in bone marrow forming niches (**Figure 1.1**, [Maes et al. 2012]) with bone niches, and vascular niches (the HSC niches) [Morrison et al. 2014], where hematopoietic stem cells (the same HSCs located in abluminal marrow sinus endothelial cells) are residing [Calvi et al. 2014, Sugiyama et al. 2012].

Niches are cellular and molecular microenvironments that regulate cell functions together with cell-autonomous mechanisms [Bershad et al. 2008]. The autonomous mechanisms of stem

cells include controls of the balance between quiescence and self-renewal with differentiation and the engagement of specific programs in response to stress [Cho et al. 2013]. In mammals, recent studies have incorporated the number of cell types contributing to the HSC niche including perivascular mesenchymal stem cells, macrophages, sinusoidal endothelial cells, sympathetic nerve fibers, and cells of the osteoblastic lineages [Ehninger et al. 2011].

The function of bone marrow niches is to control the balance of hBMSCs between quiescence, self-renewal, and differentiation, as well as the engagement of specific programs in response to stress or changes in microenvironments (**Figure 1.2**, [Baron et al. 2013]). However, the self-renewal and proliferation mechanisms of human mesenchymal stem cells (hBMSCs) and human hematopoietic stem cells (HSC) in these niches are unclear. Coupling of bone marrow niches with bone niches and vascular niches could form the harboring, dormant self-renewal during homeostasis [Yin et al. 2006].

1.1.2.3 Macrophages and Hematopoietic Stem Cells

Macrophages are a type of leukocytes that engulf and digest foreign microorganisms and cells via phagocytosis. During tissue damage and infection, monocytes are recruited to the tissue, where they differentiate into tissue macrophages [Mosser et al. 2008]. Macrophages reside in every tissue in different forms such as monocytes in blood and bone marrow, microglia in the nervous system, osteoclasts in the skeletal system.

Hematopoietic Stem Cells (HSCs) can differentiate to be several cell lineages such as dendritic cells, T-cells, and monocytes and macrophages [Bryder et al. 2006]. The human HSCs can differentiate into macrophages in the peripheral blood and bone marrow. The differentiated

macrophages can then migrate to the bone tissues [Takahashi 2001]. The human HSCs reside in blood, bone marrow and vascular niches.

1.1.3 Signaling Pathways

Abilities of cells perceiving and responding to their microenvironments are based on cellular and molecular signaling during tissue and skeletal development, remodeling, repair, immunity, and homeostasis. Errors in cellular information processing may be responsible for diseases and disorders. Expressions of transcription factors and genes during cellular signaling are important for molecular functions. However, cellular signaling pathways have been complicated by their ability to multifunctionality.

1.1.3.1 Skeletal and Bone Development

During skeletal and long bone development, several stages start with the formation of the initial mesenchymal condensations [Colnot et al. 2009, Colnot et al. 2012], followed by the segregation of cartilage and perichondrium [Allen et al. 2004]. The endochondral ossification begins with the vascular invasion of the perichondrium followed by cartridge hypertrophy and consequently vascular invasion [Lin et al. 2014]. The process of endochondral ossification is believed to be regulated by Hedgehog (Ihh) [Long et al. 2004], bone morphogenetic protein (Bmps) [Lowery et al. 2011], TGF-β, FGF [Du et al. 2012], Wnt/β-catenin [Day et al. 2005], VEGF [Zelzer et al. 2004] and others.

During intramembranous bone formation, Runx2 transcription factors have been believed to contribute to regulatory mechanisms throughout osteogenic differentiation. Runx2 is required

and principally linked to osteoblast proliferation and differentiation obligatory for a regulation of skeletal and bone genes [Stein et al. 2004].

Recently, the Wnt in bone marrow and vascular niches could involve in the early bone developments deriving from human bone marrow MSCs (**Figure 1.2**, [Baron et al. 2013]). In bone marrow niches at endosteum, bone-forming osteoblasts could derive from the pluripotent hBMSCs. The Wnt/β-catenin signaling has been believed to be required for the commitment of these cells to the osteoblast lineage [Day et al. 2005]. During hBMSCs commitment to osteoblasts, Wnt/β-catenin signaling inhibits adipogenic and chondrogenic cell fates. Once committed, the Wnt/β-catenin signaling in osteoblast and osteocyte could activate anti-osteoclastic factor OPG trapped RANKL inhibiting osteoclastic bone resorption [Baron et al. 2013].

1.1.3.2 Bone Formation and Remodeling

Bone formation can derive from the osteogenic differentiation of pre-osteoblasts and stem cells. Signaling pathway of Bmps/Wnts and Bmps/TGF-β can activate the osteogenic differentiation and upregulated Runx2 [Chen et al. 2012]. However, Bmp2 binding to the heterodimeric receptor could activate Smads, promoting the adipogenesis by upregulating PPARg [Lin et al. 2011]. Coupling Wnts/Bmps with Wnt/β-catenin signaling pathways activate osteogenic markers and the Runx2 transcription. However, the phosphorylation of β-catenin by GSK3 is targeted for ubiquitination and proteasome degradation [Davis et al. 2008]. The Bmp2/TGF-β could control osteoblastogenesis but the Bmp4/TGF-β controlled chondrocytogenesis of bone marrow MSCs [Ohlstein et al. 2004].

During bone remodeling, new bone formation occurs at bone resorption sites in each cycle of the bone turnover when osteoblasts crosstalk with osteoclasts to maintain bone homeostasis [Cao et al. 2011]. In the bone matrix, the primary coupling factors of TGF-β and probably IGF-1 [Locatelli et al. 2014] are released in response to osteoclastic bone resorption and simultaneously TGF-β induces the migration of osteoblastic cells [Tang et al. 2009]. RhoA acts as the mediator of these coupling mechanisms of osteoclasts-osteoblasts at the matricellular signaling of TGF-β and IGF-1 [Papadimitriou et al. 2012, McBeath et al. 2004].

During osteoblastogenesis, FGF2 is upregulated but FGF4 and FGF7 were found to be involved in chondrogenesis. The FGF23/MAPK pathway inhibited bone formation and calcification in human bone marrow MSCs [Xiao et al. 2013]. Fibroblast growth factors (e.g. FGF2, FGF4, FGF7) use a parathyroid dependent pathway and an endocrine feedback loop to regulate vitamin D in bone metabolism [Pi et al. 2013]. Integrins (ITα5β1, ITαvβ3) of osteoblasts are believed to recognize and monitor changes in proteins (e.g. fibronectin), ECM, and basement fibers [Zaidel-Bar et al. 2013].

Excessive and aging osteoblasts are resorbed during osteoclastogenesis in bone niches by TNF recruiting inflammatory macrophages, increasing osteoclastogenesis with upregulated RANKL [Udagawa et al. 2003]. The communication between osteoblasts and osteoclasts balances osteocytogenesis with osteoblasts differentiated into osteoclasts (osteoclastogenesis) [Mansour et al. 2012].

In bone osteogenic formation, the hBMSC proliferation could upregulate VEGF in the marrow niches, causing an increasing angiogenesis [Wu et al. 2010]. The hBMSCs in bone marrow niches also work on balancing upregulated Runx2-induced osteoblastogenesis with upregulated PPARg-induced adipogenesis of brown marrow [Rosen et al. 2009]. The increasing

hBMSCs driven osteoblastogenesis in bone marrow niches can activate osteoblasts towards osteocytogenesis (osteoblasts derived osteocytes) in bone niches and calcification in the bone matrix. The upregulation of PPARg induced adipogenic differentiation can be suppressed by OPG induced Runx2 [Muruganandan et al. 2009], as a negative feedback loop in controlling bone homeostasis. The overexpression of PPARg can induce inflammatory macrophages [Díaz-Gandarilla et al. 2013], causing osteoclastic differentiation in the marrow. Additionally, macrophage induced osteoclastogenesis (osteoblast differentiated osteoclasts) can be influenced by TGF-β induced inflammation [Morrison 2014]. However, the synchronously coupling mechanisms of hBMSCs driven osteoblastogenesis can trigger the macrophages in the vascular niches to promote molecular switches from anti-inflammatory to pro-healing macrophages [Makita et al. 2014]. By maintaining osteoblastogenesis in balance with osteoclastogenesis, bone homeostasis can be promoted starting in the bone marrow [Wu et al. 2010].

One of the possible self-renewal mechanisms of human stem cells may come from stem cell mobilization in response to granulocyte colony-stimulating factor (gm-CSF) of macrophages in the vascular niche. Increasing HSCs during angiogenesis can promote fibroblast growth factors 2 and 4 (FGF2, FGF4). FGF2 and FGF4 are believed to promote PI3K/Akt and ERK1/2 signaling in the homeostasis of stem cell proliferation [Choi et al. 2008]. Upregulated FGF2 and FGF4 may stimulate PI3K/Akt to induce the stem cell proliferation, especially within the first 15 minutes of upregulated Akt. The prolonged upregulation of Akt (after 12-24 hours of upregulated Akt) may activate ERK1/2 towards c-Jun that induced apoptosis in the cell cycle, modulating the self-renewal.

During interconnection of cellular signaling networks, Akt may be critical in controlling malign tumor and cancer angiogenesis [Radisavljevic et al. 2013]. Targeting angiogenic integrative Akt locus can block all signals, including the VEGF, HIF, H_2O_2, HGF, and other growth factor signals. Akt is upstream of mTOR activated by reactive oxygen species such as H_2O_2. The Akt activation by H_2O_2 induces proliferation through the H_2O_2/PI3K/Akt/mTOR pathway and causes oxidative apoptosis [Nogueira et al. 2008].

Using human adipose-derived MSCs, we were previously unable to link increased CX43 with Akt1 [Uzer et al. 2013]. There could be several reasons for this such that Akt1 is the reflector of ROS where the changes in ROS affected the Akt1. The activity of Akt controls the phosphorylation of Cx43, but Cx43 ubiquitination is not necessary for its regulation [Dunn et al. 2012]. Therefore, linking Akt1 with gap junctions (GJa1) and CX43 may need to include reactive oxygen species (ROS) and H_2O_2 including nitroactive radicals [Chen et al. 2006]. The dephosphorylation of Cx43 at Ser365 can cause the loss of Cx43 function in gap junctions [Jain et al. 2005, Solan et al. 2007]. The H_2O_2 causes hyperphosphorylation of the Cx43, leading to the loss of the gap junction function [Upham et al. 1997] and compromising the function [Pries et al. 2010].

1.1.3.3 Bone Homeostasis and Healing

Physiology of bone homeostasis balancing new bone formation and bone resorption starts in bone marrow niches (**Figure 1.1**, [Maes et al. 2012]). The bone formation could derive from the osteogenic differentiation of hBMSCs in the bone marrow and the osteoblasts differentiated osteocytes [Kini et al. 2012] in bone niches. During bone formation, the hBMSCs differentiated osteoblasts could upregulate osteocalcin, Runx2, and collagen-I, while laying down the osteoid

and transforming into osteocytes. The osteocytes embedding in the calcified bone matrix could upregulate collagen-I, alkaline phosphate (Alp1), and Runx2 [Franz-Odendaal et al 2006].

During bone resorption, transforming growth factor-β (TGFβs) and its families may be released before initiating local bone formation [Rodan et al. 1998]. Recently, mouse genetic studies have proposed the canonical Wnt/β-catenin signaling in the regulation of bone homeostasis (**Figure 1.2**, [Baron et al. 2013]). During multilineage hBMSCs enduring adipogenesis in the old marrow, the progressive adipogenesis could also activate bone resorption in old bone [Lowe et al. 2011]. This osteoclastogenesis (derived from inflammatory macrophages [Cao et al. 2011] and excessive aged osteoblasts) could be the major cause of the bone resorption. The resorption cycle stops when the cytokine receptor osteoprotegerin (OPG) is overexpressed in osteoblasts and osteocytes. OPG can trap RANKL receptors, consequently inhibiting osteoclastogenesis [Baron et al. 2013].

Dynamic bone homeostasis could derive from direct intercommunication between osteoblasts and osteoclasts through gap junction cell communication [Civitelli et al. 2008]. Recently, communication of hBMSCs and macrophages in bone marrow niches has been extensively studied to understand osteoimmunodifferentiation [Teti et al. 2010]. Coupled with bone formation, upregulated OPG induced RANK/RANKL can mediate osteoclast differentiation during bone resorption using negative feedback [Baron et al. 2013]. Bone-resorbing osteoclasts derived from macrophage lineage precursors are under the potential control of macrophage-colony stimulating factor (m-CSF) and granulocyte macrophage-CSF (gm-CSF) [Jaguin et al. 2013]. In vivo, the gm-CSF generates adherent mouse macrophages capable of

differentiating into osteoclasts. However, m-CSF could suppress gm-CSF induced RANKL osteoclastogenic differentiation.

The transforming growth factor-β (TGF-β) has been found to stimulate osteoclastogenesis of gm-CSF macrophages but potently suppressed m-CSF driven osteoclastogenic differentiation independent of endogenous interferon α/β production even with upregulated RANKL [Lari et al. 2007]. Macrophages can dynamically polarize between inflammatory (M1) and pro-healing (M2a, M2b, M2c, M2d) phenotypes in adaptations to changes of local and global cytokine microenvironments [Davis et al. 2013].

Human gm-CSF and m-CSF factors are involved in the phenotype polarization towards inflammatory and anti-inflammatory (pro-healing) macrophages, respectively [Stein et al. 1992]. The cytokine profiles of TNF and IL-23 are specific to inflammatory macrophage subtypes while the cytokine IL-10 is specific for anti-inflammatory macrophages [Mantovani et al. 2004]. One of the greatest challenges in conducting research with macrophages in vitro is that the markers defining inflammatory and pro-healing polarization are different between mouse and human macrophages [Martinez et al. 2013]. There are no human homologs of the mouse pro-healing markers Ym1 and Fizz1 including arginase-1 that have been studied extensively [Murry et al. 2011]. Recently, the multifunctional enzyme transglutaminase-2 (TGM2) has been discovered as a conserved marker, providing a consistent activation for both human and mouse pro-healing macrophages including monocytes in circulating blood [Martinez et al. 2013].

During bone inflammation, macrophages can differentiate to be osteoclasts and contribute to bone resorption [Arboleya et al. 2013]. During bone formation, overexpressing Bmps and angiopoietin-1 (Ang1) in osteoblasts may control homeostasis of the hematopoietic tissues [Guerrouahen et al. 2011], including HSC self-renewals, survival and fates [Taichman et

al. 2005]. The matrix glycoprotein osteopontin (OPN) expressed by osteoblasts also supports the adhesion of HSCs to the osteoblastic niches and negatively regulates HSC proliferation, maintaining the HSC quiescent state [Nilsson et al. 2005]. The high concentration of calcium [Ca^{2+}] in the bone marrow endosteal regions may mediate HSC homing and lodging in the osteoblastic bone niches through calcium sensor receptors [Adams et al. 2006]. Possibly, Ang1 in mouse osteoblasts interacts with the tyrosine kinase (Tie-2) receptor of mouse HSC and activates OPG/β1-integrins induced N-cadherin, enhancing adhesion and contributing to the maintenance of the stem cell quiescence [Kinashi et al. 1994].

During bone healing, the macrophages that are involved in inflammation phase could trigger hBMSC driven endochondal ossification and induce intramembraneous ossification via RANKL/OPG before commencing bone remodeling [Jeganathan et al. 2014]. Biological functions of activated inflammatory macrophages are effectors in cellular immune responses. Alternatively, activated pro-healing macrophages are involved in immunosuppression and tissue repair [Ehninger et al. 2011]. After inflammation, macrophages need to restore their homeostatic population through proliferation of the peripheral blood monocytes and macrophage tissues [Davies et al. 2011]. The IL-4 from macrophage tissues, not blood monocytes, has been found to trigger macrophage proliferation after inflammation [Jenkins et al. 2011]. In bone niches, the interfacial bone marrow niches and macrophage tissues are the osteal tissues intercalating throughout human and mouse bone lining tissues [Chang et al. 2008].

Angiogenesis is essential in bone fracture healing and survivals for restoring and regenerating blood flow to the fracture site and the newborn bone formation. The most potent regulator of angiogenesis is the vascular endothelial growth factor (VEGF) also known as a

vascular permeability factor in organ development, wound healing, and tissue regeneration [Folkman et al. 1987]. The delicate interplay of osteoblastogenesis and blood vessel development occurs during embryogenesis and bone healing [Ehninger et al. 2011]. After the inflammatory phase, the pro-healing macrophages can promote VEGF to hBMSC driven osteoblastogenesis [Wu et al. 2010]. However, increased VEGF levels have been correlated with rheumatic arthritis and causing the development of malignant phenotypes like cancer, lymphoma, and leukemia [Ehninger et al. 2011]. Excessive levels of VEGF in acute promyelocytic leukemia and plasma endostatin caused severe peril to survival [Zelzer et al. 2004].

In the pathogenesis of bone destruction associated with rheumatoid arthritis, the synovium is an active site interplaying between immune and bone cells [Baron et al. 2013]. The interaction between T cells and osteoclasts is critical in osteoimmunology [Takayanagi et al. 2009]. The interleukin-17-producing T-helper cells (T_H17) induce the expression of receptor activator of RANKL in synovial cells, which, together with inflammatory cytokines, stimulates the differentiation and activation of bone-resorbing osteoclasts.

1.1.4 Cellular and Nuclear Structures

Cells contain genetic codes, cytokines, chemokines, proteins and information that can transfer to adjacent cells, daughter cells and reproductive cells. Cell structures contain organelles, cell membranes (made of lipid bilayers), cytoplasms, and nucleus (**Figure 1.3**). At the outermost cell membrane, hBMSCs have the adherent junction (n-cadherins) and cilia. At the cell basement membrane, there are several molecules, cytokines and components such as

focal adhesion kinase, vinculin, talin and tubulin [Humphries et al. 2007]. In the cytoplasm, organelles, cytoskeletons and mictubules are located [Janmey et al. 1998]. The hBMSC has double nuclear membranes; the outer nuclear envelope and the inner nuclear membrane [Khatau et al. 2012].

1.1.4.1 Adherent Junction – Cytoskeleton Interface

The HSCs have been found to directly bind to osteoblasts via adhesion molecules at adherent junctions (N-cadherin) [Calvi et al. 2003]. At bone surfaces, osteoblasts (named spindle-shaped N-cadherin positive+CD45 osteoblastic cells, SNOB or OB^{+}) expressing a high level of N-Cadherin could function as HSC progenitors [Zhang et al. 2003]. The CD45 is known as hematopoietic stem cells antigen. Though, the majority of HSC progenitors attaches to N-$Cadherin^{+}$ positive osteoblastic cells in the endosteum. Repressed c-Myc causing by TGF-β during retardant proliferation could maintain the HSC quiescent states if N-cadherin was upregulated [Yin et al. 2006]. However, the N-cadherin OBs^{+} might not be the only factor controlling HSC quiescent states in bone-marrow-HSC niches [Kiel et al. 2009]. Recently, cell-cell interactions via n-cadherins have been extensively studied [Engl et al. 2014, Huveneers et al. 2013, Kiel et al. 2009, Li et al. 2010, Yonemura et al. 2011].

1.1.4.2 Cytoskeleton

Under cyclic stretch, cytoskeletons could form cytoskeletal bundles [Scott et al. 2008]. The mechanism could be that the focal adhesion kinase (FAK) could translocation from the cytosol to the cytoskeleton [Cohen et al. 2008]. Without actin cytoskeletons, mammalian cells could disintegrate during cell activities and mobility [Hotulainen et al. 2005]. The changes of

cytoskeletons could affect the relative modulus of osteoblasts (>20KPa) and of cardiomyocytes (>200-300KPa) [Du et al. 2011, Kuznetsova et al. 2007]. These data strongly supported that changes in cytoskeletons could affect the cellular mechanics.

During osteogenic differentiation of hBMSCs, the actin cytoskeletal organization was drastically changed correlatively with the cell morphological alterations (a drastic change of cytoskeleton during the stem cell changes phenotype to osteoblasts) [Born et al. 2009]. The actin cytoskeleton changed from thin bundles randomly across the cytoplasm to thick bundles at the outmost periphery in the osteoblastogenic cells [Rodriguez et al. 2004]. With the cytoskeletal disruption, the hMSCs differentiated osteoblasts showed a radical decrease in the cellular moduli (i.e. a decrease of the force-volume by atomic force microscope) [Yourek et al. 2007]. Their data supported that the cytoskeleton is mainly responsible for cellular mechanical properties. With blocking actin dynamics, the cytoskeletons were disassembled and could not rearrange, causing interruption of the ROCK cellular signaling [Peng et al. 2011]. These data supported that the actin dynamics control the cell signaling. The cytoskeletal rearrangement coupling with the overexpressing TGF-β1 could stimulate the cellular accumulation of collagen-I [Hubchak et al. 2003].

1.1.4.3 NuAnCE-LiNC

To bridge cytoskeletons with the nuclear basement filament (laminins, chromatins) [Folker et al. 2011, Rothballer et al. 2013], the NuAnCE-LiNC could anchor giant molecules to position the nuclear skeletons from the outer nuclear envelope to inside nucleus [Starr et al. 2009, Sun et al. 2006]. The NuAnCE-LiNC has been discovered [Lombardi et al. 2011] and commonly represented by the nucleoskeletal nesprins (or Synes, genes in human cells) and the complex molecules (Suns) [Lombardi et al. 2011]. The relation of nesprin2 found to maintain

the nuclear envelope architecture and composition of human dermal fibroblasts [Lüke et al. 2008]. The fluorescent images revealed strong connections of the cytoskeletal f-actinins (ACTns) with the spectrins (one type of nucleoskeletons that directly connect to nesprins) [Meng et al. 2011].

During dynamic nuclear motion, the nucleus could be deformed if the cytoskeletons were cross-linked and not aligned [Friedl et al. 2011]. The nuclear deformation during the nuclear translocation could be due to the giant structures of NuAnCe-LiNC, Kash and Tan complex [Crisp et al. 2008, Mellad et al. 2011, Luxton et al. 2011]. The interactions of cytoskeletons and the nuclear envelope have been found at nesprins [Taranum et al. 2012]. The connection of cytoskeletons and nesprins across the nuclear membrane could directly link to the Kash-Sun at the inner nuclear membrane [Starr et al. 2010]. The connections of Kash-Sun later have been referred to a part of the nucleoskeletons [Razafsky et al. 2009]. Interestingly, the movement of the cytoskeleton was synchronous with the shaking Kash-Sun [Starr et al. 2005, Zhou et al. 2010]. The data could suggest that the cytoskeleton physically connected with the nucleoskeletons from the nuclear membrane to inside the nucleus as a part of the signal transduction.

1.1.5 Mechanical Signals in Bone

1.1.5.1 Low Frequency Mechanical Signals

1.1.5.1.1 Human Exercise Studies

The skeletal system adapts to daily and external activities [Bouchard et al. 2011]. In general, human exercise tends to be a relatively low-frequency mechanical stimulus. The effectiveness depends on the number of sessions per week, intensity, duration and type of the

exercise protocol. During a relaxed walk, each single step could impose a load on the axial skeleton of 1x body weight [Marcus 1998]. Additionally, the loading magnitude could increase to 3x– 4x of the body weight from jogging and about 5x body weights from jumping hurdles [Bergmann et al. 2011]. The tennis players generally show one stronger arm (such as high bone density [Ermin et al. 2012] and increasing skeletal muscle strength [Sanchis-Moysi et al. 2012]). Swimmers showed a better bone quality and high bone turnover than non-swimmers [Gómez-Bruton et al. 2013]. These data supported that the human bone adapts to the external mechanical stimulation and the mechanical loading could regulate the bone mass and geometry [Layne et al. 1999]. Overall, the anabolic bone results depending on intensity, frequency, duration, and types of the exercise [Bailey et al. 2008].

1.1.5.1.2 In Vivo Animal Models

There are several exercise models developed for small animals such as swimming in the confined space, paddling the floating boat, running treadmill [Cassilhas et al. 2013]. Mice under treadmill training could increase the bone health and quality [Kemi et al. 2002], including the bone thickness [Kasper et al. 2013]. Swimming mice showed better bone density in the femur and tibia [Andolina et al. 2014]. Mouse performances could differ from the exercise models, and other intrinsic characteristics (such as the mouse strain) [Lerman et al 2002]. The effectiveness of the exercise models could depend on the mouse age [Yeh et al. 2001], exercise patterns (e.g. floating, diving), intensity [Carriero et al. 2014, Kemmler et al. 2014] and duration [Isaksson et al. 2009] of the exercise. For example, with regular prolong treadmill running, mice could run with a greater speed while increasing bone mass density [Lapvetelainen et al. 1995].

Therefore, complications of designing experiments for animal models can come from not only the exercise model and its effectiveness but also the animal intrinsic characteristics.

1.1.5.1.3 In Vitro Models

In vitro, the mechanical signals have been modified as the device-based stimulation depending on researchers' interests. The stretching devices (like PDVF templates) with 1-10Hz have been used in bone studies [Tabatabaei et al. 2014]. The varieties of forces can derive from sources of mechanical signal generations such as the laser tweezers [Titushkin et al. 2006], atomic force microscope [Charras et al. 2002], and stretching template [Ahmed et al. 2010, Hasegawa et al. 1985].

During laser tweezers, the human MSC cell membrane showed an increase in their mechanical properties due to the extracellular matrix and adhesion integrin responding to the dragging force [Neve et al. 2010, Titushkin et al. 2006]. During osteogenic differentiation, MSCs under the mechanical stimulation showed an increase in the cell adhesion [Wang et al. 2013] and a stronger ECM-interaction [Guilak et al. 2009] with a better differentiation. In confined spaces, stretching MSCs with a surface modification of the stretching template showed an increase in the ECM-adhesion and a better osteogenic differentiation [Higuera et al. 2012]. These data showed that cells respond to the external mechanical stimulation.

1.1.5.2 High Frequency Mechanical Signals

1.1.5.2.1 Human Studies

Studies of low-magnitude high-frequency or so called low intensity vibration (LIV) could show promising ways to maintain bone health [Rubin et al. 2014]. The dynamic physical activities regulating the musculoskeletal system can be used as the vibration therapy for patients with limited movements [Thompson et al. 2014]. The clinical study in facial bone and jawbone found that the low frequency vibration prevented the bone relapse after the orthodontic movement [Yadav et al. 2015]. Several clinical studies found that the 15-minute vibration could increase the bone density in postmenopausal women [Slatkovska et al. 2011].

The study of whole body vibration of healthy males found that the transmitting peak acceleration was the highest at the lowest frequency (10Hz) [Friesenbichler et al. 2014]. Additionally, the transmission of vibration at different locations in the vertebral column was different from the input frequency during the whole body vibration [Morgado-Ramirez et al 2013]. These data suggested that different areas of the bone (e.g periosteal- or endosteal-osteoids in calcified long bones or short bones, etc.) could perceive the different signals from the input signal. Therefore, the frequency characteristics of the input signals may be different from the actual physical activities.

1.1.5.2.2 In Vivo Animal Models

With high frequency vibration [Judex et al. 2010], the bone density of tibia with vibrated mice found to be denser than the non-vibrated mice. The acceleration magnitude, vibration duration, and the number of bouts can modulate the bone sensitivity to the LIV [Judex

et al. 2015]. The short duration of the LIV in female mice showed an increase in trabecular and cortical bone formation in growing skeleton [Xie et al. 2006.]. The studies of 6 month-old rodents under the whole body vibration showed that the increasing trabecular thickness with the 7-day resting was more effective than the daily vibration [Ma 2012]. The vibration of the hind limbs of rodents found to decrease the weight gain and increase the bone density [Yan et al. 2010]. Additionally, studies showed that the LIV could be anabolic not only to bone but also to the bone marrow. In rodents, the LIV could improve the bone marrow quality and healing ability with less osteoclastogenesis and bone resorption [Bramlett et al. 2014]. These studies have shown that the LIV can improve bone quality in the animal model.

1.1.5.2.3 In Vitro Models

The low intensity vibration devices can be different from the function generator to the vibration direction, and the signal combination. The combination of the frequency and acceleration could generate the fluid shear stress. The separation of the fluid shear stress from the acceleration showed that the peak acceleration at 1g during horizontal oscillation at the frequency of 30Hz could provide the highest fluid shear stress at 0.94Pa [Uzer et al. 2012].

In stress studies using the oscillating vibration, pre-osteoblasts (MC3T3-E1) were vibrated at the frequency of 5-100Hz under the specific controlled stress [Bacabac et al. 2006]. To control the stress, the maximal acceleration was steady at the specific velocity along the x-axis. This study showed that the highest stress (at 5Hz) could damage cells while the highest frequency (100Hz) could promote the cell health. By shaking up and down with steady

acceleration amplitude at 0.3g, the osteocytes improved calcification at a higher frequency [Lau et al. 2010]. These data have shown that the effectiveness of the vibration depends on not only the type of vibrations (e.g. shaking up-down, oscillating side-to-side) but also the frequency, acceleration, velocity, and duration, including the oftenness of the vibration. Additionally, the performance of cells could be different depending on the cell types, morphology [Bacabac et al. 2008], and cell sources, including the technique used to monitor genes and proteins, and the culture in vitro techniques.

In our previous studies, we developed a device connecting a voice coil linear actuator (NCM15-15-032-2LB, H2W Technologies, Inc.) to a function generator (DS335, Stanford Research Systems) and a frictionless base (NK2-110B, Schneeberger) in the horizontal direction (**Figure 1.4**). The frequency and acceleration of the device can be controlled and the combination of them can be adjusted. The vertical vibration device connected the sound amplifier to the vibration base vertically with 4 coils at the base to maintain the amplitude of the base moving up and down without bouncing (**Figure 1.5**). Our studies have been consistent with the selection of the signal combination. We selected the signal combination based on the fluid shear stress that was created at the bottom of the culture plate by the frequency and acceleration. For example, the frequency of 30Hz and the acceleration of 1g can provide the highest fluid shear stress at 0.94Pa.

1.1.5.3 Mechanical Signal Transduction

1.1.5.3.1 Low Frequency Mechanical Signals

Bone cells, animals, and humans are sensitive and adaptive to the mechanical stimulation. Human bone adapts to exercise and daily activities, which could identify to be low frequency (less than 10Hz), and high acceleration (1x-5x of the human weight) [Marcus 1998]. With applying the fluid flow at the cell surface shear of 1 Pa with 1 Hz, the MC3T3-E1 and MLOY4 found to have an increasing calcification [Malone et al. 2007]. The increasing calcification could be because of the upregulated OPG and PGE2.

In the human exercise, elite athletes and regular exercise non-athletes have shown an increase in mitochondrial oxidative phosphorylation that the body uses to produce the energy ATP [Niemi et al. 2005]. Additionally, the cytoskeleton (ACTn1) in skeletal muscles of these groups was upregulated higher than the sedative groups [Berman et al. 2010]. The upregulated ACTn1 believed to provide the skeletal muscle an ability to produce force at a high velocity [Eynon et al. 2013]. These data could suggest that the muscle metabolism and strength could improve from the regular exercise.

1.1.5.3.2 High Frequency Mechanical Signals

Low intensity vibration (LIV) may represent the mechanical signal combination of oscillation, stretching, and compression (i.e. stress and strain). Stretching may produce tensile forces to cells [Delaine-Smith et al. 2012]. Combinations of the frequency and acceleration magnitude can generate the fluid shear stress to the cells at the bottom of the culture plate [Uzer et al. 2012]. For example, the combination of 30Hz-1g generated the highest fluid shear stress (0.94Pa) while the 100Hz-0.15g created the lowest fluid shear (0.04Pa).

Systematic mechanoresponsive bone cells were considered to be osteocytes, osteoblasts, osteoclasts, osteoprogenitor cells, and MSCs [Thompson et al. 2012]. The

mechanosensors have been thought to primarily involve integrins, membranes, focal adhesion, ion channels, and cilia. The β-catenin, focal adhesion kinase, and MAPK were related to the calcium signaling [Thia et al. 2013]. Often time the cell-signaling pathway like Wnt/Bmp is considered to be a part of the mechanotransduction [Robling et al. 2009]. The Wnt/Bmp signaling including β-catenin have been extensively connected to the mechanotransduction related cell mechanisms and functions [Baron et al. 2013]. The integrins and protein related cytokine (e.g. FAK, ECM, ITG) have been extensively linked to the mechanotransduction pathway of LIV [Thompson et al. 2012]. For example, the signaling through cytokines and chemokines via FAK/mTOR and Akt of MSCs showed that the cytoskeleton linked with a nucleus [Uzer et al. 2015]. The TGF-β-induced ECM was thought to regulate cell shape and physical interactions [Guilak et al. 2009, Kiseleva et al. 2005].

Osteocytes in the lacunar canaliculi (voids and channels that fill with viscous bone fluid) could sense the interstitial fluid in the bone matrix. The primary cilia of osteocytes have been found to respond to the fluid shear stress [Hoey et al. 2011] and transducing the mechanical strain [Qin et al. 2014]. According to these studies, the primary cilia and osteocytes have been thought to be a mechanosensor in the bone [Chen et al. 2013], responsible for the fluid flow [Nguyen et al. 2013]. The primary cilia are organelles that extend from the cell surface of nearly every mammalian cell (sometimes cilia can be explained like a hair on the skin). In bone, the primary cilia could recruit osteocytes to promote osteogenic differentiation of the mesenchymal stem cell [Hoey et al. 2011]. Additionally, the primary cilia were responsible for the fluid shear stress mediating the calcium accumulation in osteoblasts and osteocytes [Delaine-Smith et al. 2014]. The fluid flow has been believed to be the mechanosensing signals that the bone cell could sense and transduction [Vaughan et al. 2014]. The hydrodynamic fluid load of

<10 pN on osteocytes could generate Ca^{2+} velocity of 5.6 μm/s. And, the αVβ3 integrin at the attachment site were believed to be a transducer [Thia et al. 2013]. The upregulated Cox2 could cause the upregulated OPG while the fluid flow induced the osteocyte-driven bone calcification [Rommel et al. 2007]. In stress study, the highest nitric oxide (NO, a stress response) and prostaglandinE2 (PGE2, one of the inflammatory responses induced bone resorption) was at the frequency of 5Hz and plateau after 1 hour [Bacabac et al. 2006]. The Cox2 (an anti-inflammatory cyclooxygenase-2 at the nucleus) was maximal at the least stress at 100Hz. Similarly, the osteocytes under 90Hz shaking had the highest Cox2 [Lau et al. 2010]. Without vibration, the PGE2 recently found to stimulate the osteoblastic bone formation at the periosteum, but activated the osteoclastic bone resorption at the endosteum connecting to the bone marrow [Nefussi et al. 1985].

In human stem cells and osteoblasts, the hAMSCs with the cilia depletion are still sensitive to the external mechanical environments [Ibanez-Tallon et al. 2003]. Under the tensile load of 3% strain, MSCs showed an increasing osteogenic differentiation and upregulated collagen type I (Col1a1) [Chen et al. 2008]. The chondrogenesis of MSCs under compression showed an upregulated ALP activity and increasing bone transcription factor Runx2/cbfa1. The hAMSCs under the LIV at 30Hz showed an increase in the osteogenic differentiation [Pre et al. 2013]. The mechanical coupling between cytoskeleton and nucleus could transduce the LIV signals via the focal adhesion (FAK) and Akt signaling [Uzer et al. 2015]. These data supported that the cilia and osteocytes are not the only mechanosensor in bone. The calcium signaling and MAPK could mediate the fluid-flow induced MSC-proliferation [Riddle et al. 2006] and the fluid shear stress was thought to be a bone cell mechanosensing signal [Riddle et al. 2009]. The gap junction communication of osteocytes and osteoblasts was somewhat modulated by the fluid

shear stress [User et al. 2013]. However, the hAMSCs were sensitive to the oscillation, but not the fluid flow [Uzer et al. 2014]. Therefore, the fluid flow is not the only mechanosensing signal that cells can sense.

The specific structures of bone cells in nature can influence cells responding to external mechanical stimulation. With microgravity, disruption of the actin cytoskeleton abolishes the response to stress [Tamma et al. 2009]. Their data suggested that the cytoskeleton was involved in cellular mechanotransduction. The interpretation to the microgravity catabolic to the skeleton of astronauts could be that disuse under weightlessness conditions caused disassembling cytoskeletal elements. The abilities of adherent junctions (e.g. n-cadherin) to perceive and transduce mechanical signals have been related to cell functions and behaviors. During in vitro stretching, MSC cells could be pulled and formed the mature junctions parallel to the actin bundles [Huveneers et al. 2013]. The mature adherent junction could form a direct contact with the cytoskeleton, increasing the mature junction-cytoskeleton interfaces [Yonemura et al. 2011]. Cytoskeletons related adherent junctions have been exclusively studied [Malone et al. 2007]. The RhoA/Rock signaling was thought to responsible for cytoskeletal remodeling [Shi et al. 2012]. The vinculin was believed to physically connect the adherent junctions to the cytoskeletons [Bays et al. 2005].

1.2 Hypotheses and Specific Aims

Bone cells including bone marrow MSCs and adipose derived MSCs of animals and human are sensitive to low intensity vibration. However, the mechanotransduction of the LIV in these cells has been unclear. Understanding the underlying mechanotransduction of the LIV is important to bone and could lead to developing non-pharmacological approaches towards personalized precision medicine. To find clues regarding the mechanotransduction pathway, we tested our hypotheses using horizontal LIV (hLIV) or vertical LIV (vLIV) at 30Hz or 100Hz with accelerations of 0.15g or 1g.

1.2.1 Hypothesis 1: Human bone marrow mesenchymal stem cells can sense LIV direction.

Specific Aim 1: To investigate hBMSC proliferation and osteogenic differentiation in response to hLIV and vLIV

Rationale: LIV generates fluid shear stress in horizontal vibration that are much greater than in the vertical direction. If vibration in different directions could modulate different cellular behaviors and responses, monitoring these different responses could potentially provide links to a relevant mechanotransduction pathway.

Hypothesis 1.1: Proliferation of hBMSCS can be modulated by hLIV and vLIV

Specific Aim 1.1: To observe cell proliferation (using a standard MTS assay) of hBMSCs responding to the hLIV versus vLIV.

Hypothesis 1.2: LIV direction (i.e., hLIV vs vLIV) can modulate the osteogenic differentiation of hBMSCs.

Specific Aim 1.2: To determine the osteogenic differentiation of hBMSCs responding to hLIV versus vLIV at (i) the early stage on Day7 by the alkaline phosphatase activity (ALP), and (ii) the late-stage differentiation on Day14 with an alizarin red assay reflecting levels of calcification.

Hypothesis 1.3: Differences in gene expression of hMSCs induced by LIV can identify the potential mechanotransduction pathway.

Specific Aim 1.3: To monitor gene expression by the real-time PCR of hBMSCs in responses to hLIV and vLIV at specific time points.

To identify mechanotransduction pathway based on cellular and nuclear physical structures using the enrichment and cluster analysis.

1.2.2 Hypothesis 2: LIV can change the cytoskeleton and nesprin2 in the mechanotransduction pathway.

Specific Aim 2: To investigate changes in the cytoskeletal and nuclear structures

Rationale: If physical structures of the cell and nucleus shake with LIV, the interaction of these structures under LIV should link to the mechanotransduction pathway. Cytoskeletons link the outermost adherent junctions and the inner most nucleus. Monitoring cytoskeleton during LIV may provide clues of the underlying pathway.

Hypothesis 2.1: Cytoskeletons can link adherent junction and nucleus during LIV.

Specific Aim 2.1: To observe the cytoskeleton and nuclear nesprin using the two-photon confocal microscopy and antibody fluorescent staining.

Hypothesis 2.2: Changes in single cell mechanical properties can indicate changes in the cytoskeleton.

Specific Aim 2.2: To monitor the mechanical modulus of the single cell using atomic force microscopy (via relations of the force-displacement).

Hypothesis 2.3: Cytoskeletal gene knockdown will confirm the mechanotransduction of cytoskeleton through nesprins.

Specific Aim 2.3: To knock down the cytoskeletal gene (using RNA Clf-1 interference to deplete the ACTn1) and observe the gene expression (using the real-time PCR) of ACTn1 and nesprins (Syne2) so to confirm the cytoskeleton connecting nesprin2 during LIV.

1.2.3 Hypothesis 3: LIV induced cytoskeletal orientation can control the stem cell differentiation fate by supporting osteogenic but suppressing adipogenic differentiation.

Specific Aim 3: To investigate osteogenic and adipogenic differentiation of hBMSCs and hAMSCs after LIV with monitoring the cytoskeletal orientation.

Rationale: LIV has been known to anabolic to osteogenic differentiation. But the mechanism of how LIV can be anabolic has been unclear. If the cytoskeletal orientation increased after LIV as well as the osteogenic differentiation, monitoring the cytoskeletal orientation during the osteogenic differentiation under LIV could provide the mechanism of LIV in cellular and molecular functions.

Hypothesis 3.1: LIV induced the cytoskeletal orientation can increase the osteogenic differentiation of hBMSCs and hAMSCs.

Specific Aim 3.1: To determine calcification (using a standard alizarin red assay).

To observe the cytoskeletal orientation after the osteogenic differentiation of hBMSCs and hAMSCs by flow cytometry.

Hypothesis 3.2: LIV can suppress the adipogenic differentiation of hBMSCs and hAMSCs

Specific Aim 3.2: To determine lipoprotein (using the oil red assay).

To observe the cytoskeletal orientation after the adipogenic differentiation of hBMSCs and hAMSCs by flow cytometry.

1.2.4 Hypothesis 4: LIV can modulate the macrophage proliferation and polarization.

Specific Aim 4: To investigate proliferation and polarization of macrophages

Rationale: If the hBMSC proliferation and differentiation can be modulated by LIV, the macrophages should be able to sense the mechanical stimulation. If the LIV is anabolic to macrophages, the LIV could switch the phenotype toward the pro-healing macrophage. Montoring the pro-healing markers and gene expression could provide information of LIV and macrophages.

Hypothesis 4.1: LIV can increase macrophage proliferation.

Specific Aim 4.1: To monitor proliferation marker m-CSF after LIV.

To calculate the ratio of m-CSF : gm-CSF as an anabolic factor of LIV

Hypothesis 4.2: LIV can promote the pro-healing phenotype by upregulating IL-10.

Specific Aim 4.2: To monitor the IL-10 using flow cytometry.

Hypothesis 4.3: LIV can promote the pro-healing macrophages by upregulating VEGF

Specific Aim 4.3: To monitor gene expression of VEGF and TGF-β using the real-time PCR.

References

Adams GB, Chabner KT, Alley IR, Olson DP, Szczepiorkowski ZM, Poznansky MC, Kos CH, Pollak MR, Brown EM, Scadden DT. '*Stem cell engraftment at the endosteal niche is specified by the calcium-sensing receptor*.' Nature. **2006**, 439 (7076): 599–603.

Abdelmagid SM, Barbe MF, Safadi FF. '*Role of inflammation in the aging bones*.' Life Sci. **2015**; 123: 25-34. doi: 10.1016/j.lfs.2014.11.011.henrik

Ahmed WW, Kural MH, Saif TA '*A novel platform for in situ investigation of cells and tissues under mechanical strain*.' Acta Biomater. **2010**; 6 (8): 2979-2990. doi: 10.1016/j.actbio.2010.02.035.

Allen MR, Hock JM, Burr DB. '*Periosteum: biology, regulation, and response to osteoporosis therapies*.' Bone **2004**, 35: 1003–1012.

Andolina D, Maran D, Viscomi MT, Puglisi-Allegra S. '*Strain-dependent variations in stress coping behavior are mediated by a 5-HT/GABA interaction within the prefrontal corticolimbic system*.' Int J Neuropsychopharmacol. **2014**, 18 (3). doi: 10.1093/ijnp/pyu074

Bacabac RG, Smit TH, Van Loon JJWA, Doulabi BZ, Helder M, Klein-Nulend J. 'Bone cell responses to high-frequency vibration stress: does the nucleus oscillate within the cytoplasm?' FASEB. **2006**, 20: 858-864. doi: 10.1096/fj.05–4966.com

Bacabac RG, Mizuno D, Schmidt CF, MacKintosh FC, Van Loon JJ, Klein-Nulend J, Smit TH. '*Round versus flat: bone cell morphology, elasticity, and mechanosensing*.' J Biomech. **2008**; 41(7): 1590-1598. doi: 10.1016/j.jbiomech.2008.01.031.

Bailey CA, Brooke-Wavell K. '*Exercise for optimising peak bone mass in women.*' Proc Nutr Soc. **2008**, 67 (1): 9-18. doi: 10.1017/S0029665108005971.

Baron R, Kneissel M. '*Wnt signaling in bone homeostasis and disease: from human mutations to treatments'. Nature Medicine*.' **2013**, 19: 179–192. doi:10.1038/nm.3074.

Bays JL, Peng X, Tolbert CE, Guilluy C, Angell AE, Pan Y, Superfine R, Burridge K, DeMali KA. '*Vinculin phosphorylation differentially regulates mechanotransduction at cell–cell and cell–matrix adhesions*' JCB **2005**, 205 (2): 251-263.

Benjamin M, Toumi H, Ralphs JR, Bydder G, Best TM, Milz S. '*Where tendons and ligaments meet bone: attachment sites ('entheses') in relation to exercise and/or mechanical load*.' J Anat. **2006**; 208 (4): 471–490. doi: 10.1111/j.1469-7580.2006.00540.x.

Bergmann P, Body JJ, Boonen S, et al. '*Loading and Skeletal Development and Maintenance.*' J Osteoporosis. **2011**; 786752. doi:10.4061/2011/786752.

Berman Y, North KN. '*A gene for speed: the emerging role of alpha-actinin-3 in muscle metabolism*.' Physiology. **2010**, 25 (4): 250-259. doi: 10.1152/physiol.00008.2010.

Bershad AK, Fuentes MA, Krakauer DC. '*Developmental autonomy and somatic niche construction promotes robust cell fate decisions.*' J Theor Biol. **2008**; 254 (2): 408-416. doi: 10.1016/j.jtbi.2008.05.018. Epub 2008 May 24.

Birmingham E, Niebur GL, McHugh PE, Shaw G, Barry FP, McNamara LM. '*Osteogenic differentiation of mesenchymal stem cells is regulated by osteocyte and osteoblast cells in a simplified bone niche*.' Eur Cell Mater. **2012**; 23: 13-27.

Born AK, Rottmar M, Lischer S, Pleskova M, Bruinink A, Maniura-Weber K. '*Correlating cell architecture with osteogenesis: the first steps towards live single cell monitoring*.' European Cells Mat. **2009**, 18: 49-62.

Boyce BF, Yoa Z, Xing L. '*Osteoclasts have multiple roles in bone in addition to bone resorption*.' Crit Rev Eukaryot Gene Expr. **2009**,19 (3): 171-180.

Bouchard C, Rankinen T, Timmons JA. '*Genomics and Genetics in the Biology of Adaptation to Exercise*.' Compr Physiol. **2011**, 1 (3): 1603–1648. doi:10.1002/cphy.c100059.

Bramlett HM, Dietrich WD, Marcillo A, Mawhinney LJ, Furones-Alonso O, Bregy A, Peng Y, Wu Y, Pan J, Wang J, Guo XE, Bauman WA, Cardozo C, Qin W. '*Effects of low intensity vibration on bone and muscle in rats with spinal cord injury*.' Osteoporos Int. **2014**, 25 (9): 2209-2219. doi: 10.1007/s00198-014-2748-8.

Bryder D, Rossi DJ, Weissman IL. '*Hematopoietic Stem Cells The Paradigmatic Tissue-Specific Stem Cell*.' J Pathology. 2006, 169 (2): 339- 346. doi: 10.2353/ajpath.2006.060312

Calvi LM, Adams GB, Weibrecht KW, Weber JM, Olson DP, Knight MC, Martin RP, Schipani E, Divieti P, Bringhurst FR, Milner LA, Kronenberg HM, Scadden DT. '*Osteoblastic cells regulate the haematopoietic stem cell niche*.' Nature **2003**, 425: 841-846. doi:10.1038/nature02040.

Calvi LM, Link DC. '*Cellular complexity of the bone marrow hematopoietic stem cell niche*.' Calcified tissue inter. **2014**; 94 (1): 112-124. doi:10.1007/s00223-013-9805-8.

Cao X. '*Targeting osteoclast-osteoblast communication*.' Nature Medicine. **2011**, 17: 1344–1346. doi:10.1038/nm.2499

Carriero A, Bruse JL, Oldknow KJ, Millán JL, Farquharson C, Shefelbine SJ. '*Reference point indentation is not indicative of whole mouse bone measures of stress intensity fracture toughness*.' Bone. **2014**; 69: 174-179. doi: 10.1016/j.bone.2014.09.020.

Cassilhas RC, Reis IT, Venâncio DP, Fernandes J, Tufik S, de Mello MT. '*Animal model for progressive resistance exercise: a detailed description of model and its implications for basic research in exercise.'* Motriz, Rio Claro, **2013**, 19 (1): 178-184. jan./mar. 2013

Chacko JV, Zanacchi FC, Diaspro A. '*Probing Cytoskeletal Structures by Coupling Optical Superresolution and AFM Techniques for a Correlative Approach*.' Cytoskeleton. **2013**, 70: 729–740. doi: 10.1002/cm.21139

Chang MK, Raggatt L-J, Alexander KA, Kuliwaba JS, Fazzalari NL, Schroder K, Maylin ER, Ripoll VM, Hume DA, Pettit AR. '*Osteal Tissue Macrophages Are Intercalated throughout Human and Mouse Bone Lining Tissues and Regulate Osteoblast Function In Vitro and In Vivo*'. J Immunol. **2008**, 181: 1232-1244. doi: 10.4049/jimmunol.181.2.1232

Charbord P, Livne E, Gross G, Häupl T, Neves NM, Marie P, Bianco P, Jorgensen C. '*Human bone marrow mesenchymal stem cells: a systematic reappraisal via the genostem experience*.' Stem Cell Rev. **2011**, 7 (1): 32-42. doi: 10.1007/s12015-010-9125-6.

Charras GT, Horton MA. '*Single cell mechanotransduction and its modulation analyzed by atomic force microscope indentation*.' Biophys J. **2002**; 82 (6): 2970-2981.

Chen G, Deng C, Li YP. '*TGF-β and Bmp Signaling in Osteoblast Differentiation and Bone Formation*'. Int J Biol Sci. **2012**, 8 (2): 272-288. doi:10.7150/ijbs.2929.

Chen JC, Jacobs CR. '*Mechanically induced osteogenic lineage commitment of stem cells*.' Stem Cell Res Ther. **2013**, 4 (5): 107.

Chen YJ, Huang CH, Lee IC, Lee YT, Chen MH, Young TH. '*Effects of cyclic mechanical stretching on the mRNA expression of tendon/ligament-related and osteoblast-specific genes in human mesenchymal stem cells*.' Connect Tissue Res. **2008**, 49 (1): 7-14.

Cho JS, Kook SH, Robinson AR, Niedernhofer LJ, Lee BC. '*Cell autonomous and non-autonomous mechanisms drive hematopoietic stem/progenitor cell loss in the absence of DNA repair*.' Stem Cells. **2013**; 31 (3): 511–525. doi: 10.1002/stem.1261

Cho DI, Kim MR, Jeong HY, Jeong HC, Jeong MH, Yoon SH, Kim YS, Ahn Y. '*Mesenchymal stem cells reciprocally regulate the M1/M2 balance in mouse bone marrow-derived macrophages*.' Exper Mol Med. **2014**, 46: e70. doi:10.1038/emm.2013.135.

Choi SC, Kim SJ, Choi JH, Park CY, Shim WJ, Lim DS. '*Fibroblast Growth Factor-2 and -4 Promote the Proliferation of Bone Marrow Mesenchymal Stem Cells by the Activation of the PI3K-Akt and ERK1/2 Signaling Pathways*.' Stem Cells Development. **2008**, 17: 725–736. doi: 10.1089/scd.2007.0230

Cianferotti L, Brandi ML. '*Muscle-bone interactions: basic and clinical aspects*.' Endocrine. **2014**; 45 (2): 165-177. doi: 10.1007/s12020-013-0026-8.

Civitelli R. '*Cell-cell communication in the osteoblast/osteocyte lineage*.' Arch Biochem Biol. **2008**, 473: 188-192.

Clemens MW, Evans KK, Mardini S, Arnold PG. '*Introduction to Chest Wall Reconstruction: Anatomy and Physiology of the Chest and Indications for Chest Wall Reconstruction*.' Semin Plast Surg. **2011**; 25 (1): 5–15. doi: 10.1055/s-0031-1275166. PMCID: PMC3140236

Colnot C. '*Skeletal cell fate decisions within periosteum and bone marrow during bone regeneration*.' J Bone Miner Res. **2009**, 24: 274–282.

Colnot C, Zhang X, Knothe Tate ML. '*Current Insights on the Regenerative Potential of the Periosteum: Molecular, Cellular, and Endogenous Engineering Approaches*'. J Orthop Res. **2012**, 30: 1869–1878.

Compton JT, Lee FY. '*A review of osteocyte function and the emerging importance of sclerostin*.' J Bone Joint Surg Am. **2014**, 96 (19): 1659-1668. Doi: 10.2106/JBJS.M.01096.

Copp DH, Shim SS. '*The homeostatic function of bone as a mineral reservoir*.' Oral Surgery, Oral Medicine, Oral Pathology. **1963**, 16 (6): 738-744.

Coscoy S, Waharte F, Gautreau A, Martin M, Louvard D, Mangeat P, Arpin M, Amblard F. '*Molecular analysis of microscopic ezrin dynamics by two-photon FRAP*'. PANS. **2002**, 99 (20): 12813-12818. doi:10.1073/pnas.192084599.

Dallas SL, Bonewald LF. '*Dynamics of the Transition from Osteoblast to Osteocyte*.' Annals New York Acad Sci. **2010**;1192: 437-443. doi:10.1111/j.1749-6632.2009.05246.x.

Darling ED, Topel M, Zauscher S, Vail TP, Guilak F. '*Viscoelastic properties of human mesenchymally-derived stem cells and primary osteoblasts, chondrocytes, and adipocytes*.' J Biomech. **2008**, 41 (2): 454–464. doi:10.1016/j.jbiomech.2007.06.019.

Davies LC, Rosas M, Smith PJ, Fraser DJ, Jones SA, Taylor PR. '*A quantifiable proliferative burst of tissue macrophages restores homeostatic macrophage populations after acute inflammation*'. Eur. J. Immunol. **2011**, 41: 2155–2164. doi:10.1002/eji.201141817

Davis MJ. et al. '*Macrophage M1/M2 polarization dynamically adapts to change in cytokine microenvironments in Cryptococcus*.' neoformans Infection. mBio. **2013**, 4: 1-10.

Day TF, Guo X, Garrett-Beal L, et al. '*Wnt/beta-catenin signaling in mesenchymal progenitors controls osteoblast and chondrocyte differentiation during vertebrate skeletogenesis*.' Dev Cell. **2005**, 8: 739–750.

Delaine-Smith RM, Reilly GC. '*Mesenchymal stem cell responses to mechanical stimuli*.' Muscles, Ligaments Tendons J. **2012**, 2 (3): 169-180.

Delaine-Smith RM, Sittichokechaiwut A, Reilly GC. '*Primary cilia respond to fluid shear stress and mediate flow-induced calcium deposition in osteoblasts*'. FASEB J. **2014**, 28 (1): 430–439. doi: 10.1096/fj.13-231894. PMCID: PMC4012163.

Demiray L, Özcivici E. '*Bone marrow stem cells adept to low-magnitude vibrations by altering their cytoskeleton during quiescence and osteogenesis*.' Turk J Biol. **2014**, 38: 1-10. doi:10.3906/biy-1404-35

Devlin MJ. '*Why does starvation make bones fat?*' Am J Hum Biol. **2011**; 23 (5): 577–585. doi: 10.1002/ajhb.21202

DiGirolamo DJ, Kiel DP, Esser KA. '*Bone and skeletal muscle: neighbors with close ties*.' J Bone Miner Res. **2013**; 28 (7): 1509-1518. doi: 10.1002/jbmr.1969.

Du G, Ravetto A, Fang Q, den Toonder JMJ. '*Cell type can be distinguished by measuring their viscoelstic recovery times using a micro-fluidic device*.' Biomed Microdevices. **2011**, 13: 29-40.

Du X, Xie Y, Xian CJ, et al. '*Role of FGFs/FGFRs in skeletal development and bone regeneration*.' J Cell Physio. **2012**, 227 (12): 3731-43. doi: 10.1002/jcp.24083.

Efremov YM, Dzyubenko EV, Bagrov DV, Maksimov GV, Shram SI, Shaitan KV. '*Atomic Force Microscopy Study of the Arrangement and Mechanical Properties of Astrocytic Cytoskeleton in Growth Medium*.' Acta Nature. **2011**, 3 (3: 10): 93-99.

Ehninger A, Trumpp A. '*The bone marrow stem cell niche grows up: mesenchymal stem cells and macrophages move in*.' J. Exp. Med. **2011**, 208 (3): 421-428.

Ehsani S. '*Time in the cell: a plausible role for the plasma membrane*.' **2012**, 1-6.

Engl W, Arasi B, Yap LL, Thiery JP, Viasnoff V. '*Actin dynamics modulate mechanosensitive immobilization of cadherin at adherens junctions*.' NATURE CELL BIOL. **2014**, 16: 584-591. doi:10.1038/ncb297

Ermin K, Owens S, Ford MA, Bass M. '*Bone Mineral Density of Adolescent Female Tennis Players and Nontennis Players*.' J. Osteoporosis. 2012:423910. doi:10.1155/2012/423910.

Eynon N, Hanson ED, Lucia A, Houweling PJ, Garton F, North KN, Bishop DJ. '*Genes for elite power and sprint performance: ACTN1 leads the way*.' Spots Med. **2013**, 43 (9): 803-817. doi: 10.1007/s40279-013-0059-4.

Fletcher GF, Balady GJ, Amsterdam EA, Chaitman B, Eckel R, Fleg J, Froelicher VF, Leon AS, Piña IL, Rodney R, Simons-Morton DA, Williams MA, Bazzarre T. '*Exercise Standards for Testing and Training : A Statement for Healthcare Professionals From the American Heart Association*.' Circulation. **2001**, 104: 1694-1740. doi: 10.1161/hc3901.095960.

Franz-Odendaal TA, Hall BK, Witten PE. '*Buried alive: how osteoblasts become osteocytes*.' Dev Dyn. **2006**; 235 (1): 176-190.

Friesenbichler B, Lienhard K, Vienneau J, Nigg BM. '*Vibration transmission to lower extremity soft tissues during whole-bodyvibration*.' J Biomech. **2014** Sep 22;47(12):2858-62. doi: 10.1016/j.jbiomech.2014.07.028. Epub 2014 Aug 2.

Gómez-Bruton A, Gónzalez-Agüero A, Gómez-Cabello A, Casajús JA, Vicente-Rodríguez G. *Is Bone Tissue Really Affected by Swimming? A Systematic Review.* PLoS ONE. **2013**, 8 (8): e70119. doi:10.1371/journal.pone.0070119.

Grabowski P. '*Physiology of bone*.' Endocr Dev. **2009**; 16: 32-48. doi: 10.1159/000223687.

Groessner-Schreiber B, Krukowski M, Hertweck D, Osdoby P. '*Osteoclast formation is related to bone matrix age*.' Calcif Tissue Int. **1991**; 48 (5): 335-340.

Guilak F, Cohen DM, Estes BT, Gimble JM, Liedtke W, Chen CS. '*Control of stem cell fate by physical interactions with the extracellular matrix*.' Cell Stem Cell **2009**, 5: 17–26.

Guerrouahen BS, Al-Hijji I, Rafii Tabrizi A. '*Osteoblastic and Vascular Endothelial Niches, Their Control on Normal Hematopoietic Stem Cells, and Their Consequences on the Development of Leukemia*.' Stem Cells Inter. **2011** (ID 375857): pp 8. doi:10.4061/2011/375857.

Hasegawa S, Sato S, Saito S, Suzuki Y, Brunette DM. '*Mechanical stretching increases the number of cultured bone cells synthesizing DNA and alters their pattern of protein synthesis*.' Calcif Tissue Int. **1985**; 37 (4): 431-436.

Heino TJ, Hentunen TA. '*Differentiation of osteoblasts and osteocytes from mesenchymal stem cells*.' Curr Stem Cell Res Ther. **2008**; 3 (2): 131-145.

Helmchen F, Denk W. '*Deep tissue two-photon microscopy*'. Nature Methods. **2005**, 2(12): 932-940.

Henriksen K, Leeming DJ, Byrjalsen I, Nielsen RH, Sorensen MG, Dziegiel MH, Martin TJ, Christiansen C, Qvist P, Karsdal MA. '*Osteoclasts prefer aged bone*.' Osteoporos Int. **2007**; 18 (6): 751-759.

Higuera GA, van Boxtel A, van Blitterswijk CA, Moroni L. '*The physics of tissue formation with mesenchymal stem cells*.' Trends Biotechnol. **2012**, 30: 583–590.

Hipp JA, Jansujwicz A, Simmons CA, Snyder BD. '*Trabecular bone morphology from micro-magnetic resonance imaging*.' J Bone Miner Res. **1996**; 11 (2): 286-297. PMID: 8822353.

Hoey Da, Kelly DJ, Jacobs CR. '*A role for the primary cilium in paracrine signaling between mechanically stimulated osteocytes and mesenchymal stem cells*.' Biochem biophy res com. **2011**, 412:182. doi: 7.10.1016/j.bbrc.2011.07.072. PubMed: 21810408.

Hubchak SC, Runyan CE, Kreisberg JI, Schnaper HW. '*Cytoskeletal rearrangement and signal transduction in TGF-beta1-stimulated mesangial cell collagen accumulation*.' J Am Soc Nephrol. **2003**, 14 (8): 1969-1980.

Humphries JD, Wang P, Streuli C, Geiger B, Humphries MJ, Ballestrem C. '*Vinculin controls focal adhesion formation by direct interactions with talin and actin*.' J Cell Biol. **2007**, 179 (5): 1043–1057.

Huveneers S, de Rooij J. '*Mechanosensitive systems at the cadherin-F-actin interface*.' J Cell Sci. **2013**, 126: 1-11. doi: 10.1242/jcs.109447.

Ibanez-Tallon I, Nathaniel Heintz N, Omran H. '*To beat or not to beat: roles of cilia in development and disease*.' Hum. Mol. Genet. **2003**, 12 (suppl1): R27-R35. doi: 10.1093/hmg/ddg061.

Isaksson H, Tolvanen V, Finnilä MA, Iivarinen J, Turunen A, Silvast TS, Tuukkanen J, Seppänen K, Arokoski JP, Brama PA, Jurvelin JS, Helminen HJ. '*Long-term voluntary*

exercise of male mice induces more beneficial effects on cancellous and cortical bone than on the collagenous matrix.' Exp Gerontol. **2009**; 44 (11): 708-717. doi: 10.1016/j.exger.2009.08.005.

Jaguin M. et al. '*Polarization profiles of human M-CSF macrophages and comparison of M1-markers in classically activated macrophages from GM-CSF and M-CSF origin*.' Cell Immunol. **2013**, 281: 51-61.

Janmey PA. '*The cytoskeleton and cell signaling: component localization and mechanical coupling*.' Physiol Rev. **1998**, 78 (3): 763-781.

Jeganathan S, Fiorino C, Naik U, Sun Hs, Harrison RE. '*Modulation of Osteoclastogenesis with Macrophage M1- and M2-Inducing Stimuli*.' PLoS ONE. **2014**, 9 (8): e104498. doi:10.1371/journal.pone.0104498.

Jenkins SJ, Ruckerl D, Cook PC, Jones LH, Finkelman FD, van Rooijen N, MacDonald AS, Allen JE. '*Local Macrophage Proliferation, Rather than Recruitment from the Blood, Is a Signature of T_H2 Inflammation*'. Science **2011**: 332 (6035): 1284-1288. doi: 10.1126/science.1204351.

Judex J, Koh T, Xie L. '*Modulation of bone's sensitivity to low-intensity vibrations by acceleration magnitude, vibration duration and number of bouts*.' Osteoporos. Int. **2015**, 26: 1417-1428.

Judex S, Rubin CT. '*Is bone formation induced by high-frequency mechanical signals modulated by muscle activity?*' J Musculoskelet Neurinal Interact. **2010**, 10 (1): 3-11.

Kasper CE. '*Animal models of exercise and obesity*.' Annu Rev Nurs Res. **2013**, 31: 1-17. doi: 10.1891/0739-6686.31.1.

Kato Y, Windle JJ, Koop BA, Mundy GR, Bonewald LF. 'Establishment of an osteocyte-like cell line, MLO-Y4.' J Bone Miner Res. **1997**; 12 (12): 2014-2023.

Kemi OJ, Loennechen JP, Wisloff U, Ellingsen O. '*Intensity controlled treadmill running in mice: cardiac and skeletal muscle hypertrophy*.' J Appl Physiol. **2002**, 93: 1301–1309.

Kemmler W, Scharf M, Lell M, Petrasek C, von Stengel S. '*High versus Moderate Intensity Running Exercise to Impact Cardiometabolic Risk Factors: The Randomized Controlled RUSH-Study*.' BioMed Research Inter. **2014**: 843095. doi:10.1155/2014/843095.

Kennel KA, Drake MT. '*Adverse Effects of Bisphosphonates: Implications for Osteoporosis Management*.' Mayo Clin Proc. **2009**, 84 (7): 632–638. doi: 10.1016/S0025-6196(11)60752-0. PMCID: PMC2704135.

Kiel MJ, Acar M, Radice GL, Morrison SJ. '*Hematopoietic stem cells do not depend on n-cadherin to regulate their maintenance*.' Cell Stem: Cell. **2009**, 4 (2): 170–179.

Kinashi T, Springer TA, Nienhuis AW, Quesenberry PJ, Yoder. '*Adhesion molecules in hematopoietic cells*.' Blood Cells. **1994**, 20 (1): 25–44.

Khaw BA, daSilva J, Vural I, Narula J, Torchilin VP. '*Intracytoplasmic gene delivery for in vitro transfection with cytoskeleton-specific immunoliposomes*.' J Control Release. **2001**, 75 (1-2): 199-210.

Khatau SB, Kusuma S, Hanjaya-Putra D, Mali P, Cheng L, et al. '*The Differential Formation of the LINC-Mediated Perinuclear Actin Cap in Pluripotent and Somatic Cells*.' PLoS ONE **2012**, 7(5): e36689. doi:10.1371/journal.pone.0036689

Krishnan V, Dhurjati R, Vogler EA, Mastro AM. '*Osteogenesis in vitro: from pre-osteoblasts to osteocytes: a contribution from the Osteobiology Research Group, The Pennsylvania State University*.' In Vitro Cell Dev Biol Anim. **2010**; 46 (1): 28-35. doi: 10.1007/s11626-009-9238-x.

Kroeker SG, Ching RP. '*Coupling between the spinal cord and cervical vertebral column under tensile loading.*' J Biomech. **2013**; 46 (4): 773-779. doi: 10.1016/j.jbiomech.2012.11.012.

Kuznetsova TG, Starodubtseva MN, Yegorenkov NI, Chizhik SA, Zhdanov RI. '*Atomic force microscopy probing of cell elasticity.*' Micron. **2007**, 38: 824–833.

Lapvetelainen T, Nevalainen T, Parkkinen JJ, Arokoski JJP, Kiraly K, Hyttinen M, Halonen P, Helminen HJ. '*Lifelong moderate running training increases the incidence and severity of osteoarthritis in the knee joint of C57BL mice*.' Anat Rec. **1995**, 242: 159–165.

Lari R, Fleetwood AJ, Kitchener PD, Cook AD, Pavasovic D, Hertzog PJ, Hamilton JA. '*Macrophage lineage phenotypes and osteoclastogenesis—Complexity in the control by GM-CSF and TGF-β*.' Bone. **2007**, 40 (2): 323–336. doi:10.1016/j.bone.2006.09.003.

Lau E, Al-Dujaili S, Guenther A, Liu D, Wang L, You L. '*Effect of low-magnitude, high-frequency vibration on osteocytes in the regulation of osteoclasts*.' Bone. **2010**, 46 (6): 1508–1515. doi: 10.1016/j.bone.2010.02.031.

Layne JE, Nelson ME. '*The effects of progressive resistance training on bone density: a review*.' Med Sci Sports Exerc. **1999**; 31 (1): 25-30.

Lerman I, Harrison BC, Freeman K, Hewett TE, Allen DL, Robbins J, and Leinwand LA. '*Genetic variability in forced and voluntary endurance exercise performance in seven inbred mouse strains*.' J Appl Physiol. **2002**, 92: 2245–2555.

Leung RKM, Whittaker PA. '*RNA interference: From gene silencing to gene-specific therapeutics*'. Pharm Therapeutics. **2005**, 107 (2): 222-239.

Li H, Daculsi R, Grellier M, Bareille R, Bourget C, Amedee J. '*Role of neural-cadherin in early osteoblastic differentiation of human bone marrow stromal cells cocultured with human umbilical vein endothelial cells*.' Am J Physiol Cell Physiol. **2010**, 299: C422–C430. doi:10.1152/ajpcell.00562.2009.

Lin Z, Fateh A, Salem DM, Intini G. '*Periosteum: biology and applications in craniofacial bone regeneration*.' J Dent Res. **2014**, 93 (2): 109-16. doi: 10.1177/0022034513506445.

Locatelli V, Bianchi VE. '*Effect of GH/IGF-1 on Bone Metabolism and Osteoporsosis*.' Inter J Endocrin. **2014** (ID 235060): 25 pp.

Lombardi ML, Jaalouk DE, Shanahan CM, Burke B, Roux KJ, Lammerding J. '*The Interaction between Nesprins and Sun Proteins at the Nuclear Envelope Is Critical for Force Transmission between the Nucleus and Cytoskeleton*'. J Biol Chem. **2011**; 286 (30): 26743–26753 doi: 10.1074/jbc.M111.233700 PMCID: PMC3143636

Long F, Chung UI, Ohba S, et al. '*Ihh signaling is directly required for the osteoblast lineage in the endochondral skeleton*.' Development. **2004**, 131: 1309–1318.

Lowe CE, O'Rahilly S, Rochford JJ. '*Adipogenesis at a glance'*. J Cell Sci. **2011**, 124: 2681-2686 doi:10.1242/jcs.079699

Lowery JW, Pazin D, Intini G, et al. '*The role of BMP2 signaling in the skeleton*.' Crit Rev Eukaryot Gene Expr. **2011**, 21: 177–185.

Lüke Y, Zaim H, Karakesisoglou I, Jaeger VM, Sellin L, Lu W, Schneider M, Neumann S, Beijer A, Munck M, Padmakumar VC, Gloy J, Walz G, Noegel AA. '*Nesprin-2 Giant (NUANCE) maintains nuclear envelope architecture and composition in skin*.' J Cell Sci. **2008**, 121 (11): 1887-1898.

Lund FW, Lomholt MA, Solanko LM, Bittman R, Wüstner D. '*Two-photon time-lapse microscopy of BODIPY-cholesterol reveals anomalous sterol diffusion in chinese hamster ovary cells*.' BMC Biophys. **2012**, 5: 20. doi: 10.1186/2046-1682-5-20.

Ma R, Zhu D, Gong H, Gu G, Huang X, Gao Jz, Zhang X. '*High-frequency and low-magnitude whole body vibration with rest days is more effective in improving skeletal micro-morphology and biomechanical properties in ovariectomised rodents*.' Hip Int. **2012**, 22 (2): 218-226. doi: 10.5301/HIP.2012.9033.

Maes C, Carmeliet G, Schipani E. '*Hypoxia-driven pathways in bone development, regeneration and disease*'. Nature Reviews Rheumatology **2012**, 8: 358-366. doi:10.1038/nrrheum.2012.36

Makita N, Hizukuri Y, Yamashiro K, Murakawa M, Hayashi Y. '*IL-10 enhances the phenotype of M2 macrophages induced by IL-4 and confers the ability to increase eosinophil migration*'. Int. Immunol. **2014**. doi: 10.1093/intimm/dxu090

Małkiewicz A, Dziedzic M. '*Bone marrow reconversion – imaging of physiological changes in bone marrow*.' Pol. J. Radiol. **2012**, 77 (4): 45-50.

Malone AMD, Batra NN, Shivaram G, Kwon RY, You L, Kim CH, Rodriguez J, Jair K, Jacobs CR. '*The role of actin cytoskeleton in oscillatory fluid flow-induced signaling in MC3T3-E1 osteoblasts*'. Am J Physiol - Cell Physiol. **2007**, 292 (5): C1830-C1836. doi:10.1152/ajpcell.00352.2005.

Malone AM, Anderson CT, Tummala P, Kwon RY, Johnston TR, Stearns T, and Jacobs CR. '*Primary cilia mediate mechanosensing in bone cells by a calcium-independent mechanism.'* Proc Natl Acad Sci. **2007**, 104 (33): 13325-13330. pmid:17673554.

Manfrini M, Di Bona C, Canella A, Lucarelli E, Pellati A, Agostino AD, Barbanti-Brodano G, Tognon M. '*Mesenchymal stem cells from patients to assay bone graft substitutes*.' J Cell Physiol. **2012**. doi:10.1002/jcp.24276.

Mantovani A. et al. '*The chemokine system in diverse forms of macrophage activation and polarization*.' Trends Immunol. **2004**, 25: 677-686.

Marcus R. '*Exercise: Moving in the Right Direction*.' J Bone Min Res. **1998**, 13 (12): 1793-1796.

Marie PJ, Fromihue O. 'Osteogenic differentiation of human marrow-derived mesenchymal stem cells.' Regen Med. **2006**, 1 (4): 539-348.

Martin T, Gooi JH, Sims NA. '*Molecular mechanisms in coupling of bone formation to resorption*.' Crit Rev Eukaryot Gene Expr. **2009**; 19 (1): 73-88.

Martinez FO, et al. '*Genetic programs expressed in resting and IL-4 alternatively activated mouse and human macrophages: similarities and differences*.' Blood. **2013**, 121 (9): e57-e69.

Mattinzoli D, Messa P, Corbelli A, Ikehata M, Zennaro C, Armelloni S, Li M, Giardino L, Rastaldi MP. '*A novel model of in vitro osteocytogenesis induced by retinoic acid treatment*.' Eur Cell Mater. **2012**; 24: 403-425.

McBeath R, Pirone DM, Nelson CM, Bhadriraju K, Chen CS. '*Cell shape, cytoskeletal tension, and RhoA regulate stem cell lineage commitment*.' Dev Cell. **2004**, 6 (4): 483-495.

McDonald F. '*Ion channels in osteoblasts: a story of two intracellular organelles.*' Surgeon. **2004**; 2 (2): 63-69.

Meinke P, Mattioli E, Haque F, Antoku S, Columbaro M, Straatman KR, Worman HJ, Gundersen GG, Giovanna Lattanzi G, Wehnert M, Shackleton S. '*Muscular Dystrophy-Associated SUN1 and SUN2 Variants Disrupt Nuclear-Cytoskeletal Connections and*

Myonuclear Organization'. PLoS Genet. **2014**, 10 (9): e1004605. doi:10.1371/journal.pgen.1004605

Meng F, Sachs F. '*Visualizing dynamic cytoplasmic forces with a compliance-matched FRET sensor*.' J Cell Sci. **2011**, 124 (Pt. 2): 261-9. doi: 10.1242/jcs.071928. Epub 2010 Dec 20.

Meng W, Takeichi M. '*Adherens Junction: Molecular Architecture and Regulation*.' Cold Spring Harb Perspect Biol **2009**, 1: a002899

Moghadam-Kia S, Werth VP. '*Prevention and treatment of systemic glucocorticoid side effects*.' Int J Dermatol. **2010**, 49 (3): 239–248. doi: 10.1111/j.1365-4632.2009.04322.x.

Morgado-Ramirez DZ, Strike S, Lee Ry. 'Measurement of transmission of vibration through the human spine using skin-mounted inertial sensors.' Med Eng Phys. **2013**; 35 (5): 690-695. doi: 10.1016/j.medengphy.2012.12.013.

Morrison SJ, Scadden DT. '*The bone marrow niche for haematopoietic stem cells*.' Nature. **2014**, 505: 327–334. doi:10.1038/nature12984.

Mosser DM, Edwards JP. '*Exploring the full spectrum of macrophage activation*.' Nat Rev Immunol. **2008**, 8 (12): 958–969. doi:10.1038/nri2448.

Murry PJ, Wynn TA. '*Protective and pathogenic functions of macrophage subset*.' Nature Rev. Immunol. **2011**, 11: 723-737.

Muruganandan S, Roman AA, Sinal CJ. '*Adipocyte differentiation of bone marrow-derived mesenchymal stem cells: Cross talk with the osteoblastogenic program*.' Cell. Mol. Life Sci. **2009**, 66: 236 – 253. doi: 10.1007/s00018-008-8429-z

Nakahama K. '*Cellular communications in bone homeostasis and repair*.' Cell Mol Life Sci. 2010, 67(23): 4001-4009. doi: 10.1007/s00018-010-0479-3.

Nakamura M, Hiratai R, Yamashita K. '*Bone mineral as an electrical energy reservoir*.' J Biomed Mater Res A. **2012**; 100 (5): 1368-1374. doi: 10.1002/jbm.a.34076.

Nève N, Kohles SS, Winn SR, Tretheway DC. '*Manipulation of Suspended Single Cells by Microfluidics and Optical Tweezers*.' Cell Mol Bioeng. **2010**; 3 (3): 213-228.

Niemi AK, Majamaa K. '*Mitochondrial DNA and ACTN1 genotypes in Finnish elite endurance and sprint athletes*.' Eur J Hum Genet. **2005**, 13 (8): 965-969.

Nijweide PJ, van der Plas A, Olthof AA. '*Osteoblastic differentiation*.' Ciba Found Symp. **1988**; 136: 61-77.

Nilsson SK, Johnston HM, Whitty GA, Williams B, Webb RJ, Denhardt DT, Bertoncello I, Bendall LJ, Simmons PJ, Haylock DN. '*Osteopontin, a key component of the hematopoietic stem cell niche and regulator of primitive hematopoietic progenitor cells*.' Blood. **2005**, 106 (4): 1232–1239.

Nguyen AM, Jacobs CR. '*Emerging Role of Primary Cilia as Mechanosensors in Osteocytes*'. Bone. **2013**, 54 (2): 196–204. doi:10.1016/j.bone.2012.11.016.

Ozcivici E, Luu YK, Adler B, Qin YX, Rubin J, Judex S, Rubin CT. '*Mechanical signals as anabolic agents in bone'. Nat. Rev. Rheumatol*. **2010**; 6: 50–59. doi:10.1038/nrrheum.2009.239.

Palmer LC, Newcomb CJ, Kaltz SR, Spoerke ED, Stupp SI. '*Biomimetic Systems for Hydroxyapatite Mineralization Inspired By Bone and Enamel.*' Chem Rev. **2008**; 108 (11): 4754–4783. doi: 10.1021/cr8004422.

Papadimitriou E, Vasilaki E, Vorvis C, Iliopoulos D, Moustakas A, Kardassis D, Stournaras C. '*Differential regulation of the two RhoA-specific GEF isoforms Net1/Net1A by TGF-β and miR-24: role in epithelial-to-mesenchymal transition*.' Oncogene. **2012**, 31 (23): 2862-2875. doi: 10.1038/onc.2011.457. Epub 2011 Oct 10.

Pedersen JA, Swartz MA. '*Mechanobiology in the Third Dimension*.' Ann Biomed Eng. **2005**, 33 (11): 1469–1490. doi: 10.1007/s10439-005-8159-4

Peng GE, Wilson SR, Weiner OD. '*A pharmacological cocktail for arresting actin dynamics in living cells*.' Mol Biol Cell. **2011**, 3986-3994. doi/10.1091/mbc.E11-04-0379.

Prè D, Ceccarelli G, Visai L, Benedetti L, Imbriani M, Cusella De Angelis MG, Magenes G. '*High-Frequency Vibration Treatment of Human Bone Marrow Stromal Cells Increases*

Differentiation toward Bone Tissue.' Bone Marrow Res. 2013, 2013:803450. doi: 10.1155/2013/803450.

Qian AR, Gao X, Zhang W, Li J-B, Wang Y, Di SM, Hu LF, Shang P. '*Large Gradient High Magnetic Fields Affect Osteoblast Ultrastructure and Function by Disrupting Collagen I or Fibronectin/ab1 Integrin*'. PLoS ONE. **2013**, 8 (1): e51036. doi:10.1371/journal.pone.0051036.

Qin YX, Hu M. '*Mechanotransduction in musculoskeletal tissue regeneration: effects of fluid flow, loading, and cellular-molecular pathways*.' Biomed Res Int. **2014**: 863421. doi: 10.1155/2014/863421. Epub 2014 Aug 18.

Qiu S, Fyhrie DP, Palnitkar S, Rao DS. '*Histomorphometric assessment of Haversian canal and osteocyte lacunae in different-sized osteons in human rib.*' Anat Rec A Discov Mol Cell Evol Biol. **2003**; 272 (2): 520-525.

Rabey KN, Li Y, Norton JN, Reynolds RP, Schmitt D. '*Vibrating Frequency Thresholds in Mice and Rats: Implications for theEffects of Vibrations on Animal Health.'* Annals of Biomedical Engineering **2014** DOI: 10.1007/s10439-014-1226-y

Radisavljevic Z. '*AKT as Locus of Cancer Angiogenic Robustness and Fragility*.' J. Cell. Physiol. **2013**, 228: 21–24.

Razafsky D, Hodzic D. '*Bringing KASH under the SUN: the many faces of nucleo-cytoskeletal connections*.' JCB. **2009**, 186 (4): 461-472. doi: 10.1083/jcb.200906068

Ricci C, Cova M, Kang YS, Yang A, Rahmouni A, Scott WW Jr, Zerhouni EA. '*Normal age-related patterns of cellular and fatty bone marrow distribution in the axial skeleton: MR imaging study*.' Radiology. **1990**, 177 (1): 83-88.

Richtsmeier JT, Flaherty K. '*Hand in glove: brain and skull in development and dysmorphogenesis*.' Acta Neuropathol. 2013; 125 (4): 469–489. doi: 10.1007/s00401-013-1104-y. PMCID: PMC3652528

Riddle RC, Taylor AF, Genetos DC, Donahue HJ. '*MAP kinase and calcium signaling mediate fluid flow-induced human mesenchymal stem cell proliferation*.' Am. J. Physiol. Cell Physiol. **2006**, 290: C776–C784.

Riddle RC, Donahue HJ. '*From streaming-potentials to shear stress: 25 years of bone cell mechanotransduction*.' J. Orthop. Res. **2009**, 27: 143–149.

Robling AG, Turner CH. '*Mechanical Signaling for Bone Modeling and Remodeling*.' Crit Rev Eukaryot Gene Expr. **2009**, 19(4): 319–338.

Rodan GA. '*Bone homeostasis*.' Proc. Natl. Acad. Sci. **1998**, 95: 13361–13362.

Rodríguez JP, González M, Ríos S, Cambiazo V. '*Cytoskeletal organization of human mesenchymal stem cells (MSC) changes during their osteogenic differentiation*.' J Cell Biochem. **2004**, 93 (4): 721-731.

Rommel C, Camps M, Ji H. '*PI3K delta and PI3K gamma: partners in crime in inflammation in rheumatoid arthritis and beyond?*' Nat Rev Immunol. **2007**, 7: 191.

Rose RM, Martin RB, Orr RB, Radin EL. 'Architectural changes in the proximal femur following prosthetic insertion: preliminary observations of an animal model.' J Biomech. 1984; 17 (4): 241-249.

Rosen CJ, Ackert-Bicknell C, Juan Pablo Rodriguez JP, Pino AM. '*Marrow Fat and the Bone Microenvironment: Developmental, Functional, and Pathological Implications*.' Crit Rev Eukaryot Gene Expr. **2009**, 19 (2): 109–124.

Rubin CT. '*The Potential Benefits and Inherent Risks of Vibration as a Non-Drug Therapy for the Prevention and Treatment of Osteoporosis.'* Curr Osteoporos Rep. **2013**, 11 (1): 36-44.

Rubin CT, Seeherman H, Qin YX, Gross TS. '*The mechanical consequences of load bearing in the equine third metacarpal across speed and gait: the nonuniform distributions of normal strain, shear strain, and strain energy density*.' FASEB J. **2013**, 27 (5): 1887-1894. doi: 10.1096/fj.12-216804. Epub 2013 Jan 25.

Salmon P. '*Non-linear pattern formation in bone growth and architecture.*' Front Endocrinol. **2015**; 5: 239. doi: 10.3389/fendo.2014.00239.

Sambuceti G, Brignone M, Marini C, Massollo M, Fiz F, Morbelli S, Buschiazzo A, Campi C, Piva R, Massone AM, Piana M, Frassoni F. '*Estimating the whole bone-marrow asset in humans by a computational approach to integrated PET/CT imaging*.' Eur J Nucl Med Mol Imaging. **2012**; 39 (8): 1326-1338. doi: 10.1007/s00259-012-2141-9.

Sanchis-Moysi J, Idoate F, Serrano-Sanchez JA, Dorado C, Calbet JAL. '*Muscle Hypertrophy in Prepubescent Tennis Players: A Segmentation MRI Study*.' PLoS ONE. **2012**; 7 (3): e33622. doi:10.1371/journal.pone.0033622.

Scott MK, Akinduro O, Lo Celso C. '*In Vivo 4-Dimensional Tracking of Hematopoietic Stem and Progenitor Cells in Adult Mouse Calvarial Bone Marrow*.' J Vis Exp. **2014**, 91: e51683. doi:10.3791/51683.

Shi Y, Fu Y, Tong W, Geng Y, Lui PP, Tang T, Zhang X, Dai K. '*Uniaxial mechanical tension promoted osteogenic differentiation of rat tendon-derived stem cells (rTDSCs) via the Wnt5a-RhoA pathway*'. J Cell Biochem. **2012**, 113(10): 3133-3142. doi: 10.1002/jcb.24190.

Shiozawa Y, Taichman RS. '*Getting blood from bone: An emerging understanding of the role that osteoblasts play in regulating hematopoietic stem cells within their niche*.' Exper Hematology. **2012**, 40: 685–694.

Skerry TM. '*The response of bone to mechanical loading and disuse: fundamental principles and influences on osteoblast/osteocyte homeostasis*.' Arch Biochem Biophys. **2008**, 473:117–123.

Slatkovska L, Alibhai SM, Beyene J, Hu H, Demaras A, Cheung AM. '*Effect of 12 months of whole-body vibration therapy on bone density and structure in postmenopausal women: a randomized trial*.' Ann Intern Med. **2011**, 155 (10): 668-679, W205. doi: 10.7326/0003-4819-155-10-201111150-00005.

Sokolov I, Woodworth CD. '*Loss of elasticity of aging epithelial cells and its possible reversal*.' NSTI Nanotech **2005**: ISBN 0-9767985-0-6.

Starr DA, Fischer JA. '*KASH 'n Karry: the KASH domain family of cargo-specific cytoskeletal adaptor proteins*.' BioEssays. **2005**, 27: 1136–1146.

Starr DA, Fridolfsson HN. '*Interactions Between Nuclei and the Cytoskeleton Are Mediated by SUN-KASH Nuclear-Envelope Bridges*.' Annu Rev Cell Dev Biol. **2010**; 26: 421–444. doi: 10.1146/annurev-cellbio-100109-104037.

Stein GS, Lian JB, van Wijnen AJ, Stein JL, Montecino M, Javed A, Zaidi SK, Young DW, Choi JY, Pockwinse SP. '*Runx2 control of organization, assembly and activity of the regulatory machinery for skeletal gene expression*.' Oncogene. **2004**, 23: 4315–4329.

Stein M. et al. '*Interleukin 4 potently enhances murine macrophage mannose receptor activity: a marker of alternative immunologic macrophage activation*.' J.Exp. Med. **1992**, 176: 287-292.

Stricker J, Falzone T, Gardel ML. J Biomech. '*Mechanics of the F-actin cytoskeleton*.' **2010**, 43 (1): 9-14. doi:10.1016/j.jbiomech.2009.09.003. Epub 2009 Nov 13.

Sugiyama T, Nagasawa T. '*Bone Marrow Niches for Hematopoietic Stem Cells and Immune Cells*.' Inflamm Allergy Drug Targets. **2012**; 11 (3): 201-206. doi:10.2174/187152812800392689.

Swartz EE, Floyd RT, Cendoma M. '*Cervical Spine Functional Anatomy and the Biomechanics of Injury Due to Compressive Loading*.' J Athl Train. **2005**; 40 (3): 155–161. PMCID: PMC1250253.

Tabatabaei FS, Jazayeri M, Ghahari P, Haghighipour N. '*Effects of equiaxial strain on the differentiation of dental pulp stem cellswithout using biochemical reagents*.' Mol Cell Biomech. **2014**; 11 (3): 209-220.

Taichman RS. '*Blood and bone: two tissues whose fates are intertwined to create the hematopoietic stem-cell niche*.' Blood. **2005**, 105 (7): 2631–2639.

Takada I, Kouzmenko AP, Kato S. '*Molecular switching of osteoblastogenesis versus adipogenesis: implications for targeted therapies*.' Expert Opin Ther Targets. **2009**, 13 (5): 593-603. doi: 10.1517/14728220902915310.

Takayanagi, H. '*Osteoimmunology and the effects of the immune system on bone*'. Nat. Rev. Rheumatol. **2009**, 5: 667–676. doi:10.1038/nrrheum.2009.217

Tamma R, Colaianni G, Camerino C, di Benedetto A, Greco G, Strippoli M, Vergari R, Grano A, Mancini L, et al. '*Microgravity during spaceflight directly affects in vitro osteoclastogenesis and bone resorption*.' FASEB J. **2009**, 23: 2549–2554.

Tang Y, Wu X, Lei W, Pang L, Wan C, Shi Z, Zhao L, Nagy TR, Peng X, Hu J, Feng X, Van Hul W, Wan M, Cao X. '*TGF-beta1-induced migration of bone mesenchymal stem cells couples bone resorption with formation*.' Nat Med. **2009**, 15 (7): 757-765. doi: 10.1038/nm.1979. Epub 2009 Jul 5.

Taranum S, Sur I, Müller R, Lu W, Rashmi RN, Munck M, Neumann S, Karakesisoglou I, Noegel AA. '*Cytoskeletal Interactions at the Nuclear Envelope Mediated by Nesprins*.' Inter J Cell Biol. **2012**, ID 736524: 11 pp. doi:10.1155/2012/736524.

Teti A, Rucci N. '*The unexpected links between bone and immune system*.' Medi. **2010**, 32 (4): 341-348.

Thi MM, Suadicani SO, Schaffler MB, Weinbaum S, Spray DC. '*Mechanosensory responses of osteocytes to physiological forces occur along processes and not cell body and require αVβ3 integrin*.' Proc Natl Acad Sci. **2013**; 110 (52): 21012-21017. doi: 10.1073/pnas.1321210110.

Thia MM, Suadicanib SO, Schafflere MB, Weinbaume S, Spray DC. '*Mechanosensory responses of osteocytes to physiological forces occur along processes and not cell body and require αVβ3 integrin*.' PNAS. **2013**, 110 (52): 21012–21017.

Thompson WR, Rubin CT, Rubin J. '*Mechanical regulation of signaling pathways in bone*.' Gene. **2012**, 503:179-193.

Thompson WR**,** Yen SS**,** Rubin J**.** '*Vibration therapy: clinical applications in bone*.' Curr Opin Endocrinol Diabetes Obest. **2014**, 21 (6): 447-453. doi: 10.1097/MED.0000000000000111.

Timson BF. '*Evaluation of animal models for the study of exercise-induced muscle enlargement*.' J Appl Physiol. **1990**, 69 (6): 1935-1945.

Titushkin I, Cho M. '*Distinct membrane mechanical properties of human mesenchymal stem cells determined using laser optical tweezers*.' Biophys. J. **2006**, 90: 2582–2591.

Trappe S, Luden N, Minchev K, Raue U, Jemiolo B, Trappe TA. 'Skeletal Muscle Signature of a Champion Sprint Runner.' J Appl Physiol. **2015**: jap.00037.2015. doi: 10.1152/japplphysiol.00037.2015

Travlos GS. '*Normal Structure, Function, and Histology of the Bone Marrow*.' Toxicologic Pathology. **2006**, 34: 548–565.

Uzer G, Pongkitwitoon S, Chan ME, Judex S. '*Vibration induced osteogenic commitment of mesenchymal stem cells is enhanced by cytoskeletal remodeling but not fluid shear*'. J Biomech. **2013**, 46 (13): 2296-302. Epub 2013 Jul 17.

Uzer G, Thompson WR, Sen B, Xie Z, Yen SS, Miller S, Bas G, Styner M, Rubin CT, Judex S, Burridge K, Rubin J. '*Cell mechanosensitivity to extremely low magnitude signals is enabled by a LINCed nucleus*.' Stem Cells. **2015** Mar 18. doi: 10.1002/stem.2004

Udagawa N. '*The mechanism of osteoclast differentiation from macrophages: possible roles of T lymphocytes in osteoclastogenesis*.' J Bone Miner Metab. **2003**, 21 (6): 337-343.

Vaughan TJ, Mullen CA, Verbruggen SW, McNamara LM. '*Bone cell mechanosensation of fluid flow stimulation: a fluid-structure interaction model characterising the role integrin attachments and primary cilia*.' Biomech Model Mechanobiol. **2014** Nov 16.

Wakatsuki T, Schwab B, Thompson NC, Elson EL. '*Effects of cytochalasin D and latrunculin B on mechanical properties of cells*.' J Cell Sci. **2001**; 114:1025–1036. PubMed: 11181185.

Wagner M, Koester H, Deffge C, Weinert S, Lauf J, Francke A, Lee J, Braun-Dullaeus RC, Herold J. '*Isolation and intravenous injection of murine bone marrow derived monocytes*.' J Vis Exp. **2014**, 27 (94). doi: 10.3791/52347.

Wang Q, Ghasem-Zadeh A, Wang XF, Iuliano-Burns S, Seeman E. '*Trabecular bone of growth plate origin influences both trabecular and cortical morphology in adulthood.*' J Bone Miner Res. 2011; 26 (7): 1577-1583. doi: 10.1002/jbmr.360.

Wang YK, Yu X, Cohen DM, Wozniak MA, Yang MT, Gao L, Eyckmans J Chen CS. '*Bone morphogenetic protein-2-induced signaling and osteogenesis is regulated by cell*

shape, RhoA/ROCK, and cytoskeletal tension.' Stem Cells Dev. **2012**, 21(7): 1176-1186. doi: 10.1089/scd.2011.0293. Epub 2011 Oct 3.

Wang YK, Chen CS. '*Cell adhesion and mechanical stimulation in the regulation of mesenchymal stem cell differentiation*.' J. Cell. Mol. Med. **2013**, 17: 823–832.

Weinheimer-Haus EM, Judex S, Ennis WJ, Koh TJ. '*Low-Intensity Vibration Improves Angiogenesis and Wound Healing in Diabetic Mice*.' PLoS ONE **2014**, 9 (3): e91355. doi:10.1371/journal.pone.0091355.

Wilson A, Trumpp A, '*Bone-marrow haematopoietic stem-cell niches*.' Nature Reviews: Immunology. **2006**, 6: 93-106.

Whyte JL, Ball SG, Shuttleworth CA, Brennan K, Kielty CM. '*Density of human bone marrow stromal cells regulates commitment to vascular lineages*.' Stem Cell Res. **2011**, 6 (3): 238–250. doi: 10.1016/j.scr.2011.02.001 PMCID: PMC3223522.

Winter PW, Van Orden AK, Roess DA, Barisas BG. '*Actin-dependent clustering of insulin receptors in membrane microdomains*'. Biochem Biophys Acta. **2012**, 1818(3): 467-473. doi: 10.1016/j.bbamem.2011.10.006. Epub 2011 Oct 15.

Wu WK, Llewellyn OP, Bates DO, Nicholson LB, Dick AD. '*IL-10 regulation of macrophage VEGF production is dependent on macrophage polarization and hypoxia*.' Immunobiology. **2010**, 215 (9-10): 796-803. doi: 10.1016/j.imbio.2010.05.025. Epub 2010 Jun 4.

Xie L, Jacobson JM, Choi ES, Busa B, Donahue LR, Miller LM, Rubin CT, Judex S. '*Low-level mechanical vibrations can influence bone resorption and bone formation in the growing skeleton*.' Bone. **2006**, 39 (5): 1059-1066.

Yadav S, Assefnia A, Gupta H, Vishwanath M, Kalajzic Z, Allareddy V, Nanda R. '*The effect of low-frequency mechanical vibration on retention in an orthodontic relapse model*.' Eur J Orthod. **2015**, pii: cjv006. [Epub ahead of print]

Yan JG, Zhang LL< Yan Y, Sanger JR, Jensen ES, Matloub HS. '*Improved animal model for vibration injury study*.' Scand. J. Lab. Anim. Sci. 2010, 37 (3): 159-169.

Yeh JK. Niu Q, Evans JF, Iwamoto J, Aloia JF. '*Effect of circular motion exercise on bone modeling and bone mass in young rats: An animal model of isometric exercise*.' J Musculoskel Neuron Interact **2001**, (3): 235-240

Yin T, Li L. '*The stem cells niches in bone*.' J. Clin. Invest. **2006**, 116: 1195–1201. doi:10.1172/JCI28568.

Yonemura S. '*Cadherin-actin interactions at adherent junctions*'. Curr Opin Cell Biol. **2011**, 23(5): 515-22. doi: 10.1016/j.ceb.2011.07.001. Epub 2011 Jul 30.

Yourek G, Hussain MA, Mao JJ. '*Cytoskeletal changes of mesenchymal stem cells during differentiation*.' ASAIO J. **2007**, 53 (2): 219-228.

Zaidi M, Blair HC, Moonga BS, Abe E, Huang CL. '*Osteoclastogenesis, bone resorption, and osteoclast-based therapeutics*.' J Bone Miner Res. 2003; 18 (4): 599-609.

Zelzer E, Mamluk R, Ferrara N, et al. '*VEGFA is necessary for chondrocyte survival during bone development*.' Development. **2004**, 131: 2161–2171.

Zhang J, Niu C, Ye L, Huang H, He X, Tong W-G, Ross J, Haug J, Johnson T, Feng JQ, Harris S, Wiedemann LM, Yuji Mishina Y, Li L. '*Identification of the haematopoietic stem cell niche and control of the niche size*.' Nature. **2003**, 425 (6960): 836–841.

Zhou K, Hanna-Rose W. '*Movers and Shakers or Anchored: Caenorhabditis elegans Nuclei Achieve It With KASH/SUN*.' Developmental Dynamics. **2010**, 239: 1352–1364. doi: 10.1002/dvdy.22226.

Figure 1.1:

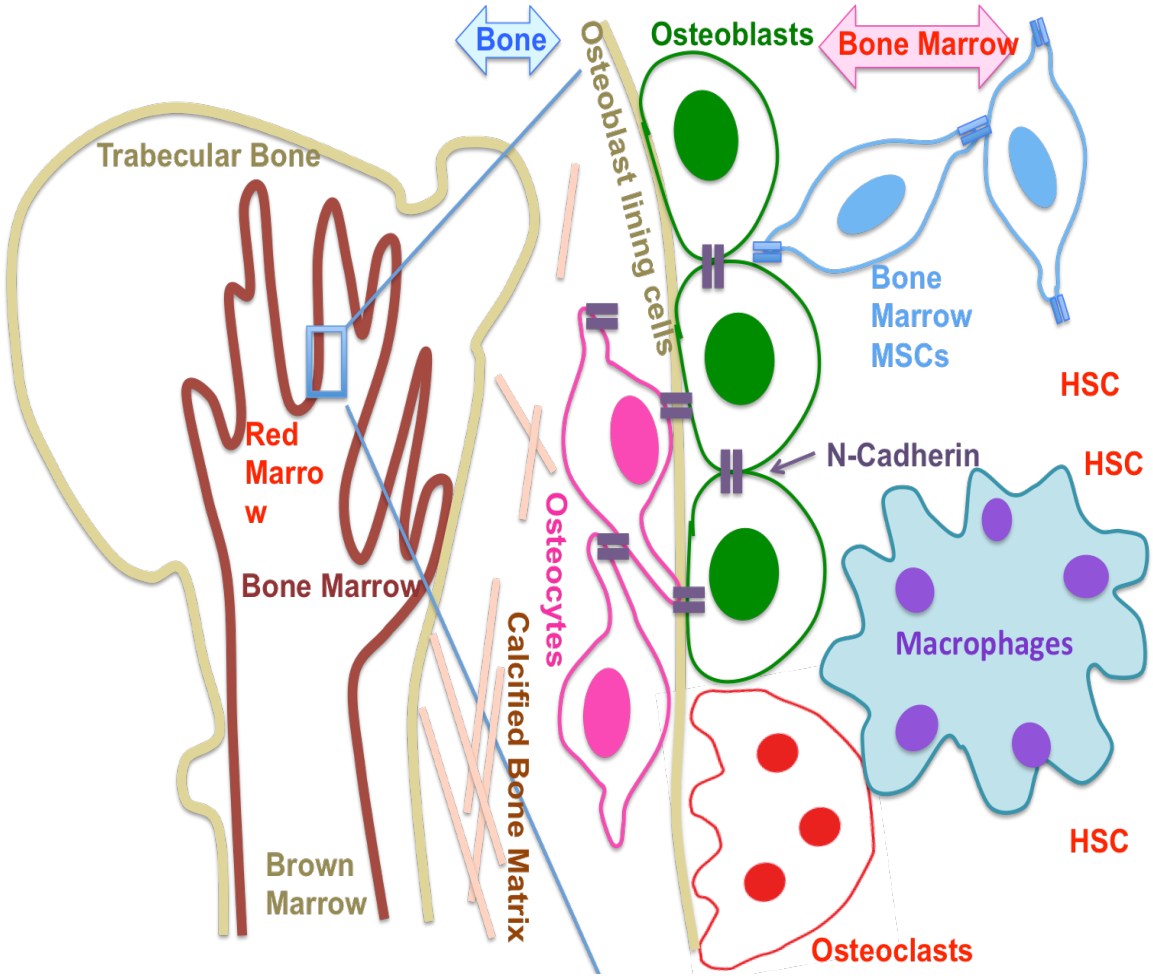
Bone
Osteoblasts
Bone Marrow
Trabecular Bone
Osteoblast lining cells
Bone Marrow MSCs
HSC
Red Marrow
N-Cadherin
HSC
Osteocytes
Bone Marrow
Macrophages
Calcified Bone Matrix
HSC
Brown Marrow
Osteoclasts

Figure 1.2:

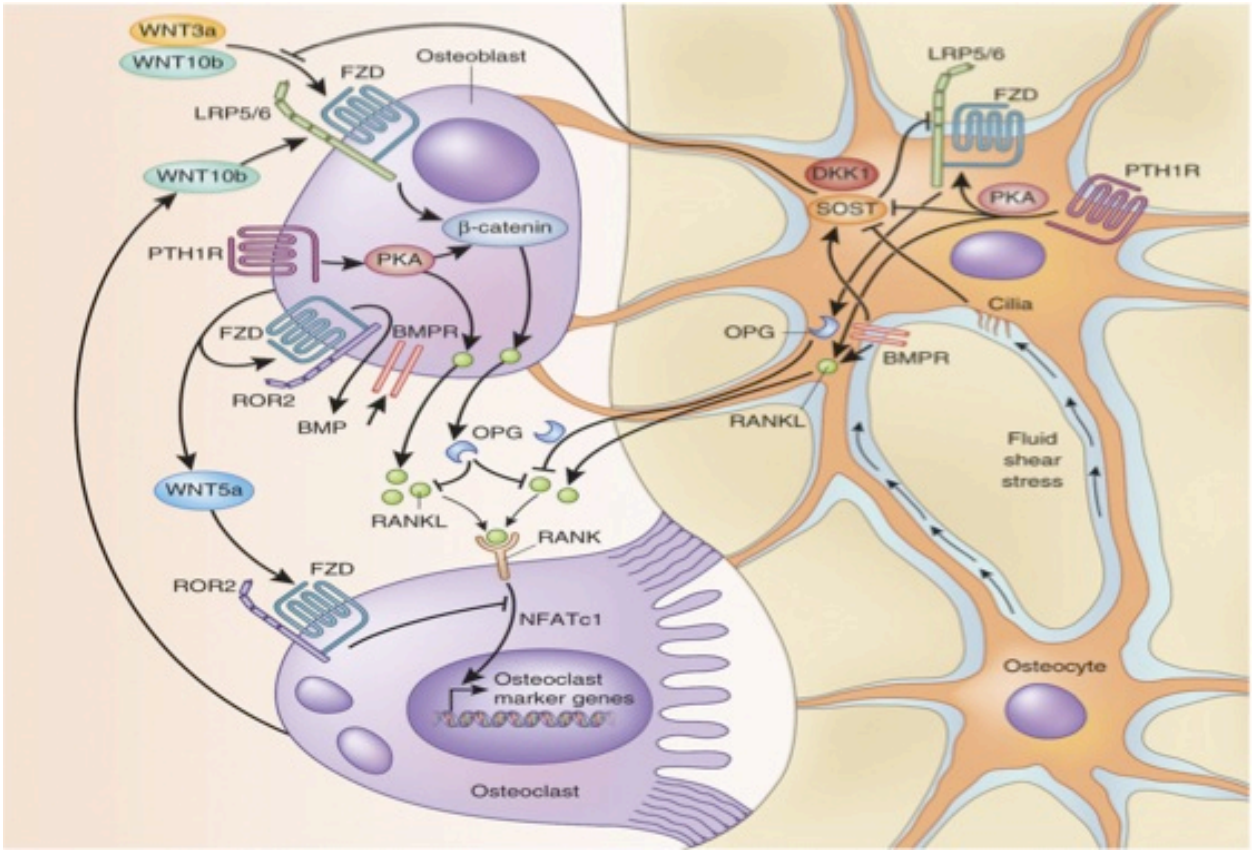
WNT3a
WNT10b
FZD
Osteoblast
LRP5/6
WNT10b
β-catenin
PTH1R
PKA
FZD
BMPR
ROR2
BMP
OPG
RANKL
RANK
WNT5a
FZD
ROR2
NFATc1
Osteoclast marker genes
Osteoclast
LRP5/6
FZD
DKK1
SOST
PKA
PTH1R
Cilia
OPG
BMPR
RANKL
Fluid shear stress
Osteocyte

Figure 1.3:

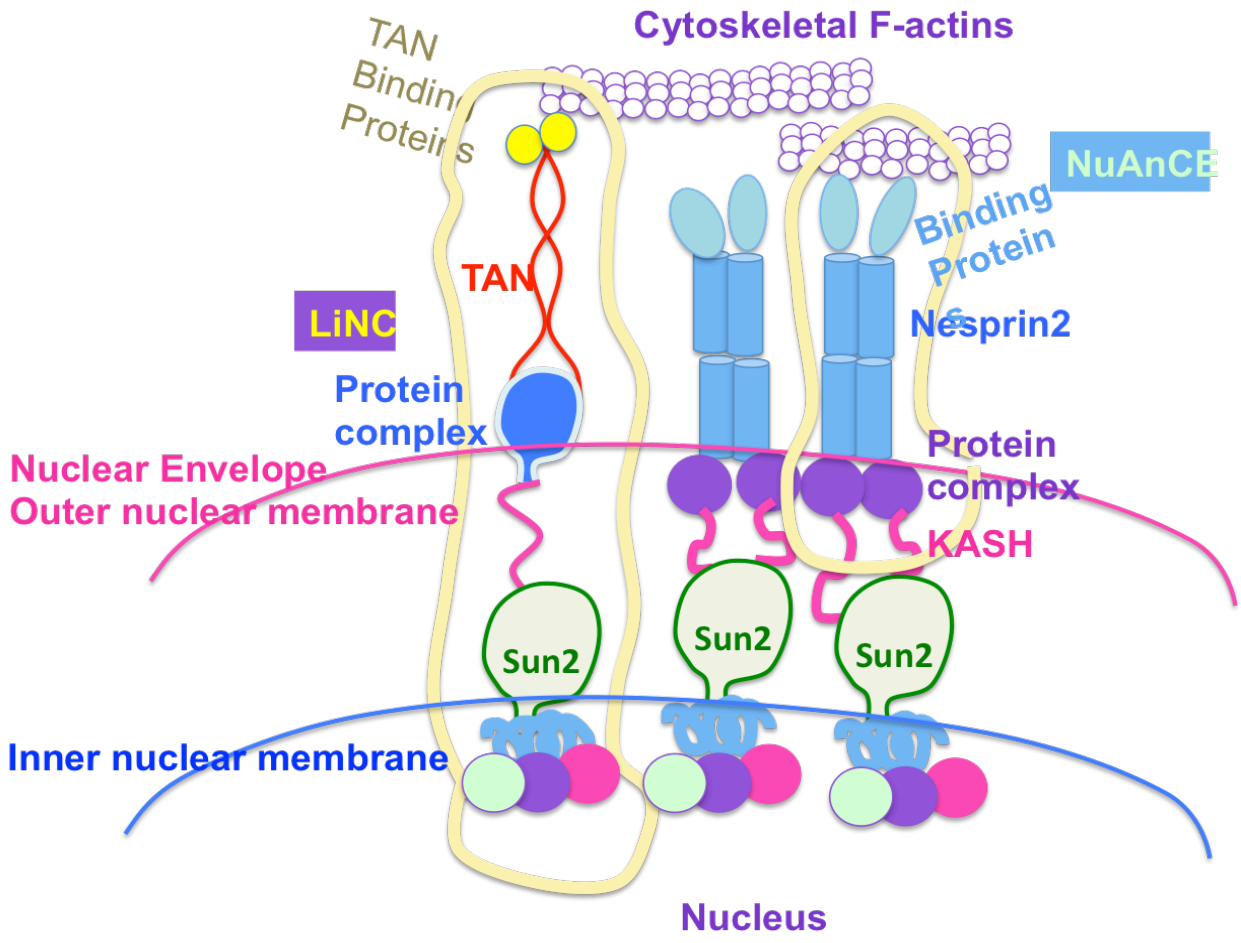
TAN
Binding
Proteins
Cytoskeletal F-actins
NuAnCE
Binding
Protein
Nesprin2
TAN
LiNC
Protein
complex
Protein
complex
KASH
Nuclear Envelope
Outer nuclear membrane
Sun2
Sun2
Sun2
Inner nuclear membrane
Nucleus

Figure 1.4:

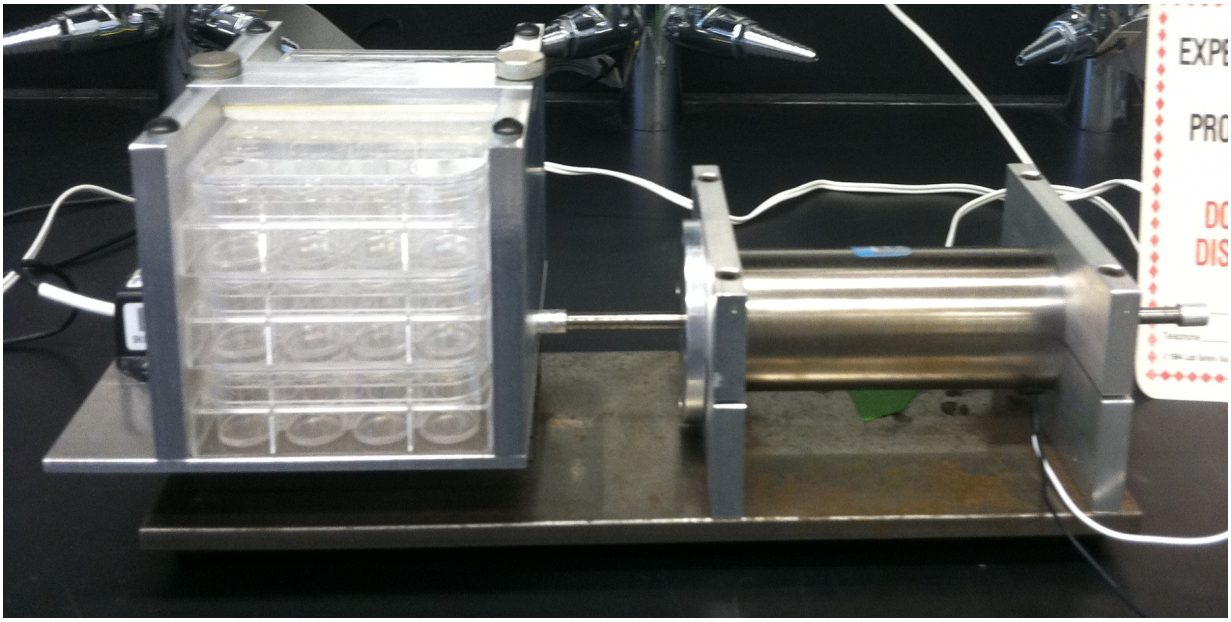

Figure 1.5:

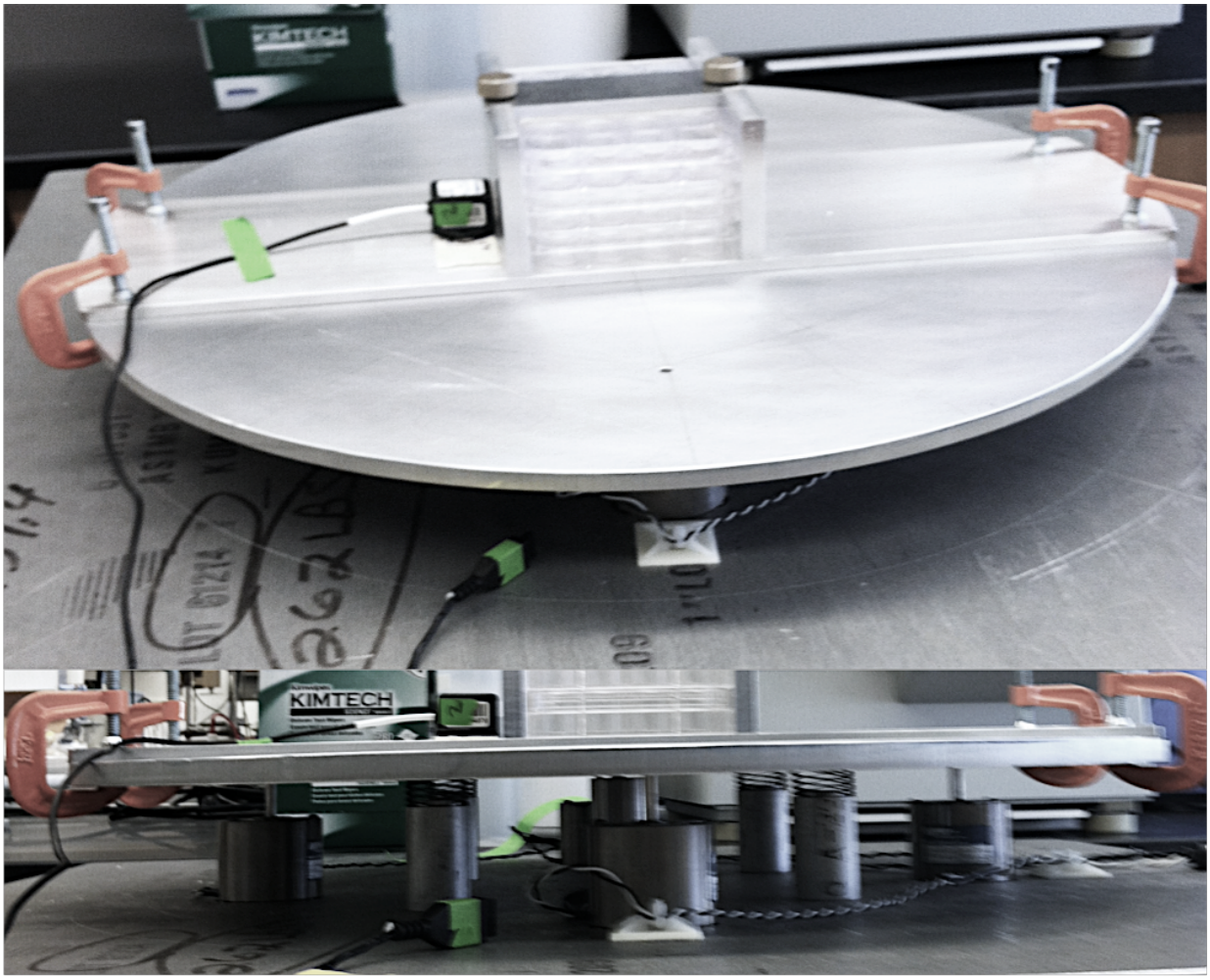

Chapter 2

Methods and Instrumentation

2. Methods and Instrumentation

2.1 Human Cell Culture In Vitro

In vitro culture of human bone marrow MSCs have been developed over the year. The fact that the human bone marrow stem cells are very sensitive to their microenvironments makes in vitro culture impossible [Golde et al. 1973]. Keeping bone marrow stem cells alive in vitro conditions has been challenging. With supplementation of the human growth factor (HGF) instead of fetal bovine serum (FBS), culture of the bone marrow stem cells can accomplish even in a long-term culture [Gartner et al. 1980]. However, HGF is very expensive and has a limited supply. Several companies have concocted their own specific media (a complete growth media such as StemLifeTM MSC Medium Complete Kit: LL-0034 [LifeLineCellTechnology]) for human bone marrow stem cells.

We used RNA recombinant to modify the proper growth factor in our media. We used FBS but modified it with human RNA recombinants of rh IGF-1 (15ng/ml) and rh FGF-β (125 pg/ml). The IGF-1 and FGF-β are rich in both fetal and adult human growth factor [Azouna et al. 2012]. One of the most crucial information is that the amino acid sequences of IGF-1 and FGF-β in bovine are different from the sequence in human [Frank et al. 2014, Honegger et al. 1986, Rinderknecht et al. 1978]. The success of in vitro culture could be that the media supplemented with human IGF-1 and FGF-β (or RNA recombinant IGF-1 and FGF-β) could improve the FBS quality similar to HGF [Merchav et al 1988]. We controlled the pH of the media with HEPES and stabilized the rh IGF-1 and rh FGF-β stock solution with DTT. We added 2.4 mM L-glutamine in the media since the HGF is also rich in L-glutamine.

We used phenol red free media because the phenol red is cytotoxic to human bone marrow stem cells. The phenol red cytotoxicity is also pH dependent [Grady et al. 1991] and UV sensitive [Stoien et al. 1974] that disrupt the stem cell growth. Additionally, the phenol red could act to be a weak estrogen for a certain cell type such as human stem cells [Welshons et al. 1988]. We supplemented the media with double antibiotics 1% penicillin/streptomycin and also added antimicrobrials/antimicrotics of 1% gentamicin because our laboratory previously had an outbreak of *Sphingomonas Paucimobilis* from humidity and moisture [Maragakis et al. 2009].

2.2 Horizontal and Vertical Vibration Devices

We used our custom made horizontal vibration device (**Figure 2.1**). The function generator (DS335, StanfordResearchSystems) controls sinusoidal frequency and acceleration (voltage from peak to peak, Vpp). The function generator can generate the frequency between 1Hz-3MHz with peak acceleration at 1.8g (400Hz) to 3g (10Hz). However, the frequency above 250Hz could create the secondary vibration of the whole system and can be eliminated by selecting 100Hz as the maximal frequency. The car amplifier with AC/DC changer was connected between the function generator and the motor (a voice coil linear actuator). The voice coil linear actuator (NCM15, H2W Technologies Inc., CA) on the frictionless base (NK2-110B, Schneeberger GmbH, Germany) was attached to the cell plate holder. The cell plate holder can hold up to 3 plates of a 24wells-plate. The accelerometer (CXL10, Moog Crossbow Inc., CA) was attached to the base to monitor the actual output acceleration (cm/t^2 or g) in real time. The computer attached to accelerometer to view whether the horizontal oscillation is the sinusoidal function and what the actual acceleration is read.

The vertical vibration device (**Figure 2.2**) is made from the loudspeaker attaching to a platform. The platform needs to be heavy enough to reduce the bouncing effect. The plate holder is secured on the platform with 4 bounce-absorbing pillars and the 4 spring linear coils (NCM02, H2W Technologies Inc., CA).

The combination of vibration frequency and acceleration determines the fluid shear stress that cells are exposed to [Uzer et al. 2012]. We used the signal combination of 30Hz-1g, 100Hz-1g, 30Hz-0.15g and 100Hz-0.15g as from the highest to lowest fluid shear stress created by horizontal vibration.

2.3 PCR Gene Expressions

Polymerase Chain Reaction (PCR) is a technique used to amplify a single copy or a piece of DNA to many billions of copies of an interested DNA sequence [Mullis et al. 1987]. The PCR uses the ability of DNA polymerase to synthesize a new strand of DNA complementary to the offered template strand. Since the DNA polymerase can add a nucleotide only onto a preexisting 3'-OH group, the PCR needs a primer (DNA sequences complementary to the target DNA) to add the first nucleotide. For example, the reversed primer sequence for Runx2 (the gene involves in the osteoblastic differentiation) is *'CTGCCTGGCTCTTCTTACTGAG'* [Niu et al 2012]. The PCR relies on the thermal cycles of repeated heating and cooling of the reaction for the DNA melting and enzymatic replication of the DNA.

To perform the real-time PCR, we first lysed cells with TRIzol (Life Technologies) and extracted the RNA using phase separation, which recently found that these protocols are feasible to use in the clinical specimen as well [Bergallo et al. 2015, and Rice et al. 2015]. The RNA was precipitated from the nucleic acid by RNeasy (Qiagen) and washed with 70% ethanol before re-dissolving by RNA-free water. We quantified the RNA concentration and determined the RNA quality using NanoDrop (ND-100 V3.3.0). The ratio of $[A_{260}/A_{280}] \geq 1.8$ is for 'pure' cDNA, and ≥ 2.0 for 'pure' RNA, validating by $[A_{260}/A_{230}]$ ~2.0-2.2 for 'pure' nucleic acid. Then, the RNA was cloned by the reversed transcriptase (Invitrogen) for the cDNA conversion. After the determination of purification and concentration, the cDNA was diluted to be the same concentration (3.33ng/μl).

We quantified gene expression by the real-time PCR using TaqMan standard protocols. The expression level was analyzed by the fold changes ($2^{-\Delta\Delta Ct}$) with respect to the control and the

GAPDH. Using StepOne 2.2, the real-time polymerase chain reaction (q-PCR) provided Ct of the interested genes for calculation of the gene expression level ($2^{-\Delta\Delta Ct}$). Several genes like Runx2, Alpl, Col1a1, Wnt10a, Bmp2, TGF-b, VEGF and more have been used to investigate bone formation and skeletal development [Zhang et al. 2012].

2.4 Western Blot

The western blot is an analytical technique to detect the specific protein expression in the cells and tissue using electrophoresis to separate the protein by length of the polypeptide. The separated polypeptide is then transferred to a membrane (generally used membranes are nitrocellulose and polyvinylidene difluoride, PVDF). To detect the specific protein of interest, the immunofluorescence staining technique with primary and specific secondary antibodies is crucial [Mahmood et al. 2012]. Since these antibodies can have cross-reactivity that implicates the protein detection. Blotting the membrane could reduce the cross-reaction of these antibodies.

We isolated the protein from the cell sample by lysis the cells with RIPA buffer (Sigma R0278) in ice-cold temperature. The protein concentration in each lysate was determined by standard BSA protein assay (BioRad) and diluted to the same concentration of 5μl/ml before conjugation with the primary and secondary antibodies. To see the protein separation, we dyed the protein with 0.004% bromophenol blue and stabilized the protein with 10% DTT.

To separate the protein by its polypeptide length (kDa), the electrophoresis of constant Amp at 200 V was applied to the running gel. The separated protein was then transferred to the transferring membrane PVDF. To prevent the non-specific protein binding to antibodies, we blotted the membrane with 5% fat-free milk in 50% BSA. After blocking non-specific binding proteins, we used two-step staining with primary and secondary antibodies. The secondary antibody can bind to the biotin or enzyme receptor (e.g. horseradish peroxidase) of one primary antibody to enhance the signal. By cleaving a chemiluminescent agent, the photoluminescence was produced in proportion to the amount of protein, which can be detected by the chemiluminescent detection.

2.5 Flow Cytometry

Flow cytometry is a laser-based technique to count, sort and detect cells, biomarkers and proteins. The suspending immunofluorescence staining cells (could be dead or live cells) in a fluid steam are forced to pass through the electronic detector. During data acquisition, the flow rate and volume of the fluid flow can be adjusted [O'Neill et al. 2013]. The detector (X-ray) could simultaneously characterize thousands of cells and particles per second with multiple parameters. The technique depends on a good immunofluorescence staining with antibodies and the proper gate setting [O'Donnell et al. 2013].

To set a proper gate, for example, the positive control (cells stained with specific antibodies) and the negative control (cells without the immunofluorescence antibodies) are required in addition to the experimental control (e.g. non-vibrated group). The program FlowJo can analyze the % cell population of the gated interests.

2.6 Two Photon Confocal Microscopy vs Confocal Microscopy

Two-photon confocal microscopy is a non-invasive fluorescent imaging technique using low energy two photons to simultaneously excite the fluorophores in one quantum event [So et al. 2000]. The most commonly used fluorophores have excitation spectra in the 400–500 nm range, whereas the laser used to excite the two-photon fluorescence lies in the ~700–1000 nm (infrared) range. The excitation process with two photons can penetrate deep inside the thick tissues with high resolution. The two-photon microscopy can use to image the live cells, animals and even in humans in clinical uses [Eggeling et al. 2005]. For example, the two-photon was used to locate osteocytes in lacunar canalicular network in murine tibia [Sano et al. 2015] and bone marrow in vivo [Turcotte et al. 2014].

The most distinction of the two-photon- from the conventional confocal- microscope is that the two-photon can image in z-direction with clear resolution by adjustable pinholes and low energy x-ray [Sako et al 1997]. With low energy x-ray, the problem of photobleaching during imaging can be diminished with shorter acquiring time. The limitation of the two-photon confocal microscopy in the in situ imaging is that it can only take 5 images in 1 second.

We double stained the cell membranes, cytoskeleton, and nuclear nesprin2 of the human cell with immunofluorescent antibodies. We used 700-1000nm (depending on the fluorophores) to excite the fluoreophore. Since the x-ray in the two-photon instrument (CMI) we used could only take one color image at a time, we used ImageJ to overlap image of cytoskeleton, cell membrane in to one image.

2.7 Atomic Force Microscopy

The atomic force microscope (AFM) operates by physical interaction of a cantilever tip with the molecules of the cell surface. During the tip dragging along the cell surface, adhesion forces between the tip and the cell surface molecule can be detected as the cantilever deflection [Trache et al. 2008]. The deflection depends on the cantilever spring constant. Advantages of AFM are (i) imaging live single cell in liquid with an atomic resolution [Chtcheglov et al. 2010] and (ii) probing single molecules in physiological conditions [Ando et al. 2013]. Currently, the AFM is the only technique that directly provides structural [Lyubchenko et al. 2009], mechanical [Kim et al. 2003], and functional information with high resolution.

We used AFM (Digital Instrument) to obtain the relative modulus with liquid mode. The drive amplitude (mV) and the lateral deflection amplitude of the cantilever (ΔX, mV) were relatively set to convert to be the force (pN) and distance (μm). The calibration was performed in Hank's balanced solution. We used a standard V-shaped cantilever (200μm) and a gold tip with a typical radius of the apex ~20nm. Before each measurement, a UV shortwave sanitized the tip for at least 2 min. The alignment of the tip on top of the cells was accomplished using a laser system. We used contact mode (scanning the tip across the surface).

2.8 RNA Interference vs. Transfection

The RNA interference is a technique to use small molecules of ribonucleic acid (RNA; shRNA, siRNA) to inhibit the gene expression [Agrawal et al. 2003]. The permanent gene depletion (the gene knockdown) is to use shRNA (complementary with the miRNA of the gene of interests) to produce non-function defected DNA of exportin (**Figure 2.3**) [Shan 2010]. The gene knockdown happens in the nucleus and so called the post-transcription gene silencing [Hannon 2002]. The double stranded RNAs that are homologous to the gene being suppressed initiate the post-transcriptional silencing. In mammalian cells, the siRNA molecules are capable of specifically silencing gene expression without induction of the unspecific interferon response pathway [Scheer et al. 2007].

However, the temporary gene silencing can also use the siRNA to silence the gene in cytoplasm before transcription (**Figure 2.4**). Generally, the gene silencing describes the epigenic regulation of the gene expression, particularly as the cell ability to expression of a certain gene. The gene transfection can silence the gene expression during transcription and/or translation [Leung et al. 2005]. Since techniques that used to knock down gene can also use to silence gene such as interference RNA (RNAi) [Scheer et al. 2003], often time the gene silencing can be confused with the gene knockdown. The gene silencing is to reduce and silence the expression but not erase the expression like the knockdown.

We knocked down the cytoskeletal f-actinins using Cofilin-shRNA (shRNA Clf1, Santa Cruz Bio) while silencing the cytoskeleton with its compromised siRNA. The Cfl1 is an actin-binding protein that regulates dynamic assembling-disassembling of g-actins during cytoskeletal polymerization [Hammond et al. 2012]. Before the gene knockdown, the cell needs to undergo

the transfection the transfecting reagent (such as opti-MEM, LifeTechnologies) overnight in 1% DMSO. The gene knockdown could cause cell dead and instabilities from the permanent depletion by shRNA and transfection with opti-MEM in DMSO. Therefore, the validation of the effectiveness and toxicity of the knockdown technique are required.

References:

Agrawal N, Dasaradhi PV, Mohmmed A, Malhotra P, Bhatnagar RK, Mukherjee SK. '*RNA interference: biology, mechanism, and applications*.' Microbiol Mol Biol Rev. **2003**, 67 (4): 657-85.

Ando T, Uchihashi T, Kodera N. '*High-speed AFM and applications to biomolecular systems*.' Annu Rev Biophys. **2013**, 42: 393-414. doi: 10.1146/annurev-biophys-083012-130324.

Azouna NB, Jenhani F, Regaya Z, Berraeis L, Othman TB, Ducrocq E, Domenech J. '*Phenotypical and functional characteristics of mesenchymal stem cells from bone marrow: comparison of culture using different media supplemented with human platelet lysate or fetal bovine serum*.' Stem Cell Research & Therapy **2012**, 3: 6 doi:10.1186/scrt97

Bergallo M, Gambarino S, Martino S, Montin D, Montanari P, Galliano I, Tovo PA. '*Comparison of Two Available RNA Extraction Protocols for microRNA Amplification in Serum Samples*.' J Clin Lab Anal. **2015**. doi: 10.1002/jcla.21848.

Chtcheglova LA, Wildling L, Waschke J, Drenckhahn D, Hinterdorfer P. '*AFM functional imaging on vascular endothelial cells*.' J Mol Recognit. **2010**, 23 (6): 589-596. doi: 10.1002/jmr.1052.

Delorme B, Charbord P. '*Culture and Characterization of Human Bone Marrow Mesenchymal Stem Cells*.' Methods in Molecular Medicine, Tissue Engineering, **2007**, 140: 67-81.

Eggeling C, Volkmer A, Seidel CAM.' *Molecular Photobleaching Kinetics of Rhodamine 6G by One- and Two-Photon Induced Confocal Fluorescence Microscopy*.' **2005** doi: 10.1002/cphc.200400509

Franke J, Abs V, Zizzadoro C, Abraham G. '*Comparative study of the effects of fetal bovine serum versus horse serum on growth and differentiation of primary equine bronchial fibroblasts*.' BMC Vet Res. **2014**; 10: 119. doi: 10.1186/1746-6148-10-119. PMCID: PMC4040117

Gartner S, Kaplan HS. '*Long-term culture of human bone marrow cells*.' Proc. Natl. Acad. Sci. **1980**, 77 (8): 4756-4759.

Golde DW, Cline MJ. '*Growth of Human Bone Marrow in Liquid Culture*.' Blood. **1973**, 41 (1): 45-57.

Grady LH, Nonneman DJ, Rottinghaus GE, Welshons WV '*pH-dependent cytotoxicity of contaminants of phenol red for MCF-7 breast cancer cells*.' Endocrinology. **1991**, 129 (6): 3321-3330.

Hammond S., Lee K.H. '*RNA interference of cofilin in Chinese hamster ovary cells improves recombinant protein productivity*'. Biotechnology and Bioengineering, **2012**, (109, 2): 528–535.

Hannon GJ. '*RNA interference*.' Nature. **2002**, 418 (6894): 244-251.

Honegger A, Humbel RE. '*Insulin-like Growth Factors I and I1 in Fetal and Adult Bovine Serum: Purification, Primary Structures, and Immunological Cross-Reactivities*.' J Biol Chem. **1986**, 261 (2): 569-575.

Kim H, Arakawa H, Osada T, Ikai A. 'Quantification of cell adhesion force with AFM: distribution of vitronectin receptors on a living MC3T3-E1 cell.' Ultramicroscopy. **2003**, 97 (1-4): 359-363.

Leung RK, Whittaker PA. '*RNA interference: from gene silencing to gene-specific therapeutics*.' Pharmacol Ther. **2005**; 107 (2): 222-239.

Lyubchenko YL, Shlyakhtenko LS, Gall AA. '*Atomic force microscopy imaging and probing of DNA, proteins, and protein DNA complexes: silatrane surface chemistry*.' Methods Mol Biol. **2009**, 543: 337-351. doi: 10.1007/978-1-60327-015-1_21.

Mahmood T, Yang PC. '*Western Blot: Technique, Theory, and Trouble Shooting*.' N Am J Med Sci. **2012** Sep; 4(9): 429–434. doi: 10.4103/1947-2714.100998 PMCID: PMC3456489

Maragakis LL, Chaiwarith R, Srinivasan A, Torriani FJ, Avdic E, Lee A, Ross TR, Carroll KC, Perl TM. '*Sphingomonas paucimobilis Bloodstream Infections Associated with Contaminated Intravenous Fentanyl*.' Emerging Infectious Diseases. **2009**, 15 (1): 12-18. doi: 10.3201/eid1501.081054

Merchav S, Tatarsky I, Hochberg Z. '*Enhancement of human granulopoiesis in vitro by biosynthetic insulin-like growth factor I/somatomedin C and human growth hormone*.' J Clin Invest. **1988**, 81(3): 791–797. doi: 10.1172/JCI113385, PMCID: PMC442527

Mullis KB, Faloona FA. '*Specific synthesis of DNA in vitro via a polymerase-catalyzed chain reaction*.' Methods Enzymol. **1987**; 155: 335-50.

Niu DF, Kondo T, Nakazawa T, Oishi N, Kawasaki T, Mochizuki K, Yamane T, Katoh R. '*Transcription factor Runx2 is a regulator of epithelial-mesenchymal transition and invasion in thyroid carcinomas*.' Nature. Lab Invest. **2012**, 92 (8): 1181-1190. doi: 10.1038/labinvest.2012.84.

O'Donnell EA, Ernst DN, Hingorani R. '*Multiparameter Flow Cytometry: Advances in High Resolution Analysis*.' Immune Netw. **2013**, 13 (2): 43–54. doi: 10.4110/in.2013.13.2.43

O'Neill K, Aghaeepour N, Spidlen J, Brinkman R. '*Flow Cytometry Bioinformatics*'. PLoS Comput Biol. **2013**, 9 (12): e1003365. doi: 10.1371/journal.pcbi.1003365

Rice J, Roberts H, Burton J, Pan J, States V, Rai SN, Galandiuk S. '*Assay Reproducibility in Clinical Studies of Plasma miRNA*.' PLoS One. **2015**, 10 (4): e0121948. doi: 10.1371/journal.pone.0121948. eCollection 2015.

Rinderknecht E, Humbel RE. '*The amino acid sequence of human insulin-like growth factor I and its structural homology with proinsulin*.' The Journal of Biological Chemistry. **1978,** 253: 2769-2776.

Sako Y. Sekihata A. Yanagisawa Y. Yamamoto M. Shimada Y. Ozaki K. Kusumi A. '*Comparison of two-photon excitation laser scanning microscopy with confocal laser*

scanning microscopy in three-dimensional calcium imaging using the fluorescence indicator Indo-1'. J. Microscopy. **1997**, 185 (1): 9-20.

Sano H, Kikuta J, Furuya M, Kondo N, Endo N, Ishii M '*Intravital bone imaging by two-photon excitation microscopy to identify osteocytic osteolysis in vivo.'* Bone. **2015**, 74: 134-139. doi: 10.1016/j.bone.2015.01.013.

Shan G. '*RNA interference as a gene knockdown technique*.' Int J Biochem Cell Biol. **2010**; 42 (8): 1243-1251. doi: 10.1016/j.biocel.2009.04.023.

Scherr M, Eder M. '*Gene silencing by small regulatory RNAs in mammalian cells*.' Cell Cycle. **2007**; 6 (4): 444-449.

Scherr M, Morgan MA, Eder M. '*Gene silencing mediated by small interfering RNAs in mammalian cells*.' Curr Med Chem. **2003**; 10 (3): 245-256.

So PTC, Dong CY, Masters BR, Berland KM. '*Two-Photon Excitation Fluorescence Microscopy*.' Ann Rev Biomed Eng. **2000**, 2: 399-429. doi: 10.1146/annurev.bioeng.2.1.399

Stoien JD, Wang RJ. '*Effect of Near-Ultraviolet and Visible Light on Mammalian Cells in Culture II: Formation of Toxic Photoproducts in Tissue Culture Medium by Blacklight (human cells/cell lethality/photodynamic action/riboflavin-tryptophan-tyrosine)*.' Proc. Nat. Acad. Sci. **1974**, 71 (10): 3961-3965.

Trache A, Meininger GA. '*Atomic force microscopy (AFM)*.' Curr Protoc Microbiol. **2008**, Chapter 2: Unit 2C. 2. doi: 10.1002/9780471729259.mc02c02s8.

Turcotte R, Alt C, Mortensen LJ, Lin CP. *'Characterization of multiphoton microscopy in the bone marrow following intravital laser osteotomy.'* Biomed Opt Express. **2014**, 5 (10): 3578–3588. doi: 10.1364/BOE.5.003578

Welshons WV, Wolf MF, Murphy CS, Jordan VC. '*Estrogenic activity of phenol red*.' Mol Cell Endocrinol. **1988**, 57 (3): 169-178.

Zhang Y, Xie RL, Gordon J, LeBlanc K, Stein JL, Lian JB, van Wijnen AJ, Stein GS. '*Control of Mesenchymal Lineage Progression by MicroRNAs Targeting Skeletal Gene Regulators Trps1 and Runx2*.' J Biol Chem. **2012**, 287 (26): 21926 –21935.

Figure 2.1:

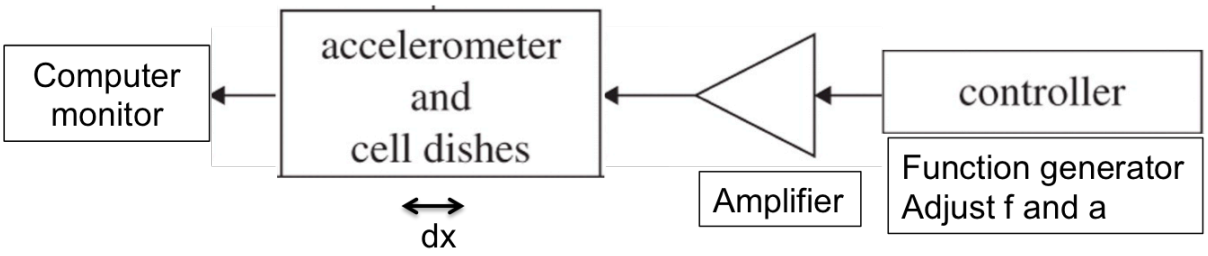
Computer monitor
accelerometer and cell dishes
dx
Amplifier
controller
Function generator
Adjust f and a

Figure 2.2:

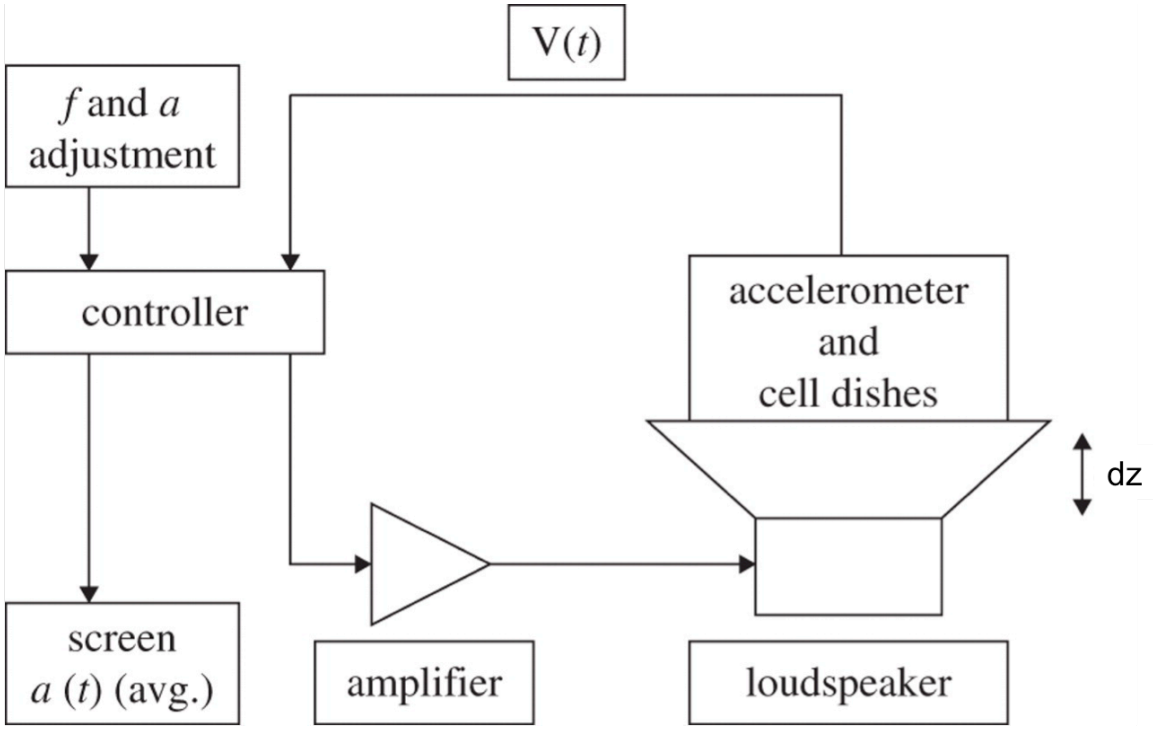
V(t)
f and a adjustment
controller
accelerometer and cell dishes
dz
screen a (t) (avg.)
amplifier
loudspeaker

Figure 2.3:

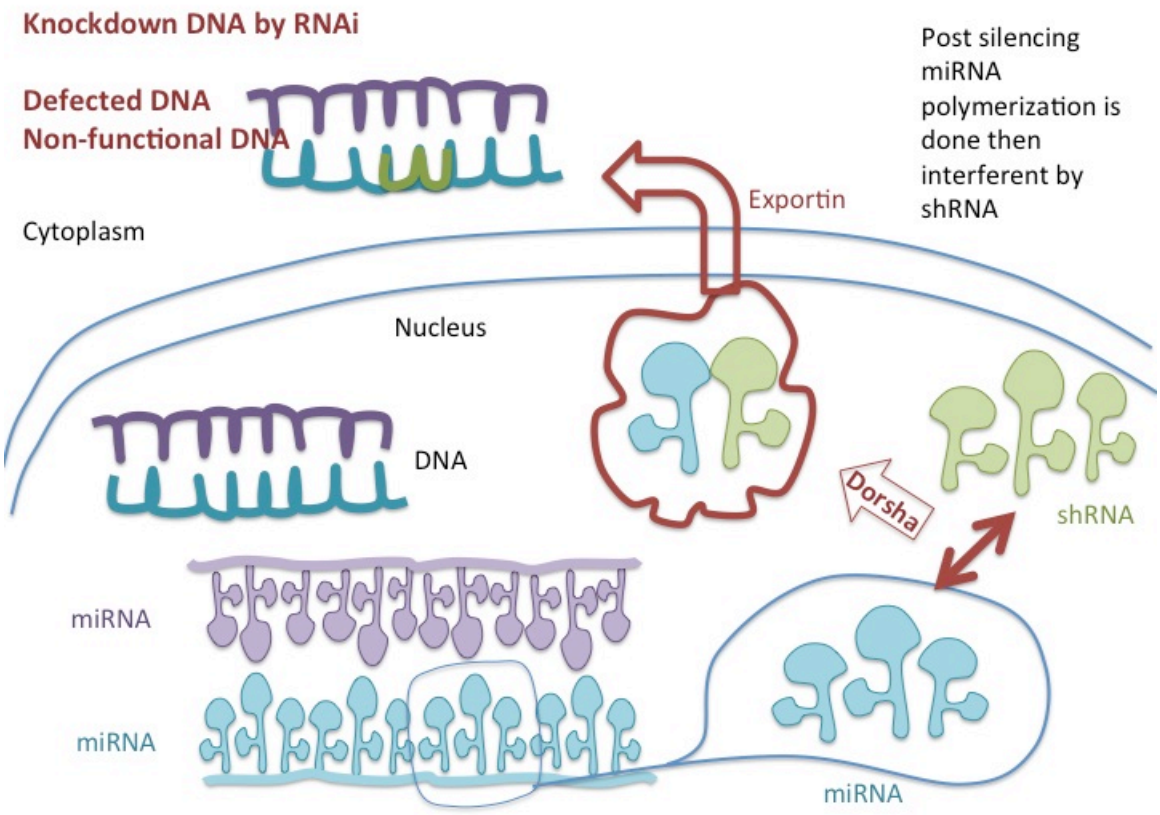
Knockdown DNA by RNAi
Defected DNA
Non-functional DNA
Post silencing miRNA polymerization is done then interferent by shRNA
Exportin
Cytoplasm
Nucleus
DNA
Dorsha
shRNA
miRNA
miRNA
miRNA

Figure 2.4:

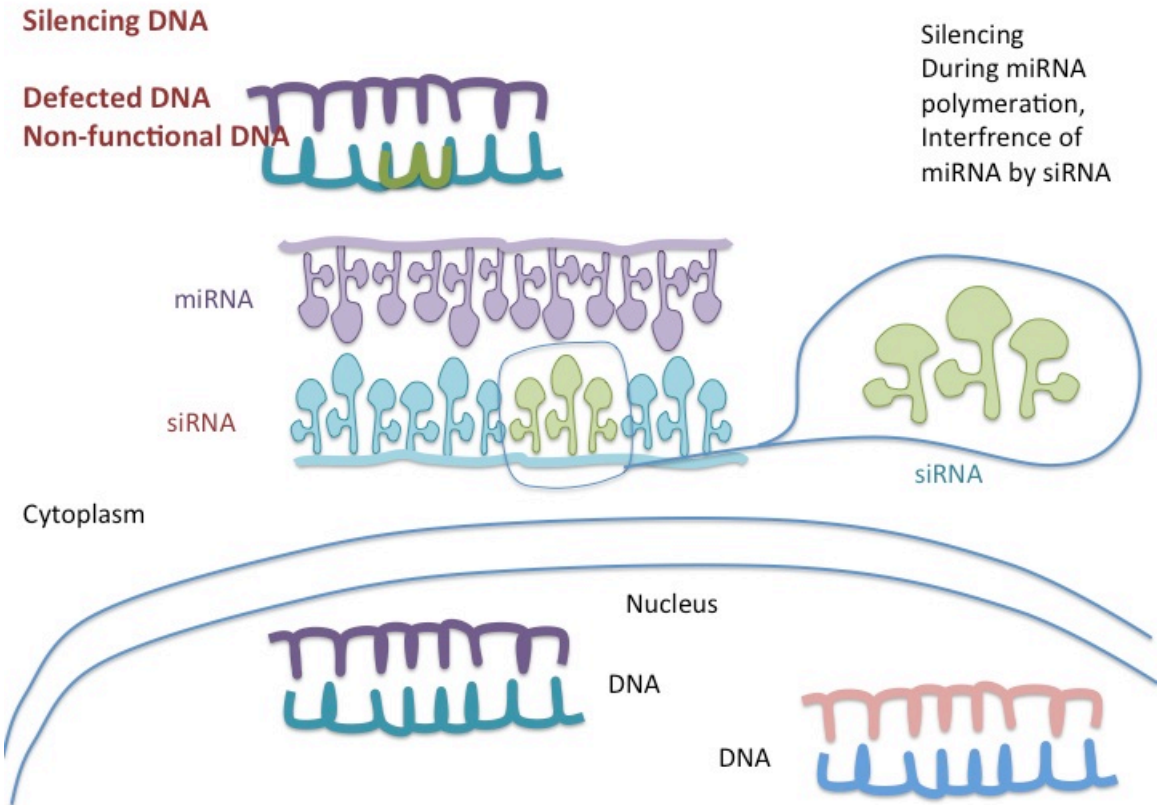
Silencing DNA
Defected DNA
Non-functional DNA
Silencing
During miRNA
polymeration,
Interfrence of
miRNA by siRNA
miRNA
siRNA
siRNA
Cytoplasm
Nucleus
DNA
DNA

Chapter 3

Mechanotranduction of Low Intensity Vibration in Mesenchymal Stem Cells:

Evidence towards Interactions between Nuclear and Cellular Structures

(Pending publication and/or patent)

Abstract

Human bone marrow mesenchymal stem cells (hBMSCs) are sensitive to the low intensity vibration (LIV) in vitro and in vivo, however, the specific components that play a role in cellular and molecular mechanotransduction are largely unknown. Here, we hypothesized that the different LIV conditions, differentially causing interactions between cellular and nuclear structures, modulate the gene expression profile of hBMSCs. We applied horizontal and vertical LIV with the signal combination of the frequency (30Hz or 100Hz) and the acceleration amplitude (0.15g or 1g). Profiling gene expression of the structure related genes with their functions, we identified the mechanotransduction pathway. The cell proliferation of the vibrated group was ~1.5x-2.3x more than that of the control. The proliferation was modulated by the frequency and acceleration amplitude, but not the direction. However, the direction significantly influenced osteogenic differentiation. The upregulated ALPL gene expression and the increased alkaline phosphatase activity supported the progressive osteogenic differentiation in the LIV group. An overexpression of Runx2 confirmed an increasing cellular calcification in the LIV group. The physical structure related genes such as adherent junction (CDH11), cytoskeletal f-actin including alpha actinin (ACTn1), and nesprin2 (Syne2) were upregulated in the LIV group. The cytoskeletal remodeling kinase (Whamm) was upregulated with the upregulated ACTn1. Additionally, an increase in the upregulation of the NuAnCE-LiNC (Syne2 and Sun2) was similar to the increased cytoskeleton. These data supported that the physical connection of the cell and nucleus could directly involve in the mechanotransduction pathway.

3.1 Introduction

Though human bone marrow mesenchymal stem cells are sensitive to the LIV, the mechanotransduction of the LIV in hBMSCs, however, has been unclear [Thompson et al. 2012]. The hBMSCs are multipotent precursors for bone regeneration in vivo and in vitro [Potier et al. 2010]. The LIV is anabolic to bone in animals and humans [Ozcivici et al. 2010, Thompson et al. 2014]. Combinations of the frequency and acceleration can create the fluid shear stress [Uzer et al. 2012]. For example, the 30Hz-1g can generate the highest fluid shear (0.94Pa) while the 100Hz-0.15g provides the lowest fluid shear (0.04Pa).

Mechanical stimulation has been shown to activate several signaling pathways stimulating molecular functions. The proliferation of murine MSCs showed that the PI3K controlled the Akt [Choi et al. 2008] and could regulate by β-catenin/Akt [Kushwaha et al. 2014]. The complication of relating the signaling pathway with the mechanotransduction pathway mainly comes from multiple molecular functions of each signaling pathway. During osteogenic differentiation, the upregulated β-catenin/Akt could activate the PPARg/ cEBPα, causing a progressive adipogenic differentiation [Metcalfe et al. 2011, Hart et al. 1998, Palsggard et al. 2012]. Additionally, the mechanical stimulation induced the upregulated bone morphogenetic protein 2 (Bmp2) could cause the elevated Smad1 activated PPARg [Hata et al. 2003]. These data have suggested that the signaling related mechanotransduction could omit the actual transduction system inside the cell and nucleus.

Several studies have shown that the mechanical stimulation could change the physical interaction of the cellular and nuclear structure. Under the dynamic oscillation, fluorescence images showed the cytoskeleton forming bundles [Stricker et al. 2010] during the MSC

osteogenic differentiation [Malone et al. 2007]. The Nucleoskeleton (nesprin2) could directly link to the sun molecule [Rothballer et al. 2013] during the force transmission from the cytoskeleton to the nucleus [Lombardi et al. 2011]. The nesprin2 is a part of the nuclear skeletal complex (NuAnCE-LiNC) [Lombardi et al. 2011, Zhen et al. 2002]. The NuAnCE-LiNC was composed of (1) KASH, (2) sun family, and (3) TAN giant molecules [Tapley et al. 2013]. The cytoskeletal remodeling (upregulated Whamm) could anchor the NuAnCE-LiNC from the outer nuclear envelope across the inner nuclear membrane [Rothballer et al. 2013, Tapley et al. 2013]. The anchorage could further organize the laminin at the nuclear basement membrane [Libotte et al. 2005, Rothballer et al. 2013, Tapley et al. 2013].

Here, we aim to connect physical interactions of the cell and the nucleus under the LIV with the mechanotransduction pathway. We profiled changes of the structure related genes (e.g. ACTn1 and Syne2) with their molecular function related genes (e.g. Runx2, Whamm). The association of these genes with the cellular behavior (e.g. ALP activities and calcification) could provide the important clue of the LIV induced mechanotransduction pathway.

3.2 Materials and Methods

3.2.1 Experimental design

To connect the dynamic changes in physical interactions of structures with the mechanotransduction pathway, we investigated changes in gene expression levels and cellular behaviors under different LIV conditions.

To monitor cellular behaviors, we investigated proliferation and osteogenic differentiation of hBMSCs. The LIV of horizontal and vertical directions at signal combinations

of frequencies (30Hz or 100Hz) and acceleration (0.15g or 1g) was applied. Changes in cell density over 3-day proliferation were observed by the standard MTS assay and reported the normalized average-cell-density. To investigate the osteogenic differentiation, we observed ALP activities, calcification (by alizarin red assay) and gene expression levels of ALPL and Runx2. The GAPDH was selected to be housekeeping gene due to its stability and constant under observed conditions.

To observe dynamic changes in the physical structure of the cell and nucleus, and the interaction between neighboring cells under different LIV conditions, we determined changes in gene expression levels by the real-time PCR. To investigate physical interactions of the neighboring cell-cell and the cellular-nuclear structure, we observed structure-related genes (e.g. CDH11, ACTn1, Syne2). To evaluate potentials of the proposed mechanotransduction, these genes were associated with their molecular functional levels. We analyzed the effect of the LIV or non-LIV by statistic one-way ANOVA. The effect of frequency, acceleration and direction was analyzed by three-way ANOVA with the significance at $p \leq 0.05$.

3.2.2 Cell culture and Mechanical stimulation

3.2.2.1 Culture human bone marrow mesenchymal stem cells (hBMSCs)

hBMSCs were aspirated from bone marrow of 25 years old African American female patient (Life Technologies) tested negative HIVs. hBMSCs were cultured in alpha-MEM without phenol red containing 7.5% heat inactivated fetal bovine serum (Gibco), 5μM L-glutamine and specific growth factors of recombinant 15nM IGF-1 and 125pM FGF-β. To sustain properties under different environments, 1mM DTT (LifeLine D1532) and 0.1% BSA (Sigma A2058) were added to the stock solution of the growth factors. Since hBMSCs is very

sensitive to changes in pH and $\%CO_2$, we added 25 mM HEPES to preserve the pH at 7.4, and protected the cells with 1% penicillin/streptomycin.

3.2.2.2 Selected signal combination of low intensity vibration (LIV)

We selected signal combinations of frequency and acceleration from the highest to lowest fluid shear stress at 30Hz-1g, 100Hz-1g, 30Hz-0.15g, and 100Hz-0.15g, respectively. We vibrated cells in horizontal- and vertical- directions with non-vibrated cells as a control. Cells were vibrated in 2 sessions a day, for 20 minutes in each session, with 2-hour rest in between sessions as the loading cycles [Qin et al. 1998] and duration of vibration could control cell behaviors.

3.2.3 Cell viability by Live Dead assay

To test the cell viability, we used techniques of double stain of living cells with 2mM ethidium homodimer, Eth-D1 (Invitrogen L3224) and incubated at 37°C for 45 minutes, following by incubation with 4mM Calcein AM (Invitrogen L3224) for another 3 hours. We qualified the viable cells by fluorescent images (Zeiss Axio), where green represents living cells and red color is for dead cells. We quantified %living cells by flow cytometric analysis.

3.2.4 Cell proliferation

To observe the cell proliferation, we plated hBMSCs with low concentration of 7,500 cells/cm^2 on the day prior to the experimental day. We monitored cell density (cells/cm^2) using a standard spectrophotometric MTS assay (XTT reagent, ACTT) immediately after the second vibration of each combination, in every day, for 3 consecutive days. The second-generation

tetrazolium salt XTT reduced to its derivatives, when mixing with cellular surface effectors, and developed bright orange color that can be monitored by fluorescence absorption. The standard curve of known cell density (cells/cm^2) was established by plotting the cell density against the absolute specific absorbance [A_{475}], where [A_{475}] is the differences of specific absorbance at 475nm from the unspecific absorbance at 660nm between the sample and blank. The normalized averaged cell density, $[\delta] = \frac{averaged\ cell\ density,\left(\frac{cells}{cm^2}\right)_{LIV}}{averaged\ cell\ density,\left(\frac{cells}{cm^2}\right)_{non-LIV}}$, was reported. To ensure that LIV do no harm to inherent cellular behaviors, we observed doubling time over additional 10 consecutive days. The LIV proliferation exhibited doubling time within 1-2 days, similar to an early passage hBMSCs [Teixeira et al. 2010], indicating LIV did not change inherent characteristics of human cells.

3.2.5 Osteoblastogenic differentiation

Our proliferation showed that the hBMSCs expressed doubling time within 1-2 days for all LIV groups. To prevent cell proliferation interfering with cell differentiation, we plated cells 2 days prior to the experiment with cell density at 18,000 cells/cm^2. After 2 days of the first inoculation, the hBMSCs were induced with osteoblastogenic media containing 100nM dexamethasone, 10mM β-glycerol phosphate, and 0.05mM L-ascorbic acid-2-phosphate. The vibration was performed right after the osteoblastogenic induction. All observations were performed at the end of the second vibration on Day1, Day7, and Day14. The first day of osteoblastogenic induction was called Day1.

3.2.6 Alkaline phosphatase assay, [ALP]

Alkaline phosphatase activity is a standard estimation of ALP activity in μg/ml that presents in cells as an early marker for osteoblastogenic differentiation. 0.5mM p-nitrophenyl phosphate, p-NP (Sigma N7660) is a phosphatase substrate that turns yellow (λ_{max}= 405 nm) when dephosphorylated by the ALP. After the second vibration, hBMSCs were rinsed with sterilized distilled water before adding 75μl of 0.5mM p-NP, and after one hour, adding 0.2M NaOH to stop the reaction. The standard curve of an absorbance (A_{405}) of the known ALP concentration was established to estimate ALP activity (μg/ml). The average of ALP activity in each condition was n=6 for Day1 and Day7. The normalization of the averaged ALP activity, [ALP] was presented, $[\text{ALP}] = \frac{\text{averaged ALP activity},(\frac{\mu g}{ml})_{LIV}}{\text{averaged ALP activity},(\frac{\mu g}{ml})_{non-LIV}}$.

3.2.7 Western blot analysis

The samples were lysed to extract the protein using RIPA buffer (Sigma R0278) in ice-cold temperature. The protein concentration in each lysate was determined by standard BSA protein assay (BioRad). The protein lysates of all conditions were diluted to the same concentration (5μl/ml) before conjugation with primary ALP antibody and IgG secondary antibody. The 0.004% bromophenol blue and 10% DTT were added for each lysate. Electrophoresis of the running gel was performed at constant 350mAmp of 200volts for at least 2 hours or until seeing the protein separation. The running gel (30%Protogel) and buffer (pH 8.3) composed of 25mM Tris, 190mM Glycine and 0.1% SAS was prepared at least 24 hours prior to the experiment. The separated protein was then transferred to PVDF membrane with the transferring buffer in the electrophoresis at 200V for an hour. The transferred protein in PVDF

was then blotted in 5% fat-free milk of 50% BSA, Tween20 buffer at 4°C overnight. The next day, PVDF was washed several times with BSA-tween buffer before adding ALP conjugated primary antibody (1:2,000) in DMEM and rotation at low speed for 2 hours (in the dark). The secondary antibody IgG (Invitrogen A21109) and AlexaFlour680 were added and incubated for another 2 hours at 4°C. The chemiluminescence was developed in the dark room and Bio Rad detected the protein. From standard protein on the farthest left (Figure was not shown here.), ALP showed molecular weight at ~53K and H100Hz-0.15g showed the biggest band, confirming the best ALP activity.

3.2.8 Cellular calcification (μg/ml) by Alizarin red assay

After fixed cells with ice-cold 100% ethanol, cells were several rinsed with sterilized distilled ice-cold water (sd-H_2O). The fixed cells were then added in with 40mM Alizarin Red S (Sigma A5533) solution and incubated in the dark for 45 minutes at room temperature. The samples were then several washed with sd-H_2O before incubation with dPBS for another 15 minutes. Qualified cellular calcification by fluorescent images showed that horizontal LIV at 100Hz-0.15g exhibited the darkest red color (the highest calcification). The development of red color indicated progress in cellular calcification of hBMSCs (images were not showed).

To quantify calcification [Ca^{2+}] in μg/ml, the alizarin red-stained cells were then destained by 10% cetylpyridinium chloride, CPC (Sigma C0732) for 15 minutes in the dark at room temperature. The CPC was prepared following the standard protocols. The fluorescent absorbance at 562 nm was measured with 3 measurements for each well and each condition had 6 wells. The A_{562} was then compared to an established standard curve of known amount of

$[Ca^{2+}]$. The ratio of the averaged calcification of LIV with the control $[Ca^{2+}]_{CT}$ provides the normalized calcification $[Ca^{2+}]$, $[\frac{\text{averaged Calcification},(\frac{\mu g}{ml})_{LIV}}{\text{averaged Calcification},(\frac{\mu g}{ml})_{non-LIV}}]$.

3.2.9 Gene expression by real-time PCR

3.2.9.1 Justification of our selected housekeeping gene

We selected Glyceraldehyde 3-phosphate dehydrogenase (GAPDH) as the housekeeping gene and justified the selection by comparison the average expression level with 18S ribosomal RNA (18S), β_2-microgrobulin (B2M), β-actin (ACTβ) and Cyclophilin (Cyp). The analysis of stability (M) by NormFinder [Tan et al. 2012] validated that GAPDH was the most stable (the lowest M and constant at all different conditions).

3.2.9.2 Real-time PCR for gene expression (fold changes, $2^{-\Delta\Delta Ct}$)

We quantified gene expression by real-time PCR using TaqMan standard protocols with n=6 in each condition. The expression level was analyzed by the fold changes ($2^{-\Delta\Delta Ct}$) with respect to the control and the GAPDH. After vibration, these cells were lysed by TRIzol (Life Technologies) and the RNA extraction was done by phase separation with chloroform. The RNA was precipitated from nucleic acid by RNeasy (Qiagen) and washed with 70% ethanol before re-dissolving by RNA-free water. To quantify RNA concentration and determine the RNA quality, we used NanoDrop (ND-100 V3.3.0). The ratio of $[A_{260}/A_{280}]$ ≥1.8 is for 'pure' cDNA, and ≥2.0 for 'pure' RNA, validating by $[A_{260}/A_{230}]$ ~2.0-2.2 for 'pure' nucleic acid. Then, the RNA was cloned by the reversed transcriptase (Invitrogen) for cDNA conversion. After the determination of purification and concentration, cDNA was diluted to be the same

concentration (3.33ng/μl). Using StepOne 2.2, the real-time polymerase chain reaction (q-PCR) provided Ct of the interested genes for calculation of the gene expression level ($2^{-\Delta\Delta Ct}$).

3.2.9.3 Pooled cDNA for customized 96-gene array

To profile genes, we customized a 96-gene array. The RNA was reversed the transcription by the SyBrGreen master mix (BC3, LifeTechnologies). The cDNA dilution of n=6 at each condition was equally pooled into one. We compared the gene expression level of ACTn1, Akt1, ALPL, β-catenin, Bmp2, CDH11, COL1α1, FAK, FN1, PPARg, Runx2, Syne2, Sun2, Wnt10α including housekeeping genes (ACTβ and GAPDH) for both pooled and averaged data. The similarity of the expression trends confirmed the liability of the results and the array.

3.2.9.4 Cluster analysis of gene expression level

The cluster analysis is to qualitatively see gene expression into one profile [D'haeseleer et al. 2005]. By adding the raw Ct in the built-in template (SABioScience), relations of the interested genes can be plotted in a heat-diagram or clustergram. However, our customized array was not matched with the built-in template and the built-in program can only compare with the control at one-time point. With modified the heat diagram using MatLab, we were able to compare the data with the control at the specific time point. Qualitatively, the similar expression compared to the control is in bright green and the most difference is in red. In general, we found more red color in osteoblastogenesis and upregulated cytoskeletal and nuclear-related genes in the horizontal than in the vertical LIV.

3.2.9.5 Enrichment analysis by DAVID program (NIH)

The enrichment analysis is a mining tool that relates gene names by their functions and groups them into possible relations with statistic significance [Huang et al. 2009]. Although, the

the relation between these gene names was based on known pathway cascades that rely on cytokines, chemokine, or secreted proteins, the relation provided confident links of these genes. In Table 2.1, selective genes in our customized array were related together significantly in these categories; human mesenchymal stem cells, calcium and bone pathways, osteoblastogenesis, cell/actin/nuclear binding and cytoskeleton. Remarkably, we could predict the relation of these genes by adding the gene names and their up/down-expression levels in the table.

3.2.10 Flow cytometric analysis

The measurement of % cell populations by laser-based flow cytometric analysis relies on effective immunofluorescent staining and conjugated antibodies. We prepared samples by lifting the attached cells with 0.05% trypsin/EDTA. We performed immunofluorescent staining of living cells with (1) EtD1/CalceinAM for viability, (2) primary ACTn1 human monoclonal antibody (Santa Cruz sc-17829) and IgG, or (3) Phalloidin AlexaFluor594 (LifeTechonologies) to see cytoskeletons. To acquire the data, we set the % gated cells positive to specific immunofluorescence with at least 10,000 events and FlowJo analyzed the % cell population. We reported the normalized average %population as [%P] ($\frac{Averaged\ \%\ Population,LIV}{Averaged\ \%\ Population,non-LIV}$), n=6.

3.2.11 Statistic analysis

Statistic one-way analysis of variance, ANOVA (SPSS) with Tukey post hoc test analyzed the effect of LIV vs non-LIV. Each condition in each experiment was repeated at least n=6. Each experiment was at least duplicated. The results were statistically significant when $p < 0.05$, and p values were reported as *<0.05, **<0.01.

Effects of frequency, acceleration and direction on the proliferation (cell-density), ALP-activity, calcification and gene expression were analyzed by three-way ANOVA (MatLab syntax for N-way ANOVA, p = anovan(y, {g_1 g_2 g_3}) p, where g_n can be matrix). The gene relation to their functions was statically analyzed by DAVID, NIH program (Table 2.1).

3.3 Results

3.3.1 Frequencies Modulated Cell Proliferation

The fluorescence images (**Figures 3.1a and b**) qualitatively showed viable human cells under LIV and non-LIV (green color). Flow cytometric analysis quantitatively confirmed the similar %living cell in all vibrations (>99.7%±2% in LIV vs >99.2% ±3% in non-LIV), indicating no damage of human cells by LIV.

Normalizations of the averaged cell density [δ] of the 30Hz and 100Hz group were higher than the density of the control on Day1, Day2 and Day3 (**Figure 3.1c**). The signal combination of 100Hz-0.15g in horizontal LIV provided the highest cell density, implying that the LIV but not the fluid shear could induce the stem cell proliferation. The increment of [δ] over 3 days was increased in 100Hz groups (from ~2x to 3x) but decreased in 30Hz groups (from 1.7x to 1.5x). The different trend with different frequency suggested that the frequency not the direction could influence the stem cell proliferation (these significant differences confirmed by the statistic 3-way ANOVA).

3.3.2 Directions Influenced Osteoblastogenic Differentiation

The normalized [ALP] of LIV was ~2-3x higher than that of the control (confirmed by western blot analysis), (**Figure 3.2a**). The differences of $[ALP]_{Day7}$ - $[ALP]_{Day1}$ were much more

noticeable than the $[ALP]_{Day14}$ - $[ALP]_{Day7}$. The data confirmed that the ALP behaviors exhibited in the early osteogenic differentiation.

Quantitatively, the averaged normalized $[Ca^{2+}]$ of LIV was slightly higher than that of the control in the early days (>1.2x in Day1), (**Figure 3.2b**). However, $[Ca^{2+}]$ was much higher in the later days (>3x), supporting that the stem cell differentiated toward the functioning mature osteoblast. The data supported that the alizarin red assay can monitor the late commitment of the osteogenic differentiation. The normalized $[Ca^{2+}]$ of the horizontal LIV prominently increased from Day7 to Day14, indicating a significant effect of the direction on functioning mature osteoblasts.

The fluorescent images of alizarin red assay of samples were presented in the **Appendex A, Figures A2 and A3**.

3.3.3 Transcriptional Changes and Gene Expression

The averaged ALPL and Runx2 gene expression level in the LIV group was overexpressed (**Figures 3.3a and b**). The overexpressed ALPL and Runx2 confirmed the improved cellular function of the elevated ALP activity and the increased calcification in the LIV above the non-LIV. The upregulation of the averaged ALPL gene expression was higher than the control (~>2-4 ± 0.2 folds) and the highest expression was at the hLIV-100Hz-0.15g (**Figures 3.3a**). Similarly, the pooled data showed the higher gene expression in the LIV group. The ALPL levels under 100Hz provided higher upregulated folds (~3–4x) than that of 30Hz (~2–3x). The horizontal LIV expressed the ALPL 2x folds more than the vertical LIV.

We confirmed the expression of ALP by the western blot (**Figure A1**).

The averaged Runx2 expression levels were upregulated (~2–3 folds ±0.03–0.07) in all vibration groups. Additionally, the Runx2 overexpression in the horizontal LIV was ~2x higher than the vertical groups (**Figure 3.3b**). Higher frequencies in 100Hz groups provided a better upregulated fold (>2x) than that in the 30Hz groups.

To make sure we selected a proper housekeeping gene for our experiment, we tested stability of 5 housekeeping genes: 18S, β_2-microgrobulin, ACTb, GAPDH, and cyclophillin (**Figures A4-A9**). We found that the GAPDH is the most stable in all LIV conditions (**Figures A4, and A8**).

Gene profiles by cluster analysis (**Figure A10**) found that the genes related osteogenic differentiation and the gene related structural dynamics exhibited strong overexpression levels under the LIV. The changes in cellular and nuclear structures showed a strong involvement in the osteogenic differentiation.

Enrichment analysis (**Table 3.1**) provided a statistic confidence in the relation of genes with one another and with their functions. The gene related osteogenic differentiation (e.g. ALPL, Bmp2, Runx2, Wnt10α, **Figure A11**) was upregulated. Similarly, the structure related genes of cytoskeletal and nuclear genes (e.g. ACTn1, Syne2, Sun2) were upregulated. With upregulated ACTn1, the Whamm related cytoskeletal remodeling was significantly upregulated. An overexpression of Whamm was known as a nucleation-promoting factor like WASp, and binding to Arp2/3 complexes during the cellular dynamics with upregulated Rho family [Gad et al. 2012]. The upregulated Whamm with ACTn1 could support that the cytoskeletal function improved with the dynamic change in the cellular structure during the LIV. These data could verify that the physical interaction between the cellular and nuclear structures were well involved in the mechanotransduction pathway.

3.3.4 Structural Changes and Interactions Incorporated Mechanotransduction

The function-related gene Whamm of the pooled data was the most upregulated level in the H100Hz-0.15g (**Figure 3.4a**), suggesting that the LIV influenced the cytoskeletal remodeling. The increased overexpression of Whamm in the horizontal LIV and the 100Hz group was ~2-4x more than that of the vertical LIV and the 30Hz group.

Identically following the trend of Whamm, the averaged gene expression level of the structure-related gene ACTn1 was upregulated in the H100Hz-0.15g (**Figure 3.4b**). Similarly, the pooled data of the horizontal LIV groups provided ~2-6x higher upregulation than the vertical groups. These data suggested a strong connection of the cytoskeletal f-actin and the remodeling with the mechanotransduction pathway.

Our data showed that the up-regulated nesprin2 and sun2 were significant and synchronized with the overexpressed cytoskeletal f-actins. So, we used Syne2 and sun2 to monitor the NuAnCE-LiNC. The adherent junction (CDH11), cytoskeleton and binding actinin (ACTn1), Nucleoskeletal Syne2 and Sun2 expression levels were upregulated in all vibration groups (**Figure 3.5a**). The increment of the ACTn1 and Syne2 expression level was drastically changed from Day1 to Day7 (was >3-5 folds different). The data could verify that the LIV could cause changes in the cellular and nuclear structures. Interestingly, the increased pattern of the cytoskeleton was similar to the nucleoskeletons as upregulated ACTn1 increasing Syne2.

To see the effect of the competitive mechanisms of the other differentiated lineages, we calculated the ratio of the Sox9 to Runx2 expression levels, $[\frac{2^{-\Delta\Delta Ct,\mathrm{Sox9}}}{2^{-\Delta\Delta Ct,\mathrm{Runx2}}}]$. The data showed that

all LIV groups had the ratio less than 1. These data indicated that the competitive osteochondocytogenesis could not disturb the osteogenic differentiation during the LIV.

To confirm the relation of these genes, we additionally used techniques of antibody immunofluorescence staining with the secondary conjugation. Flow cytometric analysis of the % cytoskeletal f-actins conjugated with ACTn1 antibody was equivalent to %population positive to the Phalloidin594 staining in all LIV groups (Figure was not shown here). These data confirmed that the ACTn1 well represented the cytoskeletal f-actins including cytoskeletal bundles and binding actinin. The normalized averaged %positive population, [%P], of CDH11, ACTn1 and Syne2 on Day1 was increased in all LIV groups (**Figure 3.5b**). The horizontal LIV at 100Hz-0.15 exhibited >~2x higher than the [%P] of the control. The data showed the analogous pattern of the increasing [%P] of CDH11 and Syne2 with the ACTn1 in all LIV groups.

We found that both ECM1 and FAK were upregulated under the LIV (**Figure 3.6 and Figure A12**) but at least >3 folds less than the ACTn1. The data suggested that the strong impact of the physical structure but not only kinases could influence the gene expression related mechanotransduction. The Bmp2, Wnt10a, b-catenin, PI3K and Akt1 were upregulated (>2.5folds) but the SMAD1 and PPARg were down regulated as if the PI3K controlled Akt1 to suppress SMAD1, causing down-regulated PPARg similarly to the non-canonical Wnt (**Figure A11**). These profile expressions could suggest the mechanotransduction pathway toward more accurate based on the physical interaction of structures in the cell and the nucleus.

3.4 Discussion

We investigated gene expression of hBMSCs during proliferation and differentiation under the LIV. The relation of changes in cellular and nuclear structures related genes was profiled and included into the mechanotransduction pathway. During the stem cell proliferation, the averaged cell density of hBMSCs increased with the frequency, but not acceleration. During early osteogenic differentiation, ALP activity that was confirmed by the upregulated ALPL gene expression level was increased with frequency and direction. Similarly, Runx2 confirming the alizarin calcification in the late differentiation was overexpressed more prominently with the LIV direction. The data indicated that hBMSCs could sense the frequency during the proliferation while sensing the direction during the osteogenic differentiation. The structure-related gene of cytoskeletal f-actin binding proteins (ACTn1) was upregulated with an overexpression of the nucleoskeleton (Syne2 and Sun2). The data could provide the relation of the cytoskeletal f-actin anchoring NuAnCE-LiNC. Interestingly, the differences in gene expression of the early days were much more noticeable than in the latter days.

Our date may suggest that the changes in the cellular and nuclear structures in an early differentiation could involve the drastic structural changes from the hBMSC to the pre-osteoblast. However, a more gradual change of the structure in the late differentiation could involve the development of the molecular functions of the pre-osteoblast to the calcified osteoblast bone cell. Therefore, the structural changes in the cell and nucleus significantly influenced the gene expression. The relation of these genes could provide the physical interaction based mechanotransduction pathway that has been overlooked in the commonly known signaling pathway.

A limitation of this study was that some certain cellular and nuclear structures have not been yet identified. As examples of the NuAnCE-LiNC, it has been acceptable to use nesprins and suns in the representation of these nucleoskeletal complexes [Lombardi et al. 2011]. The connection of such structure-related genes with their potential functions in DAVID could only be speculated relying on the known protein-synthesis-based signaling pathways. The gene expression depends on the protein synthesis mechanism, which is time sensitive, and the activated or inactivated protein synthesis can cause complications in determining gene levels [Kadauke et al. 2009]. Overall cellular behaviors like alkaline phosphate activities [ALP] and calcification [Ca^{2+}] could represent the temporal molecular changes through accumulations or subtractions of the subtle dynamic spatial changes [Serafini et al. 2014]. The end results could only represent slight differences, often causing incomparable with the regional gene expression.

3.4.1 Human stem cells sense frequency of LIV

The proliferation of human bone marrow MSCs under the LIV stimulation was agreeable with our previous data (in human adipose derived MSCs [Uzer et al. 2014], murine MSCs, and macrophages). The similarity suggested that both human and animal cells of any sizes could sense the LIV. Importantly, the averaged cell density in 100Hz-groups was much higher than that of the 30Hz groups, indicating that hBMSC cells could sense the high frequency during their proliferation.

The interesting question was that how human and animal cells with different types and sizes could comparably sense the high frequency. One possibility could be that the force through

the frequency could affect the cell and nucleus. All cells are composed of the cytoplasm that is less rigid than the nucleus. The MC3T3-E1 differentiated osteoblasts showed that the nucleus was >3 times more rigid than the cytoplasm [Bacabac et al. 2006]. From this estimation, if we used the Stokes-Einstein relation to model the force, we could estimate the force that nucleus might perceive during the oscillation. The maximal force at the nucleus can be directly dependent on the frequency at ω^2 (, where frequency=$\omega/2\pi$). This estimation could possibly answer that the human stem cell could respond well with the high frequency due to this frequency dependent force at the nucleus.

3.4.2 LIV Direction Modulated Gene Expressions of the Underlying Pathway

The ALPL and Runx2 gene expression level was upregulated with the increased ALP activity and the alizarin calcification in all LIV groups. The upregulated ALPL gene expression could confirm the temporal ALP activity behavior in an early progressive osteogenic differentiation [Prins et al. 2014]. The increasing alizarin calcification [Ca2+] confirmed the osteoblast functioning to deposit the calcium [Okura et al. 2014] and the commitment of the mature osteoblast [Wang et al. 2006]. These data supported that the LIV advanced the stem cell osteogenic differentiation and improved the functioning mature osteoblast.

Additionally, the upregulated ALPL and Runx2 of the horizontal LIV was much higher than that of the vertical group. These data could indicate that the hBMSCs could sense the different directions during their osteogenic differentiation. Here, the data were for the first able

to separate the specific mechanical signal that hBMSCs could sense during the proliferation and the osteogenic differentiation.

In living bone tissue, the Runx2 transcription factor found to control not only the osteogenic differentiation, but also the overall calcification [Benjamin et al. 2004]. Though, pathways regulating Runx2 remain unclear [Franceschi et al. 2003]. Our data showed that the Runx2 was upregulated corresponding with the upregulated cytoskeleton and confirmed by the flow cytometric analysis. The data could provide strong possible relations of the cytoskeleton regulated Runx2. Surprisingly, hBMSC proliferation and calcification cultured in the 3D honeycomb scaffolds of biocompatible polylactic acid (PLA) showed similar patterns to the 2D in vitro across the vibration condition. The similar trend of our data in 2D and 3D (**Figure A24**) could imply the similar mechanism of the signal transduction [Tong et al. 2013].

3.4.3 Mechanotransduction is based on cellular and nuclear interactions

During osteogenic differentiation, the CDH11, ACTn1, and Syne2 were found up-regulated with overexpressed Runx2. The overexpressed CDH11 found to involve in the β-catenin/Wnts activating Rho families [Wang et al. 2012], and during the n-cadherin connecting the cytoskeleton via the vinculin and talin at the cell basement membrane [Yao et al. 2014]. During the Wnts upregulated RhoA, the cytoskeletal bundles could form to overexpress ACTn1 under the mechanical stress [Arnsdorf et al. 2009, Cawthorna et al. 2012]. During LIV upregulated CDH11 and ACTn1, the adherent junction formed a mature junction with the cytoskeleton as a direct connection from the outer cell membrane to the cytoplasm. During the

upregulated ACTn1, Syne2, and Sun2 were upregulated. The nesprin2 has been found to physically connect with the sun molecules by bridging the giant molecule called NuAnCE-LiNC [Rothballer et al. 2013]. To maintain nuclear integrity during the dynamic LIV, the cytoskeleton could activate the nesprin2 to bridge the giant molecule. The cytoskeleton anchoring the nuclear structure could form the physical connection across the double nuclear membrane without the nuclear deformation. By connecting the cellular and nuclear structures with the gene expression change related their functions, the mechanotransduction pathway could be identified as CDH11-ACTn1-Syne2.

To prove the existing of the proposed mechanotransduction pathway, we further used the underlying pathway to predict the gene expression and interpret the related function. The mechanotransduction could start when the hBMSCs sensed the direction of the interaction of the adherent junction between neighboring cells. Subsequently, the cytoskeletal orientation connecting with the mature junction could anchor the nucleoskeleton throughout the nucleus.

For example, several studies believed that the pathway controlling the MSC osteogenic differentiation started from the substrate to the extracellular matrix (ECM). The activated ECM could then stimulate the integrin (ITGα5) at the cell basement. The integrin ITGα5 linked to the FAK kinase could induce the adhesion protein (α5β1) activating the cytoskeleton and the collagen type 1 (COL1α1) via upregulated Akt/Rho [Wang et al. 2013]. From this assumption, the ECM-upregulated FAK with the FAK-upregulated Akt/RhoA has been widely thought as the completed mechanotransduction [Ng et al. 2014].

However, if the mechanotransduction was via the FAK acting mechanical effector, the upregulated FAK should be prominent. Our data showed that the upregulated FAK, ECM, Akt and RhoA was increased much less than the overexpressed ACTn1 and COL1α1 (**Figure A12**).

Our data supported that something else could substantially influence the expression levels [Engl et al. 2014]. It could be that the well-known cytokine-related FAK-Akt-Rho pathway could omit the actual mechanisms of the physical connection of the cellular and nuclear structures. Therefore, our proposed mechanotransduction pathway of the CDH11-ACTn1-Syne2 provided sufficient interpretation and prediction of the gene expression.

We profiled the gene expression of structure related gene with their functions. We could propose the potential pathway for the cytoskeletal regulation (**Figure A13**) and the calcification pathway (**Figure A14**). The growth factors (FGFs) and integrin (ITGs) could be activated during LIV and upregulated PI3K to stimulate Rock/RhoA in polymerization of actins (Figure A13). During LIV, The stem cell could release the excess energy from the stimulation through the enery consumption of ATP (Figure A14). The losen phophates were then deposited in collagen, causing the upregulated ALP. The progressive phosphate deposition in collagen was increased with the upregulated SPP1 and IBSP.

3.5 Conclusion

This work demonstrates that the expression of several cellular- and nuclear- structure related genes is upregulated during the LIV. The data indicate strong involvements of the physical structure in the gene expression and transcriptional levels toward the mechanotransduction pathway. The gene expression profile and cellular behaviors of different signal combinations and directions define specific mechanical signals that hBMSCs sense. Although the majority of these genes is known, their cellular functions related molecular characterizations remain novel. Analyzes of gene expressions evaluate the proposed mechanisms of changes in the physical structures of human bone marrow stem cells modulating the mechanotransduction under LIV. The information on cellular and molecular mechanisms definitely provides great insights as the first step toward determining physiological stages of mammalian bone adaptive to the mechanical stimulation.

References

Alves RD, Demmers JA, Bezstarosti K, van der Eerden BC, Verhaar JA, Eijken M, van Leeuwen JP. '*Unraveling the human bone microenvironment beyond the classical extracellular matrix proteins: a human bone protein library*.' J Proteome Res. **2011**, 10 (10): 4725-33. doi: 10.1021/pr200522n. Epub 2011 Sep 21.

Arnsdorf EJ, Tummala P, Jacobs CR. '*Non-Canonical Wnt Signaling and N-Cadherin Related β-Catenin Signaling Play a Role in Mechanically Induced Osteogenic Cell Fate*'. PLoS ONE **2009**, 4(4): e5388. doi:10.1371/journal.pone.0005388

Benjamin A. Byers BA, García AJ. '*Exogenous Runx2 Expression Enhances in Vitro Osteoblastic Differentiation and Mineralization in Primary Bone Marrow Stromal Cells'*. Tissue Eng. **2004**, 10 (11-12): 1623-1632. doi:10.1089/ten.2004.10.1623.

Cawthorna WP, Breea AJ, Yaoa Y, Dua B, Hematia N, Martinez-Santibañezc G, MacDougald OA. 'Wnt6, Wnt10a and Wnt10b inhibit adipogenesis and stimulate osteoblastogenesis through a β-catenin-dependent mechanism'. Bone. **2012**, 50 (2): 477–489. doi:10.1016/j.bone.2011.08.010.

Choi SC, Kim SJ, Choi JH, Park CY, Shim WJ, Lim DS. '*Fibroblast Growth Factor-2 and -4 Promote the Proliferation of Bone Marrow Mesenchymal Stem Cells by the Activation of the PI3K-Akt and ERK1/2 Signaling Pathways*'. Stem Cells and Development. **2008**, 17(4): 725-736. doi:10.1089/scd.2007.0230.

D'haeseleer P. '*How does gene expression clustering work?*' Nature Biotech. **2005**, 23: 1499 – 1501. doi:10.1038/nbt1205-1499.

Edlund S, Landström M, Heldin CH, Aspenström P. '*Transforming growth factor-beta-induced mobilization of actin cytoskeleton requires signaling by small GTPases Cdc42 and RhoA*.' Mol Biol Cell. **2002**, 13(3): 902-914.

Engl W, Arasi B, Yap LL, Thiery JP, Viasnoff V. '*Actin dynamics modulate mechanosensitive immobilization of cadherin at adherens junctions*'. NATURE CELL BIOL. 2014, 16: 584-591. doi:10.1038/ncb297.

Franceschi RT, Xiao G, Jiang D, Gopalakrishnan R, Yang S, Reith E. '*Multiple Signaling Pathways Converge on the Cbfa1/Runx2 Transcription Factor to Regulate Osteoblast Differentiation*'. Connect Tissue Res. **2003**, 44 (1): 109–116.

Gad AK, Nehry V, Ruusala A, Aspenström P. '*RhoD regulates cytoskeletal dynamics via the actin nucleation-promoting factor WASp homologue associated with actin Golgi membranes and microtubules.*' Mol Biol Cell. **2012**; 23(24): 4807-19. doi: 10.1091/mbc.E12-07-0555.

Hampton CM, Taylor DW, Taylor KA. '*Novel Structures for α-Actinin: F-Actin Interactions and their Implications for Actin–Membrane Attachment and Tension Sensing in the Cytoskeleton*'. J Mol Biol. **2007**, 368 (1): 92–104.

Hart MJ, de los Santos R, Albert IN, Rubinfeld B, Polakis P, '*Downregulation of* β*-catenin by human Axin and its association with the APC tumor suppressor,* β*-catenin and GSK3*β'. Current Biology. **1998**, 8: 573–581. doi: 10.1016/S0960-9822(98)70226-X

Hata K, Nishimura R, Yamashita K, Matsubara T, Nokubi T, Yoneda T. '*Differential roles of Smad1 and p38 kinase in regulation of peroxisome proliferator-activating receptor gamma during bone morphogenetic protein 2-induced adipogenesis'.* Mol Biol Cell. **2003**, 14 (2): 545-555.

Huang DW, Sherman BT, Lempicki RA. '*Systematic and integrative analysis of large gene lists using DAVID Bioinformatics Resources*'. Nature Protoc. **2009**; 4 (1): 44-57.

Huang DW, Sherman BT, Lempicki RA. '*Bioinformatics enrichment tools: paths toward the comprehensive functional analysis of large gene lists*'. Nucleic Acids Res. **2009**; 37 (1): 1-13.

Huveneers S, de Rooij J. '*Mechanosensitive systems at the cadherin-F-actin interface*.' J Cell Sci. **2013**, 126: 1-11. doi: 10.1242/jcs.109447.

Kadauke S, Blobel GA. '*Chromatin loops in gene regulation: Review*'. Biochimica et Biophysica Acta - Gene Regulatory Mechanisms. **2009**, 1789 (1): 17-25. doi: 10.1016/j.bbagrm.2008.07.002

Kushwaha P, Khedgikar V, Gautam J, Dixit P, Chillara R, Verma A, Thakur R, Mishra DP, Singh D, Maurva R, Chattopadhyay N, Mishra PR, Trivedi R. '*A novel therapeutic approach with Caviunin-based isoflavonoid that en routes bone marrow cells to bone formation via BMP2/Wnt-β-catenin signaling*'. Cell Death Differ. **2014**, 5e1422. doi:10.1038/cddis.2014.350

Libotte T., Zaim H., Abraham S., Padmakumar V.C., Schneider M., Lu W., Munck M., Hutchison C. Wehnert M., Fahrenkrog B., Sauder U., Aebi U., Noegel A.A., Karakesisoglou, L. '*Lamin A/C–dependent Localization of Nesprin-2, a Giant Scaffolder at the Nuclear Envelope*' Mol Biol Cell. **2005**, 16 (7): 3411–3424. doi: 10.1091/mbc.E04-11-1009 PMCID: PMC1165422

Lombardi M.L., Jaalouk D.E., Shanahan C.M., Burke B., Roux K.J., Lammerding J. *'The Interaction between Nesprins and Sun Proteins at the Nuclear Envelope Is Critical for Force Transmission between the Nucleus and Cytoskeleton'.* J Biol Chem. **2011**; 286 (30): 26743–26753 doi: 10.1074/jbc.M111.233700 PMCID: PMC3143636

Malone AMD, Batra NN, Shivaram G, Kwon RY, You L, Kim CH, Rodriguez J, Jair K, Jacobs CR. '*The role of actin cytoskeleton in oscillatory fluid flow-induced signaling in MC3T3-E1 osteoblasts'.* Am J Physiol - Cell Physiol. **2007**, 292 (5): C1830-C1836. doi**:**10.1152/ajpcell.00352.2005

Mathieu PS., Loboa EG. '*Cytoskeletal and focal adhesion influences on mesenchymal stem cell shape, mechanical properties, and differentiation down osteogenic, adipogenic, and chondrogenic pathways***.** Tissue Eng Part B Rev. **2012**, 18(6):436-44. doi: 10.1089/ten.TEB.2012.0014. Epub 2012 Aug 6.

Meinke P, Mattioli E, Haque F, Antoku S, Columbaro M, Straatman KR, Worman HJ, Gundersen GG, Giovanna Lattanzi G, Wehnert M, Shackleton S. '*Muscular Dystrophy-Associated SUN1 and SUN2 Variants Disrupt Nuclear-Cytoskeletal Connections and Myonuclear Organization*'. PLoS Genet. **2014**, 10 (9): e1004605. doi:10.1371/journal.pgen.1004605

Metcalfe C, Bienz M. '*Inhibition of GSK3 by Wnt signalling – two contrasting models*'. J Cell Sci. **2011**, 124: 3537–3544.

Ng CP, Sharif AR, Heath DE, Chow JW, Zhang CB, Chan-Park MB, Hammond PT, Chan JK, Griffith LG. '*Enhanced ex vivo expansion of adult mesenchymal stem cells by fetal mesenchymal stem cell ECM*.' Biomaterials. **2014**, 35 (13): 4046-4057. doi: 10.1016/j.biomaterials.2014.01.081. Epub 2014 Feb 21.

Okura H, Sato S, Kishikawa S, Kaneto S, Nakashima T, Yoshida N, Takayanagi H, Kiyono H. '*Runx2-I Isoform Contributes to Fetal Bone Formation Even in the Absence of Specific N-Terminal Amino Acids*'. PLoS ONE. **2014**, 9(9): e108294. doi:10.1371/journal.pone.0108294

Ozcivici E, Luu YK, Adler B, Qin YX, Rubin J, Judex S, Rubin CT. '*Mechanical signals as anabolic agents in bone*'. Nat. Rev. Rheumatol. **2010**; 6: 50–59. doi:10.1038/nrrheum.2009.239.

Palsgaard J, Emanuelli B, Winnay JN, Sumara G, Karsenty G, Kahn CR. '*Cross-talk between Insulin and Wnt Signaling in Preadipocytes: Role of protein-5 (LRP5) Lipoprotein Receptor-Related WNT co-receptor low density*'. J. Biol. Chem. **2012**, 287: 12016-12026. doi: 10.1074/jbc.M111.337048

Prins HJ, Braat AK, Gawlitta D, Dhert WJA, Egan DA, Tijssen-Slump E, Yuane H, Coffer PJ, Rozemuller H, Martens AC. '*In vitro induction of alkaline phosphatase levels predicts in vivo bone forming capacity of human bone marrow stromal cells*'. Stem Cell Res. **2014**, 12: 428–440.

Potier E, Noailly J, Ito K. *'Directing bone marrow-derived stromal cell function with mechanics'*. J Biomech. **2010**; 43(5): 807-17. doi: 10.1016/j.jbiomech.2009.11.019.

Qin YX, Rubin CT, McLeod KJ, '*Nonlinear dependence of loading intensity and cycle number in the maintenance of bone mass and morphology.*' J Orthop Res. **1998**, 16: 482-489.

Reddy P, Deguchi M, Cheng Y, Hsueh AJW. *'Actin Cytoskeleton Regulates Hippo Signaling'*. PLoS ONE **2013**, 8(9): e73763. doi:10.1371/ journal.pone.0073763

Rothballer A, Kutay U. '*The diverse functional LINCs of the nuclear envelope to the cytoskeleton and chromatin*'. Chromosoma **2013**, 122: 415–429. Doi: 10.1007/s00412-013-0417-x

Schaller MD. '*Cellular functions of FAK kinases: insight into molecular mechanisms and novel functions*'. J Cell Sci. **2010**, 123 (7): 1007-1013. doi:10.1242/jcs.045112

Serafini M, Sacchetti B, Pievani A, Redaelli D, Remoli C, Biondi A, Riminucci M, Bianco P. '*Establishment of bone marrow and hematopoietic niches in vivo by reversion of chondrocyte differentiation of human bone marrow stromal cells*'. Stem Cell Res. **2014**, 12(3): 659–672.

Sjöblom B, Salmazo A, Djinović-Carugo K. '*Alpha-actinin structure and regulation*.' Cell Mol Life Sci. **2008**, 65 (17): 2688-701. doi: 10.1007/s00018-008-8080-8.

Shen QT, Hsiue PP, Sindelar CV, Welch MD, Campellone KG, Wang HW. '*Structural insights into WHAMM-mediated cytoskeletal coordination during membrane remodeling*'. J Cell Biol. **2012**, 199 (1): 111–124. doi: 10.1083jcb.201204010

Stricker J, Falzone T, Gardel ML. J Biomech. '*Mechanics of the F-actin cytoskeleton.'* **2010**, 43 (1): 9-14. doi:10.1016/j.jbiomech.2009.09.003. Epub 2009 Nov 13.

Tan SC, Carr CA, Yeoh KK, Schofield CJ, Davies KE, Clarke K. '*Identification of valid housekeeping genes for quantitative RT-PCR analysis of cardiosphere-derived cells preconditioned under hypoxia or with prolyl-4-hydroxylase inhibitors*'. Mol Biol Rep **2012**; 39:4857–4867. doi: 10.1007/s11033-011-1281-5

Tapley EC, Starr D. '*Connecting the nucleus to the cytoskeleton by SUN-KASH bridges across the nuclear envelope*'. Curr Opin Cell Biol. **2013**; 25(1): 57–62. doi: 10.1016/j.ceb.2012.10.014. PMCID: PMC3578026. NIHMSID: NIHMS417735

Teixeira CC, Liu Y, Thant LM, Pang J, Palmer G, Alikhani M. '*Foxo1, a novel regulator of osteoblast differentiation and skeletogenesis*'. J Biol Chem. **2010**, 285 (40): 31055-31065. doi: 10.1074/jbc.M109.079962. Epub 2010 Jul 22.

Thompson WR, Rubin CT, Rubin J. '*Mechanical regulation of signaling pathways in bone*'. Gene **2012**, 503: 179–193. doi:10.1016/j.gene.2012.04.076

Thompson WR, Yen SS, Rubin J. '*Vibration therapy: clinical applications in bone*'. Curr Opin Endocrinol Diabetes Obes. **2014** 21 (6): 447-53. doi: 10.1097/MED.0000000000000111.

Triplett JW, Pavalko FM. '*Disruption of alpha-actinin-integrin interactions at focal adhesions renders osteoblasts susceptible to apoptosis*'. Am J Physiol Cell Physiol. **2006**, 291: C909 –C921.

Tong Z, Duncan RL, Jia X. '*Modulating the Behaviors of Mesenchymal Stem Cells Via the Combination of High-Frequency Vibratory Stimulations and Fibrous Scaffolds*' Tissue Eng Part A. **2013**, 19(15-16): 1862-1878. doi: 10.1089/ten.TEA.2012.0694

Uzer G., Manske SL., Chan ME., Chiang FP., Rubin CT., Frame MD., Judex S. '*Separating Fluid Shear Stress from Acceleration during Vibrations in Vitro: Identification of Mechanical Signals Modulating the Cellular Response*'**.** Cell Mol Bioeng. **2012**, 5 (3): 266-276.

Uzer G., Pongkitwitoon S., Chan ME., Judex S. '*Vibration induced osteogenic commitment of mesenchymal stem cells is enhanced by cytoskeletal remodeling but not fluid shear'*. J Biomech. **2013**, 46 (13): 2296-302. Epub 2013 Jul 17.

Uzer G., Pongkitwitoon S., Cheng I., Thompson WR., Rubin J., Chan ME., Judex S. '*Gap junctional communication in osteocytes is amplified by low intensity vibrations in vitro'*. PLoS One **2014**, 9 (3): e90840. Epub 2014 Mar 10.

Wang YK, Chen CS. '*Cell adhesion and mechanical stimulation in the regulation of mesenchymal stem cell differentiation'*. J Cell Mol Med. **2013**, 17 (7): 823-832. doi: 10.1111/jcmm.12061. Epub 2013 May 15

Wang YH, Liu Y, Maye P, Rowe DW. '*Examination of Mineralized Nodule Formation in Living Osteoblastic Cultures Using Fluorescent Dyes*'. Biotechnol Prog. **2006**, 22 (6): 1697–1701. doi: 10.1021/bp060274b

Wang YK, Yu X, Cohen DM, Wozniak MA, Yang MT, Gao L, Eyckmans J Chen CS. '*Bone morphogenetic protein-2-induced signaling and osteogenesis is regulated by cell shape, RhoA/ROCK, and cytoskeletal tension.*' Stem Cells Dev. **2012**, 21(7): 1176-1186. doi: 10.1089/scd.2011.0293. Epub 2011 Oct 3.

Yao M, Goult BT, Chen H, Cong P, Sheetz MP, Yan J. '*Mechanical activation of vinculin binding to talin locks talin in an unfolded conformation*'. Nature Sci Rep. **2014**, 4: 4610. doi: 10.1038/srep04610.

Yonemura S. '*Cadherin-actin interactions at adherent junctions*'. Curr Opin Cell Biol. **2011**, 23(5): 515-22. doi: 10.1016/j.ceb.2011.07.001. Epub 2011 Jul 30.

Zhen YY, Libotte T, Munck M, Noegel AA, Korenbaum E. '*NUANCE, a giant protein connecting the nucleus and actin cytoskeleton'*. J Cell Sci. **2002**, 115(15): 3207-3222.

Zhou G, Zheng Q, Engin F, Munivez E, Chen Y, Sebald E, Krakow D, Lee B. '*Dominance of SOX9 function over RUNX2 during skeletogenesis.'* Proc Natl Acad Sci. **2006**, 103 (50): 19004-19009.

Tables

Table 3.1: Enrichment analysis of genes in our customized 96-gene array showed that genes in the array were related to functions with statistic significance. By adding related gene names and their up/down-regulation levels, we could surprisingly predict any connections of structure-related gene expression levels with their functions, confirming physical interactions incorporated mechanotransduction.

Table 3.1: Enrichment analysis of genes in 96 gene array showed functional genes relative to the whole array with acceptance more than 95% confidence.

Functions	-regulated	Related Genes	p-Value
Human bone marrow MSCs and Osteoblasts related-			
Biomineralization, Calcium binding, Osteogenesis, Differentiation, Bone	Up	ALPL, BGLAP (osteocalcin), COLa1a, IBSP, SPP1 (Osteopontin), SP7 (Osterix), Runx2	4-9.8E-06
Angiogenesis	Up	VEGF	2.80E-04
Duplication and Cell Division	Up	CDC42, GDF10	4.80E-03
	Down	CSF-1	
Bmp/Wnt signaling pathway	Up	Bmp2, (BMP4, BMP7 mild up then decreased), b-Catenin (CTNNb1), Wnt10a, FrZB, FZD1, Runx2	1.20E-07
	Down	SMAD1, SMAD4	
Adipogenesis	Down	Adipoq, FAbP4, PPARD, PPARg, RSPO1, SOST, UCP1 (related to brown MSCs)	5.30E-08
Signaling Cytokine	Up	GJA1, (Akt1 mild up), PI3K	1.9-2.6E-09
	Down	PTK2, STAT3	
Growth factor	Up	(FGF1, FGF2, IGF1, TGF-b mild up), VEGF	6.80E-10
	Down	FGF23	
Cytoskeleton or Nucleus related-			
Cell binding, Cell adhesion	Up	CDH11, COL1a1, ECM1, FN1, (ICAM1, LrFN5, PDGFRL mild)	3.4-6.9E-02
Actin-binding, Collagen binding	Up	ACTn1, ACTβ, CDH11, COL1a1, RhoA, ROCK	2.8-6.7E-03

Cytoskeleton	Up	ACTn1, TLN1 (talin), TUBB3 (tubulin), WHAMM	3.40E-03
Nuclear-binding	Up	LAMA1, Syne1, Syne2, Sun1, Sun2	5.80E-02
Extracellular matrix	Up	ECM1	2.30E-06
Membrane and Integrin related-			
Cell membrane, Integrin	Up	IBSP, ITGav, ITGa5, ITGb3	1.6-5.6E-02
Activities and Energy related-			
Energy (Acetylation, Methylation)	Up	CREB1, CREBBP, NADPH, PAK1	7.30E-02
Inflammatory	Down	PTK2, TNF, TNFSF11, TRAF6, TRAF3IP2	5.60E-02

Figure 3.1a:

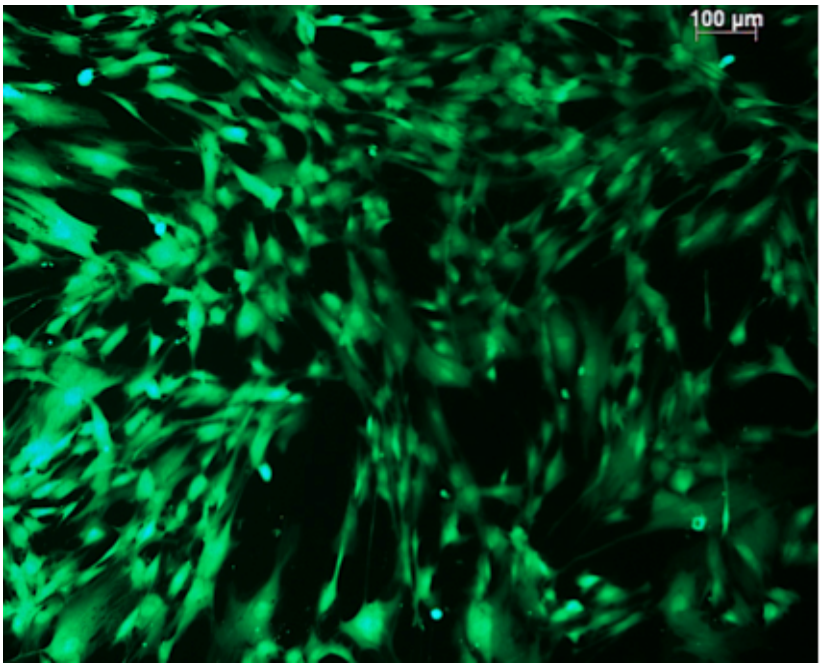

Figure 3.1b:

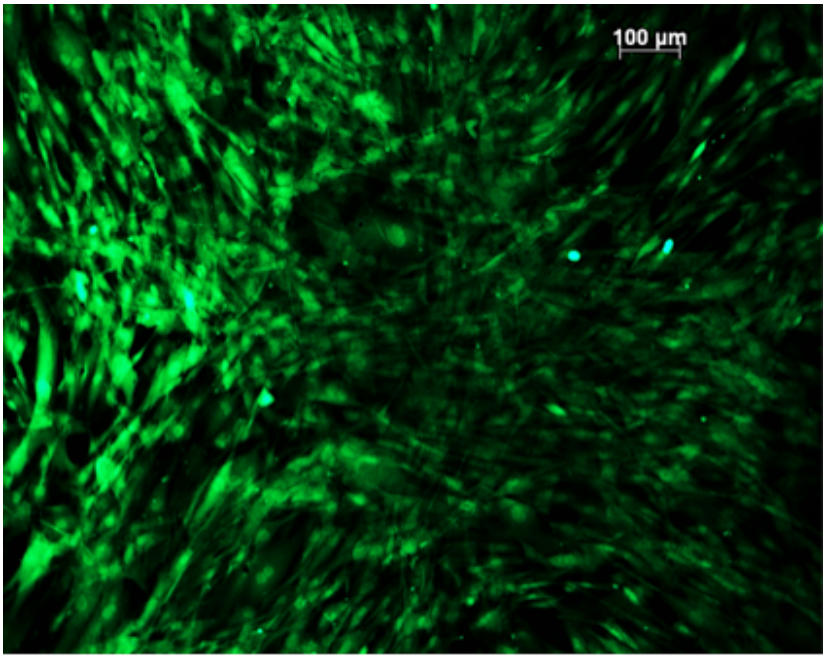

Figure 3.1c:

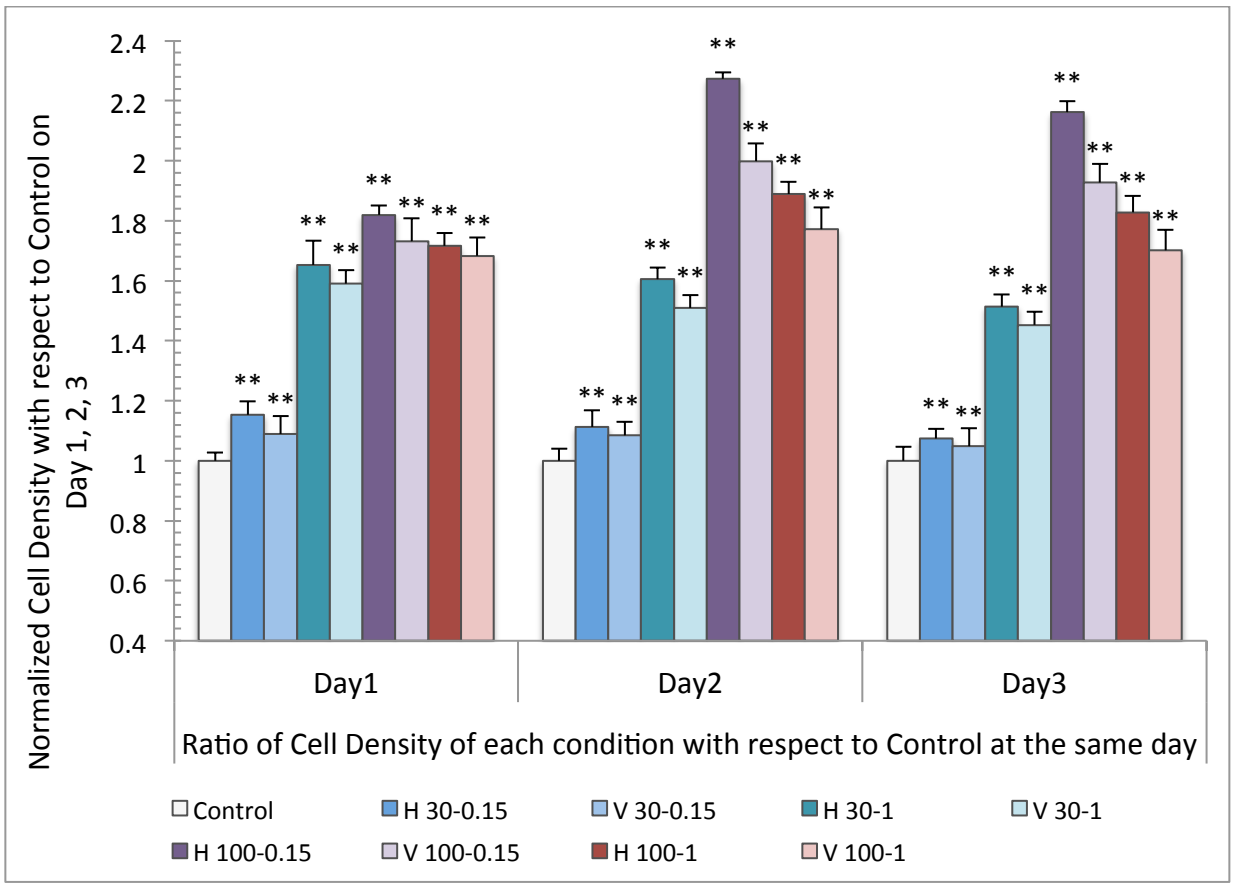
Normalized Cell Density with respect to Control on Day 1, 2, 3
2.4
2.2
2
1.8
1.6
1.4
1.2
1
0.8
0.6
0.4
**
Day1
Day2
Day3
Ratio of Cell Density of each condition with respect to Control at the same day
Control
H 30-0.15
V 30-0.15
H 30-1
V 30-1
H 100-0.15
V 100-0.15
H 100-1
V 100-1

Figure 3.2a:

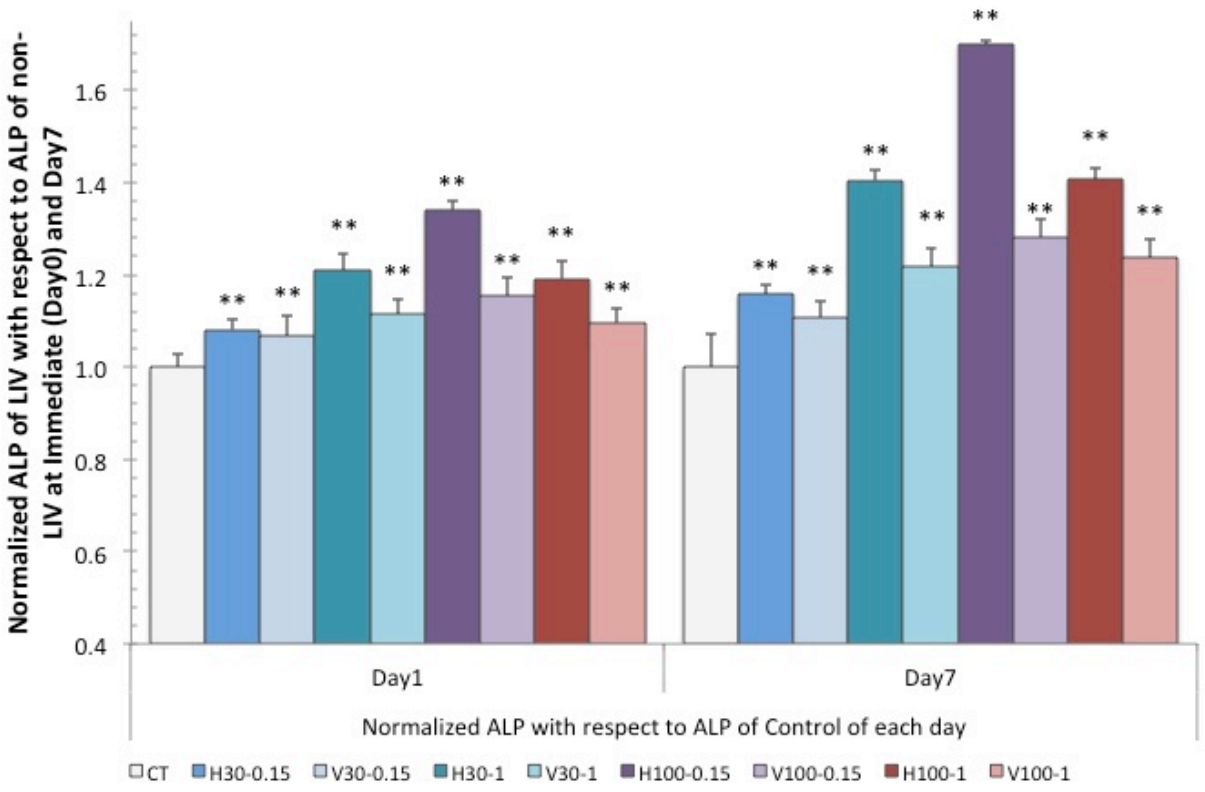
Normalized ALP of LIV with respect to ALP of non-LIV at Immediate (Day0) and Day7
1.6
1.4
1.2
1.0
0.8
0.6
0.4
**
Day1
Day7
Normalized ALP with respect to ALP of Control of each day
CT
H30-0.15
V30-0.15
H30-1
V30-1
H100-0.15
V100-0.15
H100-1
V100-1

Figure 3.2b:

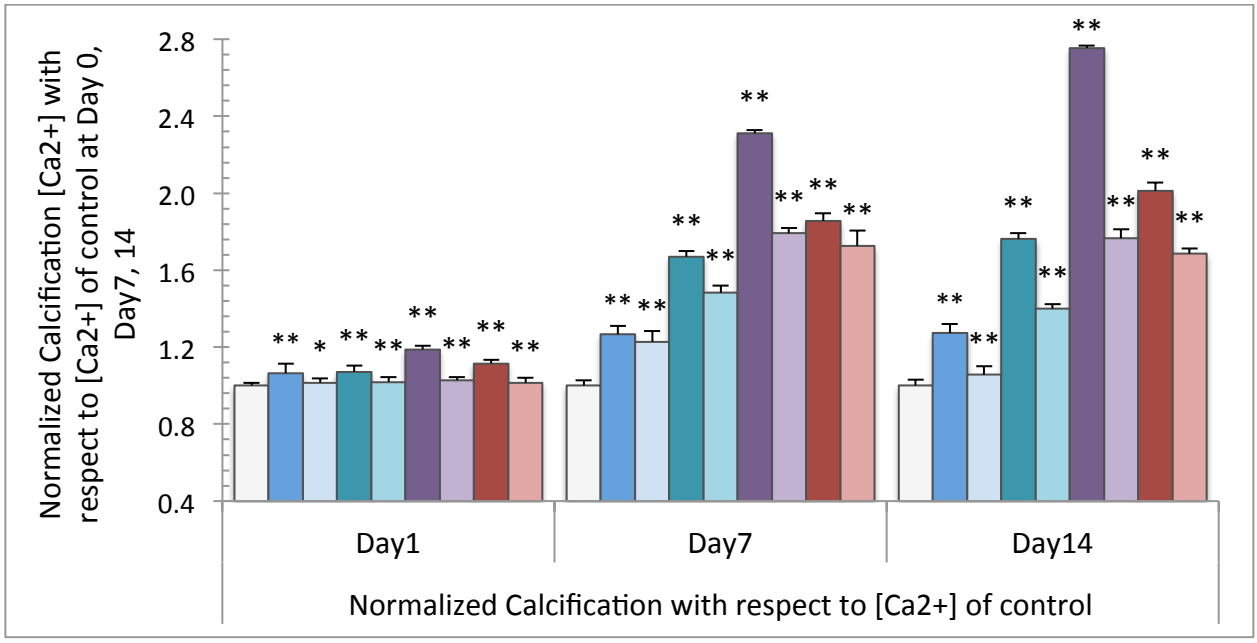
Normalized Calcification [Ca2+] with respect to [Ca2+] of control at Day 0, Day7, 14
2.8
2.4
2.0
1.6
1.2
0.8
0.4
Day1
Day7
Day14
Normalized Calcification with respect to [Ca2+] of control

Figures 3.3a and b:

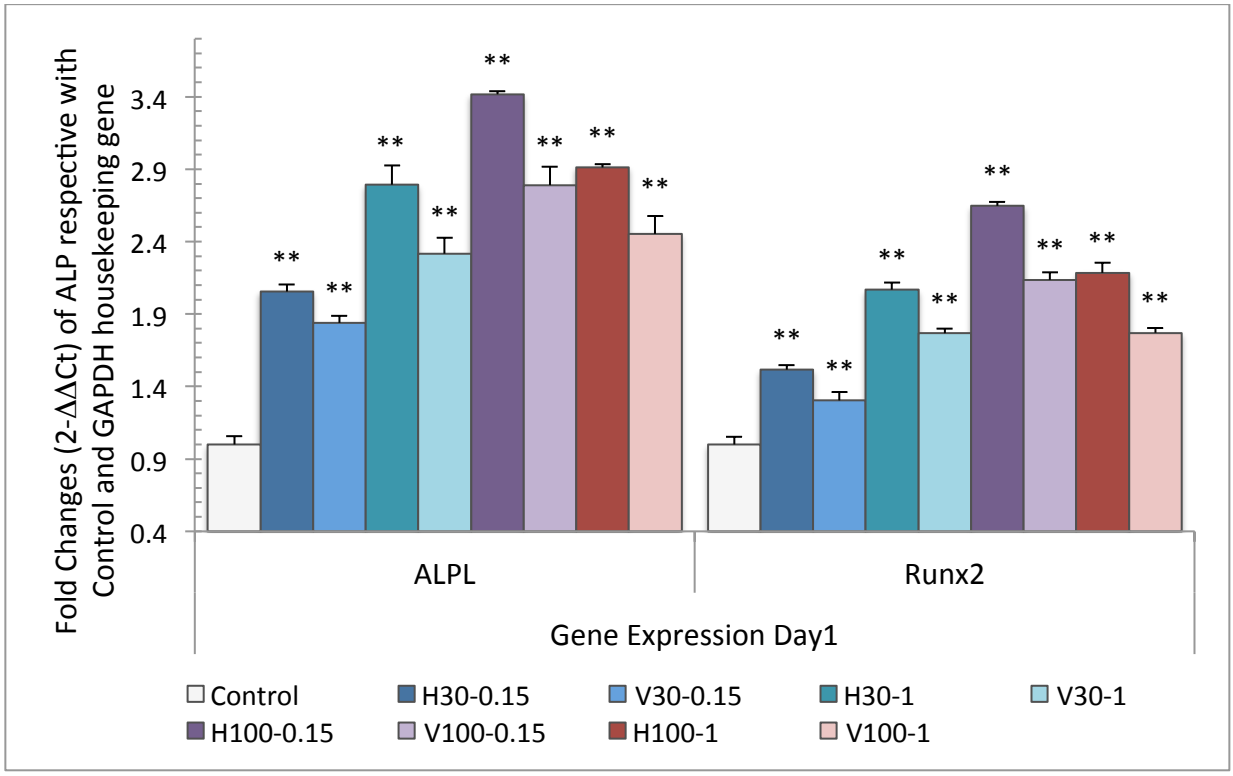

Figure 3.4a:

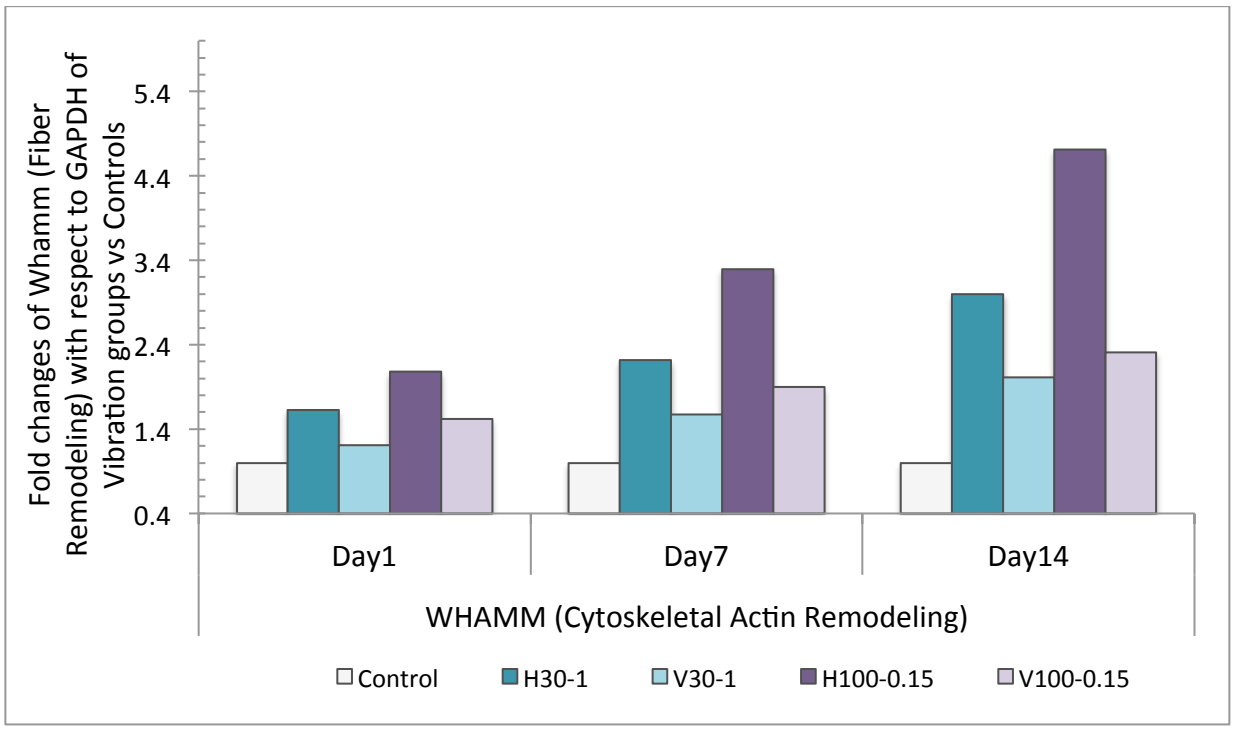
Fold changes of Whamm (Fiber Remodeling) with respect to GAPDH of Vibration groups vs Controls
5.4
4.4
3.4
2.4
1.4
0.4
Day1
Day7
Day14
WHAMM (Cytoskeletal Actin Remodeling)
Control
H30-1
V30-1
H100-0.15
V100-0.15

Figure 3.4b:

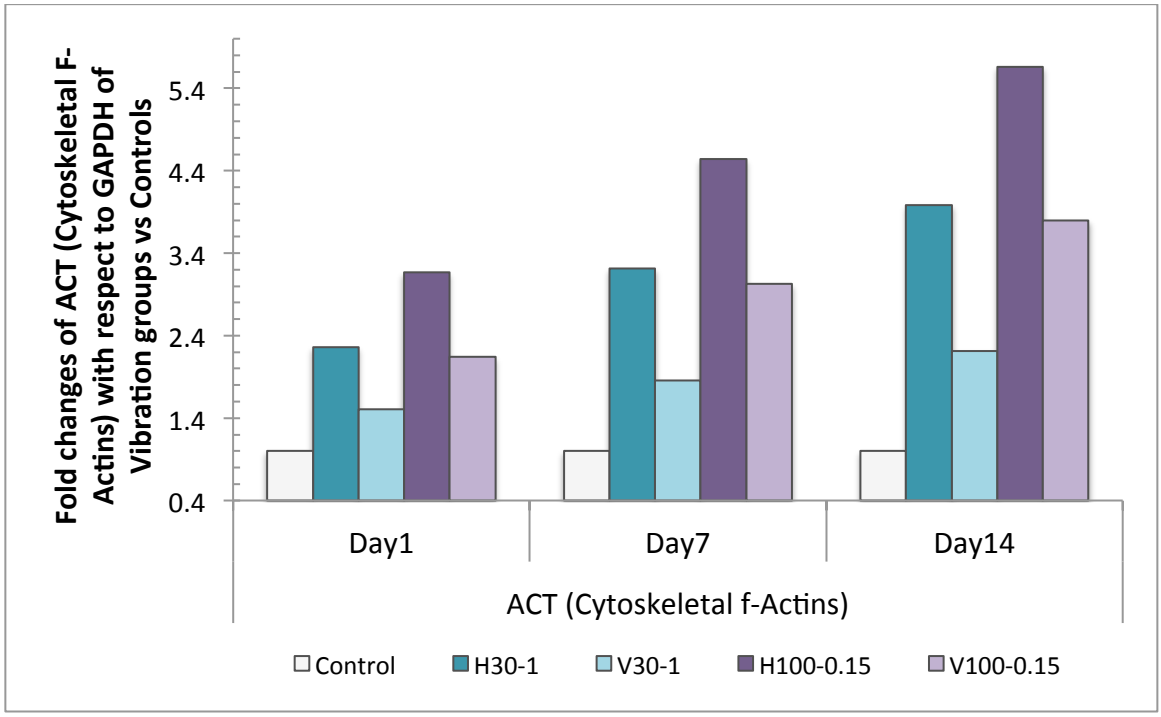
Fold changes of ACT (Cytoskeletal F-Actins) with respect to GAPDH of Vibration groups vs Controls
5.4
4.4
3.4
2.4
1.4
0.4
Day1
Day7
Day14
ACT (Cytoskeletal f-Actins)
Control
H30-1
V30-1
H100-0.15
V100-0.15

Figure 3.5a:

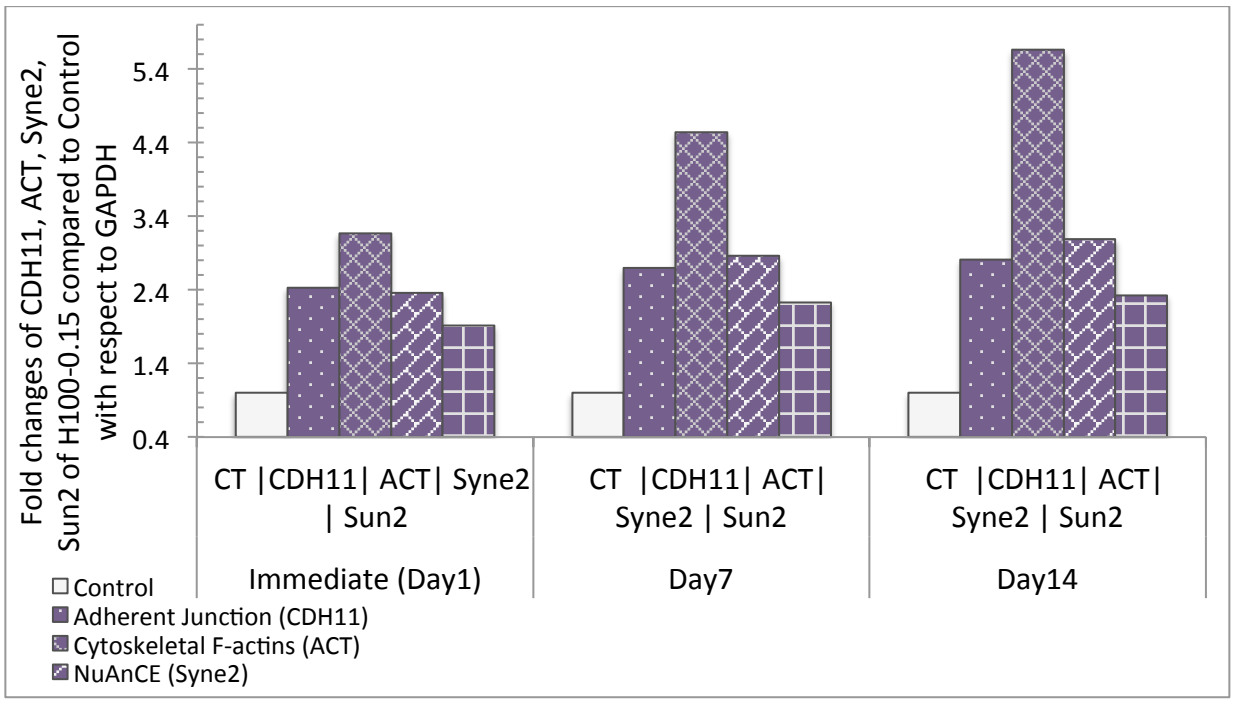
Fold changes of CDH11, ACT, Syne2, Sun2 of H100-0.15 compared to Control with respect to GAPDH
5.4
4.4
3.4
2.4
1.4
0.4
CT |CDH11| ACT| Syne2 | Sun2
CT |CDH11| ACT| Syne2 | Sun2
CT |CDH11| ACT| Syne2 | Sun2
Immediate (Day1)
Day7
Day14
Control
Adherent Junction (CDH11)
Cytoskeletal F-actins (ACT)
NuAnCE (Syne2)

Figure 3.5b:

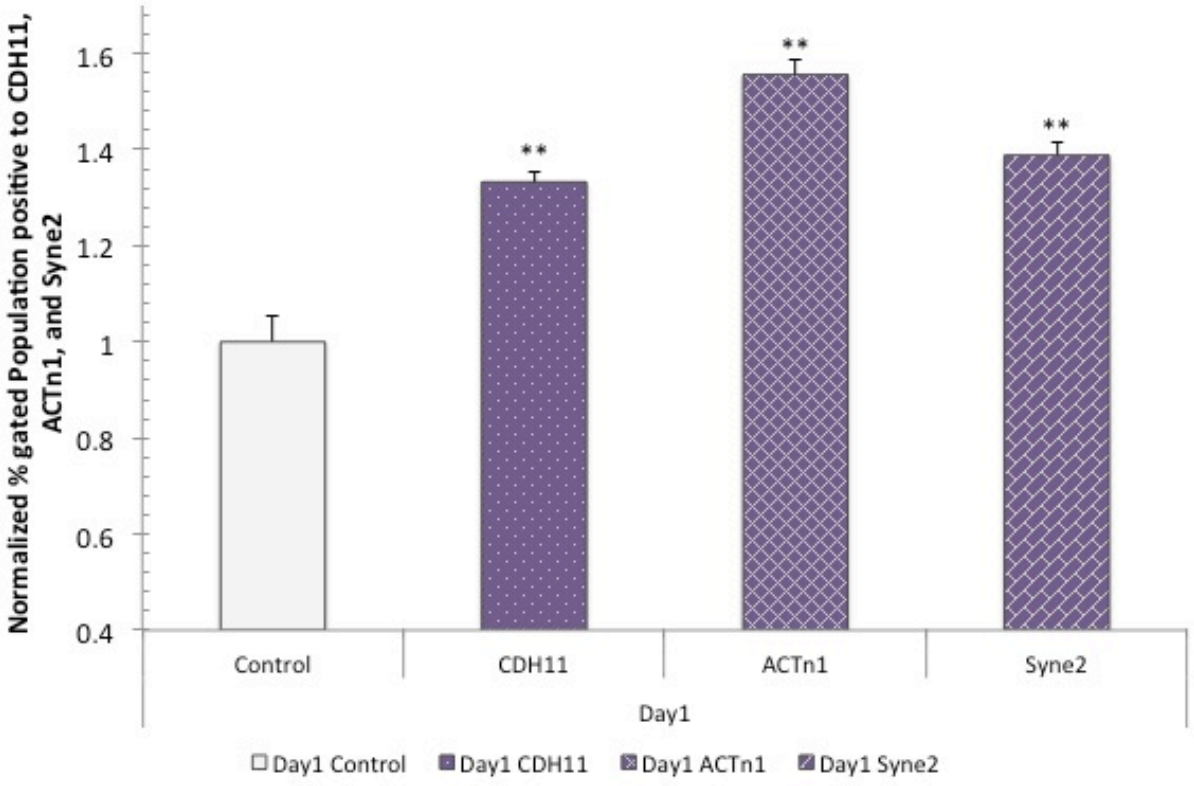
Normalized % gated Population positive to CDH11, ACTn1, and Syne2
1.6
1.4
1.2
1
0.8
0.6
0.4
**
**
**
Control
CDH11
ACTn1
Syne2
Day1
Day1 Control
Day1 CDH11
Day1 ACTn1
Day1 Syne2

Figure 3.6:

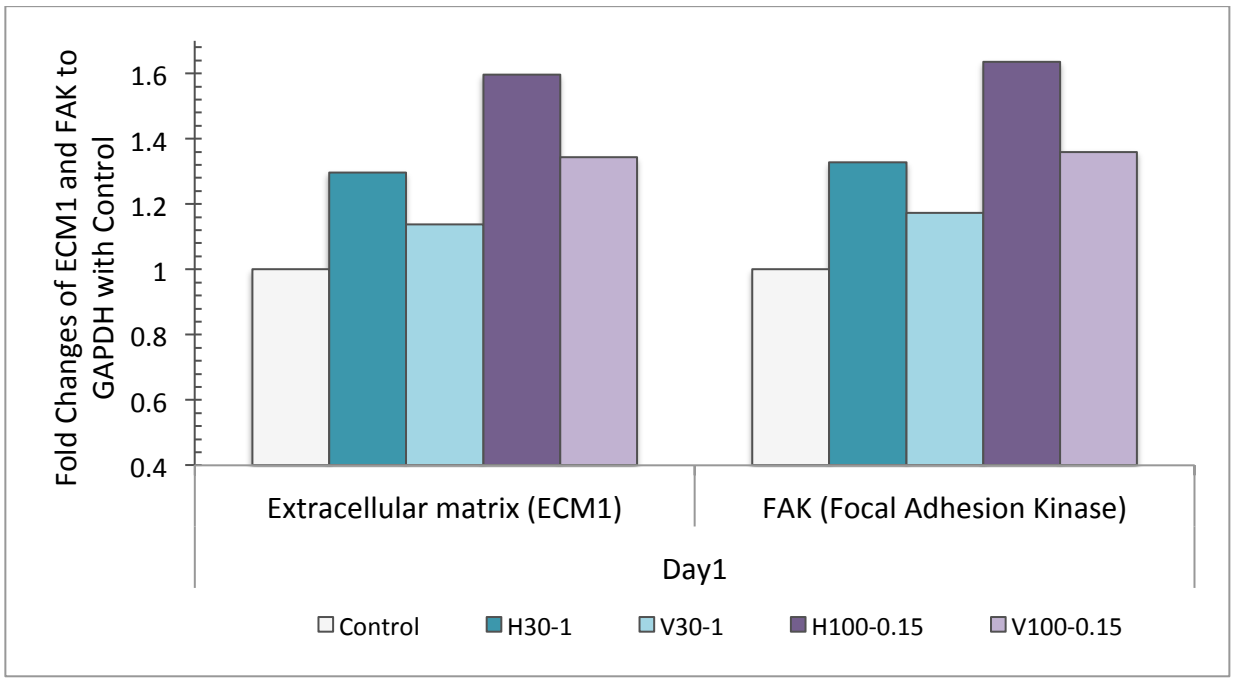
Fold Changes of ECM1 and FAK to GAPDH with Control
1.6
1.4
1.2
1
0.8
0.6
0.4
Extracellular matrix (ECM1)
FAK (Focal Adhesion Kinase)
Day1
Control
H30-1
V30-1
H100-0.15
V100-0.15

Chapter 4

Mechanical Vibrations Alter the Cytoskeleton and Nuclear Adhesions

(Pending publication and/or patent)

Abstract

Previously we found that human bone marrow mesenchymal stem cells in vitro are sensitive to acceleration amplitudes, frequency, and direction of the low intensity vibration. We have identified the mechanotransduction pathway through the cellular and nuclear structures. Here, we aim to validate our pathway through the physical connection of the CDH11-ACTn1-Syne2. We hypothesized that the cytoskeletal orientation could anchor NuAnCE-LiNC during LIV. We observed the cytoskeletal orientation under the horizontal and vertical LIV at the signal combination of 100Hz-0.15g comparable with the non-LIV. We visualized the cytoskeletal orientation by the two-photon confocal microscopy. We used the antibody immunofluorescence staining specific to the actin cytoskeleton and nesprin2. The two-photon images revealed significant cytoskeletal orientations under the hLIV. Quantitative cytoskeletal orientations showed that the hLIV provided the cytoskeletal orientation >2x more than the vLIV (with the statistic significance by 3-way ANOVA). The averaged gene expression level of CDH11 and Syne2 was upregulated with the overexpressing ACTn1. The data could confirm that the cytoskeletal orientation anchor the NuAnCE-LiNC from the outer- across the inner- nuclear membrane. Flow cytometric analysis confirmed an increase in the gene expression level of the cytoskeletal orientation. A quantification of the relative modulus by atomic force microscopy supported that the increased relative modulus could come from the cytoskeletal orientation under the LIV. The RNA interference confirmed that without cytoskeleton, the mechanotransduction through the CDH11-ACTn1-Syne2 pathway was incomplete due to the impaired cytoskeleton anchoring nucleoskeleton (nesprin2). With the RNA transfection, the silencing cytoskeleton could not connect with the nesprin2, confirming that the completion of the CDH11-ACTn1-Syne2 pathway requires the actin cytoskeleton.

4.1 Introduction

Human bone marrow mesenchymal stem cells (hBMSCs) in vitro can sense the frequency, direction, and acceleration amplitude of the low intensity vibration during the stem cell proliferation and osteogenic differentiation [Pongkitwitoon et al. 2014]. We have demonstrated the potential mechanotransduction pathway through the physical connection of the cellular and nuclear structure. However, the mechanotransduction pathway has been yet unconfirmed.

Cytoskeletons related adherent junctions (such as n-cadherin) have been exclusively studied [Malone et al. 2007]. During in vitro stretching, cells were pulled and could form the mature adherent junction parallel to the actin bundle [Huveneers et al. 2013]. In responses to forces, the cell could form the cadherin-cytoskeleton interface through the physical connection by vinculin [Bays et al. 2005]. The interface could delegate the locally physical force through the cytoskeletal organization, transformation and remodeling [Yonemura et al. 2011]. The RhoA/Rock signaling pathway was extensively believed to be responsible for the cytoskeletal remodeling [Shi et al. 2012]. The upregulated CDH11, ACTn1, and Syne2 of hBMSCs under the LIV in vitro could support the physical connection of the adherent junction, cytoskeleton and nucleoskeletons [Pongkitwitoon et al. 2014]. The nucleoskeletal NuAnCE-LiNC has been discovered and commonly represented by nesprin2 (Syne2) and sun2 [Lombardi et al. 2011]. The up- and down- regulation of the sun2 expression level could be impaired without the Syne2 [Meinke et al. 2014], indicating that the Syne2 could sufficiently represent the anchoring NuAnCE-LiNC.

To optically observe the physical connection of the cell and nucleus, the two-photon confocal microscopy revealed that the cytoskeletal f-actins including alpha actinin (ACTn1) connected to the nesprin2 at the spectrin [Meng et al. 2011]. The atomic force microscopy (AFM) could probe the 3D structure of the cytoskeleton [Chacko et al. 2013] and the dynamic random orientation [Efremov et al. 2011]. The resolution of the AFM for probing the living cells is as high as probing <200nm [Kuznetsova et al. 2007]. The AFM could confirm the structural change in the cell by determining the relative modulus. The relative modulus of osteoblast was >20KPa during the dynamic change of the cytoskeleton [Kuznetsova et al. 2007, Du 2011].

Here, we aim to confirm the CDH11-ACTn1-Syne2 mechanotransduction based physical interactions of cells and nucleus under the LIV. We visualized cytoskeletal orientations by the two-photon confocal microscopy. Quantified fiber orientation was related to the CDH11, ACTn1, and Syne2 gene expression level. Changes in the cellular and nuclear structure that influenced the cellular mechanics were monitored by the atomic force microscopy. To confirm the physical connection of the CDH11, ACTn1, and Syne2, we depleted the cytoskeletons by the RNA interference and transfection. The knockdown and silencing cytoskeletons substantially validated the cytoskeleton anchoring nesprin2 as the underlying transduction pathway.

4.2 Materials and Methods

4.2.1 Experimental design

To validate the CDH11-ACTn1-Syne2 mechanotransduction pathway, we visualized cytoskeletons by the two-photon confocal microscopy. We confirmed the finding by the knockdown and silencing the cytoskeleton.

To monitor changes in cellular and nuclear structures under the LIV, we optically observed the cytoskeletal and nuclear filaments of hBMSCs. From our previous data, the osteogenic differentiation of hBMSCs could sense directions and frequencies of the LIV. The LIV of horizontal and vertical directions at 100Hz-0.15g was applied. To investigate changes in cellular and nuclear structures, we used the two-photon confocal microscopy to visualize the antibody immunofluorescence stained cytoplasm, cell membrane, cytoskeleton, and nucleoskeletal nesprin2. To observe the dynamic changes in the physical structures of the cell and nucleus, we determined the mechanical change by the atomic force microscopy.

To confirm gene expression of the CDH11-ACTn1-Syne2 pathway, we used flow cytometric analysis of immunofluorescence staining and conjugated antibodies. To evaluate the potential mechanotransduction, we depleted and silencing cytoskeletons by the RNA interference and transfection. The RNA interference is to permanently deplete genes by inhibition of the encoding miRNA during the DNA polymerization in the nucleus [Leung et al. 2005]. The RNA transfection (or silencing RNA) is to disrupt the DNA transcription by breaking down miRNA in the cytoplasm, causing compromising nucleotide sequences [Khaw et al. 2001].

Statistic one-way and three-way ANOVA analyzed the effects of the LIV vs non-LIV and the direction, respectively, with significance at $p \leq 0.05$.

4.2.2 Cell culture and Mechanical stimulation

4.2.2.1 Culture human bone marrow mesenchymal stem cells (hBMSCs)

hBMSCs were aspirated from bone marrow of 25 years old African American female patient (Life Technologies) tested negative HIVs. hBMSCs were cultured in alpha-MEM

without phenol red containing 7.5% heat-inactivated fetal bovine serum (Gibco), 5μM L-glutamine and specific growth factors of recombinant 15nM IGF-1 and 125pM FGF-β. To sustain properties under different environments, 1mM DTT (LifeLine D1532) and 0.1% BSA (Sigma A2058) were added to the stock solution of the growth factors. Since hBMSCs is very sensitive to changes in pH and $\%CO_2$, we added 25 mM HEPES to preserve the pH at 7.4, and protected the cells with 1% penicillin/streptomycin.

4.2.2.2 Selected signal combination of low intensity vibration (LIV)

We selected the best cell responding signal combinations of frequency and acceleration at 100Hz-0.15g [Pongkitwitoon et al. 2014]. We vibrated cells in horizontal- and vertical-directions with non-vibrated cells as a control. We vibrated cells in 2 sessions a day, for 20 minutes in each session, with 2-hour rest in between sessions as the loading cycles and duration of vibration could control cell behaviors.

4.2.3 Osteoblastogenic differentiation

Our proliferation showed that the hBMSCs expressed doubling time within 1-2 days for all LIV groups. To prevent cell proliferation interfering with cell differentiation, we plated cells 2 days prior to the experiment with cell density at 18,000 cells/cm^2 in 24wells/plate. After 2 days of the first inoculation, the hBMSCs were induced with osteoblastogenic media containing 100nM dexamethasone, 10mM β-glycerol phosphate, and 0.05mM L-ascorbic acid-2-phosphate. The vibration was performed immediately after the osteoblastogenic induction. All observations were performed at the end of the second vibration on Day1 (i.e. the first day of the induction).

4.2.4 Gene expression by real-time PCR, (fold changes, $2^{-\Delta\Delta Ct}$)

Real time PCR quantified gene expression using TaqMan standard protocols (n=6). After vibration, cells were lysed by TRIzol (Life Technologies). To extract the RNA, the lysates were phase separated by chloroform. The RNA was precipitated from nucleic acid by RNeasy (Qiagen) and re-dissolved by RNA-free water. NanoDrop (ND-100 V3.3.0) quantified RNA, cDNA, and nucleic acid concentration and determined their quality. The ratio of [A_{260}/A_{280}] ≥1.8 is for 'pure' cDNA and ≥2.0 for 'pure' RNA, validating by [A_{260}/A_{230}] ~2.0-2.2 for 'pure' nucleic acid. After cDNA conversion by the reversed transcriptase (Invitrogen), the cDNA was diluted to 3.33ng/µl. The real time PCR by StepOne 2.2 provided Ct of the interested genes and the gene expression level was calculated (fold changes, $2^{-\Delta\Delta Ct}$) with respect to the control and the GAPDH housekeeping gene.

4.2.5 Flow cytometric analysis

The measurement of % cell populations by laser-based flow cytometric analysis relies on effective immunofluorescent staining and conjugated antibodies. We prepared samples by lifting the attached cells with 0.05% trypsin/EDTA. We performed immunofluorescent staining of cytoskeletal f-actins with (i) primary ACTn1 human monoclonal antibody (Santa Cruz sc-17829) and IgG, or (ii) Rhodamine Phalloidin AlexaFluor594 (LifeTechonologies). To acquire the data, we set the % gated cell population positive to specific immunofluorescence with at least 10,000 events and FlowJo analyzed the % cell population. We reported the normalized average %population as [%P] ($\frac{Averaged\ \%\ Population,LIV}{Averaged\ \%\ Population,non-LIV}$), n=6.

4.2.6 Two photon confocal microscopy

To visualize the cytoskeleton, we made sure the cells were intact and not damaged using immunofluorescent staining cytoplasm and cell membranes along with cytoskeletons and nuclear filaments. The images taken by 40x oil lens and 63x water lens were probed with TRIC and FITC modes (Zeiss). The most advantage of the two-photon over the regular one-photon confocal microscopy is that the two-photon confocal microscopy can image the z-direction with (i) clearer resolutions from adjustable pinholes and (ii) deeper in living cells and tissues without damaging cells from low energy x-ray [Helmchen et al. 2005]. Limitations of Zeiss are that it can (i) only probe one x-ray at a time, and (ii) only take 5 images per seconds. Therefore, the two-photon images could only present the overall changes after LIV.

4.2.6.1 Cytoplasm and cell membranes

Cell membranes were conjugated with CD44 and incubated overnight in 4°C, and further 3-4 hours with IgG antibody and AlexaFlour560, yellowish green (λ_{560}).

4.2.6.2 Cytoskeletal f-actins

Cytoskeletal f-actins were immunofluorescent stained with specific Rhodamine Phalloidin (LifeTechonologies). Phalloidin is a highly affinity with cytoskeletal f-actins and gives red-orange fluorescence. Z-direction was probed by two-photon at $\lambda_{640/700}$ with 40x oil lens.

4.2.6.3 Nucleus

Here we used Syne2 to represent Syne2-sun2 relation in NuAnCE-LiNC [Meinke et al. 2014]. Immunofluorescent staining nucleus with DAPI (4', 6-diamidino-2-phenylindole/2HCl, specific to nuclear DNA and nucleic acid) was further incubated overnight with the nesprin2

antibody at 4°C. Nuclear skeletons were subsequently conjugated with specific IgG secondary antibody and coupling with AlexaFlour488, bluish green (λ_{488}).

4.2.6.4 Quantification of %fiber orientation

We quantified the amount of cytoskeletal and nuclear orientation by MatLab. After binary image conversion by NIH ImageJ, 'edge detection' and tensor diffusion simplified 3D matrix into a linear equation. The orientation that is perpendicular to the direction axis was defined to be the shortest distances, where the value changes from 0 to 1 in both directions. We computed angle of any two (x, y) pairs by syntax: atan2((y2 - y1), (x2 - x1)). The %fiber orientation with respect to the overall fiber was quantified and the normalized averaged %fiber orientation with respect to that of the control was reported.

4.2.7 Atomic Force Microscope

4.2.7.1 Force distance

To obtain the relative modulus, AFM (Digital Instrument) with a fluid holder was used. The drive amplitude (mV) and the lateral deflection amplitude of the cantilever (ΔX, mV) were relatively converted to be the force (pN) and distance (μm). The calibration was performed in Hank's balanced solution with the measured value within <15% of the nominal value. A standard V-shaped cantilever (200μm) and the tip (typical radius of the apex ~20nm) were sanitized before each measurement by a UV shortwave for >2 min. The tip was positioned over the cells by a laser system. The total signal on the photodetector was set at the negative set point of 0.5-1V. The scan rate was set ~2-3Hz to optimize the signal quality with 1.5μm-resolution. Each LIV condition had 6 samples (n=6) and each sample was measured in > 6 different areas. Each area was performed at least 3 different measurements.

4.2.7.2 Data analysis

The ratio of the slopes (the straight-line portion) was the relative modulus of hBMSCs (unit-less). We reported normalized averaged relative modulus of LIV with respect to non-LIV.

If the spring constant (K) is 10, therefore the indentation depth should be >48nm. Typically, cell membrane (lipid bilayer) is ~4-8nm thick. Our two-photon showed that hBMSC thickness is >10 microns and the nearest cytoskeletal is at >24-36nm from the cell membrane. Therefore, the measurement was inside cells, not at the surface of the cell membrane, and not damage the nucleus.

4.2.8 Depletion of targeted biogenes

4.2.8.1 Knockdown cytoskeletons (permanent)

To evaluate CDH11-ACTn1-Syne2 mechanotransduction, we knocked down cytoskeletal f-actins with Cofilin-shRNA (Santa Cruz Bio) before flow cytometric analysis of %CDH11, ACTn1 and %Syne2. Cofilin (Cfl1) is an actin-binding protein, regulating dynamic process of assembling/disassembling g-actins and their oligomers during cytoskeletal polymerization.

Prior to knocking down cytoskeletons, hBMSCs were changed media to Opti-MEM and incubated with 1%DMSO overnight at 37°C. The hBMSCs were subsequently incubated overnight with 10mg/ml Clf1-shRNA at 37°C [Hammond et al. 2012]. Then, hBMSCs were under hLIV and vLIV at 100Hz-0.15 and compared to the non-LIV of wild type and KO. The immunofluorescent conjugated CDH11, ACTn1 and Syne2 antibodies with IgG was performed

and hBMSCs were detached by 0.05% trypsin/EDTA, following by the flow cytometric analysis of %positive populations (n=6) at >10,000 events.

Generally, knockdown biogenes can cause unstable and dead cells. To validate the toxicity and the effectiveness of the knockdown technique, we monitored (i) cell viability, and (ii) %Population of ACTn1 for 3 consecutive days. The data showed (i) similar cell viability in all groups as no cell damage from knockdown conditions, and (ii) similar insignificant amount of %ACTn1 in all knockdown groups without toxicity as effective knockdown techniques.

4.2.8.2 Silencing cytoskeletons (transient)

Biogenetic transfection (silencing biogenes) is to disrupt DNA by breaking down miRNA in the cytoplasm after transcription, causing compromising nucleotide sequences. Before the RNA transfection, hBMSCs were changed media to Opti-MEM and incubated with 1%DMSO overnight at 37°C. The hBMSCs were then incubated overnight with 0.5mM Clf1-siRNA (Qiagen) at 37°C. Immunofluorescent staining of CDH11, ACTn1 and Syne2 before flow cytometry analysis of %CDH11, %ACTn1 and %Syne2 were performed.

4.2.9 Statistic analysis

Statistic one-way analysis of variance, ANOVA (SPSS) with Tukey post hoc test analyzed the effect of LIV vs non-LIV. Each condition in each experiment was repeated at least n=6. Each experiment was at least duplicated. The results were statistically significant when $p < 0.05$, and p values were reported as *<0.05, **<0.01.

4.3 Results

4.3.1 Two-Photon Microscopy Visualized Cytoskeletal f-actins and Fiber Orientation

The two-photon confocal microscopy showed that the cytoskeletal orientation under hLIV was aligned in one direction better than under the vLIV and the control (**Figures 4.1a and b**). The cytoskeletons under the vLIV exhibited random orientations similar to that of the control. The calculation of the surface fiber density index (which can be found in Sokolov et al. 2005) of the cytoskeleton under the hLIV was ~2-4x less than the index of the vLIV and the non-LIV. The lower index confirmed the cytoskeletal forming bundles increasing density and thickness (similar to the studies of Demiray et al. 2014). Our data supported that cytoskeletal f-actins were forming bundles during mechanical stimulations to stabilize cytoskeletons by inhibiting actin depolarization (similar to the previous studies of Coscoy et al. 2002).

Quantitative analysis of the amount of cytoskeletal and nuclear orientations showed that hLIV had higher fiber orientations (**Figure 4.2**). The normalized averaged %cytoskeletal orientation of hLIV was ~1.2-2x higher than the vLIV and non-LIV, respectively. The normalization of the averaged %nuclear orientations was 1.4x higher than both groups. The data showed that the direction of LIV controlled cytoskeletal and nuclear orientations.

4.3.2 Mechanotransduction Pathway via CDH11-ACTn1-Syne2

The averaged gene expression level of CDH11 in hLIV was 1.5-2.7x higher than that of vLIV and non-LIV, respectively (**Figure 4.3a**). The ACTn1 expression level of hLIV was 1.7-3.3x while the Syne2 expression level of hLIV was 1.4-2.5x higher than that of the vLIV and non-LIV, respectively. The data confirmed that hLIV influenced cytoskeletal orientation.

The normalized averaged %population positive to (i) Phalloidin (actin cytoskeleton) and (ii) ACTn1 (actin cytoskeleton binding protein including alpha actinins) was similar in the cytoskeletal orientation of the two-photon images. These data confirmed that the ACTn1, as well as Phalloidin, could well represent the cytoskeletal orientation. The normalized averaged %population positive to CDH11, ACTn1 and syne2 by flow cytometric analysis also confirmed overexpression levels of these genes (**Figure 4.3b**). The CDH11 expression levels of hLIV were ~1.2-1.3x higher than both groups. The ACT and Syne2 of hLIV were ~1.5-2x and ~1.2-1.4x higher than the expression levels of vLIV and non-LIV, respectively. The data confirmed CDH11-ACTn1-Syne2 pathway and supported connections of cytoskeletal induced nuclear orientation.

4.3.3 Cytoskeletal Orientations Modulated Mechanical Moduli

As we hypothesized that the changes in cellular and nuclear structures should affect changes of cellular and/or molecular mechanics. The normalized averaged relative modulus calculated from the force-displacement of AFM showed that the hBMSC under the hLIV exhibited ~1.3-1.6x higher than the relative modulus of the vLIV and non-LIV, respectively (**Figure 4.4**). The data supported that the direction and frequency of the LIV significant influenced cytoskeletal orientation and mechanics. Additionally, the relative modulus of the hBMSCs under the 100Hz-0.15g was the highest. The data could imply that the high frequency and horizontal direction could provide stronger cytoskeletons oriented in one direction. Similarly, under the zero gravity, the mechanical stimulation could increase the mechanical strength during the MSCs osteogenic differentiation. The data could imply that the acceleration might not be the only key effect of the MSC commitment [Qian et al. 2013].

4.3.4 Cytoskeleton Knockdown Proved Mechanotransduction via CDH11-ACT-Syne2

We confirmed the CDH11-ACTn1-Syne2 mechanotransduction pathway by knocking down the cytoskeleton. The viability of human cells under the knockdown condition was observed for 3 consecutive days. The flow cytometric analysis showed the similar averaged %cell population, as there were no harmful effects of the knockdown condition on the cell viability and cytotoxicity.

The effectiveness of knockdown technique was tested (**Figure 4.5a**) by observation of %ACTn1 positive population. The flow cytometric analysis of %population positive to ACTn1 showed that over 3 days the cytoskeletons were permanently depleted completely. The normalized averaged %ACTn1 population was < 0.07 in the knockdown groups with hLIV, vLIV, and non-LIV for all 3 days.

The hBMSCs with the cytoskeleton knockdown under the hLIV, vLIV, and non-LIV exhibited the depletion of ACTn1 (**Figure 4.5b**). The %ACTn1 of all knockdown groups was ~0.06-0.7 (>17x less than %ACTn1 of the wild type). The knockdown ACTn1 groups had %Syne2 (>16x) significantly less than the non-LIV, wild type hBMSCs. The normalized averaged %CDH11 population was >2x less than that of the wild type hBMSCs under non-LIV. The knockdown ACTn1 had %CDH11, %ACTn1 and %Syne2 under hLIV similar to those under vLIV and non-LIV. The data confirmed that there were significant connections of the adherent junction (CDH11) with cytoskeletal f-actins (ACTn1) [Engl et al. 2014] as the depletion of ACTn1 exhibited less CDH11. The data firmly supported that the cytoskeletal f-actins modulated anchoring NuAnCE-LiNC through the nuclear nesprin2 throughout the nuclear double membrane [Pongkitwitoon et al. 2014].

The depletion of ACT by silencing cytoskeletons showed less %ACTn1 (>3x) than in the wild type (**Figure 4.5c**). The %CDH11 and %Syne2 of silencing ACTn1 were less than the wild type (>1.5 and >2.5 less, respectively). The data demonstrated that without ACTn1, the links between CHD11-ACTn1 and ACTn1-Syne2 was significantly disconnected. The depletion of ACTn1 (by knockdown and silencing ACTn1) confirmed the connection of CDH11-ACTn1-Syne2 in the mechanotransduction.

4.4 Discussion

We investigated the physical change of the cellular and nuclear structure in the human bone marrow mesenchymal stem cell during the hLIV, vLIV, and non-LIV. We selected the best cell responding signal combinations at 100Hz-0.15g from our previous data [Pongkitwitoon et al. 2014]. We visualized orientations of cytoskeletal f-actins by the two-photon confocal microscopy for both planar 2D and deep in the z-direction. The cytoskeletal f-actins were oriented in one direction in hLIV while random orientation in vLIV and non-LIV. From two-photon images, we quantified the cytoskeletal orientation. The %cytoskeletal orientation of the hBMSCs under the hLIV was 1.5-2x higher than that under the vLIV and non-LIV, respectively. The averaged gene expression levels of CDH11, ACTn1, and Syne2 under the hLIV were >1.5x higher folds than the expression level under the vLIV and non-LIV. The upregulated Syne2 expression level was synchronized with an overexpression of ACTn1, supporting the cytoskeletons anchoring NuAnCE-LiNC in the CDH11-ACTn1-Syne2 mechanotransduction [Pongkitwitoon et al. 2014]. Flow cytometric analysis of %CDH11, %ACTn1 and %Syne2 populations confirmed the physical connection of the CDH11-ACTn1-Syne2. Changes in the physical structure of the cell and the nucleus influencing the mechanical modulus were confirmed by AFM. The linear portion in the force-displacement provided the relative modulus of hBMSCs under the mechanical stimulation. The normalized average relative modulus under the hLIV was >1.3x higher than the modulus under the vLIV and non-LIV. The data supported that changes in the cellular mechanics could directly be influenced by the cytoskeletal orientation. The depletion of ACTn1 by the knockdown and silencing ACT demonstrated that without cytoskeletons the connection of CDH11-ACTn1 and ACT-Syne2 were disrupted. The

data confirmed that the physical link of the adherent junction and the cytoskeleton anchoring nuclear skeleton is required in the mechanotransduction of LIV in hBMSCs.

Several limitations of this study were the two-photon confocal microscopic capacities. The several x-ray sources can only be employed one x-ray at a time, causing the time lapse during imaging [Lund et al. 2012, Scott et al. 2014]. The DAPI labeled nucleus cannot be imaged in this article from the lack of the x-ray source. The maximum 5 frames in a second are the upper limit of the image acquisition, causing imaging in the real time impossible. To obtain high data resolution, the AFM data acquisition requires lower speeds, which is time-consuming and loses abilities to monitor localized properties.

4.4.1 LIV induced Cytoskeletal Orientation

The two-photon confocal microscopy was able to optically observe the cellular and nuclear structure including transformations and remodeling. The most advantage of determining the cell thickness by the two-photon over AFM is that the two-photon imaging acquisition uses a non-invasive low energy x-ray. But AFM requires aggressive forces to mechanically scan the tip over cells, especially if done in a regular (air) mode [Demiray et al. 2014]. The two-photon images can provide the cell diameter (both width and length) and height (or cell thickness). Though, we commonly found that the cell morphology and thickness was observed by the AFM [Chacko et al. 2013, Demiray et al. 2014].

We found that the hBMSCs under the hLIV showed the cytoskeletal orientation in more or less one direction (**Figure A15**). But the hBMSCs under the vLIV and non-LIV seemed to

have the random orientation. These data could support that the LIV induced the cytoskeleton orientation. We also quantified the %fiber orientation to evaluate and confirm the cytoskeletal orientation under the LIV. To calculate the %fiber orientation, we first changed the two-photon images to binary images using ImageJ (**Figure A17**) before simplified calculation to linear equation (**Figure A18**). The % fiber orientation of hBMSCs under the hLIV was higher than the % under the vLIV and non-LIV. These data confirmed that the cytoskeletal orientation of hBMSCs under the hLIV was the highest. Additionally, the gene expression of the cytoskeleton (ACTn1) also supported that the LIV induced the cytoskeletal orientation. To confirm our finding, we also calculated the surface fiber density index [Sokolov et al. 2005] to evaluate the cytoskeletal bundle deriving from the cytoskeletal density during the cell responding to the mechanical stimuli. If the density index is less or close to zero, the bundle is, therefore, formed. We found that the density index of the LIV groups was less than the index of the control, meaning that there was a thicker cytoskeletal bundle formation in the LIV group than in the non-LIV. These data supported that the LIV induce the cytoskeletal orientation and bundle formation.

4.4.2 LIV induced Cellular and Nuclear Interactions

Our data showed previously that the mechanotransduction pathway of the CDH11-ACTn1-Syne2 depends on the physical interaction of the cellular and nuclear structures. We were able to confirm and demonstrate the connection of physical changes in the cellular and nuclear structure with the change in the gene expression level [Pongkitwitoon et al. 2014].

The adherent junction (CDH11) has been confirmed to connect with the cytoskeleton during the mechanical stimulation in other works as well. However, most of the studies would link the CDH11-ACTn1 to the β-catenin based signaling pathways [Huveneers et al. 2013, Engle et al. 2014], which was difficult to link with Akt1 [Uzer et al. 2013]. The connection of the cytoskeleton and nucleoskeletons were required during the force transduction in cells [Lombardi et al. 2011]. We are the first to show the relation of the cytoskeleton in the mechanotransduction not only via the two-photon fluorescence image but also the gene expression.

4.4.3 Cytoskeletal Orientations Improved Cellular Mechanics

The advantage of using the AFM with liquid mode over the air mode is that it provides a proper environment to the cell. The relative modulus estimating from the force-displacement (**Figure A22**) supported that the cytoskeletal orientation and remodeling can cause changes in the molecular mechanical properties. The increased mechanical tension of the dynamic cytoskeleton could indicate the cytoskeleton forming bundles [Meng et al. 2011]. With the orientation toward one direction, the single cell mechanical property was much improved from the non-oriented cytoskeleton in the non-vibrated control group (**Figure A16**). We assumed that the observation was the overall measurement (**Firgures A19-A21**). The hBMSCs under hLIV had >1.5x higher cytoskeletal orientation and >1.3x higher relative modulus than vLIV. The data supported that the mechanical property of cells could indicate the change in the cell and the nucleus. Additionally, the increased cytoskeletal orientation showed the improved cellular modulus (**Figure A23**).

4.4.4 Proven CDH11-ACTn1-Syne2 Mechanotransduction

From our fluorescence images (images were not shown here), the cytoskeletal knockdown showed the depleted cytoskeleton. Our data showed that the knockdown of the cytoskeleton was effective and caused no cytotoxicity after 3days. To form the cytoskeletal bundles, the repetitive polarization of many small actins and actinins, including the orientation of many actin cytoskeletons was required [Hotulainen et al. 2005]. Our data supported that the knockdown could deplete cytoskeleton by depolarization of the actin cytoskeleton and actinin.

Without the depolarized cytoskeleton (and the orientation and bundles, %ACTn1, was less than <0.07), the %Syne2 was less than <0.08. The data could suggest that the nesprin2 could not anchor from the outer nuclear envelope throughout the nucleus without the cytoskeleton oreintation. These data could confirm the CDH11-ACTn1-Syne2 mechanotransduction through the physical interaction of the cytoskeleton with the mature junction and the nucleoskeleton.

4.5 Conclusion

Our data demonstrates the visual image and for the first time that the horizontal LIV orients cytoskeletal f-actins. The data indicate strong connections of the cytoskeleton in the CDH11-ACTn1-Syne2 mechanotransduction pathway. The gene expression profiles and flow cytometric analysis define that the hBMSC senses a specific direction of the LIV through the cytoskeletal orientation. Analyses of the single cell relative modulus by the atomic force microscopy evaluate that the changes in the cytoskeleton influence the cellular mechanics. The cytoskeletal knockdown and silencing confirm the physical interaction based mechanotransduction. The confirmation of the pathway by visualization of the cytoskeletons and by measurement of the cellular mechanics definitely provides great insights toward the change in the gene expression directly derive from the change inside the cell and the nucleus. Additionally, the single cell mechanical properties can be affected directly by changes of the cellular and nuclear structure.

References

Bays JL, Peng X, Tolbert CE, Guilluy C, Angell AE, Pan Y, Superfine R, Burridge K, DeMali KA. 'Vinculin phosphorylation differentially regulates mechanotransduction at cell–cell and cell–matrix adhesions' JCB **2005**, 205 (2): 251-263.

Chacko JV, Zanacchi FC, Diaspro A. '*Probing Cytoskeletal Structures by Coupling Optical Superresolution and AFM Techniques for a Correlative Approach*.' Cytoskeleton. **2013**, 70: 729–740. doi: 10.1002/cm.21139

Coscoy S, Waharte F, Gautreau A, Martin M, Louvard D, Mangeat P, Arpin M, Amblard F. '*Molecular analysis of microscopic ezrin dynamics by two-photon FRAP*'. PANS. **2002**, 99 (20): 12813-12818. doi:10.1073/pnas.192084599.

Demiray L, Özcivici E. '*Bone marrow stem cells adapt to low-magnitude vibrations by altering their cytoskeleton during quiescence and osteogenesis*'. Turk J Biol. **2014**, 38: 1-10. doi:10.3906/biy-1404-35

Du G, Ravetto A, Fang Q, den Toonder JMJ. '*Cell type can be distinguished by measuring their viscoelstic recovery times using a micro-fluidic device*' Biomed Microdevices. **2011**, 13: 29-40.

Efremov YM, Dzyubenko EV, Bagrov DV, Maksimov GV, Shram SI, Shaitan KV. '*Atomic Force Microscopy Study of the Arrangement and Mechanical Properties of Astrocytic Cytoskeleton in Growth Medium*.' Acta Nature. 2011, 3 (3: 10): 93-99.

Engl W, Arasi B, Yap LL, Thiery JP, Viasnoff V. '*Actin dynamics modulate mechanosensitive immobilization of cadherin at adherens junctions*'. NATURE CELL BIOL. **2014**, 16: 584-591. doi:10.1038/ncb297

Hammond S, Lee KH. '*RNA interference of cofilin in Chinese hamster ovary cells improves recombinant protein productivity*'. Biotechnology and Bioengineering, **2012**, 109(2): 528–535.

Helmchen F, Denk W. '*Deep tissue two-photon microscopy*'. Nature Methods. **2005**, 2(12): 932-940.

Hotulainen P, Paunola E, Vartiainen MK, Lappalainen P. '*Actin depolarizing factor and cofilin-1 play overlapping roles in promoting rapid f-actin depolymerization in mammalian non-muscle cells*'. Mol Biol Cell. **2005**, 16: 649-664. doi:10.1091/mbc.E04-07-0555.

Huveneers S, de Rooij J. '*Mechanosensitive systems at the cadherin-F-actin interface*'. J Cell Sci. **2013**, 126: 1-11. doi: 10.1242/jcs.109447.

Khaw BA, daSilva J, Vural I, Narula J, Torchilin VP. '*Intracytoplasmic gene delivery for in vitro transfection with cytoskeleton-specific immunoliposomes*'. J Control Release. **2001**, 75 (1-2): 199-210.

Kuznetsova TG, Starodubtseva MN, Yegorenkov NI, Chizhik SA, Zhdanov RI. '*Atomic force microscopy probing of cell elasticity*'. Micron. 2007, 38: 824–833.

Leung RKM, Whittaker PA. '*RNA interference: From gene silencing to gene-specific therapeutics*'. Pharm Therapeutics. **2005**, 107 (2): 222-239.

Lombardi M.L., Jaalouk D.E., Shanahan C.M., Burke B., Roux K.J., Lammerding J. *'The Interaction between Nesprins and Sun Proteins at the Nuclear Envelope Is Critical for Force Transmission between the Nucleus and Cytoskeleton'.* J Biol Chem. **2011**; 286 (30): 26743–26753 doi: 10.1074/jbc.M111.233700 PMCID: PMC3143636

Lund FW, Lomholt MA, Solanko LM, Bittman R, Wüstner D. '*Two-photon time-lapse microscopy of BODIPY-cholesterol reveals anomalous sterol diffusion in chinese hamster ovary cells*.' BMC Biophys. **2012**, 5: 20. doi: 10.1186/2046-1682-5-20.

Malone AMD, Batra NN, Shivaram G, Kwon RY, You L, Kim CH, Rodriguez J, Jair K, Jacobs CR. '*The role of actin cytoskeleton in oscillatory fluid flow-induced signaling in MC3T3-E1 osteoblasts'.* Am J Physiol - Cell Physiol. **2007**, 292 (5): C1830-C1836. doi**:**10.1152/ajpcell.00352.2005

Meinke P, Mattioli E, Haque F, Antoku S, Columbaro M, Straatman KR, Worman HJ, Gundersen GG, Giovanna Lattanzi G, Wehnert M, Shackleton S. '*Muscular Dystrophy-Associated SUN1 and SUN2 Variants Disrupt Nuclear-Cytoskeletal Connections and Myonuclear Organization*'. PLoS Genet. **2014**, 10 (9): e1004605. doi:10.1371/journal.pgen.1004605

Meng F, Sachs F. '*Visualizing dynamic cytoplasmic forces with a compliance-matched FRET sensor.*' J Cell Sci. **2011**, 124 (Pt. 2): 261-9. doi: 10.1242/jcs.071928. Epub 2010 Dec 20.

Ozcivici E, Luu YK, Adler B, Qin YX, Rubin J, Judex S, Rubin CT. '*Mechanical signals as anabolic agents in bone*'. Nat. Rev. Rheumatol. **2010**; 6: 50–59. doi:10.1038/nrrheum.2009.239

Pedersen JA, Swartz MA. '*Mechanobiology in the Third Dimension'*. Ann Biomed Eng. **2005**, 33 (11): 1469–1490. doi: 10.1007/s10439-005-8159-4

Pongkitwitoon S. '*Mechanotransduction of low intensity vibration in human bone marrow mesenchymal stem cells and bone marrow niches' macrophages*.' Ph.D. Dissertation. **2014**.

Qian AR, Gao X, Zhang W, Li J-B, Wang Y, Di SM, Hu LF, Shang P. 'Large Gradient High Magnetic Fields Affect Osteoblast Ultrastructure and Function by Disrupting Collagen I or Fibronectin/ab1 Integrin'. PLoS ONE. **2013**, 8 (1): e51036. doi:10.1371/journal.pone.0051036

Shi Y, Fu Y, Tong W, Geng Y, Lui PP, Tang T, Zhang X, Dai K. 'Uniaxial mechanical tension promoted osteogenic differentiation of rat tendon-derived stem cells (rTDSCs) via the Wnt5a-RhoA pathway'. J Cell Biochem. **2012**, 113(10): 3133-3142. doi: 10.1002/jcb.24190.

Scott MK, Akinduro O, Lo Celso C. '*In Vivo 4-Dimensional Tracking of Hematopoietic Stem and Progenitor Cells in Adult Mouse Calvarial Bone Marrow*'. J Vis Exp. **2014**, 91: e51683. doi:10.3791/51683.

Stricker J, Falzone T, Gardel ML. J Biomech. '*Mechanics of the F-actin cytoskeleton'*. **2010**, 43 (1): 9-14. doi:10.1016/j.jbiomech.2009.09.003. Epub 2009 Nov 13.

Sokolov I, Woodworth CD. '*Loss of elasticity of aging epithelial cells and its possible reversal*'. NSTI Nanotech **2005**: ISBN 0-9767985-0-6.

Uzer G., Pongkitwitoon S., Chan ME., Judex S. '*Vibration induced osteogenic commitment of mesenchymal stem cells is enhanced by cytoskeletal remodeling but not fluid shear'.* J Biomech. **2013**, 46 (13): 2296-302. Epub 2013 Jul 17.

Wang YK, Yu X, Cohen DM, Wozniak MA, Yang MT, Gao L, Eyckmans J Chen CS. '*Bone morphogenetic protein-2-induced signaling and osteogenesis is regulated by cell shape, RhoA/ROCK, and cytoskeletal tension.*' Stem Cells Dev. **2012**, 21(7): 1176-1186. doi: 10.1089/scd.2011.0293. Epub 2011 Oct 3.

Winter PW, Van Orden AK, Roess DA, Barisas BG. '*Actin-dependent clustering of insulin receptors in membrane microdomains*'. Biochim Biophys Acta. **2012**, 1818(3): 467-473. doi: 10.1016/j.bbamem.2011.10.006. Epub 2011 Oct 15.

Yonemura S. '*Cadherin-actin interactions at adherent junctions'*. Curr Opin Cell Biol. **2011**, 23(5): 515-22. doi: 10.1016/j.ceb.2011.07.001. Epub 2011 Jul 30.

Figures 4.1a and b:

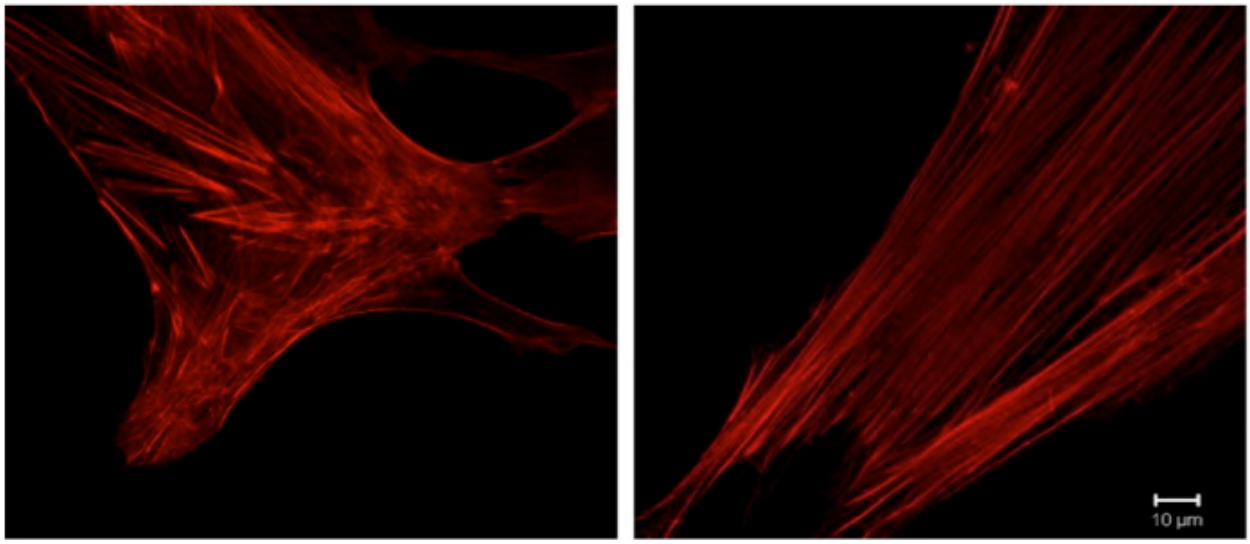

Figure 4.2:

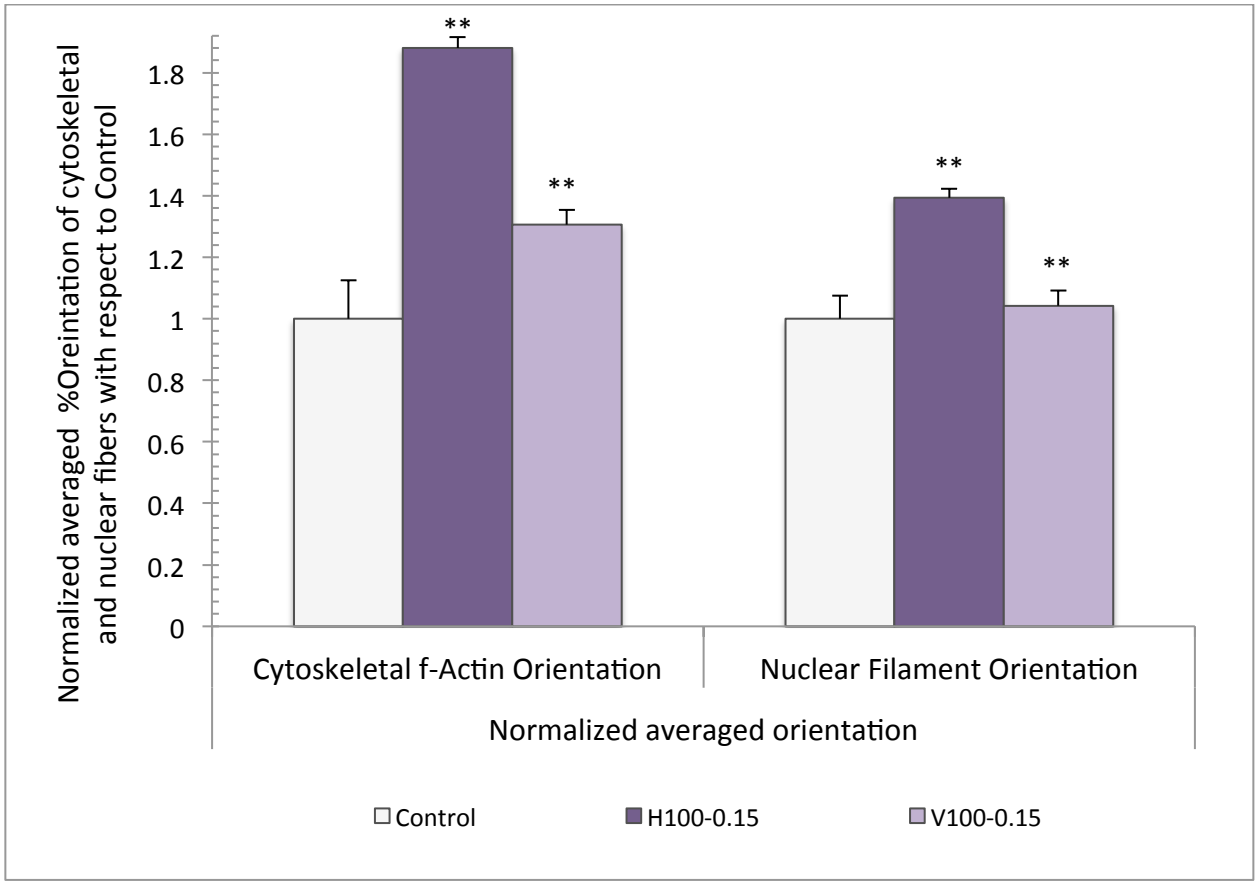
Normalized averaged %Oreintation of cytoskeletal and nuclear fibers with respect to Control
1.8
1.6
1.4
1.2
1
0.8
0.6
0.4
0.2
0
**
**
**
**
Cytoskeletal f-Actin Orientation
Nuclear Filament Orientation
Normalized averaged orientation
Control
H100-0.15
V100-0.15

Figure 4.3a:

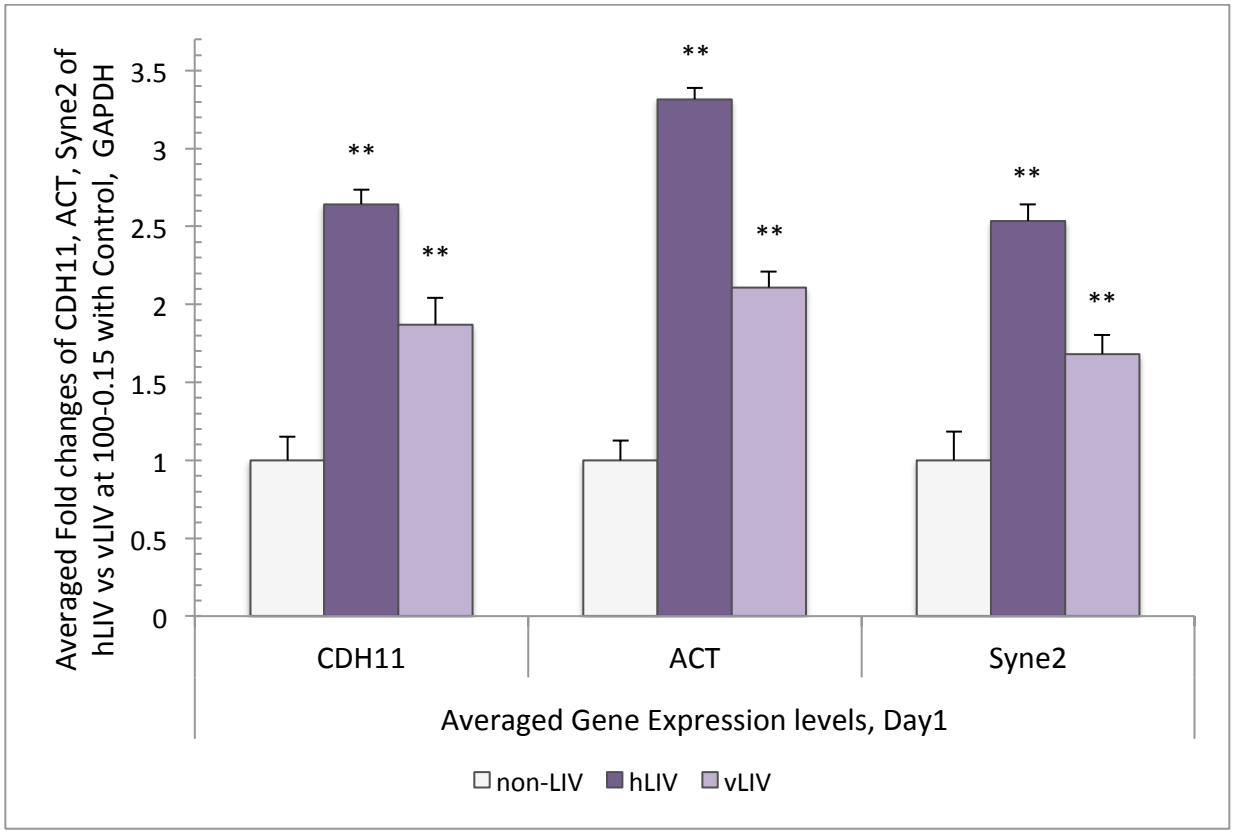
Averaged Fold changes of CDH11, ACT, Syne2 of hLIV vs vLIV at 100-0.15 with Control, GAPDH
3.5
3
2.5
2
1.5
1
0.5
0
**
**
**
**
**
**
CDH11
ACT
Syne2
Averaged Gene Expression levels, Day1
non-LIV
hLIV
vLIV

Figure 4.3b:

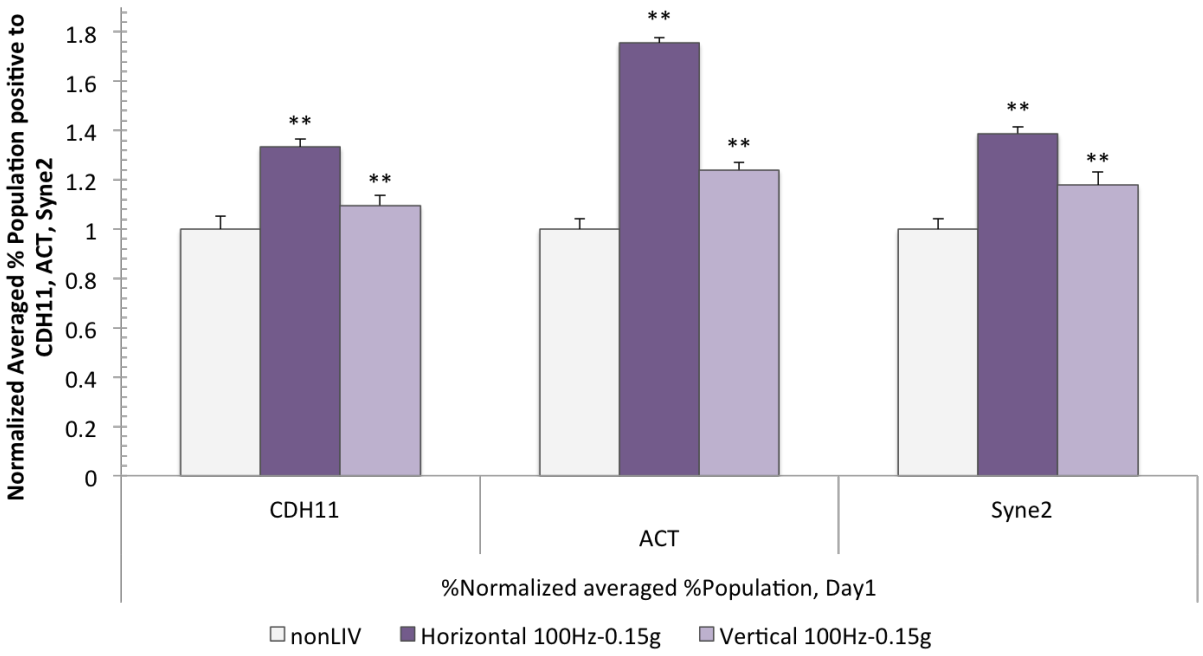
Normalized Averaged % Population positive to CDH11, ACT, Syne2
1.8
1.6
1.4
1.2
1
0.8
0.6
0.4
0.2
0
**
**
**
**
**
**
CDH11
ACT
Syne2
%Normalized averaged %Population, Day1
nonLIV
Horizontal 100Hz-0.15g
Vertical 100Hz-0.15g

Figure 4.4:

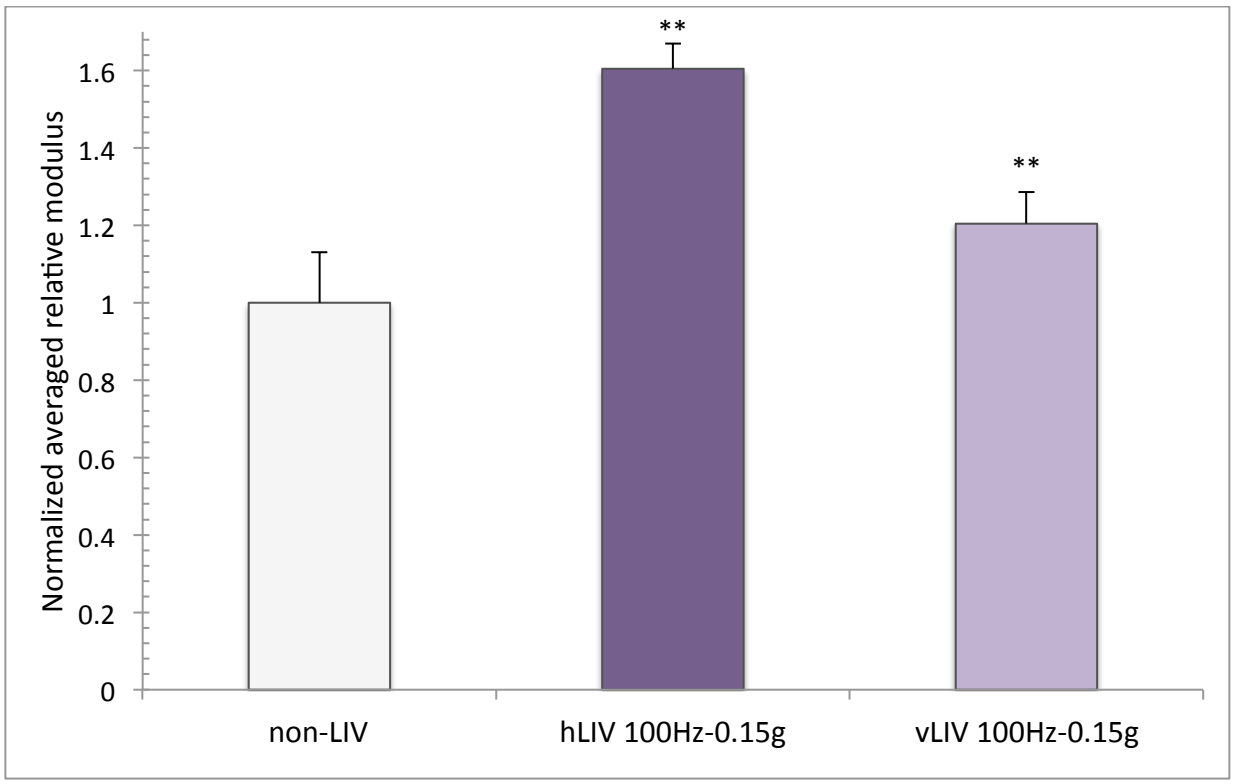
Normalized averaged relative modulus
1.6
1.4
1.2
1
0.8
0.6
0.4
0.2
0
**
**
non-LIV
hLIV 100Hz-0.15g
vLIV 100Hz-0.15g

Figure 4.5a:

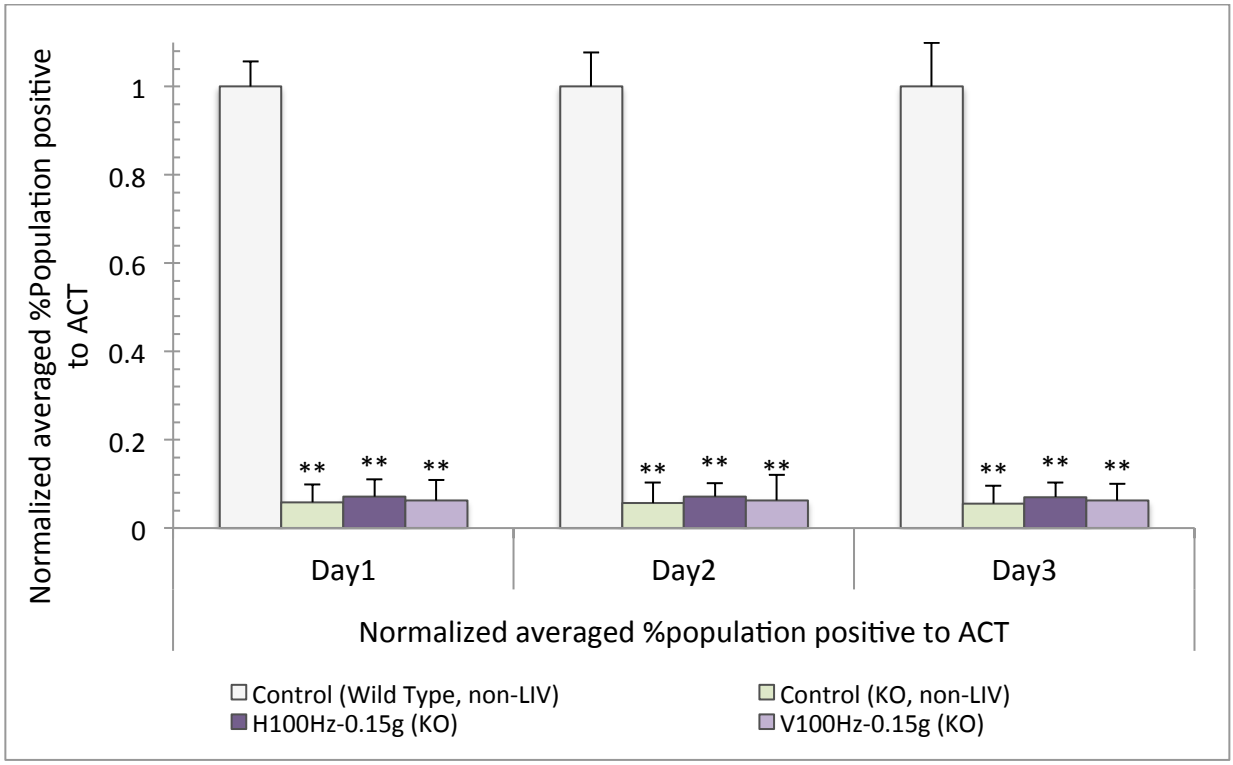
Normalized averaged %Population positive to ACT
1
0.8
0.6
0.4
0.2
0
**
**
**
**
**
**
**
**
**
Day1
Day2
Day3
Normalized averaged %population positive to ACT
Control (Wild Type, non-LIV)
Control (KO, non-LIV)
H100Hz-0.15g (KO)
V100Hz-0.15g (KO)

Figure 4.5b:

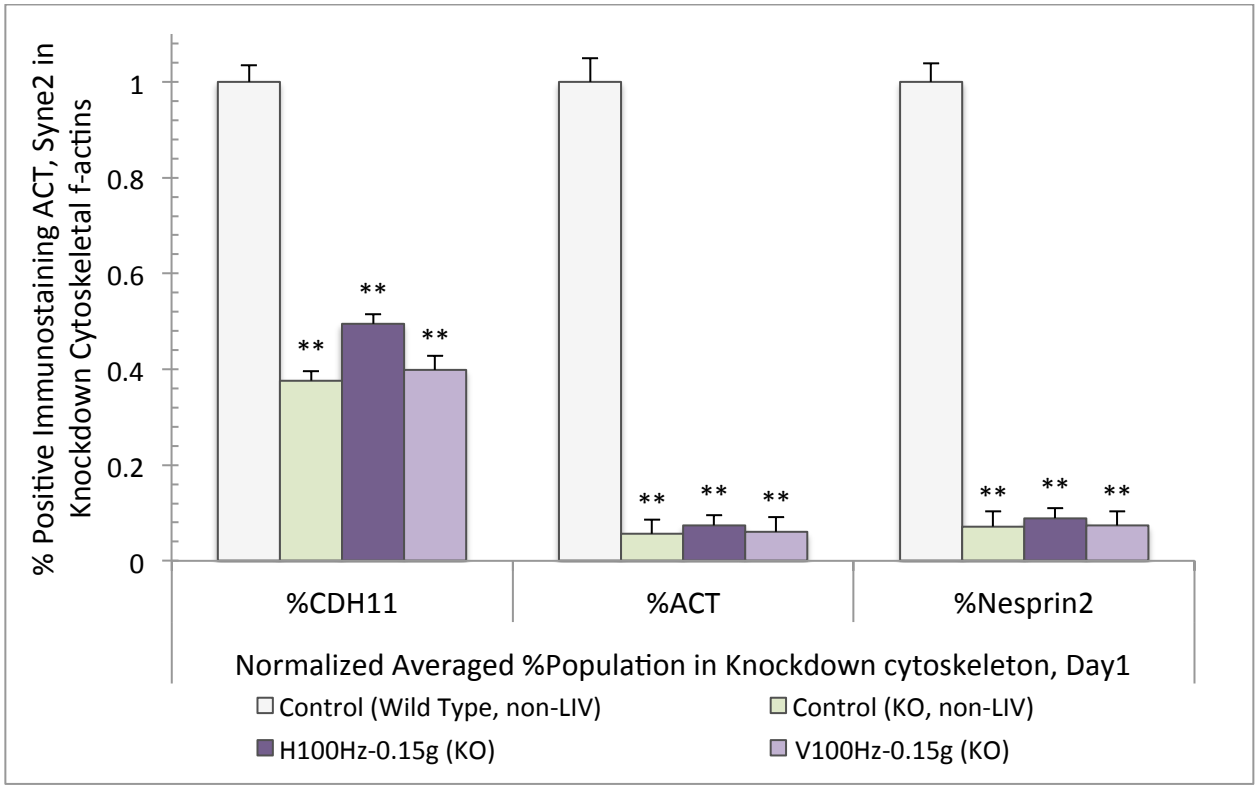
% Positive Immunostaining ACT, Syne2 in Knockdown Cytoskeletal f-actins
1
0.8
0.6
0.4
0.2
0
**
**
**
**
**
**
%CDH11
%ACT
%Nesprin2
Normalized Averaged %Population in Knockdown cytoskeleton, Day1
Control (Wild Type, non-LIV)
Control (KO, non-LIV)
H100Hz-0.15g (KO)
V100Hz-0.15g (KO)

Figure 4.5c:

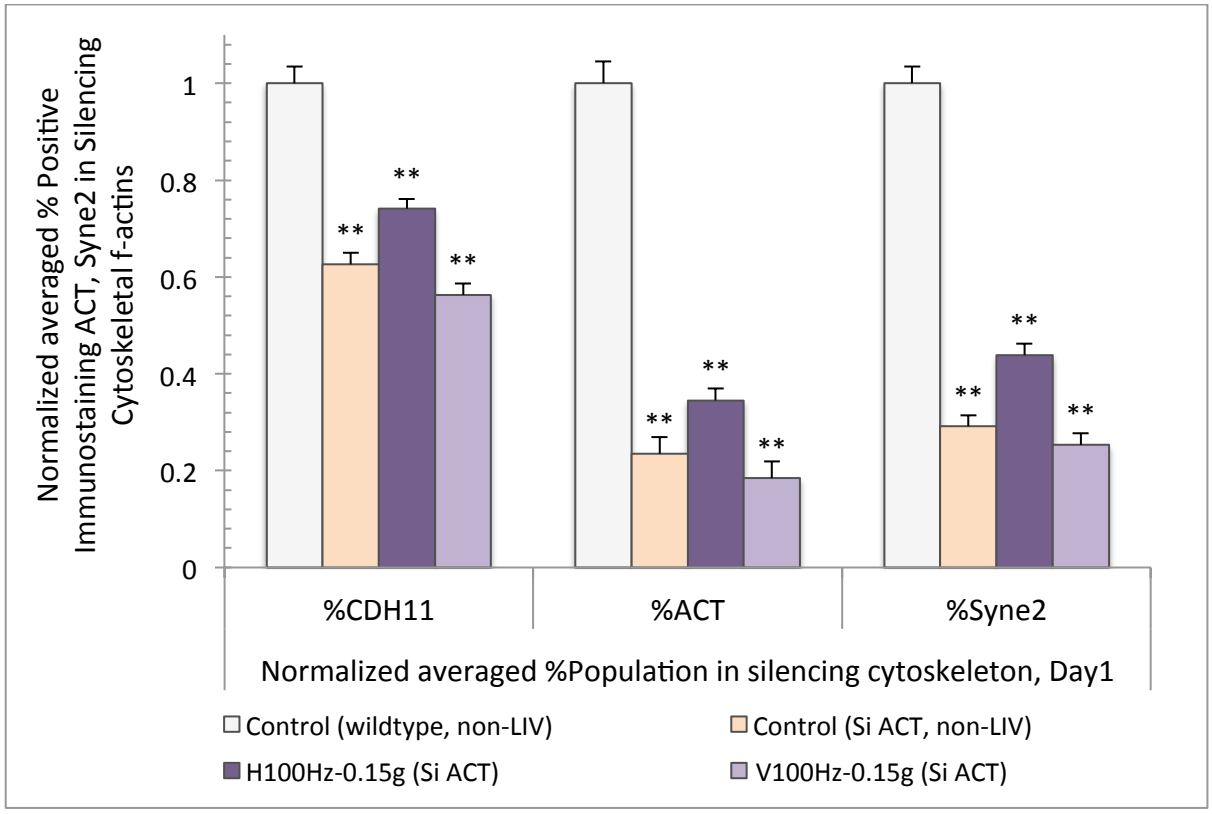
Normalized averaged % Positive Immunostaining ACT, Syne2 in Silencing Cytoskeletal f-actins
1
0.8
0.6
0.4
0.2
0
**
%CDH11
%ACT
%Syne2
Normalized averaged %Population in silencing cytoskeleton, Day1
Control (wildtype, non-LIV)
Control (Si ACT, non-LIV)
H100Hz-0.15g (Si ACT)
V100Hz-0.15g (Si ACT)

Chapter 5

Oscillatory Accelerations Modulate Stem Cell Differentiation in Human Bone Marrow and Adipose Derived MSCs

(Pending publication and/or patent)

Abstract

Human stem cells under the LIV have shown to improve osteogenic but suppress adipogenic differentiation. However, understanding whether the LIV controls the stem cell differentiation direction is still unclear. Previously we found that the human bone marrow MSCs have significantly increased the osteogenic differentiation under the LIV. Here, we investigated whether the LIV could modulate the differentiation fate of human stem cells (both human bone marrow and adipose-derived MSCs). We observed the stem cell osteogenic and adipogenic differentiation under the LIV at 100Hz-0.15g vs non-LIV. We tested whether the LIV could influence the commitment potentials of the human stem cell. The bone marrow MSCs with and without osteogenic induction media showed an increase in the cellular calcification under LIV. The upregulated Runx2 with the induction media was >1.3x higher folds than the non-induction groups. However, the PPARg levels were downregulated and much more in the groups under the LIV. Similarly, the adipose derived stem cells under the LIV showed the upregulated Runx2 (>1.2x more than the non-LIV) while down-regulated PPARg. These data suggested that the LIV directed the human stem cells towards the osteogenic lineages while suppressed the adipogenic differentiation. The data provided that the stem cells sense the LIV while the LIV promoted the osteogenic commitment of the stem cells. For the first time, we demonstrated the LIV directs the differentiation fate of the human stem cells.

5.1 Introduction

Low intensity vibration (LIV) commonly found to be anabolic to osteogenic but not adipogenic differentiation in cells, humans, and animals [Kim et al. 2012, Sen et al. 2011]. However, how the LIV promotes osteogenic or suppresses adipogenic differentiation has been unclear.

We found that human bone marrow mesenchymal stem cells (hBMSCs) during osteogenic differentiation were sensitive to frequencies, accelerations, and directions of the LIV [Pongkitwitoon et al. 2014]. Human stem cells (both human bone marrow and adipose-derived mesenchymal stem cells (hAMSCs)) are pluripotent and able to differentiate toward several lineages. Though both hBMSCs and hAMSCs show similar morphology and surface protein expression, however, the ability to differentiate towards specific lineages has been ongoing studied. The hBMSCs express higher levels of calcification than in the hAMSCs during the osteogenic differentiation [Vishnubalaji et al. 2012]. However, the hAMSCs provide higher percentages of differentiated adipocytes than in the hBMSCs [Barba et al. 2013, Takemitsu et al. 2012].

The differentiation direction of these stem cells can be modulated by pharmacological and biochemical stimulations [Autelitano, 1994, Carcamo-Orive et al. 2010]. Several studies have shown the mechanical stimulation in stem differentiation [Chen et al. 2015, Potier et al. 2010]. LIV has shown to promote osteogenic differentiation and prevent adipogenic differentiation in both animals and humans [Pre et al. 2011, Sen et al. 2011]. Furthermore, LIV has found to not only promote the stem cell proliferation [Luu et al. 2009] but also to enhance the lineage commitment of hAMSCs towards osteogenic differentiation, suggesting that MSCs

could sense the vibratory frequencies [Uzer et al. 2013]. However, understanding the LIV regulation of the stem cell fate has been significantly limited though critical to modulate the mechanism towards specific tissues.

Here, we aim to investigate the LIV in controlling the differentiation fate of the human stem cells. We observed changes in the calcification during the osteogenic and the lipoprotein accumulation during the adipogenic differentiations. The association of the amount of calcification and lipopeptide with the transcription Runx2 and PPARg levels could suggest the ability of the LIV in regulating the stem cell lineage. The results could provide the understanding of the cellular and molecular function of the LIV in the stem cell differentiation toward specific tissues.

5.2 Materials and Methods

5.2.1 Experimental design

To understand how LIV influences the human stem cell differentiation, we investigate the structure related gene of cytoskeletons [Pongkitwitoon et al. 2014] and the stem cell differentiation potentials under the horizontal LIV with respect to the non-LIV.

To monitor stem cell potentials, we investigated osteogenic and adipogenic differentiation of hBMSCs and hAMSCs with and without differentiation induction. The horizontal LIV of 100Hz-0.15g was applied. To investigate osteogenic differentiation, we observed cellular calcification by alizarin red assay and its colorimetric quantity. To confirm the osteoblastogenesis, gene expression levels of Runx2 (and GAPDH housekeeping gene) was

observed. To observe adipogenic differentiation, we quantified lipoprotein content by colorimetric oil red assay and confirmed it by PPARg gene expression levels.

To observe dynamic changes in the cytoskeletal structures, we determined changes in ACTn1 gene expression by the real-time PCR and flow cytometric analysis [Pongkitwitoon et al. 2014]. To evaluate the effect of LIV on the differentiation, we related the change of the cytoskeletal structure related gene expression with Runx2 and PPARg expression levels. We analyzed effects of LIV and non-LIV by statistic one-way ANOVA and the effect of LIV with or without induction by two-way ANOVA (significance at $p \leq 0.05$).

5.2.2 Cell culture and Mechanical stimulation

5.2.2.1 Culture human bone marrow mesenchymal stem cells (hBMSCs)

hBMSCs were aspirated from bone marrow of 25 years old African American female patient (Life Technologies) tested negative HIVs. hBMSCs were cultured in alpha-MEM without phenol red containing 7.5% heat-inactivated fetal bovine serum (Gibco), 5μM L-glutamine and specific growth factors of recombinant 15nM IGF-1 and 125pM FGF-β. To sustain properties under different environments, 1mM DTT (LifeLine D1532) and 0.1% BSA (Sigma A2058) were added to the stock solution of the growth factors. Since hBMSCs is very sensitive to changes in pH and $\%CO_2$, we added 25 mM HEPES to preserve the pH at 7.4, and protected the cells with 1% penicillin/streptomycin.

5.2.2.2 Culture human adipose-derived mesenchymal stem cells (hAMSCs)

hAMSCs were donated from 18-year-old female (Life Line Technology) and cultured in modified alpha-MEM without phenol red containing 7.5% heat inactivated FBS, 5μM L-glutamine, and 1% penicilins/streptomycin.

5.2.2.3 Selected signal combination of low intensity vibration (LIV)

We selected signal combinations of frequency, acceleration and direction of the best cell responses to the horizontal 100Hz-0.15g LIV [Pongkitwitoon et al. 2014]. We vibrated cells in 2 sessions a day, for 20 minutes in each session, with 2-hour rest in between sessions.

5.2.3 Osteoblastogenic differentiation

Our proliferation showed that the hBMSCs expressed the doubling time within 1-2 days for all LIV groups. To prevent the cell proliferation interfering with the cell differentiation, we plated cells 2 days prior to the experiment with cell density at 18,000 cells/cm^2 in 24well/plate. After 2 days of the first inoculation, the hBMSCs were induced with osteoblastogenic media containing 100nM dexamethasone, 10mM β-glycerol phosphate, and 0.05mM L-ascorbic acid-2-phosphate. The vibration was performed right after the osteoblastogenic induction. All observations were performed at the end of the second vibration on Day1 (the first day of osteoblastogenic induction).

5.2.4 Adipogenic differentiation

To prevent cell proliferation interfering with cell differentiation, we plated cells 2 days prior to the experiment with cell density at 18,000 cells/cm^2 in 24well/plate. After 2 days of the first inoculation, the hBMSCs were induced with adipogenic media containing 10μg/ml Insulin, 10μM dexamethasone, 250μM isobutylmethylxanthine (IBMX) and 200μM Indomethacin. After the second vibration, the oil red assay was performed for lipoprotein contents.

5.2.5 Calcification by Alizarin red assay

After fixing cells with ice-cold 100% ethanol, cells were several rinsed with sterilized distilled ice-cold water (sd-H_2O). The fixed cells were then added in with 40mM Alizarin Red S (Sigma A5533) solution and incubated in the dark for 45 minutes at room temperature. (Alizarin red solution was prepared according to standard protocols.) The samples were then incubated with dPBS for another 15 minutes. To quantify calcification [Ca^{2+}] in μg/ml, the alizarin red-stained cells were then destained with 10% cetylpyridinium chloride, CPC (Sigma C0732) for 15 minutes in the dark at room temperature. (The CPC solution was prepared followed standard protocols.) The fluorescent absorbance at 562 nm was measured (each well of 24wells/plate was aliquot into 3 wells of 95wells/plate for measurements, each condition had 6 wells). The A_{562} was then compared to an established standard curve of known amount of [Ca^{2+}]. The ratio of the averaged calcification of LIV with the control $[Ca^{2+}]_{CT}$ provides the normalized calcification [Ca^{2+}]

5.2.6 Lipoprotein content by Oil red assay

After cells were fixed with 10%para-formalin for 1hour, the fixed cells were washed 5times with sterilized distilled water and added the oil red stain solution. After the incubation with oil red for ~15 minutes, the stained cells were washed with sterilized distilled water and incubated with hematoxylin for 5-10 min. (Fluorescent imaging of samples was acquired by Zeiss, as red color for lipoprotein and blue for nucleus.) To quantify the lipoprotein content, destaining oil-red-stained cells were washed 3times with 60% isopropanol and incubation with 100% isopropanol for 10-15min. Each well of 24wells/plate was aliquot into 3wells of 96wells/plate for fluorescence analysis at 520nm with respect to the absorbance at 490nm. We reported normalized averaged lipoprotein accumulation of hLIV with respect to non-LIV.

5.2.7 Gene expression by real-time PCR

We quantified Runx2 and PPARg gene expression levels by real-time PCR using TaqMan standard protocols with n=6 in each condition. The expression level was analyzed by the fold changes ($2^{-\Delta\Delta Ct}$) with respect to the control and the GAPDH housekeeping gene. After vibration, cells were lysed by TRIzol (Life Technologies) and the RNA extraction was done by phase separation with chloroform. The RNA was precipitated from nucleic acid by RNeasy (Qiagen) and washed with 70% ethanol before re-dissolving by RNA-free water. To quantify RNA concentration and determine the RNA quality, we used NanoDrop (ND-100 V3.3.0). The ratio of [A_{260}/A_{280}] ≥1.8 is for 'pure' cDNA, and ≥2.0 for 'pure' RNA, validating by [A_{260}/A_{230}] ~2.0-2.2 for 'pure' nucleic acid. Then, the RNA was converted to cDNA by reversed transcriptase (Invitrogen). After the determination of purification and concentration, cDNA was

diluted to be the same concentration (3.33ng/µl). Using StepOne 2.2, the real-time polymerase chain reaction (q-PCR) provided Ct of the interested genes for calculation of the gene expression level ($2^{-\Delta\Delta Ct}$).

5.2.8 Flow cytometric analysis

The measurement of % cell populations by laser-based flow cytometric analysis relies on effective immunofluorescent staining and conjugated antibodies. We prepared samples by lifting the attached cells with 0.05% trypsin/EDTA. We performed immunofluorescent staining of (i) ALP activity, (ii) calcification with alizarin red, (iii) lipoprotein with oil red, and (iv) cytoskeletal orientation with conjugated primary ACTn1 human monoclonal antibody (Santa Cruz sc-17829) and IgG. Data acquisition was set the %gated cell population positive to specific immunofluorescence with at least 10,000 events and FlowJo analyzed the %cell population. We reported the normalized average %population, n=6.

5.2.9 Statistic analysis

Statistic one-way analysis of variance, ANOVA (SPSS) with Tukey post hoc test analyzed the effect of hLIV vs non-LIV and three-way ANOVA for effects of hLIV, non-LIV, with and without induction. Each condition in each experiment was repeated at least n=6. Each experiment was at least duplicated. The results were statistically significant when $p < 0.05$, and p values were reported as *<0.05, **<0.01.

5.3 Results

5.3.1 Cellular calcification of osteoblastogenesis

The cellular calcification [Ca^{2+}] by the alizarin red assay of hLIV groups was >1.3-1.8x higher than non-LIV. The normalized average [Ca2+] of hBMSCs was >1.2x higher than [Ca2+] of hAMSCs (**Figure 5.1a**). The normalized averaged [Ca^{2+}] of hBMSCs with osteogenic induction (OS) was >1.13x more than [Ca^{2+}] without an OS as the induction had no significant effect on osteoblastogenesis of hBMSCs under hLIV (statistic three-way ANOVA). The calcification of hBMSCs with the OS was similar to the calcification without an OS, indicating hBMSCs were naturally osteoblastic precursors even without the osteogenic induction (and similar to the studies of Kanczler et al. 2008). The normalized averaged [Ca^{2+}] of hAMSCs with OS was >1.2x more than [Ca^{2+}] without OS.

Flow analysis of %population of cellular calcification (%calcification) confirmed calcification by alizarin red (**Figure 5.1b**). The normalized average %calcification of hBMSCs was higher than that of hAMSCs. %Calcification of hBMSCs and hAMSCs with the OS was >1.2x and >1.09x more than that without an OS, respectively.

5.3.2 Lipoprotein content in adipogenesis

The lipoprotein accumulation, [Lipoprotein], of hBMSCs in hLIV groups was ~1.3-1.4 less than [Lipoprotein] in non-LIV. However, the normalized average [Lipoprotein] of hAMSCs in hLIV and non-LIV was similar. [Lipoprotein] in hAMSCs was ~1.3-1.6x higher than that in hBMSCs (**Figure 5.2a**). The normalized average [Lipoprotein] of hAMSCs with adipogenic differentiation (AD) was >1.2x higher than [Lipoprotein] without AD. Contrary, [Lipoprotein]

of hBMSCs with AD was similar to [Lipoprotein] without AD, supporting no effect of the induction media on hBMSCs under LIV. The data suggested that even with adipogenic induction hBMSCs were difficult to differentiate to be adipocytes (as similarly seen in Hamam et al. 2014).

Normalized averaged %population of oil red (%Lipoprotein) confirmed higher lipoprotein accumulation in hAMSCs (**Figure 5.2b**). %Lipoprotein of hAMSCs with AD was >1.2x higher than %Lipoprotein without AD. However, %Lipoprotein of hBMSCs with and without AD was similar as though hBMSCs was natural adipogenic resistance (as also seen in Matsuoka et al. 2013).

5.3.3 Transcriptional Runx2 and PPARg

Runx2 expression levels of hBMSCs and hAMSCs under hLIV were upregulated (**Figure 5.3a**), supporting the significant effect of hLIV on osteoblastogenesis. The average Runx2 expression level of hBMSCs had ~1.3x folds higher than that of hAMSCs. The Runx2 expression level of hBMSCs with the OS was >1.35x more than the expression without an OS. However, the Runx2 expression levels of hAMSCs with and without an OS were quite similar. The data suggested that hLIV improved osteogenic differentiation and hBMSCs were effortlessly osteoblastogenesis even without OS.

The averaged PPARg expression levels of hLIV groups were downregulated (**Figure 5.3b**), confirming hLIV-suppressing adipogenesis. The PPARg of hAMSCs was >1.4x higher than that of hBMSCs. Without AD, hAMSCs had ~1.3 less PPARg than with AD as if hAMSCs were ready to differentiate to be adipocytes with the right induction [Linero et al. 2014]. However, hBMSCs with and without AD had downregulated PPARg, especially under hLIV.

5.3.4 LIV elevated osteoblastogenesis but suppressed adipogenesis

The normalized averaged of %population positive to cytoskeleton in the osteogenic and adipogenic differentiation of the LIV groups was monitored by flow cytometry (**Figure 5.4a**). The %cytoskeleton of hBMSCs and hAMSCs during osteogenic differentiation (upregulated Runx2 >2-3x folds) under the horizontal LIV was >1.2-1.9x higher than the %cytoskeleton under non-LIV. During adipogenesis (downregulated PPARg <0.6-1 folds), the %cytoskeleton under hLIV was >1.1-1.5x higher than that under non-LIV.

The %cytoskeleton during osteogenic differentiation of hBMSCs was >1.4-1.6x higher than the %cytoskeleton of hAMSCs. Corresponding with the upregulated Runx2 of hBMSCs was >1.2-1.3 folds higher than Runx2 of hAMSCs. During osteogenic differentiation, hBMSCs with OS had 1.5x higher %cytoskeletons than without OS. Significantly, increasing %cytoskeleton of hBMSCs under hLIV during the osteogenic differentiation confirmed that the hLIV induced the cytoskeletal orientation as seen in the two-photon images [Pongkitwitoon et al. 2014]. During adipogenic differentiation, the %cytoskeleton of hBMSCs was ~1.3x higher than that of hAMSCs, while hBMSCs had >1.3x less PPARg than hAMSCs.

To understand the mechanism of LIV on the differentiation, we observed the structure related cytoskeleton (ACTn1) and Runx2 gene expression levels. We found that the amount of cytoskeleton (%ACTn1) correlated with the cytoskeletal orientation (>86.3%±1.02). If the cytoskeletal orientation assisted the osteogenic differentiation, the elevation of Runx2 and calcification should synchronize with an increase in cytoskeletal orientation. The %ACTn1 cytoskeleton was re-plotted against a progress of osteogenic and adipogenic differentiation of hBMSCs (**Figure 5.4b**). As the cytoskeleton increased, the osteogenic differentiation was raised with an increasing upregulated Runx2. But during adipogenic differentiation, the cytoskeleton

was increased with the decreasing PPARg. The highest cytoskeleton caused the lowest down-regulated PPARg. The data could provide for the first time that the cytoskeleton involved in the LIV controlling the differentiation fate by increasing osteogenic but suppressing adipogenic differentiation.

5.4 Discussion

We investigated the osteogenic and adipogenic differentiation of hBMSCs and hAMSCs under the LIV. We selected the best responding signal combinations of the horizontal LIV at 100Hz-0.15g [Pongkitwitoon et al. 2014]. We observed (i) the calcification during the osteogenic differentiation by the alizarin red assay, and (ii) the lipoprotein accumulation during adipogenic differentiation by an oil red assay. The hBMSCs are natural osteoblast precursors as they progressed through the osteogenic differentiation even without the osteogenic induction or LIV stimulation. The increased calcification of hBMSCs was >1.2x more than of hAMSCs. The Runx2 expression levels of hBMSCs were >1.5x folds higher than that of hAMSCs. Flow cytometric analysis of the %cytoskeleton of hBMSCs was increased with upregulated Runx2 and elevating calcification. The data suggested, for the first time, that the cytoskeleton involved in the LIV regulating the osteogenic differentiation. The cytoskeleton gene expression level was increased under LIV and the increase in hBMSCs was more than in hAMSCs. The relation of the cytoskeleton increased with the progressive osteogenic differentiation could indicate the LIV improving osteoblastogenesis though the cytoskeleton. The lipoprotein accumulation of hAMSCs was >1.5x higher than that of hBMSCs under non-LIV (**Figure A25**). The down-regulation of PPARg expression levels in LIV confirmed that the adipogenic differentiation under the LIV was less progressive than the non-LIV. The highest increased cytoskeleton (1.5x) had the lowest PPARg expression levels (0.07x) during the LIV. These data could indicate that the LIV supported osteoblastogenesis but suppressed adipogenesis.

A limitation of this study was that the intermediate cellular and molecular processes are time dependent. While the biological assays mainly relied on the time-dependent protein

synthesis, the biological responsiveness could only be captured as overall responses only after a certain experimental duration. These observations could omit transitional details of the local reaction, but exclusively represented the overall cell responses.

5.4.1 LIV Supported Osteoblastogenesis but Suppressed Adipogenesis

Since amounts of the calcium deposition and the lipoprotein accumulation increase with cell density, here we made sure that the cells are confluent at the same concentration by plating cells 2 days prior to the induction and LIV. Therefore, changes in the calcification and the lipoprotein here indicate the cell responsiveness to the LIV or the induction media. Additionally, with our technique the cell proliferation could not interfere with the differentiation.

The mechanical stimulation able to promote bone formation and decrease lipid accumulation has been extensively studied [Sen et al. 2008]. Mechanical shear stress found to induce the osteogenic differentiation [Yourek et al. 2010] while mechanical strain found to inhibit adipogenic differentiation through β-catenin in human stem cells [Sen et al. 2008].

Though the mechanical stimulation could provide an anabolic to osteogenic- while catabolic to adipogenic- differentiation. Some uncertainties of the uncontrollable mechanical signals could deliver counterproductive results. Under cyclic strain, the stem cell could undergo a progressive adipogenic- instead of osteogenic- differentiation because the coupling GSK3β mechanism could deplete the β-catenin, increasing adipogenic differentiation [Sen et al. 2011]. Additionally, the overexpressed TGF-β during slow cyclic stress could also upregulate insulin-like growth factor-1 (IGF-1), which prompts to increase adipogenic differentiation [Lowe et al. 2011].

With LIV, the undesirable results can be curbed here through a precise control of frequency and acceleration. Our data (not shown here) also provided that the LIV could maintain the upregulated β-catenin and TGF-β in proper levels of controlling differentiation toward the preferable osteogenic direction. Our data showed that the upregulated Runx2 and Wnt10α were increased with an elevated cytoskeletal orientation. These data were similar to the common finding of the upregulated Runx2 and Wnt10α promoting the osteogenic differentiation in human stem cells [Giuliani et al. 2013]. Although the pathway regulating the transcriptional Runx2 has been unclear, the Runx2 was found to be abundant in the pre-osteoblasts and osteoblast bone cells, including stem cells during the progressive osteogenic differentiation [Meyer et al. 2014].

5.4.2 LIV Functions to Control Stem Cell Fates

Control multilineage potentials of human stem cells have been extensively studied in biochemistry and nanomaterials for medicines. In well-defined surface nanomaterials, the extracellular matrix was thought to control the stem cell fates through their physical interactions [Guilak et al. 2009]. The increasing modulus of the substrate could cause the ECM upregulating FAK with β-catenin [Parekh et al. 2011]. However, the fact that ECM of osteoblast bone cells is in the calcified collagen matrix that is very rigid. The transduced forces could aggravate from their resonance exceeding 100% more than the input forces in calcified matrix [Rubin et al. 2003]. Therefore, the interaction between the ECM in the rigid matrix might only be exacerbated to cells to impossibly withstand such excessive transduced forces.

Previously, we found that the cytoskeletal orientation (by the two-photon imaging) was better aligned in one direction during the LIV whereas the stem cells expressed the upregulated ACTn1 structure related gene expression with an increased %ACTn1 positive population [Pongkitwitoon et al. 2014]. Here, the upregulated ACTn1 during the LIV was synchronized with the upregulated Runx2 but downregulated PPARg. These data could indicate that the increased cytoskeletal orientation could advance the osteogenic differentiation while restraining the adipogenic differentiation. The data showed the ability of LIV in regulating the stem cell fate through controlling the cytoskeleton.

5.4.3 LIV Directs Stem Cell Differentiation Direction

Though the mechanical signal delivery throughout the cell relevant to the human physiology remains unclear. By optimization of the LIV loading parameters, we were able to apply a wide range of the well-defined mechanical signal to the biological stem cell responsiveness. However, the identification of cellular and molecular mechanisms of the LIV that control these stem cell adaptive responses is still unclear.

Here, for the first time, we were able to demonstrate that the cytoskeleton could be the biological mechanism of the LIV regulating the stem cell differentiation toward osteogenic while suppressing adipogenic lineages [Pongkitwitoon et al. 2014]. We found that human stem cells are sensitive to acceleration amplitude, frequency, and direction through the vibration-oriented cytoskeletons.

To maintain the cellular integrity, the intracellular force transmission could start from the cytoskeletal orientation [Lombardi et al. 2011], and remodeling [Shafrir et al. 2002]. Such orientation and remodeling could prevent the nuclear deformation [Friedl et al. 2010, Rothballer et al. 2013], and the damaged nuclear laminins [Houben et al. 2007], including chromatins that could cause the impaired gene expression [Folker et al. 2011]. Previously, we found that the cytoskeletal orientation increased with the progressive osteogenic differentiation under the LIV by quantifying the two-photon images [Pongkitwitoon et al. 2014]. Several findings have supported the role of cytoskeleton in the cytoskeletal orientation [Hinoue et al. 2005, Pongkitwitoon et al. 2014], including in cell division [Triplett et al. 2006], molecular functions [Reddy et al. 2013]. The fact is that the actin cytoskeletons including cytoskeleton binding protein alpha actinins (ACTn1) can form a lattice-like structure that regulates the cytoskeletal organization [Sjöblom et al. 2008]. Additionally, the cytoskeletal orientation has been found to control the cell morphology. The stem cells with accumulated leaner and longer morphology were found to commit to the osteogenic differentiation, while the round shape became adipogenesis [Matsuoka et al. 2013].

In surface modification to direct the stem cell lineage, the higher modulus nanostructure provided an increased calcification during the stem cells osteogenic differentiation [Parekh et al. 2011]. Interestingly, from their results we saw that the difference in the cytoskeletal orientation not the substrate modulus could also be the key to the increased osteogenic differentiation. These data supported that the cytoskeleton involved in the LIV controlling the stem cell differentiation direction.

5.4.4 LIV Suppresses Adipogenesis

An increase in fatty acid-binding protein-4 (Fabp4) and hormone adiponectin (Adipoq) was believed to upregulated PPARg and further maturation of the lipogenesis [Menssen et al. 2011]. Increasing the dissembled cytoskeletons could promote a round morphology of the stem cells, stimulating the adipogenesis [Feng et al. 2010]. Previously, we found the downregulated Adipoq and Fabp4 with decreasing the PPARg in LIV groups [Pongkitwitoon et al. 2014]. The mechanism could derive from the LIV induced the cytoskeletal orientation promoting (i) an increase in the cytoskeletal assembling (upregulated ACTn1), and (ii) the long and lean morphology, ultimately suppressing the adipogenesis. We could in the future measure the length to width ratio (L/W) of adipocytes, and osteoblasts. The prediction would be that human osteoblasts would have an L/W ratio >> 1 (long and lean), and adipocytes = 1 (round).

In relation of the upregulated PPARg with the cellular structure, several studies showed that the upregulated PPARg during adipogenesis could cause defects in the cilia formation [Marion et al. 2009] and disrupted cytoskeletons [Farmer 2005]. The cilia have known to be one of the cell mechanical receptors, responsible for cell movements, sensing and signaling [Thompson et al. 2012]. The lack of cilia and cilia deformation [Mukhopadhyay et al. 2013] could cause cytoskeletal disruption [Pedersen et al. 2012] and impaired Wnt/β-catenin [Lancaster et al. 2009], increasing the PPARg induced adipogenesis [Huang et al. 2011]. The Wnt/β-catenin was believed to induce the cytoskeletal remodeling [May-Simera et al. 2012].

Here, our data supported that the LIV restrain a progress in the adipogenic differentiation, which could be through the cytoskeleton.

5.5 Conclusion

Our data demonstrate for the first time that the LIV directs the stem cell differentiation towards the osteogenic lineages. We demonstrated the mechanism of LIV in modulating the stem cell differentiation direction is via the cytoskeletal orientation. The data indicate the specific cellular and molecular function of the LIV in regulating the stem cell lineages. The information provides great insights into the non-pharmacological precision control of human stem cells towards specific tissues, eventually determining the physiological stage of the mammalian bone anabolism.

References

Alves RD, Demmers JA, Bezstarosti K, van der Eerden BC, Verhaar JA, Eijken M, van Leeuwen JP. '*Unraveling the human bone microenvironment beyond the classical extracellular matrix proteins: a human bone protein library*.' J Proteome Res. 2011, 10 (10): 4725-33. doi: 10.1021/pr200522n. Epub 2011 Sep 21.

Autelitano DJ. '*Glucocorticoid regulation of c-fos, c-jun and transcription factor AP-1 in the AtT-20 corticotrope cell*.' J Neuroendocrinol. 1994; 6 (6): 627-637.

Barba M, Cicione C, Bernardini C, Michetti F, Lattanzi W. '*Adipose-Derived Mesenchymal Cells for Bone Regereneration: State of the Art*.' BioMed Research Inter. 2013: ID 416391. http://dx.doi.org/10.1155/2013/416391

Carcamo-Orive I, Gaztelumendi A, Delgado J, Tejados N, Dorronsoro A, Fernandez-Rueda J, Pennington DJ, Trigueros C. '*Regulation of Human Bone Marrow Stromal Cell Proliferation and Differentiation Capacity by Glucocorticoid Receptor and AP-1 Crosstalk*'. J Bone Min Res. 2010, 25 (10): 2115–2125. doi: 10.1002/jbmr.120.

Chen X, He F, Zhong DY, Luo ZP. '*Acoustic-Frequency Vibratory Stimulation Regulates the Balance between Osteogenesis and Adipogenesis of Human Bone Marrow-Derived Mesenchymal Stem Cells*.' BioMed Research Inter. 2015: ID 540731. http://dx.doi.org/10.1155/2015/540731

Farmer SR. '*Regulation of PPARgamma activity during adipogenesis*.' Int J Obes (Lond). 2005; 29 Suppl 1: S13-S16.

Feng T, Szabo E, Dziak E, Opas M. '*Cytoskeletal disassembly and cell rounding promotes adipogenesis from ES cells*.' Stem Cell Rev. 2010, 6(1): 74-85. doi: 10.1007/s12015-010-9115-8.

Friedl P, Wolf K, Lammerding J. '*Nuclear mechanics during cell migration*'. Curr Opin Cell Biol. 2010, 23: 55-64. doi:10.1016/j.ceb.2010.10.015

Giuliani N, Lisignoli G, Magnani M, Racano C, Bolzoni M, Dalla Palma B, Spolzino A, Manferdini C, Abati C, Toscani D, Facchini A, Aversa F. *'New insights into osteogenic and chondrogenic differentiation of human bone marrow mesenchymal stem cells and their potential clinical applications for bone regeneration in pediatric orthopaedics.'* Stem Cells Int. 2013:312501. doi: 10.1155/2013/312501. Epub 2013 May 23.

Guilak F, Cohen DM, Estes BT, Gimble JM, Liedtke W, Chen CS. '*Control of stem cell fate by physical interactions with the extracellular matrix*'. Cell Stem Cell. 2009, 5 (1): 17-26. doi:10.1016/j.stem. 2009.06.016

Hamam D, Ali D, Vishnubalaji R, Hamam R, Al-Nbaheen M, Chen L, Kassem M, Aldahmash A, Alajez NM. '*microRNA-320/RUNX2 axis regulates adipocytic differentiation of human*

mesenchymal (skeletal) stem cells'. Cell Death and Disease. 2014, 5, e1499; doi:10.1038/cddis.2014.462

Hinoue A, Takigawa T, Miura T, Nishimura Y, Suzuki S, Shiota K. '*Disruption of actin cytoskeleton and anchorage-dependent cell spreading induces apoptotic death of mouse neural crest cells cultured in vitro*.' Anat Rec A Discov Mol Cell Evol Biol. 2005, 282 (2): 130-137.

Houben F, Ramaekers FC, Snoeckx LH, Broers JL. '*Role of nuclear lamina-cytoskeleton interactions in the maintenance of cellular strength.*' Biochim Biophys Acta. 2007, 1773 (5): 675-686.

Huang HY, Hu LL, Song TJ, Li X, He Q, Sun X, Li YM, Lu HJ, Peng-Yuan Yang PY, Tang QQ. '*Involvement of Cytoskeleton-associated Proteins in the Commitment of C3H10T1/2 Pluripotent Stem Cells to Adipocyte Lineage Induced by BMP2/4*.' Mol Cell Proteomics. 2011; 10 (1): M110.002691. doi: 10.1074/mcp.M110.002691. PMCID: PMC3013452

Kanczler JM, Oreffo ROC. '*Osteogenesis and angiogenesis: the potential for engineering bone*'. Euro Cells Mat. 2008, 15: 100-114.

Kim IS, Song YM, Lee B, S.J. Hwang SJ. '*Human Mesenchymal Stromal Cells are Mechanosensitive to Vibration Stimuli*.' JDR. 2012, 91 (12): 1135-1140. doi:10.1177/0022034512465291

Lancaster MA, Louie CM, Silhavy JL, Sintasath L, DeCambre M, Nigam SK, Karl Willert K, Gleeson JG. '*Impaired Wnt/β-catenin signaling disrupts adult renal homeostasis and leads to cystic kidney ciliopathy*.' Nature Medicine. 2009, 15: 1046-1054. doi:10.1038/nm.2010

Linero I, Chaparro O. '*Paracrine Effect of Mesenchymal Stem Cells Derived from Human Adipose Tissue in Bone Regeneration*'. PLoS ONE. 2014, 9(9): e107001. doi:10.1371/journal.pone.0107001

Lombardi ML, Lammerding J. '*Keeping the LiNC: the importance of nucleoskeletal coupling in intracellular force transmission and cellular function*'. Biochem Soc Trans. 2011, 39: 1729-1732. doi:10.1042/BST20110686.

Lowe CE, O'Rahilly S, Rochford JJ. '*Adipogenesis at a glance'*. J Cell Sci. 2011, 124: 2681-2686 doi:10.1242/jcs.079699

Luu YK, Capilla E, J Rosen CJ, Gilsanz V, Pessin JE, Judex S, Clinton T Rubin CT. '*Mechanical Stimulation of Mesenchymal Stem Cell Proliferation and Differentiation Promotes Osteogenesis While Preventing Dietary-Induced Obesity*.' J. Bone Min Res. 2009, 24 (1): 50-61.

Marion V, Stoetzel C, Schlicht D, Messaddeq N, Koch M, Flori E, Danse JM, Mandel JL, Dollfus H. '*Transient ciliogenesis involving Bardet- Biedl syndrome proteins is a*

fundamental characteristic of adipogenic differentiation.' Proc. Natl. Acad. Sci. 2009, 106: 1820-1825.

Matsuoka F, Takeuchi I, Agata H, Kagami H, Shiono H, Kiyota Y, Honda H, Kato R. '*Morphology-Based Prediction of Osteogenic Differentiation Potential of Human Mesenchymal Stem Cells*'. PLoS ONE. 2013, 8(2): e55082. doi:10.1371/journal.pone.0055082

May-Simera HL, Kelley MW. '*Cilia, Wnt signaling, and the cytoskeleton*.' Cilia. 2012, 1: 7. http://www.ciliajournal.com/content/1/1/7

Menssen A, Häupl T, Sittinger M, Delorme B, Charbord P, Ringe J. '*Differential gene expression profiling of human bone marrow-derived mesenchymal stem cells during adipogenic development*.' BMC Genomics 2011, 12: 461.

Meyer MB, Benkusky NA, Pike JW. '*The RUNX2 cistrome in osteoblasts: characterization, down-regulation following differentiation, and relationship to gene expression.'* J Biol Chem. 2014, 289 (23): 16016-31. doi: 10.1074/jbc.M114.552216. Epub 2014 Apr 24.

Mukhopadhyay S, Jackson PK. '*Cilia, tubby mice, and obesity.*' Cilia. 2013; 2: 1. doi: 10.1186/2046-2530-2-1. PMCID: PMC3626941

Parekh SH, Chatterjee K, Lin-Gibson S, Moore NM, Cicerone C, Young MF, Simon CG. '*Modulus-Driven Differentiation of Marrow Stromal Cells in 3D Scaffolds That Is Independent of Myosin-based Cytoskeletal Tension*.' Biomaterials. 2011, 32 (9): 2256–2264. doi:10.1016/j.biomaterials.2010.11. 065.

Pedersen LB, Schrøder JM, Satir P, Christensen ST. '*The ciliary cytoskeleton*.' Compr Physiol. 2012 Jan;2(1):779-803. doi: 10.1002/cphy.c110043.

Pongkitwitoon S. '*Mechanotransduction of LIV in human bone marrow mesenchymal stem cells and bone marrow niches*'. Ph.D. Dissertation 2014.

Potier E, Noailly J, Ito K. '*Directing bone marrow-derived stromal cell function with mechanics*.' J Biomech. 2010, 43: 807–817.

Prè D, Ceccarelli G, Gastaldi G, Asti A, Saino E, Visai L, Benazzo F, Cusella De Angelis MG, Magenes G. '*The differentiation of human adipose-derived stem cells (hASCs) into osteoblasts is promoted by low amplitude, high frequency vibration treatment*.' Bone. 2011, 49 (2): 295–303.

Reddy P, Deguchi M, Cheng Y, Hsueh AJW. *'Actin Cytoskeleton Regulates Hippo Signaling'*. PLoS ONE 2013, 8(9): e73763. doi:10.1371/ journal.pone.0073763

Rothballer A, Kutay U. '*The diverse functional LiNCs of the nuclear envelop to the cytoskeleton and chromatin*'. Chromosome 2013, 122: 415-429. doi:10.1007/s00412-013-0417-x

Rubin C, Pope M, Fritton JC, Magnusson M, Hansson T, McLeod K. '*Transmissibility of 15-hertz to 35-hertz vibrations to the human hip and lumbar spine: Determining the physiologic feasibility of delivering low-level anabolic mechanical stimuli to skeletal regions at greatest risk of fracture because of osteoporosis*.' SPINE. 2003, 28 (23): 2621-2627. doi: 10.1097/01.BRS.0000102682.61791.C9

Sjöblom B, Salmazo A, Djinović-Carugo K. '*Alpha-actinin structure and regulation*.' Cell Mol Life Sci. 2008, 65 (17): 2688-701. doi: 10.1007/s00018-008-8080-8.

Sen B, Xie Z, Case N, Styner M, Rubin CT, Rubin J. '*Mechanical Signal Influence on Mesenchymal Stem Cell Fate is Enhanced by Incorporation of Refractory Periods into the Loading Regimen*'. J Biomech. 2011, 44 (4): 593–599. doi:10.1016/j.jbiomech.2010.11.022.

Sen B, Xie Z, Case N, Ma M, Rubin C, Rubin J. '*Mechanical Strain Inhibits Adipogenesis in Mesenchymal Stem Cells by Stimulating a Durable β-Catenin Signal*'. Endocrinology. 2008, 149 (12): 6065– 6075. doi: http://dx.doi.org/10.1210/en.2008-0687.

Shafrir Y, Forgacs G. '*Mechanotransduction through the cytoskeleton*.' Am J Physiol Cell Physiol. 2002, 282 (3): C479-C486.

Takemitsu H, Zhao D, Yamamoto I, Harada Y, Michishita M, Arai T. '*Comparison of bone marrow and adipose tissue-derived canine mesenchymal stem cells*.' BMC Vet Res. 2012, 8: 150. doi:10.1186/1746-6148-8-150.

Thompson WR, Rubin CT, Rubin J. '*Mechanical regulation of signaling pathways in bone*' Gene. 2012, 503: 179–193.

Triplett JW, Pavalko FM. '*Disruption of alpha-actinin-integrin interactions at focal adhesions renders osteoblasts susceptible to apoptosis*'. Am J Physiol Cell Physiol. 2006, 291: C909 – C921.

G. Uzer, S. Pongkitwitoon, M. Ete Chan, and S. Judex, '*Vibration induced osteogenic commitment of mesenchymal stem cells is enhanced by cytoskeletal remodeling but not fluid shear*.' J Biomech. 2013, 46 (13): 2296–2302.

Vishnubalaji R, Al-Nbaheen M, Kadalmani B, Aldahmash A, Ramesh T. '*Comparative investigation of the differentiation capability of bone-marrow- and adipose-derived mesenchymal stem cells by qualitative and quantitative analysis*.' Cell Tissue Res. 2012; 347 (2): 419-427. doi: 10.1007/s00441-011-1306-3.

Yourek G, McCormick SM, Mao JJ, Reilly GC. '*Shear stress induces osteogenic differentiation of human mesenchymal stem cells*'. *Regen Med*. 2010, 5 (5): 713–724. doi:10.2217/rme.10.60.

Figure 5.1a:

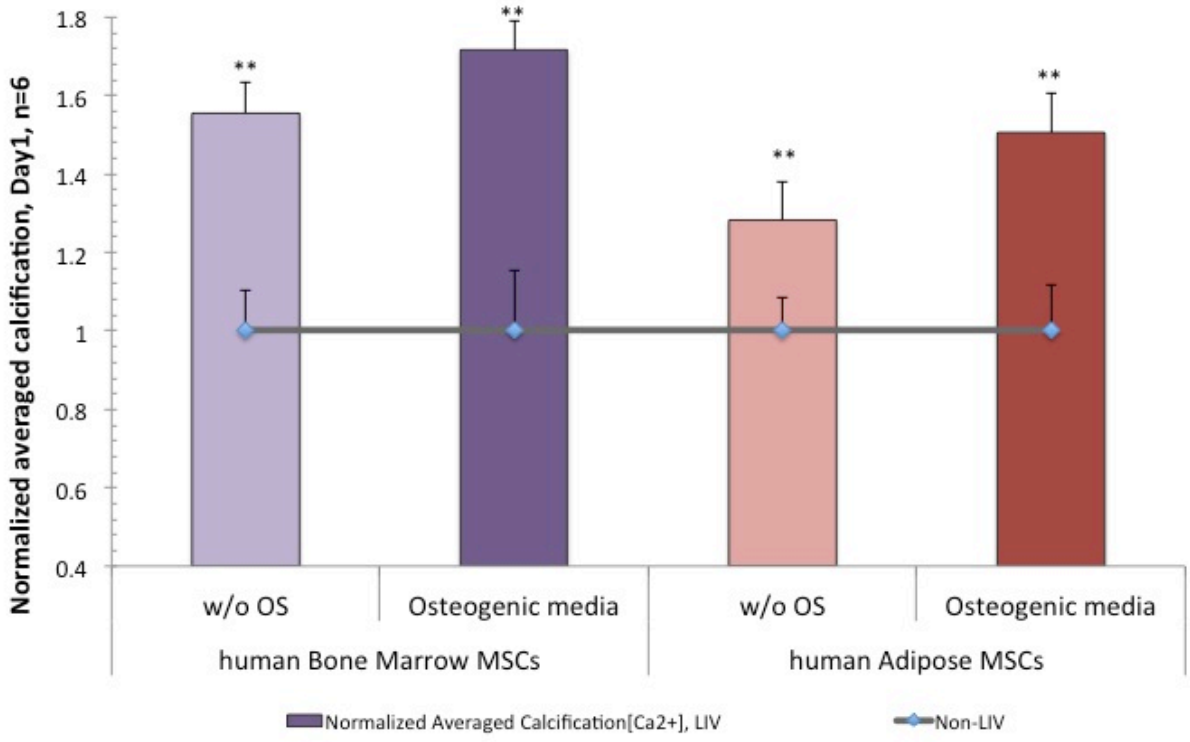
Normalized averaged calcification, Day1, n=6
1.8
1.6
1.4
1.2
1
0.8
0.6
0.4
**
**
**
**
w/o OS
Osteogenic media
w/o OS
Osteogenic media
human Bone Marrow MSCs
human Adipose MSCs
Normalized Averaged Calcification[Ca2+], LIV
Non-LIV

Figure 5.1b:

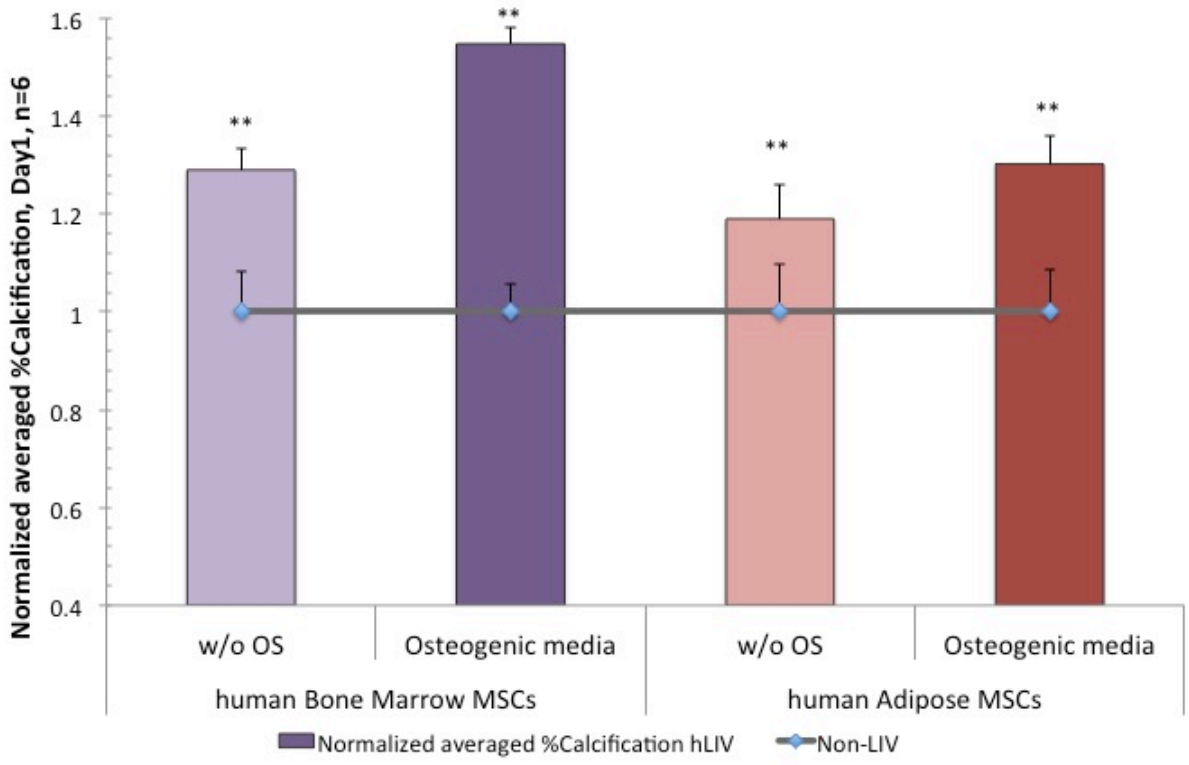
Normalized averaged %Calcification, Day1, n=6
1.6
1.4
1.2
1
0.8
0.6
0.4
**
**
**
**
w/o OS
Osteogenic media
w/o OS
Osteogenic media
human Bone Marrow MSCs
human Adipose MSCs
Normalized averaged %Calcification hLIV
Non-LIV

Figure 5.2a:

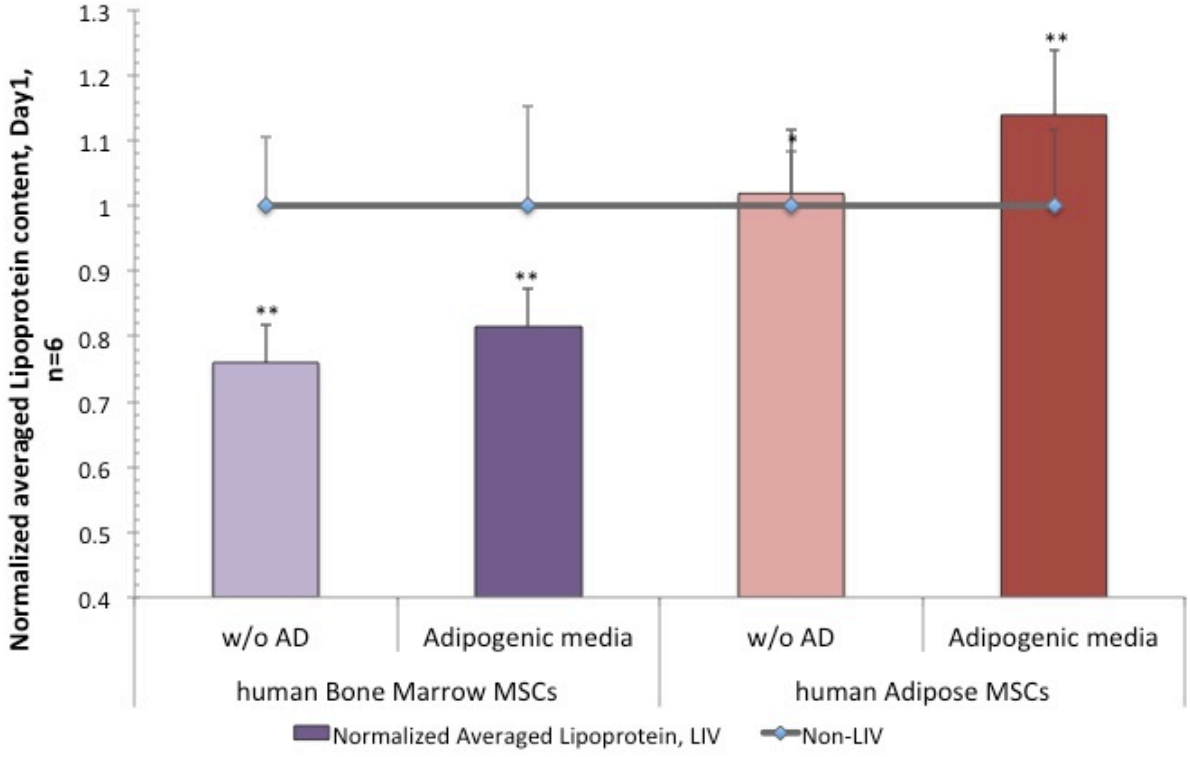
Normalized averaged Lipoprotein content, Day1, n=6
1.3
1.2
1.1
1
0.9
0.8
0.7
0.6
0.5
0.4
**
**
*
**
w/o AD
Adipogenic media
w/o AD
Adipogenic media
human Bone Marrow MSCs
human Adipose MSCs
Normalized Averaged Lipoprotein, LIV
Non-LIV

Figure 5.2b:

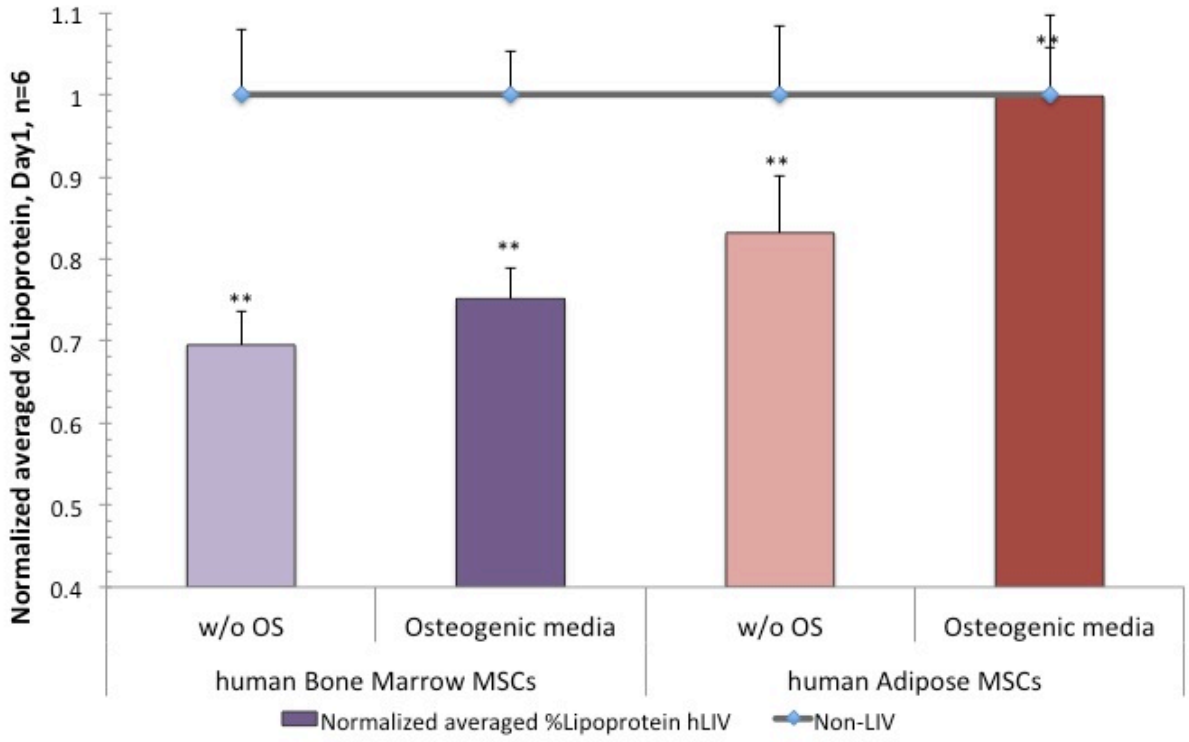
Normalized averaged %Lipoprotein, Day1, n=6
1.1
1
0.9
0.8
0.7
0.6
0.5
0.4
**
**
**
**
w/o OS
Osteogenic media
w/o OS
Osteogenic media
human Bone Marrow MSCs
human Adipose MSCs
Normalized averaged %Lipoprotein hLIV
Non-LIV

Figure 5.3a:

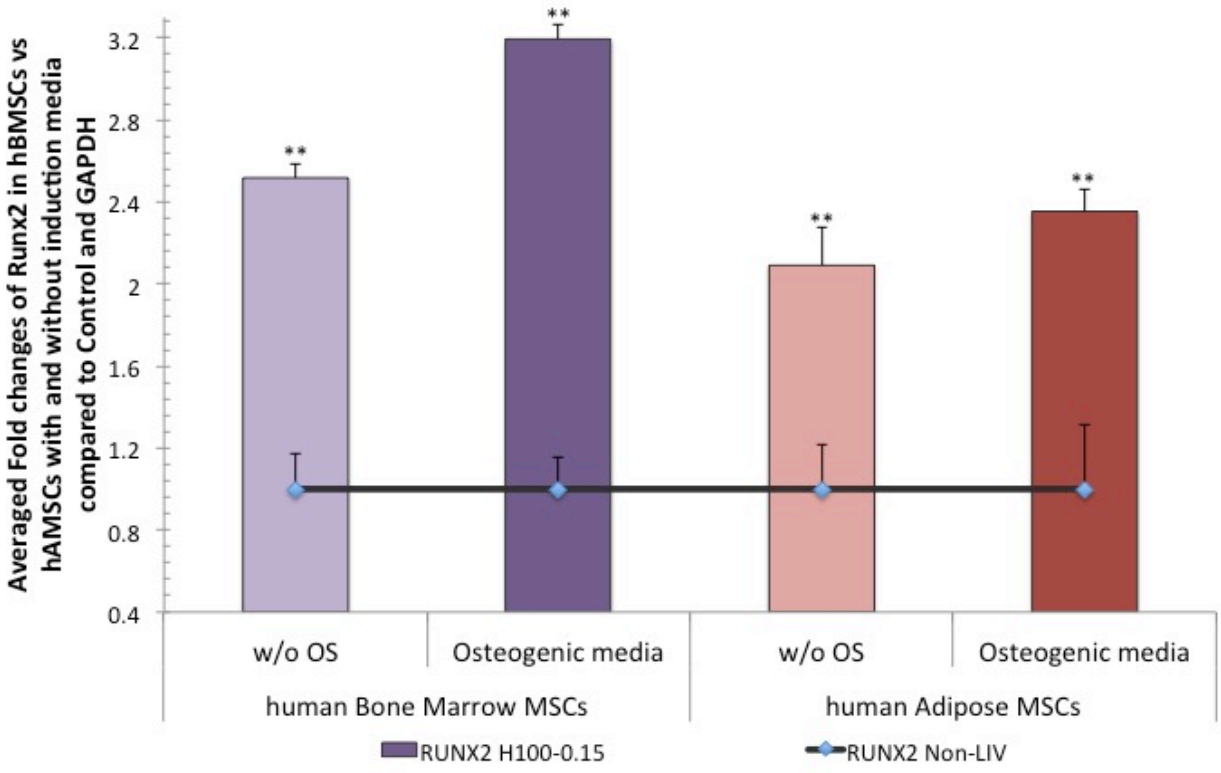
Averaged Fold changes of Runx2 in hBMSCs vs hAMSCs with and without induction media compared to Control and GAPDH
3.2
2.8
2.4
2
1.6
1.2
0.8
0.4
**
**
**
**
w/o OS
Osteogenic media
w/o OS
Osteogenic media
human Bone Marrow MSCs
human Adipose MSCs
RUNX2 H100-0.15
RUNX2 Non-LIV

Figure 5.3b:

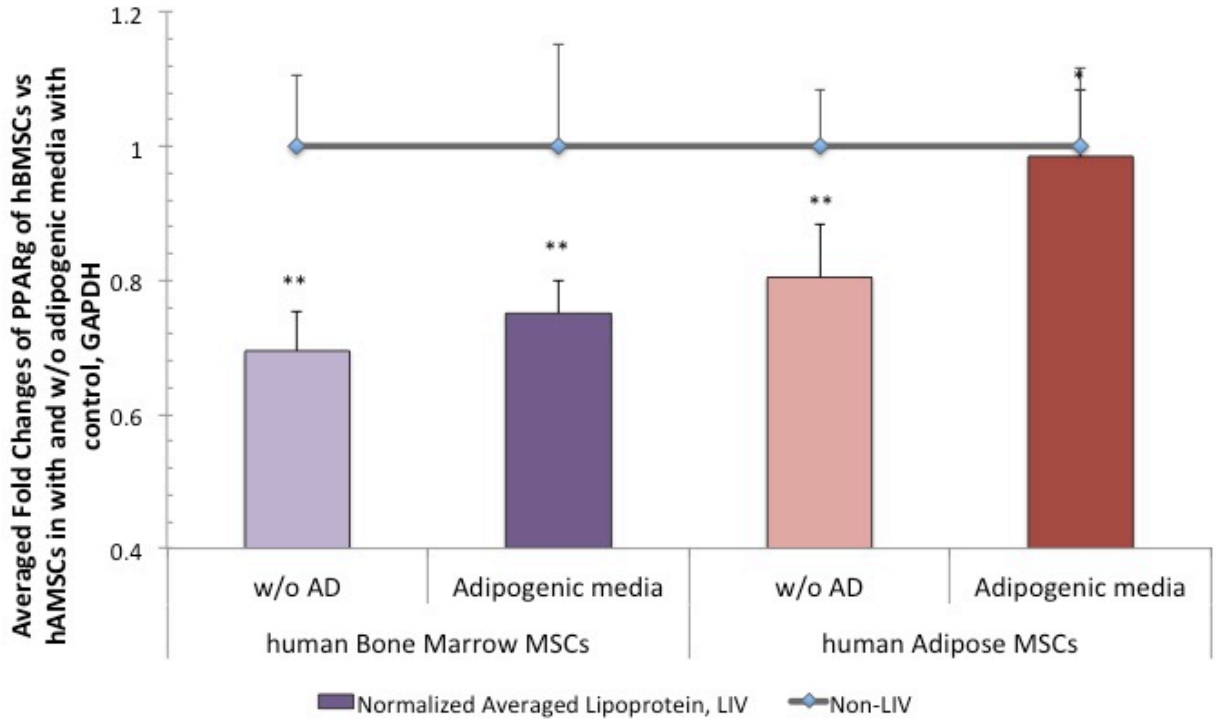
Averaged Fold Changes of PPARg of hBMSCs vs hAMSCs in with and w/o adipogenic media with control, GAPDH
1.2
1
0.8
0.6
0.4
**
**
**
*
w/o AD
Adipogenic media
w/o AD
Adipogenic media
human Bone Marrow MSCs
human Adipose MSCs
Normalized Averaged Lipoprotein, LIV
Non-LIV

Figure 5.4a:

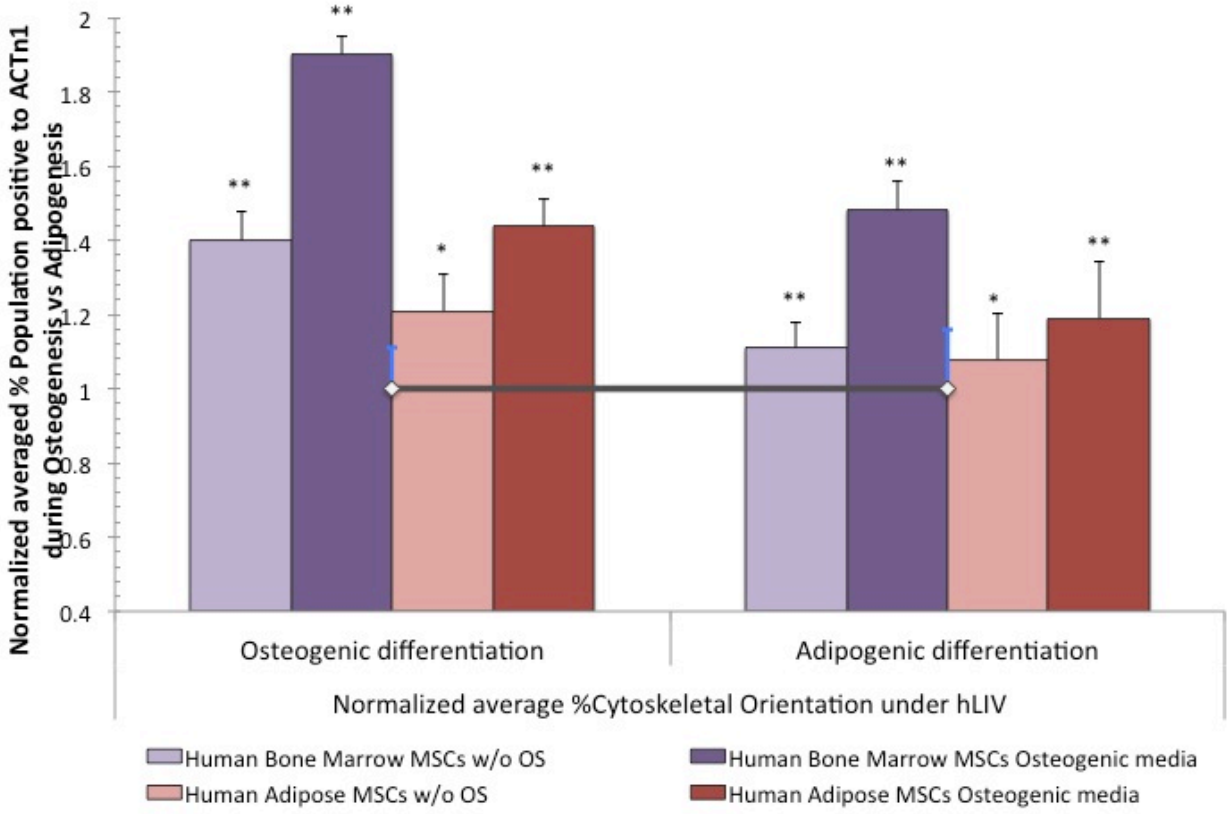
Normalized averaged % Population positive to ACTn1 during Osteogenesis vs Adipogenesis
2
1.8
1.6
1.4
1.2
1
0.8
0.6
0.4
**
**
*
**
**
**
*
**
Osteogenic differentiation
Adipogenic differentiation
Normalized average %Cytoskeletal Orientation under hLIV
Human Bone Marrow MSCs w/o OS
Human Bone Marrow MSCs Osteogenic media
Human Adipose MSCs w/o OS
Human Adipose MSCs Osteogenic media

Figure 5.4b:

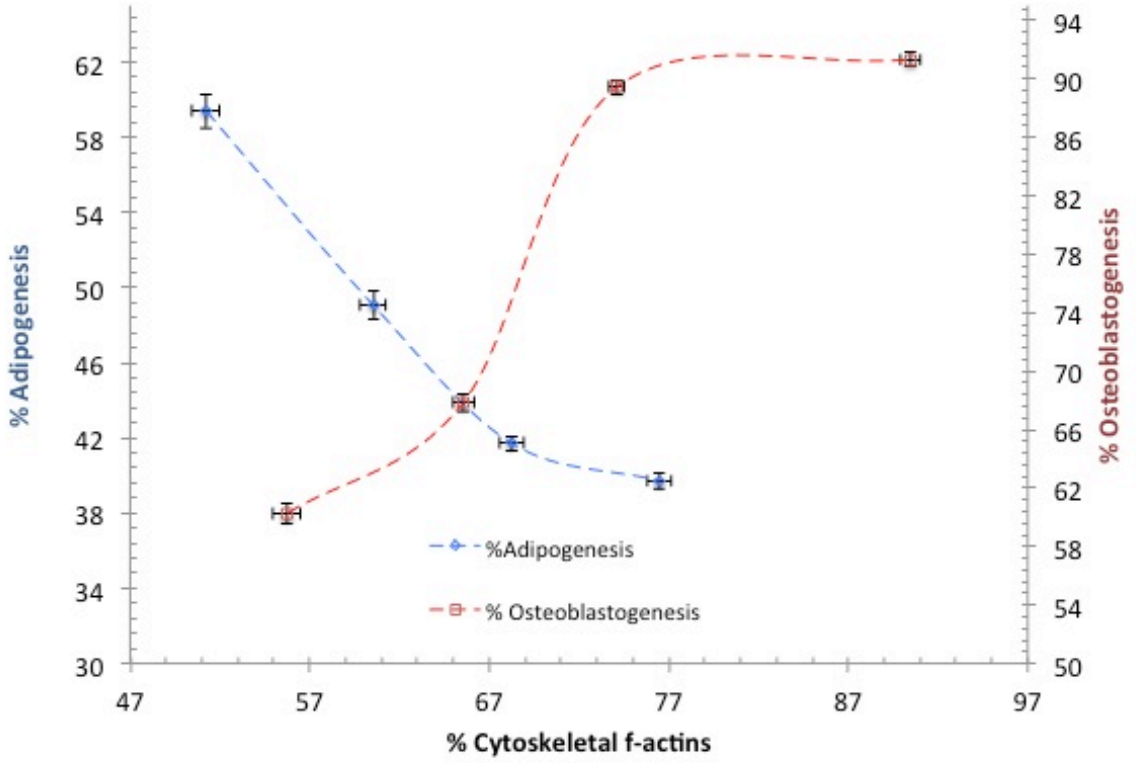
% Adipogenesis
% Osteoblastogenesis
% Cytoskeletal f-actins
%Adipogenesis
% Osteoblastogenesis
62
58
54
50
46
42
38
34
30
94
90
86
82
78
74
70
66
62
58
54
50
47
57
67
77
87
97

Chapter 6

Altering Macrophage Proliferation and Phenotype with Low Intensity Vibrations

(Pending publication and/or patent)

Abstract

Macrophages play ubiquitous roles in cell physiology. Their sensitivity to mechanical signals is largely unexplored but could open up an array of opportunities from manipulating bone resorption to enhancing healing. Here, we applied low intensity vibrations (LIV) to macrophages to test their influence on cell proliferation and polarization. Two different LIV signal frequencies (30Hz or 100Hz) were combined with two acceleration magnitudes (0.15g or 1g) to generate four distinct LIV signals. Murine macrophages (J774.1) were exposed to each of the four different LIV signals for 20min per session, 2x/d. We monitored cell viability, proliferation, polarization, as well as VEGF and TGF-β gene expression. Cell viability was unaffected by LIV. Macrophage proliferation was increased significantly (1.5x-2.5x, $p<0.05$) by each of the four LIV signals on days 1, 2, and 3. The 100Hz/0.15g was consistently the most effective signal for all three days. Flow cytometry showed that the ratio of pro-healing to inflammatory phenotypes was significantly greater (2x-2.5x, $p<0.05$) in LIV groups than in controls, with a preference of 100Hz signals over 30Hz signals. IL-10 was up-regulated up to 2-fold with LIV ($p<0.05$). Transcriptional levels of VEGF were 2.6x greater ($p<0.05$) in the 100Hz/0.15g group with smaller increases for the other LIV signals. LIV also increased gene expression of TGF-β, albeit to a lesser extent, and there were no significant differences between individual LIV groups. These data demonstrate the sensitivity of macrophages to high-frequency oscillations applied at low intensities. Interestingly, LIV not only enhanced macrophage proliferation but also modulated a change in phenotype from pro-inflammatory to pro-healing macrophages. Increased VEGF expression induced by LIV may contribute towards angiogenesis and ultimately may facilitate healing and survival of the pro-healing macrophages. Whether low intensity vibrations

may directly attenuate macrophage induced osteoclastogenesis and whether enhanced healing associated with LIV is driven by changes to macrophage phenotype remains to be investigated.

6.1 Introduction

Macrophages are immune cells derived from committed hematopoietic stem cells located in the bone marrow [Murray et al. 2011]. Within a tissue, they can be highly specific such as osteoclasts in bone, or monocytes in blood [Varol et al. 2015]. Impaired inflammation and delayed healing can cause infections and non-healing chronic wounds in diabetic patients [Koh et al. 2011, Mehta et al. 2010]. Generally, macrophages play a critical role in inflammatory and healing processes [Butterfield et al. 2006]. Changes in the cell's cytokine and chemokine environment can modulate a cell phenotype from and to pro-inflammatory and pro-healing macrophages [Davis et al. 2013]. Though the mechanism underlying the initiation of polarization has not been fully identified [Lawrence et al. 2011], changes in IL-4, for instance, can polarize macrophages towards pro-healing macrophages [Deng et al. 2012, Makita et al. 2014, Wynn 2015].

Interestingly, macrophages are not only sensitive to changes in their cytokine environment but also to mechanical signals [Pugin et al. 1998]. For instance, stretch applied to human macrophages may enhance macrophage function by activating adherent mediated cytokines [Martin et al. 1995]. Efficacy of cyclic mechanical deformations has not only been observed in vitro but also in vivo where mechanically stimulated human macrophages may more effectively serve tissue repair functions [Ennis et al. 2008, Yang et al. 2000]. While most if not all eukaryotic cells can respond to mechanical signals, it has generally been assumed that signals have to be relatively large (>1% stretch) in magnitude (Krishnan et al. 2009, Van Vliet et al. 2003). More recently, we and others have demonstrated that the magnitude of mechanical stimulus can be drastically reduced when the frequency is raised from less than 10Hz to greater

than 25Hz (Bacabac et al. 2006, Holguin et al. 2011). These oscillatory vibrations can enhance (and suppress) cellular activity both in vitro and in vivo (Rubin et al. 2003, Rubin et al. 2006).

In diabetic mice, low intensity vibrations (LIV) may improve delayed wound healing [Weinheimer-Haus et al. 2014] but the mechanism by which this was achieved was not clear. Conceivably, LIV modulated the expression of VEGF by macrophages, ultimately increasing epithelialization [Safferling et al. 2013, Spagnol et al. 2014]. Here, in an effort towards identifying a potential cellular mechanisms controlling LIV enhanced wound healing, we probed the responsivity of macrophages to LIV by investigating macrophage proliferation, polarization and gene expression in vitro.

6.2 Materials and Methods

6.2.1 Experimental design

The response of macrophages to different levels of low intensity vibrations (LIV) was quantified in terms of cell viability, proliferation, polarization, and gene expression by flow cytometric analysis and the real-time PCR.

To understand dynamic mechanisms of macrophages in bone marrow niches, we investigate changes in gene expression levels, during proliferation and phenotype polarization, under different hLIV conditions.

To monitor cellular behaviors, we investigated proliferation of macrophages. The horizontal LIV at signal combinations of frequencies (30Hz or 100Hz) and acceleration (0.15g or 1g) was applied. Changes in the cell density over 3-day proliferation were observed by the standard MTS assay and reported the normalized average-cell-density. To observe the effects of

hLIV on the dynamic pro-healing : inflammatory phenotype, we observed %population positive to m-CSF and gm-CSF without the pro-healing induction media.

Flow cytometric analysis of the %IL-10 (a pro-healing marker) could investigate the pro-healing polarization under hLIV. To see the effect of hLIV on pro-healing phenotypes, we determined changes in the gene expression level by real-time PCR. To investigate the association of healing and inflammatory macrophages, we observed VEGF and TGF-β gene expression. To evaluate the potentials of macrophages in bone marrow niches, we associated gene expression levels of macrophages with related genes of hBMSCs. Statistic one-way ANOVA analyzed the effects of hLIV and non-LIV with significance at $p \leq 0.05$.

6.2.2 Cell culture and Mechanical stimulation

6.2.2.1 Culture macrophages

Murine macrophages (J774.1, ACTT) were cultured in RPMI 1640 (Gibco) supplemented with 10% heat inactivated Fetal Bovine Serum (FBS) and 1% penicillin/streptomycin.

6.2.2.2 Selected signal combination of low intensity vibration (LIV)

We selected signal combinations of frequency and acceleration at 30Hz-1g, 100Hz-1g, 30Hz-0.15g, and 100Hz-0.15g. We found that the combination of frequency and acceleration could generate the fluid shear stress in the cell culture plate. The highest fluid shear stress is at 30Hz-1g and the lowest fluid shear stress is at 100Hz-0.15g. We vibrated cells in 2 sessions a day, for 20 minutes in each session, with 2-hour rest in between sessions as the loading cycles and duration of vibration could control cell behaviors.

6.2.2 Cell viability by Live Dead assay

To test the cell viability, we used techniques of double stain of living cells with 2mM ethidium homodimer, Eth-D1 (Invitrogen L3224) and incubated at 37°C for 45 minutes, following by incubation with 4mM Calcein AM (Invitrogen L3224) for another 3 hours. Florescence images (Zeiss Axio) qualified the cell viability, (green for living cells and red for dead cells). Flow cytometric analysis quantified %living cells. We reported the normalized average %living cells.

6.2.3 Cell proliferation

Changes in the cell density over 3-day proliferation were observed by the standard MTS assay and reported the normalized average-cell-density. To determine cell proliferation, we plated macrophages with low concentration of 7,500 cells/cm^2 in 6wells/plate on the day prior to the experimental day. We monitored cell density (cells/cm^2) using the standard spectrophotometric MTS assay (XTT reagent, ACTT) immediately after the second vibration of each combination, in every day, for 3 consecutive days. The XTT is a common assay for cell proliferation [Bancos et al. 2012]. The second-generation tetrazolium salt XTT reduced to its derivatives, when mixing with cellular surface effectors, and developed bright orange color that can be monitored by the fluorescence absorbance. The standard curve of known cell density (cells/cm^2) was established by plotting the cell density against the absolute specific absorbance [A_{475}], where [A_{475}] is the differences of specific absorbance at 475nm from the unspecific absorbance at 660nm between the sample and blank. The normalized averaged cell density, $[\delta] = \frac{\text{averaged cell density,}\left(\frac{\text{cells}}{\text{cm}^2}\right)_{\text{LIV}}}{\text{averaged cell density,}\left(\frac{\text{cells}}{\text{cm}^2}\right)_{\text{non-LIV}}}$, was reported. The proliferation of macrophages under LIV

and non-LIV exhibited doubling time within 1-2 days similar to other reports [Zhuang et al. 1997], indicating LIV did not change inherent characteristics of the cell.

6.2.4 Pro-healing macrophage polarization

Our proliferation data showed that macrophages expressed the doubling time within 1-2 days for all LIV groups. To prevent cell proliferation interfering with cell differentiation, we plated cells 2 days prior to the experiment with cell density at 18,000 cells/cm^2 in 6wells/plate.

After 2 days of the first inoculation, the macrophages were induced with pro-healing M2-induction media containing RPMI 1640 (Gibco) supplemented with 10% heat-inactivated FBS, 2mM L-glutamine, 25ng/ml recombinant murine m-CSF (Life Technology) solubilized in dPBS containing 0.1% BSA, 25 mM HEPES, and 1% penicillin/streptomycin. All observations were performed at the end of the second vibration on Day1 (the first day of M2 induction).

6.2.5 Gene expression by real-time PCR

We quantified gene expression by real-time PCR using the TaqMan standard protocols with n=6 in each condition. The expression level was analyzed by the fold changes ($2^{-\Delta\Delta Ct}$) with respect to the control and the GAPDH. After vibration, cells were scraped, collected and centrifuged at 1350rpm for 3-4 minutes. After aspirating out the supernatant, cells were lysed by TRIzol (Life Technologies)

The RNA extraction was done by phase separation with chloroform. The RNA was precipitated from nucleic acid by RNeasy (Qiagen) and washed with 70% ethanol before re-dissolving by RNA-free water. To quantify RNA concentration and determine the RNA quality, we used NanoDrop (ND-100 V3.3.0). The ratio of [A_{260}/A_{280}] $\geq$1.8 is for 'pure' cDNA, and $\geq$2.0

for ‘pure’ RNA, validating by [A_{260}/A_{230}] ~2.0-2.2 for ‘pure’ nucleic acid. Then, the RNA was cloned by the reversed transcriptase (Invitrogen) for cDNA conversion. After the determination of purification and concentration, cDNA was diluted to be the same concentration (3.33ng/µl). Using StepOne 2.2, the real-time polymerase chain reaction (q-PCR) provided Ct of the interested genes for calculation of the gene expression level ($2^{-\Delta\Delta Ct}$).

6.2.6 Flow cytometric analysis

The measurement of % cell populations by laser-based flow cytometric analysis relies on effective immunofluorescence staining and conjugated antibodies. We prepared samples by scraping the cells. We performed immunofluorescence staining of living cells with (1) EtD1/CalceinAM for viability, (2) primary gm-CSF polyclonal antibody (abcam 9741), (3) m-CSF monoclonal antibody (abcam 66236) and (4) IL-10 conjugated with IgG. To acquire data, we set the %gated cells positive to the specific immunofluorescence with at least 10,000 events and FlowJo analyzed %cell populations. The normalized average %population of [pro-healing macrophages : inflammatory macrophages] ($\frac{Normalized\ averaged\ \%\ m-CSF}{Normalized\ averaged\ \%\ gm-CSF}$), n=6 of all hLIV with respect to non-LIV was reported.

6.2.7 Statistic analysis

Statistic one-way analysis of variance, ANOVA (SPSS) with Tukey post hoc test analyzed the effect of LIV vs non-LIV. Each condition in each experiment was repeated at least n=6. Each experiment was at least duplicated. The results were statistically significant when $p < 0.05$, and p values were reported as *<0.05, **<0.01.

6.3 Results

6.3.1 Horizontal LIV modulated macrophage proliferation

The fluorescence images (**Figures 6.1a and 1b**) qualitatively showed viable macrophages under LIV and non-LIV (green color). Similar to hBMSCs, flow cytometric analysis quantitatively found that the %living macrophages in all vibrations were the same (>99.7±2%), indicating hLIV is not cytotoxicity.

Normalizations of the averaged cell density [δ] of hLIV groups were >1.3 – 2.5x higher than the normalized density of the non-LIV across Day1, Day2 and Day3 (**Figure 6.2**). The signal combination of 100Hz-0.15g in horizontal LIV provided the highest [δ] for all 3days, indicating the vibration, but not the fluid shear that induced macrophage proliferation. The proliferation of 100Hz groups was increased >1.5-2x higher than the proliferation of 30Hz groups, suggesting the frequency, not the direction induced macrophage proliferation (, confirmed by statistic 3-way ANOVA analysis). The increment from Day1 to Day2 was less than (<1.1-1.2) the increment from Day3 to Day2, as hLIV was effective over time. Interestingly, the macrophage proliferation was similar to the proliferation of human bone marrow MSCs under hLIV [Pongkitwitoon et al. 2014]. These data indicated that the frequency of hLIV influenced the proliferation of animal and human cells in bone marrow niches.

6.3.2 Frequency induced pro-healing macrophages

Flow cytometric analysis confirmed that hLIV improved pro-healing macrophages without induction media. After monitoring cell proliferation, we observed %gm-CSF and %mCSF by flow cytometric analysis (**Figure 6.3**). Flow cytometric analysis of normalized average %m-CSF was divided by normalized average %gm-CSF. The ratio of %m-CSF to

%gm-CSF was presented as the ratio of pro-healing macrophages to inflammatory macrophages. The ratio of pro-healing : inflammatory macrophages under hLIV was 1.9-2.5x higher than that of non-LIV, confirmed that hLIV promoted pro-healing phenotypes. The ratio of pro-healing : inflammatory macrophages of 100Hz groups was ~1.3x higher than the 30Hz groups, supporting that the frequency directed pro-healing macrophages. The data indicated that hLIV feasibly switched phenotypes of macrophages to pro-healing macrophages.

6.3.3 Elevated IL-10 promoted pro-healing macrophages

Fluorescence images of pro-healing macrophages showed that macrophages formed colonization in hLIV groups better than in non-LIV during the induced polarization.

The normalized average %IL-10 by flow cytometric analysis showed that IL-10 under hLIV was >1.2-1.8x higher than that of the non-LIV (**Figure 6.4**). The data supported that the hLIV could increase IL-10 induced M2 phenotypes. The IL-10 of the 30Hz-1g was >1.1x higher than the IL-10 of 30Hz-0.15g. The IL-10 of 100Hz-0.15g was >1.3x higher than that of 100Hz-1g. The 100Hz groups had IL-10 >1.1-1.6x higher than that of 30Hz groups, indicating that the frequency could activate IL-10.

6.3.4 Up-regulated VEGF inhibiting Bone Resorption

The averaged VEGF expression levels (n=6) of hLIV were upregulated >1.6-2.5x folds higher than the expression level of the non-LIV (**Figure 6.5a**). The 100Hz groups provided higher VEGF expression levels (>1.2-1.6x folds) than the 30Hz groups. The 30Hz-1g had

~1.2folds higher than VEGF of 30Hz-0.15g. The 100Hz-0.15g had ~1.3folds higher than VEGF of 100Hz-1g. The data supported that hLIV improved pro-healing abilities in macrophages.

The averaged TGF-β expression levels (n=6) of hLIV were upregulated >1.4-1.5x folds higher than that of the non-LIV (**Figure 6.5b**). Though the upregulated TGF-β levels of the hLIV were very similar in all hLIV but the hLIV maintained TGF-β levels. The data suggested that hLIV sustained balance abilities in macrophages and relation with hBMSCs in bone marrow niches.

6.4 Discussion

We investigated gene expression levels of macrophages during proliferation and polarization under horizontal LIV. The relation of changes in cellular phenotypes was associated with gene expression levels. During proliferation, the averaged cell density of macrophages increased with frequency, but not acceleration as if macrophages sensed mechanical signals of frequency. Over 3 days, hLIV effectively promoted the proliferation. Without induction, hLIV seemed to switch macrophage phenotypes to pro-healing macrophages (the ratio of M2 : M1 was higher in hLIV). The data supported that the frequency improved pro-healing macrophage phenotypes. In pro-healing induced polarization, hLIV increased IL-10 promoting macrophage pro-healing phenotypes. The upregulated VEGF in hLIV supported that the frequencies of the hLIV induced healing abilities of macrophages. However, upregulated TGF-β remained the same level in all hLIV conditions as though hLIV maintain the balancing abilities of macrophages.

A limitation of this study was that the real system of macrophages residing in bone marrow environments has not been imitated yet. Even though co-culture techniques and bioreactor technologies have been improved over the year, but they are still far the real automatic biological-biochemical responsive system in human bodies.

6.4.1 Frequency Promoted Self-Renewals in Bone Marrow Niches

The proliferation of murine macrophages, J774.1 under LIV stimulation was similar to our previous data in human bone marrow and adipose-derived MSCs [Pongkitwitoon et al. 2014], suggesting both human and animal cells of any sizes could sense LIV. Importantly, the

averaged cell density in 100Hz-groups was much higher than that of the 30Hz groups, indicating that the macrophages could sense the frequency during their proliferation.

6.4.2 Cells dwelling in Bone Marrow Niches Sense Frequency, Acceleration and Direction

Our previous data showed that the frequency, acceleration and direction of LIV, but not the fluid shear stress had an effect on hBMSCs, osteoblasts and macrophages in proliferation or differentiation [Pongkitwitoon et al. 2014]. However, osteocytes naturally sense the fluid shear as the communication of osteocyte like cells and osteoblasts through gap junction relied on the fluid shear. The observation could indicate that cell inheritances formed different responsiveness to hLIV. In fact, the hBMSCs and macrophages reside in viscous bone marrow in nature [Gurkan et al. 2008]. The osteoblasts are dwelling at interfacial with bone marrow niches (**Figure A26**). The osteocytes are inside calcified collagen matrix, which is more rigid (higher modulus with less viscosity) [Graham et al. 2013]. The information could indicate that the osteocytes were naturally affected by fluid shear stress as though their morphology easily noticed the change of interstitial fluid flow.

6.4.3 LIV Switched Macrophages to Anabolic Phenotypes

The ratio of pro-healing macrophages (M2) to inflammatory macrophages (M1) in horizontal LIV groups was much higher than the ratio in the non-LIV, which indicated predominant pro-healing phenotypes of macrophages in hLIV. From the fluorescent images, the macrophages under the LIV showed more colonized cells than non-LIV (**Figure A27**). It could

be that macrophages sensed the frequency of the hLIV, and switched the phenotypes in responses to the mechanical stimulations. Normally, biochemical reagents could activate the pro-healing macrophage phenotypes, but these data firmly gave the new clue to activate pro-healing macrophages by non-pharmacological stimulation.

Though without mechanical stimulation, IL-4 in inflammatory macrophages could induce an increase in IL-10 [Makita et al. 2014]. In turn, the elevated IL-10 could assist switching the inflammatory macrophage phenotype into the pro-healing phenotypes, supporting muscle growth and regeneration [Deng et al. 2012]. During pro-healing polarization, the IL-10 under hLIV was increased much higher than non-LIV. The data indicated that the hLIV was driving the macrophages toward pro-healing phenotypes.

6.4.4 LIV induced VEGF for Bone Healing Angiogenesis

During macrophages induced tissue repair, anti-inflammation processes in pro-healing macrophages could enhance the differentiation of human bone marrow MSCs to osteoblastogenesis [Sesia et al. 2014]. However, increased inflammatory macrophages could induce adipogenesis [Díaz-Gandarilla et al. 2013]. These data supported the communication of hBMSCs and macrophages in bone marrow niches as if macrophage phenotypes controlled hBMSC differentiation decisions.

The expression level of VEGF during induced pro-healing macrophages was upregulated in responses to horizontal LIV. The data supported that hLIV enhanced pro-healing macrophage phenotypes and functions. The VEGF stimulation in blood peripheral endothelial cells could

increase interactions between cytoskeleton and nucleus and increased angiogenesis [Spagnol et al. 2014]. During angiogenesis, rapid and transient growth of new capillaries in human hematopoietic stem cells could reverse human bone marrow induced chondrogenesis into osteoblastogenesis [Serafini et al. 2014]. These data supported that increases in VEGF of macrophages supported increase bone marrow niches' communication with hematopoietic niches [Shiozawa et al. 2012] as the VEGF could direct hBMSCs toward osteoblastogenesis while supporting the vascular commitment of hHSC [Farhadi et al. 2005, Whyte et al. 2011].

6.4.5 LIV induced TGF-β in Balancing Bone Homeostasis

The TGF-β expression levels of pro-healing macrophages were upregulated but independent of the hLIV signal combinations as though hLIV maintained TGF-β. The TGF-β and IGF-1 are primary coupling factors in bone matrix. In responses to osteoclastogenesis bone resorption, human bodies release IGF-1 upregulated TGF-β [Wang et al. 2006]. Changes in cytoskeletal transformations from osteoblasts toward osteoclasts could trigger TGF-β induced RhoA to activate osteoblastogenesis in hBMSCs [Cao et al. 2011]. Therefore, the upregulated TGF-β should be maintained to balance bone homeostasis.

6.5 Conclusion

This work demonstrated for the first time that hLIV was non-pharmacological stimulation altering inflammatory toward pro-healing macrophages. Gene expression levels and cellular behaviors of different signal combinations defined specific mechanical signals that macrophages can sense. The data indicated strong involvements of frequencies in transcriptional levels toward switching phenotypes. Analyses of gene expressions evaluated the association of macrophages with human bone marrow MSCs in bone marrow niches. The relation of macrophage phenotypes and these genes with their cellular and molecular functions in bone marrow niches remains novel. The information on cellular and molecular mechanisms definitely provided great insights as the first step toward determining physiopathological stages of bone homeostasis and heals.

References

Bancos S, Tsai DH, Hackley V, Weaver JL, Tyner KM, '*Evaluation of Viability and Proliferation Profiles on Macrophages Treated with Silica Nanoparticles In Vitro via Plate-Based, Flow Cytometry, and Coulter Counter Assays.*' Nanotechnology. **2012**, 454072: 11 pp. doi:10.5402/2012/454072.

Byon CH, Sun Y, Chen J, Yuan K, Mao X, Heath JM, Anderson PG, Tintut Y, Demer LL, Wang D, Chen Y. '*Runx2-Upregulated Receptor Activator of Nuclear Factor kB Ligand in Calcifying Smooth Muscle Cells Promotes Migration and Osteoclastic Differentiation of Macrophages*.' Arterioscler Thromb Vasc Biol. **2011**, 31: 1387-1396. doi: 10.1161/ATVBAHA.110.222547.

Cao X. *'Targeting osteoclast-osteoblast communication*', Nature Medicine **2011**, 17: 1344–1346. doi: 10. 1038/nm.2499.

Cho DI, Kim MR, Jeong HY, Jeong HC, Jeong MH, Yoon SH, Kim YS, Ahn Y. '*Mesenchymal stem cells reciprocally regulate the M1/M2 balance in mouse bone marrow-derived macrophages*.' Exp Mol Med. **2014**, 46: e70. doi:10.1038/emm.2013.135.

Deng B, Wehling-Henricks M, Villalta SA, Wang Y, Tidball JG. *'IL-10 triggers changes in macrophage phenotype that promote muscle growth and regeneration.'* J Immunol. **2012**, 189 (7): 3669-80. Epub 2012 Aug 29.

Díaz-Gandarilla JA, Osorio-Trujillo C, Hernández-Ramírez VI, Talamás-Rohana P. '*PPAR Activation Induces M1 Macrophage Polarization via cPLA2-COX-2 Inhibition, Activating ROS Production against Leishmania mexicana'*. BioMed Res Inter. **2013**, ID 215283, 13 pp. doi: 10.1155/2013/215283.

Edlund S, Landström M, Heldin CH, Aspenström P. '*Transforming growth factor-beta-induced mobilization of actin cytoskeleton requires signaling by small GTPases Cdc42 and RhoA*.' Mol Biol Cell. **2002**, 13(3): 902-914.

Farhadi J, Jaquiery C, Barbero A, Jakob M, Schaeren S, Pierer G, Heberer M, Martin I. '*Differentiation-dependent up-regulation of BMP-2, TGF-beta1, and VEGF expression by FGF-2 in human bone marrow stromal cells*.' Plast Reconstr Surg. **2005**, 116 (5): 1379-86.

Fleetwood AJ, Dinh H, Cook AD, Hertzog PJ, Hamilton JA. '*GM-CSF- and M-CSF-dependent macrophage phenotypes display differential dependence on Type I interferon signaling*.' Journal of Leukocyte Biology. **2009**, 86 (2): 411-2421. doi:10.1189/jlb.1108702August 2009.

Graham JM, Ayati BP, Holstein SA, Martin JA. '*The Role of Osteocytes in Targeted Bone Remodeling: A Mathematical Model.'* PLoS ONE **2013**, 8 (5): e63884. doi:10.1371/journal.pone.0063884

Gralow JR, Biermann JS, Farooki A, Fornier MN, Gagel RF, Kumar RN, Shapiro CL, Shields A, Smith MR, Srinivas S, Van Poznak CH. '*Bone Health in Cancer care*'. J Natl Compr Canc Netw. **2009** 7(Suppl 3): S1–S35. NIHMSID: NIHMS272543, PMCID: PMC3047404

Gurkan UA, Akkus O. '*The Mechanical Environment of Bone Marrow: A Review*'. Annal Biomed Eng. **2008**, 36 (12): 1978–1991. doi: 10.1007/s10439-008-9577-x.

Hardy R, Cooper MS. '*Bone loss in inflammatory disorders'*. J Endocrinol. **2009**, 201: 309320.

Hubchak SC, Runyan CE, Kreisberg JI, Schnaper HW. '*Cytoskeletal Rearrangement and Signal Transduction in TGF-β1–Stimulated Mesangial Cell Collagen Accumulation*.' JASN. **2003**, 14 (8): 1969-1980. doi:10.1097/01.ASN.0000076079.02452.92

Makita N, Hizukuri Y, Yamashiro K, Murakawa M, Hayashi Y. 'IL-10 enhances the phenotype of M2 macrophages induced by IL-4 and confers the ability to increase eosinophil migration'. Int. Immunol. **2014**, doi: 10.1093/intimm/dxu090.

Moustakas A, Heldin CH. '*Dynamic control of TGF-beta signaling and its links to the cytoskeleton*.' FEBS Lett. **2008**, 582 (14): 2051-65. doi: 10.1016/j.febslet.2008.03.027. Epub 2008 Mar 28.

Paul PK, Gupta SK, Bhatnagar S, Panguluri SK, Darnay BG, Choi Y, Kumar A. '*Targeted ablation of TRAF6 inhibits skeletal muscle wasting in mice'*. **2010**, 191 (7): 1395-1411. doi: 10.1083/jcb.201006098.

Pongkitwitoon S. '*Mechanotransduction of low intensity vibration in human bone marrow mesenchymal stem cells and bone marrow niches' macrophages*.' Ph.D. Dissertation. **2014**.

Sanjabi S, Zenewicz LA, Kamanaka M, Flavell RA . '*Anti-inflammatory and pro-inflammatory roles of TGF-beta, IL-10, and IL-22 in immunity and autoimmunity*.' Curr Opin Pharmacol. **2009**, 9 (4): 447-53. doi: 10.1016/j.coph.2009.04.008. Epub 2009 May 29.

Serafini M, Sacchetti B, Pievani A, Redaelli D, Remoli C, Biondi A, Riminucci M, Bianco P. '*Establishment of bone marrow and hematopoietic niches in vivo by reversion of chondrocyte differentiation of human bone marrow stromal cells*'. Stem Cell Res. **2014**, 12(3): 659–672.

Sesia SB, Duhr R, da Cunha CM, Todorov A, Schaeren S, Padovan E, Spagnoli G, Martin I, Barbero A. '*Anti-inflammatory/tissue repair macrophages enhance the cartilage-forming capacity of human bone marrow-derived mesenchymal stromal cells*.' J Cell Physiol. **2014** Nov 21. doi: 10.1002/jcp.24861.

Shiozawa Y, Taichman RS. '*Getting Blood from Bone: An Emerging Understanding of the Role That Osteoblasts Play In Regulating Hematopoietic Stem Cells Within Their Niche*'. Exp Hematol. **2012**, 40 (9): 685–694. doi:10.1016/j.exphem.2012.05.004.

Stournaras C, Moustakas A, Heldin CH. '*Dynamic control of TGF-β signaling and its links to the cytoskeleton***.**' FEBS Lett. **2008**, 582: 2051–2065. doi:10.1016/j.febslet.2008.03.027.

Spagnol ST, Weltz JS, Xue Y, Dahl KN. '*Mechanical coupling of the endothelial cytoskeleton and nucleus with VEGF stimulation*'. Cell Mol Bioeng. **2014**, 7 (2): 225-230.

Thorpe SD, Buckley CT, Vinardell T, O'Brien FJ, Campbell VA, Kelly DJ. '*The response of bone marrow derived mesenchymal stem cells to dynamic compression following TGF-b3 induced chondrogenic differentiation*' Ann. Biomedi Eng. **2010**, 38 (9): 2896-2909.

Vasanthi P, Nalini G, Rajasekhar G. '*Role of tumor necrosis factor-alpha in rheumatoid arthritis: a review*'. J Rheumatology **2007**; 10: 270–274.

Wang Y, Nishida S, Elalieh HZ, Long RK, Halloran BP, Bikle DD. '*Role of IGF-I signaling in regulating osteoclastogenesis*'. J Bone Miner Res. **2006**, 21 (9): 1350-8.

Whyte JL, Ball SG, Shuttleworth CA, Brennan K, Kielty CM. '*Density of human bone marrow stromal cells regulates commitment to vascular lineages*'. Stem Cell Res. **2011**, 6 (3): 238–250. doi: 10.1016/j.scr.2011.02.001. PMCID: PMC3223522.

Wu AC, Raggatt LJ, Alexander KA, Pettit AR. '*Unraveling macrophage contributions to bone repair*'. BoneKEy Reports. **2013**: 373. doi:10.1038/bonekey.2013.107.

Weinheimer-Haus EM, Judex S, Ennis WJ, Koh TJ. '*Low-Intensity Vibration Improves Angiogenesis and Wound Healing in Diabetic Mice*'. PLoS ONE **2014**, 9 (3): e91355. doi:10.1371/journal.pone.0091355.

Yavropoulou MP, Yovos JG. '*The role of the Wnt signaling pathway in osteoblast commitment and differentiation*'. Hormones **2007**, 6 (4): 279-294.

Figures 6.1a and b:

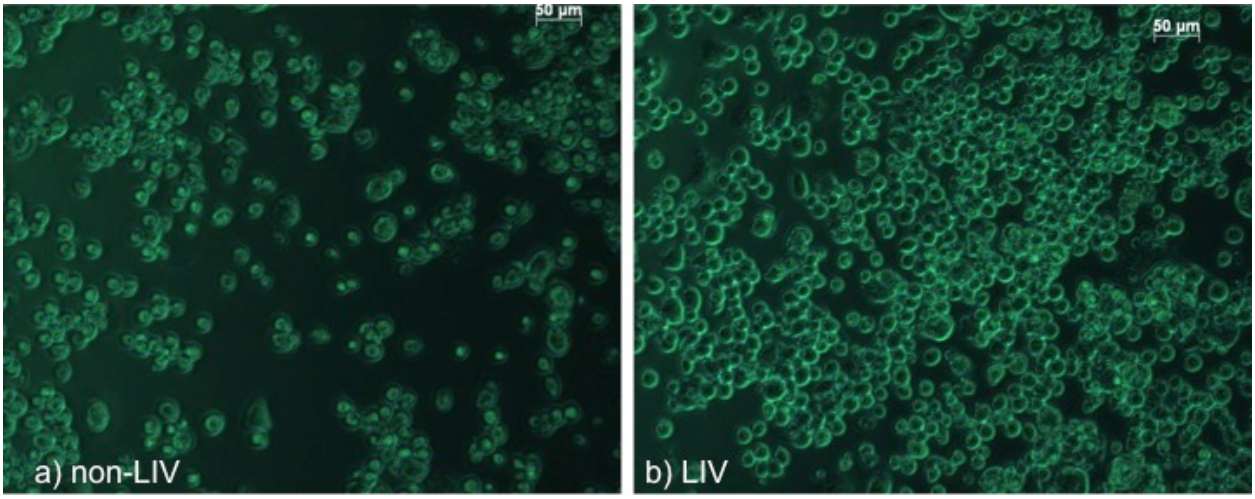

Figure 6.2:

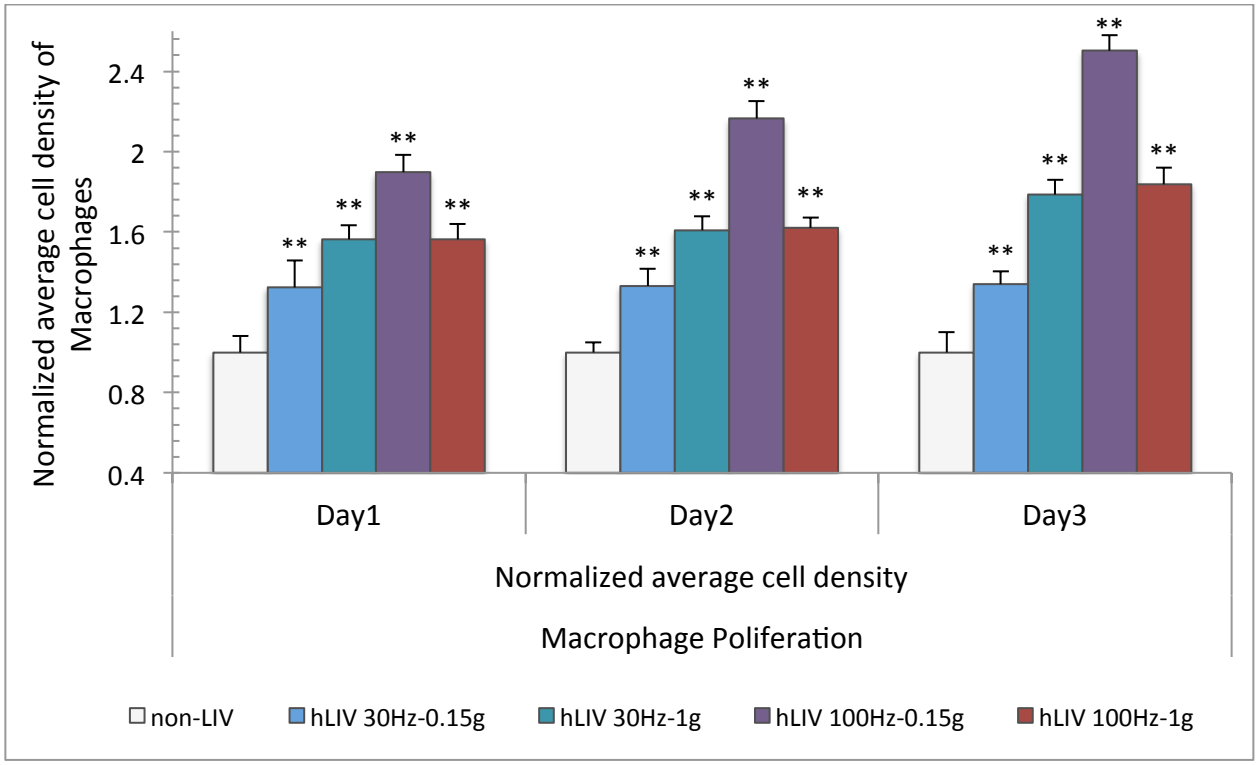
Normalized average cell density of Macrophages
2.4
2
1.6
1.2
0.8
0.4
**
Day1
Day2
Day3
Normalized average cell density
Macrophage Poliferation
non-LIV
hLIV 30Hz-0.15g
hLIV 30Hz-1g
hLIV 100Hz-0.15g
hLIV 100Hz-1g

Figure 6.3:

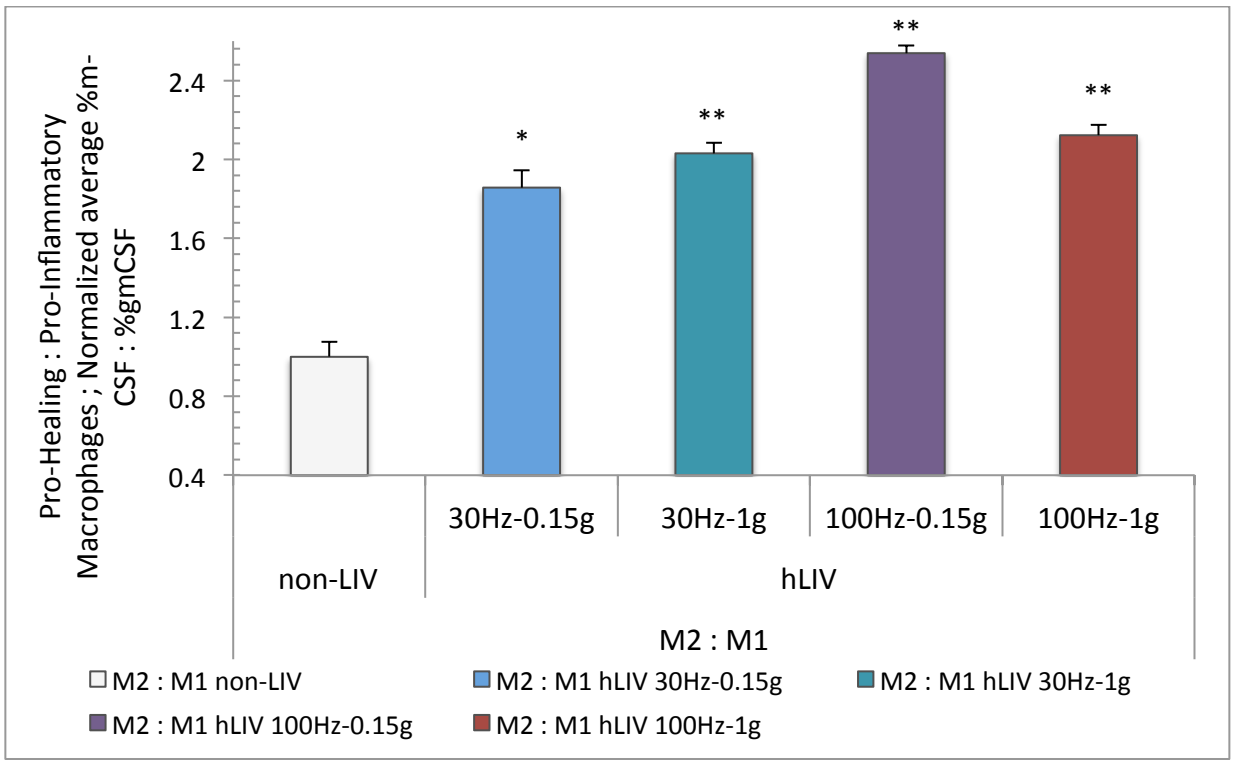
Pro-Healing : Pro-Inflammatory Macrophages ; Normalized average %m-CSF : %gmCSF
2.4
2
1.6
1.2
0.8
0.4
*
**
**
**
non-LIV
30Hz-0.15g
30Hz-1g
100Hz-0.15g
100Hz-1g
hLIV
M2 : M1
M2 : M1 non-LIV
M2 : M1 hLIV 30Hz-0.15g
M2 : M1 hLIV 30Hz-1g
M2 : M1 hLIV 100Hz-0.15g
M2 : M1 hLIV 100Hz-1g

Figure 6.4:

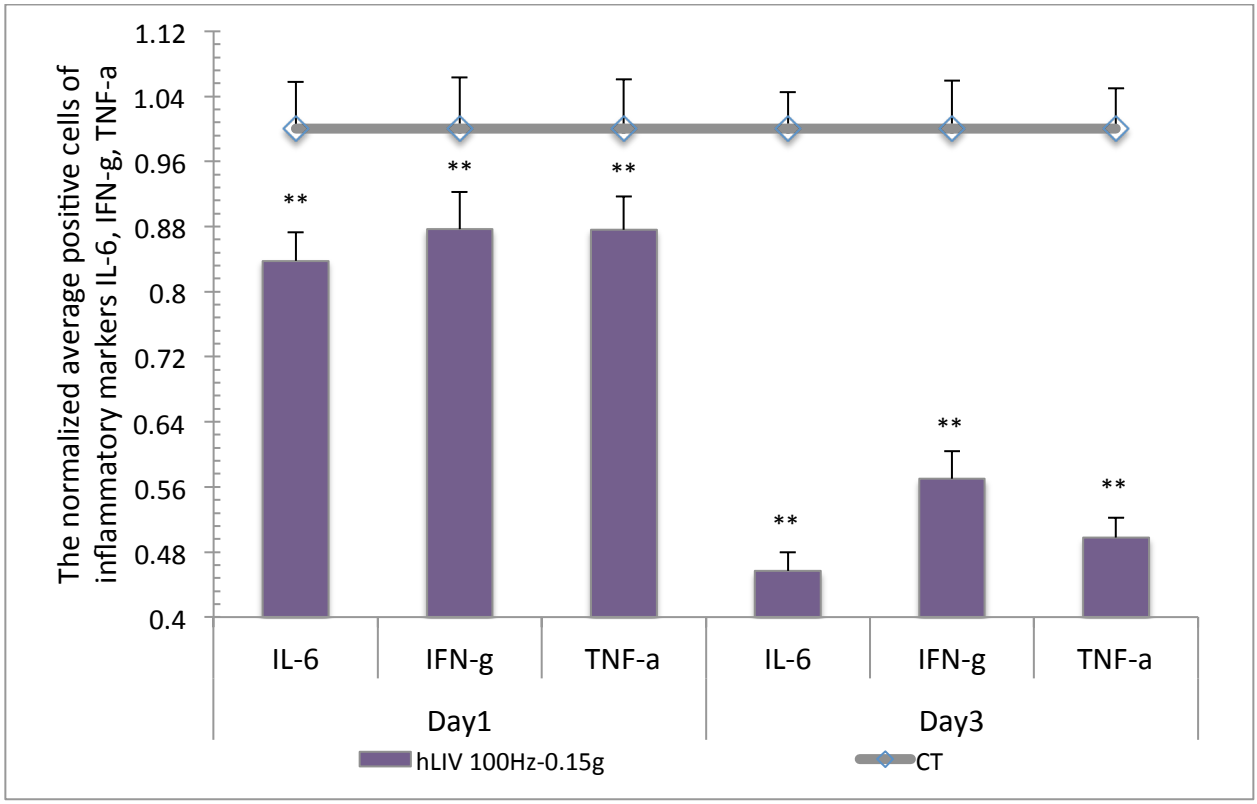
The normalized average positive cells of inflammatory markers IL-6, IFN-g, TNF-a
1.12
1.04
0.96
0.88
0.8
0.72
0.64
0.56
0.48
0.4
**
IL-6
IFN-g
TNF-a
IL-6
IFN-g
TNF-a
Day1
Day3
hLIV 100Hz-0.15g
CT

Figures 6.5:

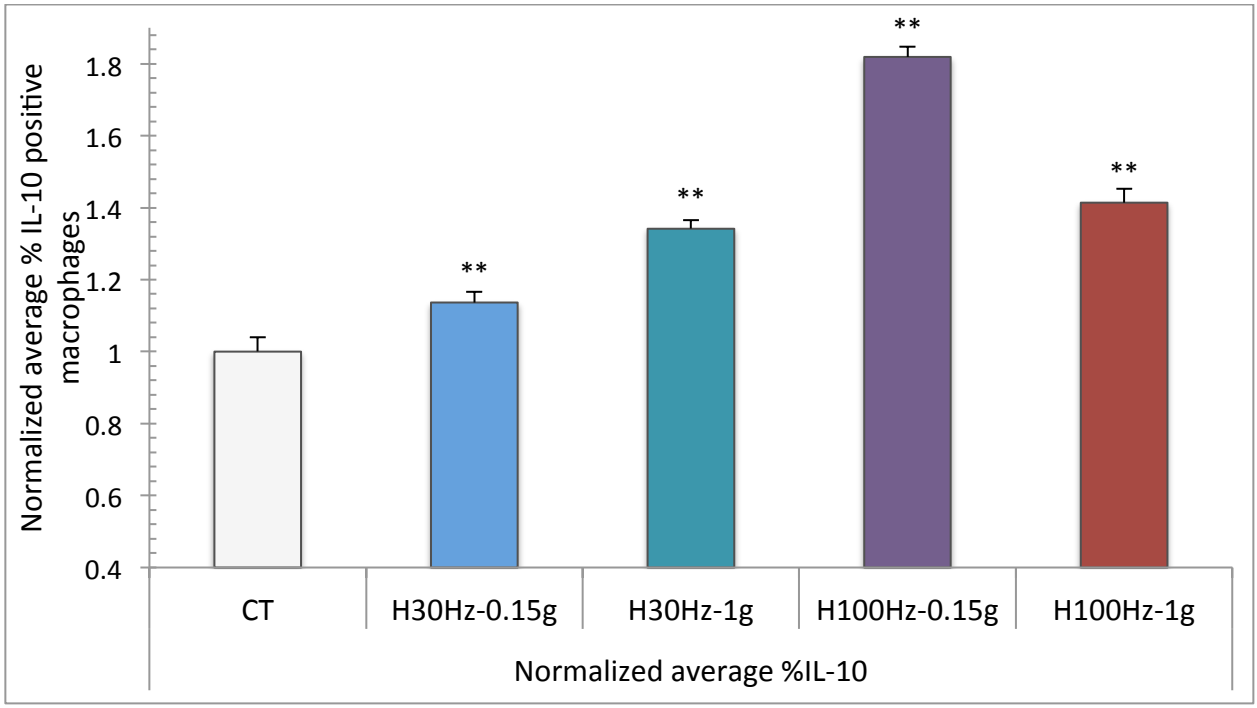
Normalized average % IL-10 positive macrophages
1.8
1.6
1.4
1.2
1
0.8
0.6
0.4
**
**
**
**
CT
H30Hz-0.15g
H30Hz-1g
H100Hz-0.15g
H100Hz-1g
Normalized average %IL-10

Figures 6.6a and b:

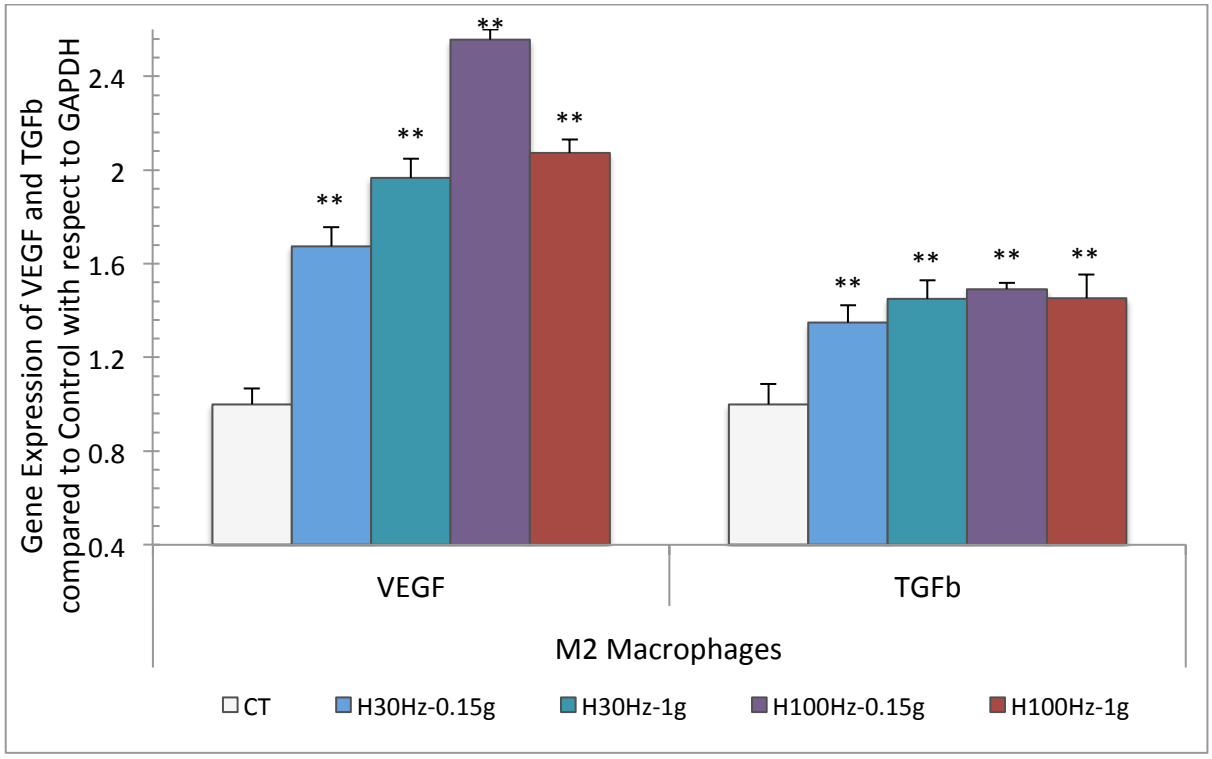

7. Discussion

(Pending publication and/or patent)

We investigated the gene expression profile and cellular behaviors of hBMSCs during the proliferation and differentiation under the hLIV and vLIV. We used mechanical signal combinations (either 30Hz or 100Hz frequency with either 0.15g or 1g acceleration amplitude) related fluid shear stress (from 0.04Pa to 0.94Pa). Cells adapt to external forces by dynamic remodeling of their cellular and nuclear structures. Observations of changes in the gene expression related cellular-nuclear structures and functions should provide the information on how LIV influences cell behaviors and functions, including the mechanotransduction pathway. We related gene profiles of the structures related genes with the functions related genes to define the potential mechanotransduction. The dynamic remodeling and changes in the cellular – nuclear structures with the mechanical stimulation could affect the cellular mechanical property. We observed structural changes in the cytoskeletal orientation and determined the relative mechanical modulus. To confirm the proposed underlying pathway, we knocked down the cytoskeletal biogene in the stem cell and observed the change in the gene profile. We found that the connection of mature junctions and nuclear nesprin2 with the cytoskeleton confirmed the CDH11-ACTn1-Syne2 mechanotransduction pathway. To understand the molecular functions of the pathway on multilineage abilities, we investigated the cytoskeletal orientation of hBMSCs and hAMSCs during the stem cell differentiation. The effect of LIV in controlling the stem cell differentiation toward preferable lineages was supported by the gene expression related cytoskeletal structures. The effect of the LIV on bone marrow residing cells like macrophages were observed in order to understand mechanical regulations of LIV in bone marrow niches'

cells. We observed proliferation and phenotype polarization of macrophages under the horizontal LIV. The effect of LIV on the macrophage showed anabolic stimulation toward pro-healing macrophage phenotypes. The data demonstrated that the LIV directs stem cells and immune cells toward anabolic bone pathway.

Our data showed, for the first time, what could be the specific mechanical signal that the human bone marrow mesenchymal stem cell could sense during the normal behavior and molecular functions. The physical changes in cellular and nuclear structures related genes showed that the specific mechanical signal modulated hBMSC proliferation were different from the signal directed the stem cell osteogenic differentiation. We found that during proliferation, human stem cells were sensitive to frequency, but during differentiation they were sensitive to the direction. Our data provided insight information on how to reprogram human stem cells. For examples, the frequency of the hLIV was able to sustain self-renewals and retain stem cell youth. The direction of the LIV could change cell phenotypes and switch stem cells and macrophages towards preferential phenotypes for the osteogenic bone formation and healing angiogenesis. The LIV was able to maintain cellular functions and programs cellular phenotypes towards anabolic mechanisms.

The relation of gene profiles with structures-, and function-related genes provided insight information for the underlying CDH11-ACTn1-Syne2 mechanotransduction pathway in human bone marrow MSCs. The mechanisms of LIV in hBMSC cells could potentially start with the LIV activating the interaction between cells and their neighboring cells to form mature adherent junctions (with an overexpressed CDH11). The mature junction upregulated CDH11 potentially formed connections with the cytoskeleton through the dynamic cytoskeletal orientation (by upregulating ACTn1). During upregulated ACTn1, the cytoskeletal orientation anchored

nucleoskeletons from the outer nuclear envelope throughout the nuclear membranes (with upregulating Syne2 and sun2). Even though links of adherent junctions with cytoskeleton or cytoskeleton with nucleoskeletons have been extensively studied, we for the first time connected adherent junctions with cytoskeletal orientations anchoring nucleoskeletons as the underlying mechanotransduction pathway.

The cytoskeletal orientation anchoring nucleoskeletons could be revealed by the two-photon confocal microscopy. This optical observation of the cytoskeletal and nucleoskeletal anchorage firmly supported that the upregulated ACTn1 with Syne2 during LIV could have the physical based mechanisms through the cytoskeletal orientation anchoring nucleoskeletons. As hBMSCs dynamically adapted to the external mechanical stimulation, the cytoskeletal orientation influenced molecular modulus should be measured. The data showed that better cytoskeletal orientations during horizontal LIV provided higher mechanical moduli. The data could translate that LIV oriented cytoskeletons induced stronger moduli in order to support osteoblastogenesis. The cytoskeleton knockdown showed no ACTn1-Syne2, confirming that the lacking of cytoskeletons could cause an incompletion in the CDH11-ACTn1-Syne2 pathway. Without cytoskeletons, the bridge from CDH11 to the nucleus was damaged, consequently causing disrupted mechanotransduction.

Our data demonstrated that the cytoskeletal orientation could function to control the stem cells fate. The hLIV induced cytoskeletal orientation could have molecular functions to support the osteoblastogenesis (upregulated Runx2) while suppressing the adipogenesis (downregulated PPARg). During the stem cell sensing the LIV, the adaptive morphology of the cytoskeletal orientation could promote the osteogenic differentiation. On molecular mechanisms, the hLIV

switched hBMSCs phenotypes towards preferential bone-forming phenotypes, as if hLIV induced adipogenic suppression.

Though the self-renewal mechanisms of the stem cells and immune cells have been unidentified. Our data could be the first to show that the LIV could maintain the cellular self-sufficient renewals of the bone marrow niches' cells. The ability of LIV in maintaining the self-renewals could be confirmed by the increased proliferation of both hBMSCs and macrophages under the LIV. Additionally, the LIV could have molecular functions as the phenotype switching activator toward anabolic mechanisms. The hLIV switched macrophage phenotypes and promoted pro-healing macrophages. Similarly, the hBMSCs' phenotypes were promoted towards the oriented cytoskeletal stimulated osteoblastogenesis. Furthermore, the upregulated VEGF of the pro-healing macrophage supported that the hLIV promoted angiogenesis, which is crucial for survival and remodeling of the hBMSC osteogenic differentiation.

Several limitations of our studies were such as the intrinsic capacities of the observation techniques and availabilities of the antibodies and immunofluorescence dyes. The two-photon confocal microscopy had a time lapse during imaging [Lund et al. 2012, Scott et al. 2014], which causes challenges in the live imaging. Monitoring the gene expression could be for overall, but not intermediated observations [Chang et al. 2008]. The cell observation assays are relied on the invasive techniques of immunofluorescence staining and antibody conjugations. Both of these techniques take time and rely on availabilities of biological agents. However, the protein expressions and synthesis in the gene expression were sensitive to time, temperatures and biological environments [Baron et al. 2013]. The combinations of time-dependent expressions and changes in environments could lead to different expression levels of the observation from the actual events. Moreover, the known signaling pathways mainly depend on protein syntheses,

integrin and cytokine [Chen et al. 2013, Vaughan et al. 2014]. Therefore, connecting genes that were not in the known pathways could be really complicated or even impossible, in which there may not be primer available. Additionally, the accuracy of linking these genes together depends strongly on how well we understand the possible interaction between these known signaling pathways and the cellular – nuclear structures.

7.1 Mechanotransduction via Physical Interactions

We for the first time identified that the hBMSCs can sense the direction of LIV, especially during the osteogenic differentiation [Pongkitwitoon et al. 2014]. Additionally, we separated the signal that the stem cell can sense at a certain molecular function. For example, we demonstrated that the stem cell proliferation preferred high frequency signals while the stem cell osteogenic differentiation was selective to the signal direction.

As previous section, we have demonstrated that the relation of the signaling pathway alone could not represent the mechanotransduction pathway. For example, the upregulated FAK/Akt was a lot less than the ACTn1/Syne2, which could be because the signaling pathway might have omit the structural changes and remodeling during the transduction. By including the cellular and nuclear structures, we confirmed that the CDH11-ACTn1-Syne2 pathway was the mechanotransduction in the human bone marrow MSCs.

If the oscillatory vibration could cause the stem cell to interact with its neighboring cells, the interaction between the cell and its neighbors could trigger changes in the cellular and nuclear structures, causing changes in the gene expression. By linking these structure related genes with their functions, the mechanotransduction pathway could be identified.

During vibrating cells, the upregulated CDH11 with overexpressed ACTn1 could demonstrate the formed mature junction with the cytoskeleton. The upregulated Whamm (cytoskeletal remodeling) with ACTn1 (cytoskeletal orientation and bundles) showed the cytoskeleton remodeling through orientation. The upregulated ACTn1 with Syne2-Sun2 could provide the cytoskeletal orientation anchoring the nuclear complex across the double nuclear membranes.

The mechanotransduction was confirmed by the cytoskeletal knockdown techniques. We identified molecular functions of LIV that the LIV-driven cytoskeletal orientation exhibited biological mechanisms as to promote osteoblastogenesis but to suppress adipogenesis.

7.1.1 LIV induced Cytoskeletal Orientation during Mechanotransduction

The two-photon confocal microscopy visually revealed cytoskeletal orientations, cell diameter, and thickness similar to the AFM [Chacko et al. 2013, Demiray et al. 2014]. Differently from these works, we evaluated quantifications of the %fiber orientation and the mechanical modulus. Similar to other works [Born et al. 2009, Engl et al. 2014], we were able to find the relation of cytoskeletal orientations with osteogenic differentiation. These data agreed with others that the cytoskeletal orientation into one preferential direction including thicken in bundles under mechanical stimulation. The cytoskeletal orientation could represent physical changes and transformations in responses to mechanical stimulation [Delaine-Smith et al. 2012, Demiray et al. 2014]. Even though most of tissue engineering would relate physical interactions with extracellular matrix [Bay et al. 2005, Guilak et al. 2009], the agreeable interpretation was that cells responded to external mechanical stimulation via physical changes in cells and nucleus

[Higuera et al 2012]. Recent works have shown one of the mechanosensitive systems was cadherin-cytoskeleton interfaces of forming mature junctions paralleled to cytoskeletons [Huveneers et al. 2013]. Although most of bone research has been concentrated on cilia of osteocytes and interstitial fluid flow [Ibanez-Tallon et al. 2003, Li et al. 2010], several visualized cytoskeletal images [Efremov et al. 2011] including gene expression and immunoprofiles [Khaw et al. 2001, Malone et al. 2007] have been showed the involvement of cytoskeletal orientation with mechanical sensing mechanisms. Changes in cytoskeletal rearrangements related overexpression of RhoA could be linked with increased in osteogenic differentiation, suggesting cytoskeletal orientation modulated osteoblastogenesis [McBeath et al. 2004, Yourek et al. 2007]. The arrangement of cytoskeletons in cytoplasm has been well related to the nucleus [Meinke et al. 2014, Starr et al. 2010]. Recent structures of NuAnCE-LiNC nucleoskeletons have been discovered to compose of at least nesprins, sun molecules, KASH, and Tan giant molecules [Lombardi et al. 2011 Luke et al. 2008]. Even though, the identifications of these structural molecules have been unclear, the known nesprin- and sun- gene expression levels have been used to observe changes in these structures [Lombardi et al. 2011, Meinke et al. 2014]. Without nesprins, the KASH and sun could not anchor from the outer nuclear envelope into the inner nuclear membranes [Razafsky et al. 2009, Starr et al. 2005, Zhou et al. 2010]. The complexity could arrive from multiple sub-filamental molecules in the same families such as Syne1, Syne2, Sun1, and Sun2 in human cells and/or sub-filaments of 3, and 4 in mouse cells [Meinke et al. 2014]. From our pooled data, we found that Syne2 and Sun2 were overexpressed more prominent than Syne1 and Sun 1. Our data monitored Nesprines (, which was Syne2 in human bone marrow MSCs) and/or Sun (Sun2) for the NuAnCE-LiNC observation.

7.1.2 Cytoskeletal Orientation Modulated Cellular Mechanics

We demonstrated that mechanical stimulation induced cytoskeletal orientation could influence mechanical modulus. Similarly found in other works, the modulus of cells was decreased during cytoskeletal disruption because the cytoskeletal bundles were responsible for cell mechanical properties [Wakatsuki et al. 2001]. Interestingly, cellular mechanical properties like viscoelasticity were used to distinguish cell types and their functions [Du et al. 2011]. From their data, longer and leaner cytoskeletons of osteoblasts provided better mechanical moduli. Our data found that cytoskeletal orientations of horizontal LIV were higher than of vertical LIV. Additionally, the relative mechanical modulus of hLIV was also increased much noticeable, comparable to the modulus of vLIV.

Correspondingly with the increased cytoskeletal orientation, the transcriptional Runx2 was upregulated much higher in hLIV than in vLIV. These data indicated strong links of cytoskeletal orientation and cellular mechanics with osteogenic differentiation, similarly to other works. During osteogenic differentiation, MSCs with cytoskeletal disruption had decreases in the expression of both ALP and Runx2 [Yourek et al. 2007]. Possibly during differentiation from hBMSCs to osteoblasts, the cytoskeletal orientation in one direction could facilitate the dynamic nuclear positioning and nucleation [Razafsky et al. 2009, Taranum et al. 2012]. Visually, stem cells tended to align cytoskeleton in one preferential direction before osteogenic differentiation and then back to a random orientation in the quiescent stage [Efremov et al. 2011]. The disassembled cytoskeletons of stem cells have been found to promote adipogenesis [Feng et al. 2010, Winter et al. 2012]. These findings supported our data that the cytoskeletal orientation increased in LIV groups could cause adipogenesis suppression.

In pharmacological studies of neutrophil migration, the cytoskeletal arrangements caused a spatial overexpression of Rac during dynamic actin polarizations towards one preferential direction [Peng et al. 2011]. However, the overall upregulated Rac maintained quite the same level over time as the dynamic cytoskeletal arrangement towards one preferential direction. Similarly, cytoskeletal arrangements towards one direction were required for Rac activating RhoA during the nuclear translocation phase in cell migrations [Rodríguez et al. 2004]. The upregulated Rac with RhoA signaling was corresponding well with cytoskeletal arrangement images towards one direction [Taranum et al. 2012]. We found that the increased cytoskeletal orientation in hLIV higher than in vLIV was corresponding with the upregulated Rac and RhoA. The overall upregulated Rac and RhoA remained somewhat the same upregulated levels over time. These data supported that physical structures and interactions of dynamic cytoskeletal arrangements towards one preferential direction caused overall upregulated Rac and RhoA (possibly up to the threshold) that cells still maintained their integrity during cellular activities over time.

7.1.3 Mechanotransduction of CDH11-ACTn1-Syne2

The CDH11-ACTn1-Syne2 mechanotransduction pathway [Pongkitwitoon et al. 2014] was confirmed by cytoskeleton knockdown. The biogene knockdown was permanent and happened in the nucleus (but not in the cytoplasm like the siRNA transfection) [Leung et al. 2005]. Without cytoskeletons, the expression of ACTn1-Syne2 was depleted. Though, the CDH11 was upregulated but decreased from the wild-type hBMSCs.

During cellular transduction of mechanical signals, the adherent junctions found to interact with cytoskeletons [Yonemura et al. 2011]. The mechanisms of these interactions have been proposed to derive from firstly the formation of mature adherent junctions before secondly the cytoskeletal arrangements [Engl et al. 2014, Huveneers et al. 2013]. The physical interactions of cytoskeletons and nucleoskeletons have been critical to anchoring NuAnCE-LiNC [Lombardi et al. 2011, Starr et al. 2010]. The transmission of mechanical signals could start when cytoskeletal rearrangements [Starr et al. 2010]. Following cytoskeletal activities, nesprins formed mature bonds towards KASH-Sun filament complex [Libotte et al. 2005, Taply et al. 2013] connecting laminins with chromatins [Kadauke et al. 2009, Rothballer et al. 2013]. We found that during an increase in the cytoskeletal orientation the upregulated Syne2 and sun2 were synchronized as the cytoskeletal orientation interacting with nucleoskeletons anchor NuAnCE-LiNC towards nuclear basement membrane laminins.

However, when cytoskeletons were depleted, the ACTn1-Syne2 was depleted. The depletion of ACTn1-Syne2 in the cytoskeletal knockdown indicated that there was no cytoskeletal arrangement anchoring nucleoskeleton [Lombardi et al. 2011, Hotulainen et al. 2005]. The decreased of upregulated CDH11 in the cytoskeletal knockdown from the wild-type hBMSCs was possibly because the mature adherent junctions could not form properly without cytoskeletons [Hammond et al. 2012]. These data of the cytoskeleton knockdown firmly verified the strong link of CDH11-ACTn1-Syne2 pathway.

7.2 LIV Functions as Self-Renewal Induction in Bone Marrow Niches

The cell doubling time can test the stem cell's ability of self-renewals [Roobrouck et al. 2008]. The hBMSCs primary cells obtained from orthopedic patients grown on Mg-doped hydroxyapatite showed the doubling time of 3.2 days on the 5th passage [Manfrini et al. 2012]. Our data showed that hBMSCs of 2nd and 3rd passages under LIV had the doubling time of 1-2 days at the same as the 1st and 2nd passages. These results indicated that LIV could retain self-renewing abilities of hBMSCs.

Even though the mechanisms of self-renewal have been unidentified, the abilities of cells to proliferation have been thought to be one of the self-renewal mechanisms [Deregowski et al. 2006]. In stem cells, most of data related the re-proliferation with CSF overexpression while the osteoblast progenitors could re-proliferate by upregulated Notch signaling [Chau et al. 2009]. However, an extreme overexpression of Notch could inhibit osteoblastogenesis of progenitors via severe suppression of Wnt/β-catenin [Deregowski et al. 2006]. Similarly, our data have shown that the upregulated CSF-1 and Notch1 in LIV groups were decreased over progressive osteoblastogenesis overtime. Indicating, as they were first proliferation before progression through differentiation in control of the upregulated Wnt10a and β-catenin.

In recent publications, macrophages had shown their ability to reproduce after acute inflammation [Davies et al. 2011]. The acute inflammation has found to be activated by TNF/Traf6 induced apoptosis [Paul et al. 2010], which is still unclear of how the proliferation was activated. One of the recent data showed that co-culture of mouse bone marrow MSCs with macrophages had a balance of pro-healing and inflammatory macrophage populations from Arg1-induced IL-10 [Cho et al. 2014]. However, as we have known that human macrophages do

not have Arg1 homolog. The IL-10 functioned as anti-inflammation by suppressing TNF levels, which promoted muscle growth and regeneration in open wounds [Deng et al. 2012]. TNF/Traf6 also found to activate autoimmune rheumatoid arthritis [Vasanthi et al. 2007]. Our data showed that hLIV increased macrophage proliferation in LIV groups corresponding with an increase in the ratio of pro-healing : inflammatory macrophages. Additionally, the increased pro-healing macrophages were in sync with upregulated IL-10 levels. These data indicated that the increased macrophage population of LIV groups were mainly pro-healing macrophages. The LIV could maintain an increased IL-10 level of functioning as anti-inflammation by suppressing TNF.

7.3 LIV Reprograms Molecular Switch towards Anabolic Phenotypes

In stem cell therapies for autoimmune imperfectae, the controls of molecular switches between osteoblastogenesis and adipogenesis found to be strongly related to inherent characteristics of stem cells [Takada et al. 2009]. Here, we found that under LIV multilineage potentials of hBMSCs including hAMSCs moved forward to preferential osteogenic not adipogenic phenotypes. Additionally, we found that LIV switched macrophage phenotypes toward pro-healing. It could be that one of the cellular and molecular functions of LIV was to control cells towards anabolic phenotypes.

Molecular reprogramming between osteogenic and adipogenic differentiation needs drastic controls of biochemistry [Takada et al. 2009]. For instance, in canonical Wnt/Bmp/β-catenin signaling pathway, the upregulated Wnt/Bmp could induce osteoblastogenesis to inhibit adipogenesis if only the β-catenin was activated to suppress Smad3 [Lowe et al. 2011]. The

peroxisome proliferator-activated receptor gamma (PPARg) is a prime inducer of adipocytes while inhibiting osteoblastogenesis [Shiozawa et al. 2012]. Here, we found that LIV controlled the molecular switch of both hBMSCs and hAMSCs towards osteoblastogenesis even without osteogenic or adipogenic inductive media. The LIV reprogrammed human stem cells during the determination phase to their commitments and the termination phase to their differentiation lineage. In the future, several possibilities of signaling studies could be that the LIV upregulated Wnt10a/Bmp2 to activate PI3K that induced Akt to suppress Smad3/PPARg. The LIV could control adipocytes crosstalk with osteoblasts by the upregulated Bmp2 suppressing Smad3, consequently inhibiting cEBP/PPARg.

7.4 Upregulated VEGF induced Macrophage Bone Healing Angiogenesis

Our data showed that the hLIV increased macrophage proliferation of pro-healing (the ratio of pro-healing : inflammatory macrophages > 1). Additionally, the pro-healing macrophages showed increasing IL-10 in the hLIV groups. These results suggested that hLIV could potentially act as anti-inflammation by assisting pro-healing macrophage proliferation at the macrophage osteal tissues intercalating osteoblast bone-lining tissues during homeostatic mechanisms after inflammation.

The upregulated VEGF in pro-healing macrophages increasing with bone marrow MSCs-driven osteoblastogenesis strongly indicated the potentials of bone repairs and survivals by angiogenesis of coupling mechanisms between macrophages and bone marrow MSCs [Schipani et al. 2009]. The upregulated TGFβ have been found to be steady as preferable dose to maintain bone homeostasis in marrow niches [Chen et al. 2012]. Our data showed that the increased IL-

10 in pro-healing macrophages was corresponding with upregulated VEGF and TGFβ. The upregulated VEGF was much more noticeable while the upregulated TGFβ was maintained somewhat similar in all signal conditions. These data suggested that hLIV could assist bone homeostasis in maintaining an upregulation of TGFβ and promoted bone healing angiogenesis.

The upregulated VEGF found to increase vascularization from bone marrow MSCs differentiation towards vascular lineages [Whyte et al. 2011]. The upregulated VEGF in coupling bone-marrow-vascular niches found to sustain osteoblast bone cell survivals while maintaining vascular regeneration [Serafini et al. 2014, Shiozawa et al. 2012]. Co-culture of hBMSCs and hUVECs found that the interaction of these two cell types at n-cadherin could upregulated VEGF increased vascularization [Li et al. 2010]. Our data showed that the upregulated VEGF were corresponding with overexpression of cadherin (CDH11) during LIV. These data suggested that the LIV increased cell-to-cell communication that upregulated CDH11. The upregulated CDH11 induced overexpression of VEGF could promote angiogenesis. In the future, the co-culture of hBMSCs and macrophages could support the potentials of LIV in improvements of intercommunications among niches. The LIV could activate crosstalk in bone marrow niches. The upregulated VEGF of macrophages under hLIV could increase angiogenesis in the coupling niches. The hBMSCs in the niches increased osteogenic differentiation under hLIV could increase osteoblast survivals from upregulated VEGF.

8. Summary:

(Pending publication and/or patent)

We are the first to successfully link cellular and nuclear architectures with the mechanotransduction pathway in human bone marrow mesenchymal stem cells. During horizontal and vertical low intensity vibration, human bone marrow MSC cells could dynamically change their cellular morphology and structures in responses to the LIV stimulation.

We demonstrated that the interaction between cells and their neighbors could form mature adherent junctions, as CDH11 of human bone marrow MSCs was upregulated. The mature junctions interacting with cytoskeletons were upregulating ACTn1 to anchor NuAnCE-LiNC (upregulated Syne2-Sun2). Theses structural dynamics monitored by gene expression were visualized by the two-photon confocal microscopy. The CDH11-ACTn1-Syne2 was the mechanotransduction pathway of hBMSCs during LIV and confirmed by the biogene knockdown technique. With cytoskeleton knockdown, the pathway of ACTn1-Syne2 was depleted. The dynamic cytoskeletal orientations were therefore required in mechanosensing systems. The LIV induced cytoskeletal orientations anchoring nucleoskeletons could function to be osteogenic activators. These data demonstrated for the first time that cellular functioning of LIV was to promote the bone formation by activation of hBMSCs driven osteogenic differentiation via the cytoskeletal orientation. The LIV could prepare the hBMSC via the cytoskeletal orientation toward the preferential phenotype and morphology ready for the osteogenic differentiation. The cytoskeletal orientation could also function to improve cellular mechanics as if to support the phase of becoming mature functioning osteoblasts. The LIV activated osteoblastogenesis could consequently suppress adipogenesis as if cytoskeletal

orientations inhibited adipocytic phenotypes suppressing adipogenic differentiation. These data demonstrated for the first time that the mechanisms of LIV supported osteoblastogenesis but suppressed adipogenesis were through the cytoskeletal orientation anchoring nucleoskeletons. The LIV has anabolic influences not only hBMSCs but also macrophages' proliferations as if LIV induced self-renewals of bone marrow niches' cells. The selective LIV could activate bone marrow niches' cells towards preferential anabolic phenotypes (such as more pro-healing macrophage populations) and maintained their functions (such as increased IL-10). The molecular functioning of LIV could promote bone healing angiogenesis and homeostasis by promotion of the bone marrow niches' cell communications. The upregulated VEGF of pro-healing macrophages supported that LIV induced bone healing angiogenesis. The maintaining upregulated TGF-β demonstrated that LIV maintained bone homeostasis in bone marrow niches.

References

Baron R, Kneissel M. '*Wnt signaling in bone homeostasis and disease: from human mutations to treatments'. Nature Medicine*.' **2013**, 19: 179–192. doi:10.1038/nm.3074.

Bays JL, Peng X, Tolbert CE, Guilluy C, Angell AE, Pan Y, Superfine R, Burridge K, DeMali KA. '*Vinculin phosphorylation differentially regulates mechanotransduction at cell–cell and cell–matrix adhesions*' JCB **2005**, 205 (2): 251-263.

Born AK, Rottmar M, Lischer S, Pleskova M, Bruinink A, Maniura-Weber K. '*Correlating cell architecture with osteogenesis: the first steps towards live single cell monitoring*.' European Cells Mat. **2009**, 18: 49-62.

Chacko JV, Zanacchi FC, Diaspro A. '*Probing Cytoskeletal Structures by Coupling Optical Superresolution and AFM Techniques for a Correlative Approach*.' Cytoskeleton. **2013**, 70: 729–740. doi: 10.1002/cm.21139

Chang MK, Raggatt L-J, Alexander KA, Kuliwaba JS, Fazzalari NL, Schroder K, Maylin ER, Ripoll VM, Hume DA, Pettit AR. '*Osteal Tissue Macrophages Are Intercalated throughout Human and Mouse Bone Lining Tissues and Regulate Osteoblast Function In Vitro and In Vivo*'. J Immunol. **2008**, 181: 1232-1244. doi: 10.4049/jimmunol.181.2.1232.

Chau JF, Leong WF, Li B. '*Signaling pathways governing osteoblast proliferation, differentiation and function*.' Histol Histopathol. 2009, 24 (12): 1593-1606.

Chen G, Deng C, Li YP. '*TGF-β and Bmp Signaling in Osteoblast Differentiation and Bone Formation*'. Int J Biol Sci. **2012**, 8 (2): 272-288. doi:10.7150/ijbs.2929.

Chen JC, Jacobs CR. '*Mechanically induced osteogenic lineage commitment of stem cells*.' Stem Cell Res Ther. **2013**, 4 (5): 107.

Cho DI, Kim MR, Jeong HY, Jeong HC, Jeong MH, Yoon SH, Kim YS, Ahn Y. '*Mesenchymal stem cells reciprocally regulate the M1/M2 balance in mouse bone marrow-derived macrophages*.' Exper Mol Med. **2014**, 46: e70. doi:10.1038/emm.2013.135.

Davies LC, Rosas M, Smith PJ, Fraser DJ, Jones SA, Taylor PR. '*A quantifiable proliferative burst of tissue macrophages restores homeostatic macrophage populations after acute inflammation*'. Eur. J. Immunol. **2011**, 41: 2155–2164. doi:10.1002/eji.201141817

Delaine-Smith RM, Reilly GC. '*Mesenchymal stem cell responses to mechanical stimuli*.' Muscles, Ligaments Tendons J. **2012**, 2 (3): 169-180.

Delaine-Smith RM, Sittichokechaiwut A, Reilly GC. '*Primary cilia respond to fluid shear stress and mediate flow-induced calcium deposition in osteoblasts*'. FASEB J. **2014**, 28 (1): 430–439. doi: 10.1096/fj.13-231894. PMCID: PMC4012163.

Demiray L, Özcivici E. '*Bone marrow stem cells adept to low-magnitude vibrations by altering their cytoskeleton during quiescence and osteogenesis*.' Turk J Biol. **2014**, 38: 1-10. doi:10.3906/biy-1404-35

Deregowski V, Gazzerro E, Priest L, Rydziel S, Canalis E. '*Notch 1 overexpression inhibits osteoblastogenesis by suppressing Wnt/beta-catenin but not bone morphogenetic protein signaling*.' J Biol Chem. **2006**, 281 (10): 6203-6210. doi: 10.1074/jbc.M508370200.

Du G, Ravetto A, Fang Q, den Toonder JMJ. '*Cell type can be distinguished by measuring their viscoelstic recovery times using a micro-fluidic device*.' Biomed Microdevices. **2011**, 13: 29-40.

Efremov YM, Dzyubenko EV, Bagrov DV, Maksimov GV, Shram SI, Shaitan KV. '*Atomic Force Microscopy Study of the Arrangement and Mechanical Properties of Astrocytic Cytoskeleton in Growth Medium*.' Acta Nature. **2011**, 3 (3: 10): 93-99.

Engl W, Arasi B, Yap LL, Thiery JP, Viasnoff V. '*Actin dynamics modulate mechanosensitive immobilization of cadherin at adherens junctions*.' NATURE CELL BIOL. **2014**, 16: 584-591. doi:10.1038/ncb297.

Feng T, Szabo E, Dziak E, Opas M. '*Cytoskeletal disassembly and cell rounding promotes adipogenesis from ES cells*.' Stem Cell Rev. **2010**, 6(1): 74-85. doi: 10.1007/s12015-010-9115-8.

Guilak F, Cohen DM, Estes BT, Gimble JM, Liedtke W, Chen CS. '*Control of stem cell fate by physical interactions with the extracellular matrix*.' Cell Stem Cell **2009**, 5: 17–26.

Hotulainen P, Paunola E, Vartiainen MK, Lappalainen P. '*Actin depolarizing factor and cofilin-1 play overlapping roles in promoting rapid f-actin depolymerization in mammalian non-muscle cells*'. Mol Biol Cell. **2005**, 16: 649-664. doi:10.1091/mbc.E04-07-0555.

Higuera GA, van Boxtel A, van Blitterswijk CA, Moroni L. '*The physics of tissue formation with mesenchymal stem cells*.' Trends Biotechnol. **2012**, 30: 583–590.

Huveneers S, de Rooij J. '*Mechanosensitive systems at the cadherin-F-actin interface*.' J Cell Sci. **2013**, 126: 1-11. doi: 10.1242/jcs.109447.

Ibanez-Tallon I, Nathaniel Heintz N, Omran H. '*To beat or not to beat: roles of cilia in development and disease*.' Hum. Mol. Genet. **2003**, 12 (suppl1): R27-R35. doi: 10.1093/hmg/ddg061.

Khaw BA, daSilva J, Vural I, Narula J, Torchilin VP. '*Intracytoplasmic gene delivery for in vitro transfection with cytoskeleton-specific immunoliposomes*.' J Control Release. **2001**, 75 (1-2): 199-210.

Leung RKM, Whittaker PA. '*RNA interference: From gene silencing to gene-specific therapeutics*'. Pharm Therapeutics. **2005**, 107 (2): 222-239.

Li H, Daculsi R, Grellier M, Bareille R, Bourget C, Amedee J. '*Role of neural-cadherin in early osteoblastic differentiation of human bone marrow stromal cells cocultured with human umbilical vein endothelial cells*.' Am J Physiol Cell Physiol. **2010**, 299: C422–C430. doi:10.1152/ajpcell.00562.2009.

Lombardi ML, Jaalouk DE, Shanahan CM, Burke B, Roux KJ, Lammerding J. '*The Interaction between Nesprins and Sun Proteins at the Nuclear Envelope Is Critical for Force Transmission between the Nucleus and Cytoskeleton*'. J Biol Chem. **2011**; 286 (30): 26743–26753 doi: 10.1074/jbc.M111.233700 PMCID: PMC3143636

Lowe CE, O'Rahilly S, Rochford JJ. '*Adipogenesis at a glance'*. J Cell Sci. **2011**, 124: 2681-2686 doi:10.1242/jcs.079699

Lund FW, Lomholt MA, Solanko LM, Bittman R, Wüstner D. '*Two-photon time-lapse microscopy of BODIPY-cholesterol reveals anomalous sterol diffusion in chinese hamster ovary cells*.' BMC Biophys. **2012**, 5: 20. doi: 10.1186/2046-1682-5-20.

Malone AMD, Batra NN, Shivaram G, Kwon RY, You L, Kim CH, Rodriguez J, Jair K, Jacobs CR. '*The role of actin cytoskeleton in oscillatory fluid flow-induced signaling in MC3T3-E1 osteoblasts*'. Am J Physiol - Cell Physiol. **2007**, 292 (5): C1830-C1836. doi:10.1152/ajpcell.00352.2005.

Manfrini M, Di Bona C, Canella A, Lucarelli E, Pellati A, Agostino AD, Barbanti-Brodano G, Tognon M. '*Mesenchymal stem cells from patients to assay bone graft substitutes*.' J Cell Physiol. **2012**. doi:10.1002/jcp.24276.

McBeath R, Pirone DM, Nelson CM, Bhadriraju K, Chen CS. '*Cell shape, cytoskeletal tension, and RhoA regulate stem cell lineage commitment*.' Dev Cell. **2004**, 6 (4): 483-495.

Meinke P, Mattioli E, Haque F, Antoku S, Columbaro M, Straatman KR, Worman HJ, Gundersen GG, Giovanna Lattanzi G, Wehnert M, Shackleton S. '*Muscular Dystrophy-Associated SUN1 and SUN2 Variants Disrupt Nuclear-Cytoskeletal Connections and Myonuclear Organization*'. PLoS Genet. **2014**, 10 (9): e1004605. doi:10.1371/journal.pgen.1004605

Paul PK, Gupta SK, Bhatnagar S, Panguluri SK, Darnay BG, Choi Y, Kumar A. '*Targeted ablation of TRAF6 inhibits skeletal muscle wasting in mice'*. **2010**, 191 (7): 1395-1411. doi: 10.1083/jcb.201006098.

Peng GE, Wilson SR, Weiner OD. '*A pharmacological cocktail for arresting actin dynamics in living cells*.' Mol Biol Cell. **2011**, 3986-3994. doi/10.1091/mbc.E11-04-0379.

Pongkitwitoon S. '*Mechanotransduction of low intensity vibration in human bone marrow mesenchymal stem cells and bone marrow niches' macrophages*.' Ph.D. Dissertation. **2014**.

Razafsky D, Hodzic D. '*Bringing KASH under the SUN: the many faces of nucleo-cytoskeletal connections*.' JCB. **2009**, 186 (4): 461-472. doi: 10.1083/jcb.200906068

Rodríguez JP, González M, Ríos S, Cambiazo V. '*Cytoskeletal organization of human mesenchymal stem cells (MSC) changes during their osteogenic differentiation*.' J Cell Biochem. **2004**, 93 (4): 721-731.

Roobrouck VD, Ulloa-Montoya F, Verfaillie CM. '*Self-renewal and differentiation capacity of young and aged stem cells*.' Exper Cell Res. **2008**, 314: 1937–1944. doi:10.1016/j.yexcr.2008.03.006.

Rothballer A, Kutay U. '*The diverse functional LiNCs of the nuclear envelop to the cytoskeleton and chromatin*'. Chromosome **2013**, 122: 415-429. doi:10.1007/s00412-013-0417-x

Schaller MD. '*Cellular functions of FAK kinases: insight into molecular mechanisms and novel functions*'. J Cell Sci. **2010**, 123 (7): 1007-1013. doi:10.1242/jcs.045112

Scott MK, Akinduro O, Lo Celso C. '*In Vivo 4-Dimensional Tracking of Hematopoietic Stem and Progenitor Cells in Adult Mouse Calvarial Bone Marrow*.' J Vis Exp. **2014**, 91: e51683. doi:10.3791/51683.

Serafini M, Sacchetti B, Pievani A, Redaelli D, Remoli C, Biondi A, Riminucci M, Bianco P. '*Establishment of bone marrow and hematopoietic niches in vivo by reversion of chondrocyte differentiation of human bone marrow stromal cells*'. Stem Cell Res. **2014**, 12(3): 659–672.

Shiozawa Y, Taichman RS. '*Getting blood from bone: An emerging understanding of the role that osteoblasts play in regulating hematopoietic stem cells within their niche*.' Exper Hematology. **2012**, 40: 685–694.

Shen QT, Hsiue PP, Sindelar CV, Welch MD, Campellone KG, Wang HW. '*Structural insights into WHAMM-mediated cytoskeletal coordination during membrane remodeling*'. J Cell Biol. **2012**, 199 (1): 111–124. doi: 10.1083jcb.201204010

Starr DA, Fischer JA. '*KASH 'n Karry: the KASH domain family of cargo-specific cytoskeletal adaptor proteins*.' BioEssays. **2005**, 27: 1136–1146.

Starr DA, Fridolfsson HN. '*Interactions Between Nuclei and the Cytoskeleton Are Mediated by SUN-KASH Nuclear-Envelope Bridges*.' Annu Rev Cell Dev Biol. **2010**; 26: 421–444. doi: 10.1146/annurev-cellbio-100109-104037. PMCID: PMC4053175. NIHMSID: NIHMS595647

Stricker J, Falzone T, Gardel ML. J Biomech. '*Mechanics of the F-actin cytoskeleton*.' **2010**, 43 (1): 9-14. doi:10.1016/j.jbiomech.2009.09.003. Epub 2009 Nov 13.

Takada I, Kouzmenko AP, Kato S. '*Molecular switching of osteoblastogenesis versus adipogenesis: implications for targeted therapies*.' Expert Opin Ther Targets. **2009**, 13 (5): 593-603. doi: 10.1517/14728220902915310.

Tapley EC, Starr D. '*Connecting the nucleus to the cytoskeleton by SUN-KASH bridges across the nuclear envelope*'. Curr Opin Cell Biol. **2013**; 25(1): 57–62. doi: 10.1016/j.ceb.2012.10.014. PMCID: PMC3578026. NIHMSID: NIHMS417735

Taranum S, Sur I, Müller R, Lu W, Rashmi RN, Munck M, Neumann S, Karakesisoglou I, Noegel AA. '*Cytoskeletal Interactions at the Nuclear Envelope Mediated by Nesprins*.' Inter J Cell Biol. **2012**, ID 736524: 11 pp. doi:10.1155/2012/736524.

Vasanthi P, Nalini G, Rajasekhar G. '*Role of tumor necrosis factor-alpha in rheumatoid arthritis: a review*'. J Rheumatology **2007**; 10: 270–274.

Vaughan TJ, Mullen CA, Verbruggen SW, McNamara LM. '*Bone cell mechanosensation of fluid flow stimulation: a fluid-structure interaction model characterising the role integrin attachments and primary cilia*.' Biomech Model Mechanobiol. **2014** Nov 16.

Wakatsuki T, Schwab B, Thompson NC, Elson EL. '*Effects of cytochalasin D and latrunculin B on mechanical properties of cells*.' J Cell Sci. **2001**; 114:1025–1036. PubMed: 11181185.

Whyte JL, Ball SG, Shuttleworth CA, Brennan K, Kielty CM. '*Density of human bone marrow stromal cells regulates commitment to vascular lineages*.' Stem Cell Res. **2011**, 6 (3): 238–250. doi: 10.1016/j.scr.2011.02.001 PMCID: PMC3223522.

Winter PW, Van Orden AK, Roess DA, Barisas BG. '*Actin-dependent clustering of insulin receptors in membrane microdomains*'. Biochem Biophys Acta. **2012**, 1818(3): 467-473. doi: 10.1016/j.bbamem.2011.10.006. Epub 2011 Oct 15.

Yonemura S. '*Cadherin-actin interactions at adherent junctions*'. Curr Opin Cell Biol. **2011**, 23(5): 515-22. doi: 10.1016/j.ceb.2011.07.001. Epub 2011 Jul 30.

Yourek G, Hussain MA, Mao JJ. '*Cytoskeletal changes of mesenchymal stem cells during differentiation*.' ASAIO J. **2007**, 53 (2): 219-228.

Zhou K, Hanna-Rose W. '*Movers and Shakers or Anchored: Caenorhabditis elegans Nuclei Achieve It With KASH/SUN*.' Developmental Dynamics. **2010**, 239: 1352–1364. doi: 10.1002/dvdy.22226.

Appendix A

(Pending publication and/or patent)

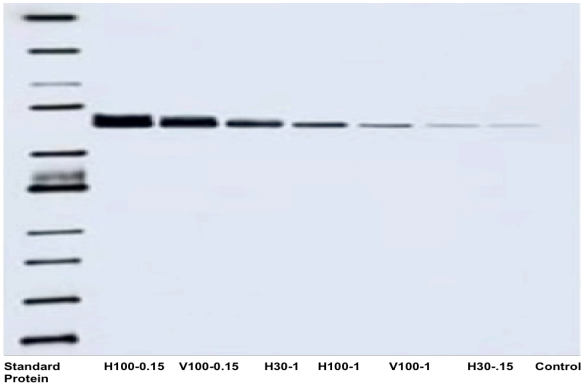

Figure A1: Western blot of the ALP in hBMSCs under LIV: Horizontal LIV at 100Hz-0.15g, Vertical LIV at 100Hz-0.15g, Horizontal LIV at 30Hz-1g, Horizontal 100Hz-1g, Horizontal 30Hz-0.15g and non-LIV was presented here. The ALP of Horizontal LIV at 100Hz-0.15g showed the strongest (darkest) and the biggest band, implying the most amount of the ALP expression in this sample.

The western blot technique is to detect the protein of interests using specific antibody to bind the specific protein. The secondary antibody of horseradish peroxidase then conjugates to the ALP and reacts to the enzyme substrate to precipitate the color on the blot that can be detected by the chemiluminescence [Kurien et al. 2003].

References:

1. Kurien BT and Scofield RH. '*Protein blotting: a review*.' J Immunol Methods. **2003**, 274, 1–15.

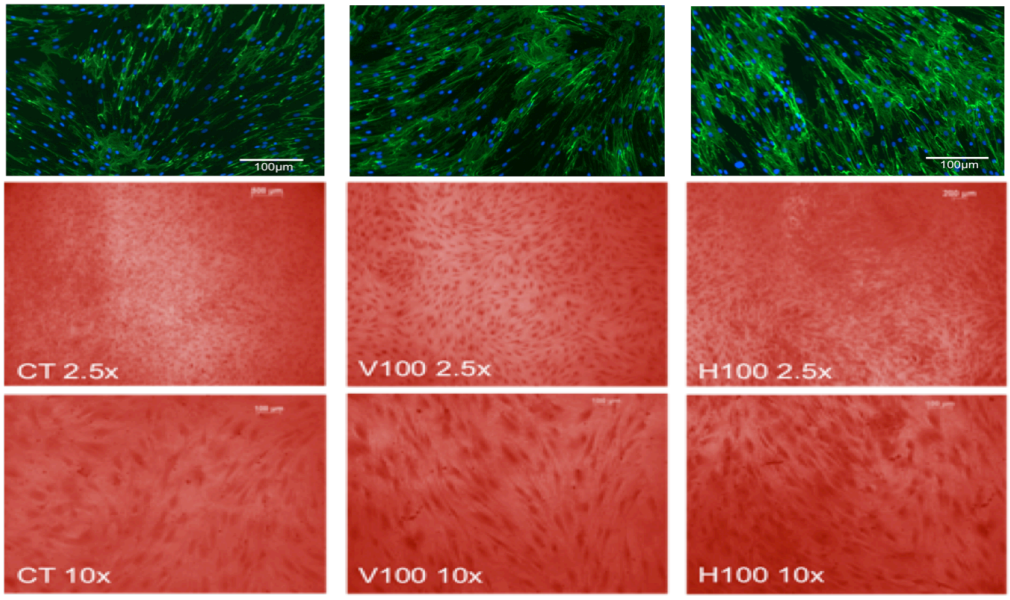

Figure A2: The human bone marrow MSCs during the osteogenic differentiation after osteogenic differentiation for 14 days expressed the collagen deposition (*in the first row*), where the green was Alxaflour488 of cytoskeletal fibers and the blue was the DAPI stained nucleus as cell are intact during imaging.

The Alizarin Red S assay of the hBMSCs after the second vibration of the osteogenic differentiation (in the second row for 2.5x and the third row for 10x magnification) showed that the osteogenic differentiation under the horizontal LIV (in the last column) was the most progressive comparing to the vertical LIV (in the middle column) and the non-LIV (in the first column).

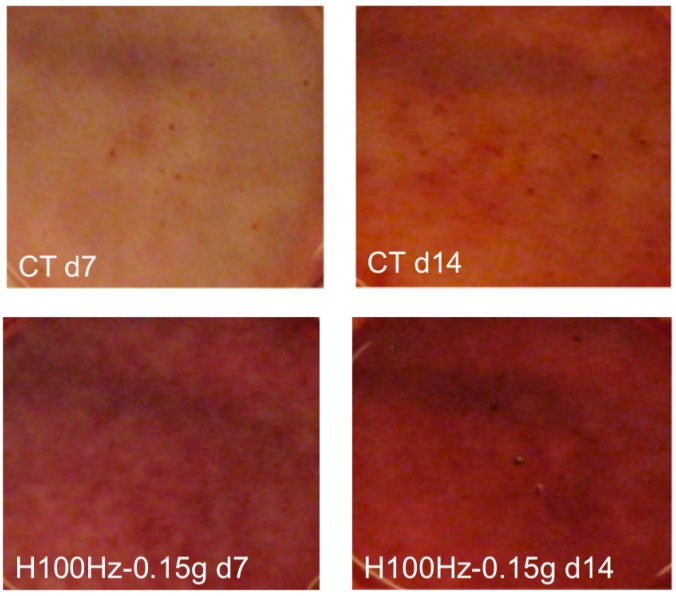

Figure A3: The Alizarin red S assay of the hBMSCS after 7 and 14 days of the osteogenic differentiation showed that the LIV group provided better calcification and had more Ca^{2+} deposition, as the color was darker in the LIV groups.

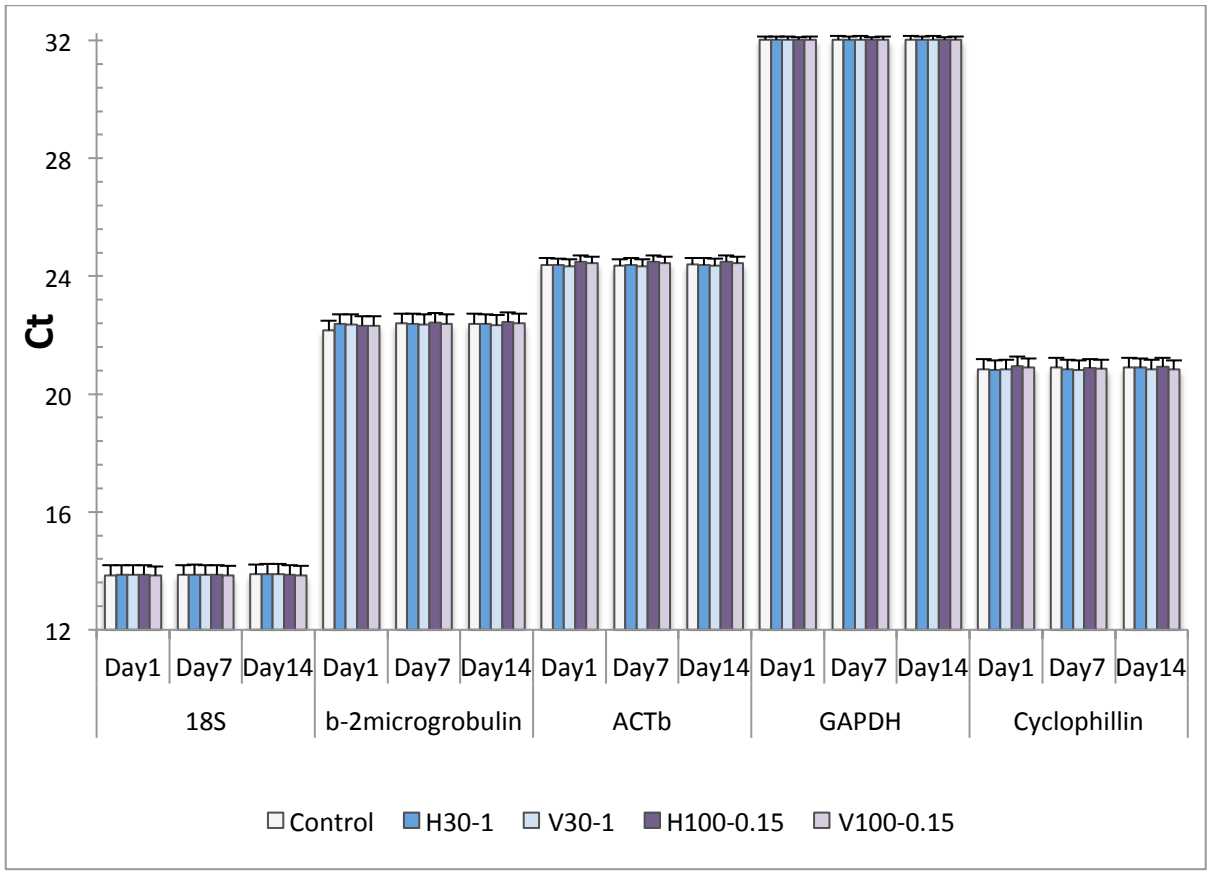

Figure A4: We tested 5 housekeeping genes shown in this figure. Since the gene expression as $2^{-\Delta(\Delta C_T)}$ (fold changes) by the real-time PCR analysis depends on how well of the selection of the housekeeping gene as a reference for normalization would be [Quiroz et al. 2010]. To justify our selection of the housekeeping gene for the human stem cells, we compared the Ct expression from the real-time PCR. We tested 5 most common uses for the housekeeping genes for human cells: 18S ribosomal RNA (18S), β_2-microgrobulin (B2M), β-actin (ACTb), cyclophilin (Cyp), and glyceraldehyde 3-phosphate dehydrogenase (GAPDH). The Ct expression of the GAPDH was the highest for all conditions (as the most abundant in the human stem cells). Additionally, the GAPDH

seemed to be the most stable without changing with the experimental conditions (somewhat flat line throughout all experimental conditions). The common used β-actin in human cells was here the second most abundant, but seemed to be slightly fluctuated (did not provide a perfect flat line) across our conditions. We used NormFinder and GeNorm [Tan et al. 2012] to qualify the stability and the GAPDH showed the most stable. From the data, we justified that GAPDH was the best housekeeping gene for human bone marrow stem cells for the PCR analysis.

Reference:

1. Quiroz FG, Posada OM, Gallego-Perez D, Higuita-Castro N, Sarassa C, Hansford DJ, Agudelo-Florez P, López LE. '*Housekeeping gene stability influences the quantification of osteogenic markers during stem cell differentiation to the osteogenic lineage*.' Cytotechnology. **2010**; 62 (2): 109–120. doi: 10.1007/s10616-010-9265-1

2. Tan SC, Carr CA, Yeoh KK, Schofield CJ, Davies KE, Clarke K. '*Identification of valid housekeeping genes for quantitative RT-PCR analysis of cardiosphere-derived cells preconditioned under hypoxia or with prolyl-4-hydroxylase inhibitors*'. Mol Biol Rep **2012**; 39: 4857–4867. doi: 10.1007/s11033-011-1281-5

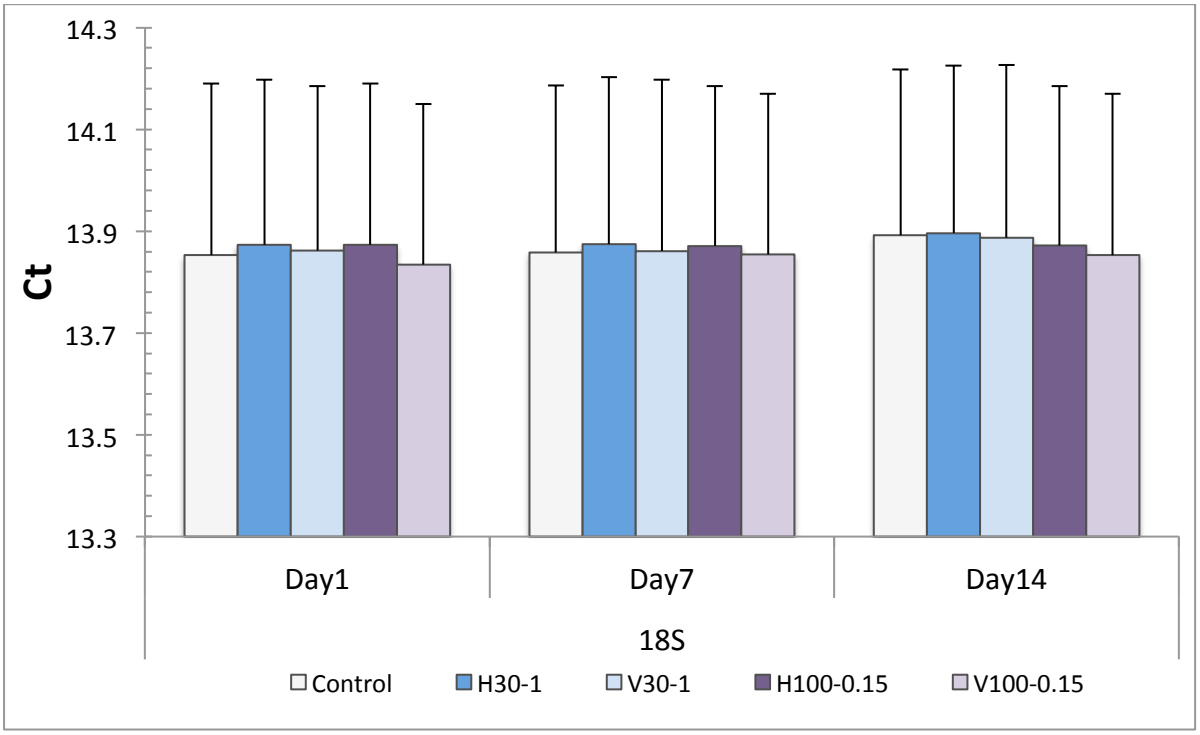

Figure A5: The 18S housekeeping gene showed some fluctuations across all experimental conditions. Additionally, when compared to other common housekeeping genes, the 18S is not the most abundant in human stem cells. Therefore, the 18S was not the best fit in our experiment. This figure was an expansion of the **Figure A4** (scalling from 13.3-14.3).

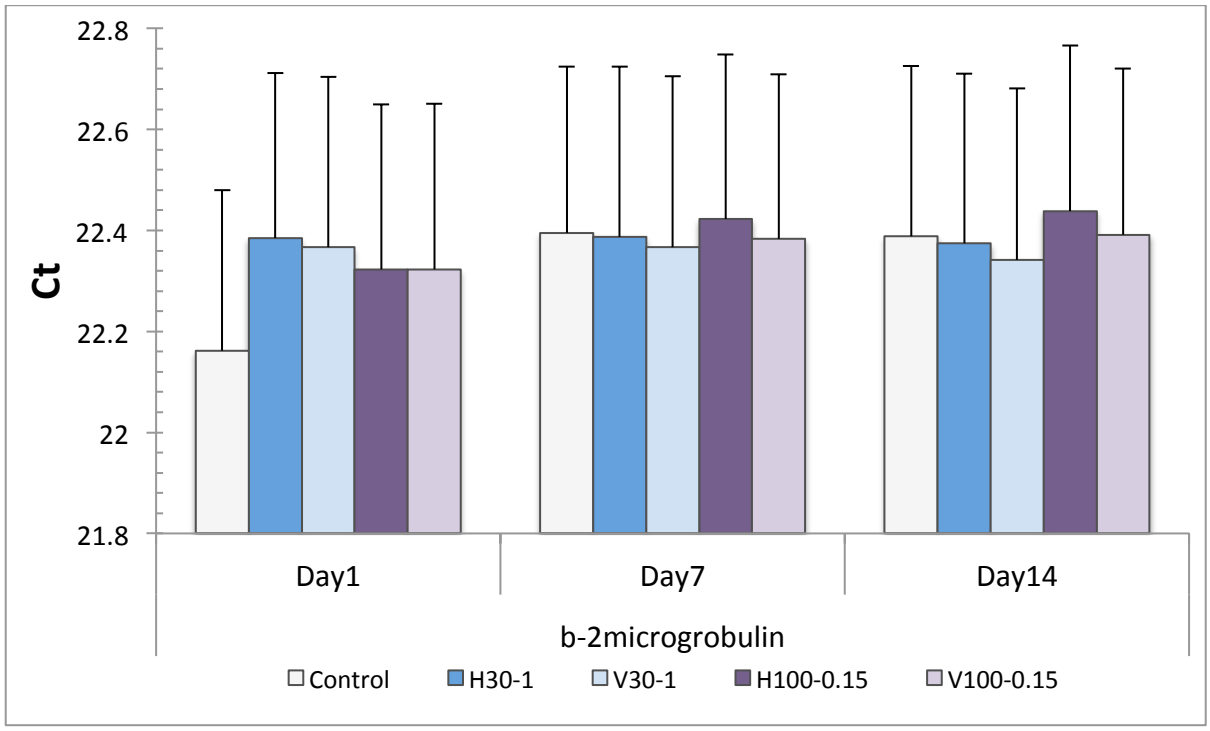

Figure A6: The expansion was in scale from 21.8-22.8 of the **Figure A4**. The β_2-microglobulin (B2M) was fairly fluctuated across all experimental conditions and as the time changed the expression seemed to have some variations as well. Therefore, the β_2-microglobulin was not the best housekeeping gene in our experiment.

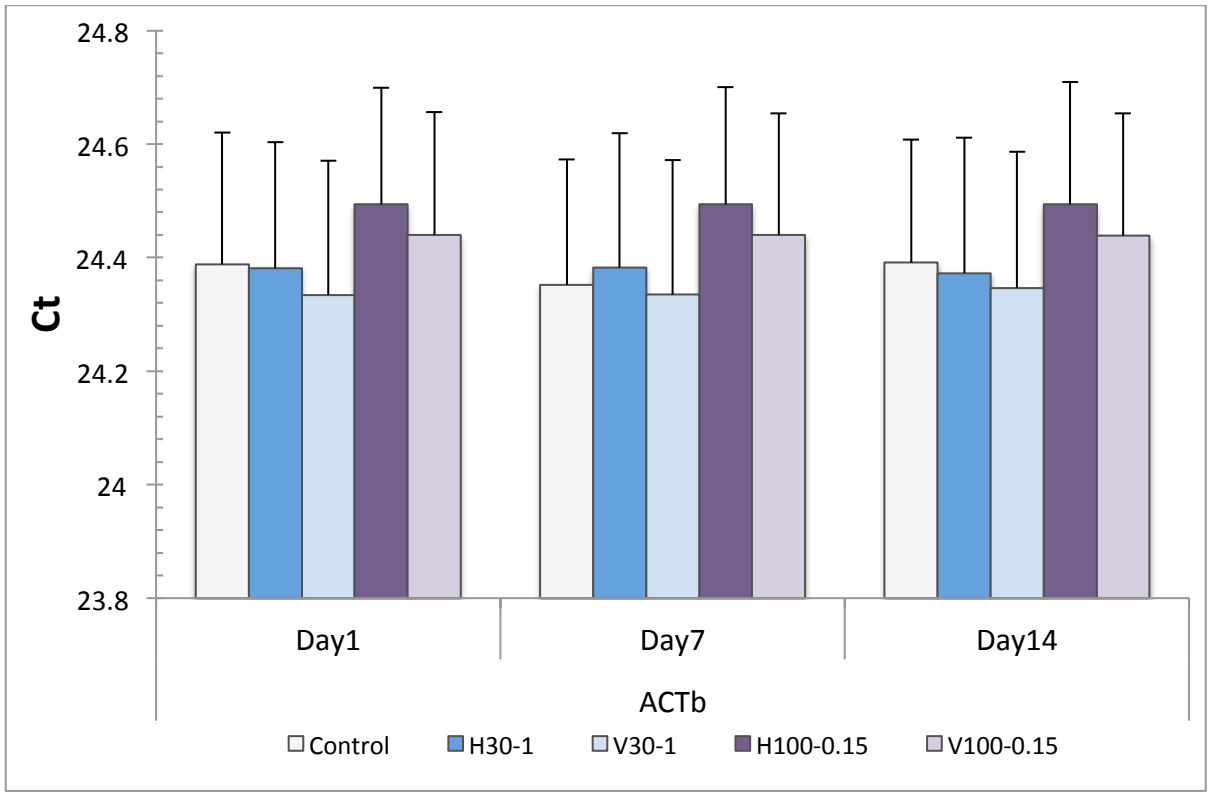

Figure A7: To see the details of the plot, the scale of the **Figure** A4 was expaneded from 23.8-24.8. The β-Actin (ACTβ) is the most common used in the real-time PCR and the western blot because it is found to be abundant in cells. Interestingly, though the β-Actin was not changed with time, however, it changed with the experimental condition. It seemed that the low fluid shear stress could manipulate the amount of the β-Actin and its expression level in human stem cells. (The stability by NormFinder confirmed the fluctuation of the β-Actin with the experimental condition.) For these reasons, we could not use the β-Actin to be our housekeeping gene.

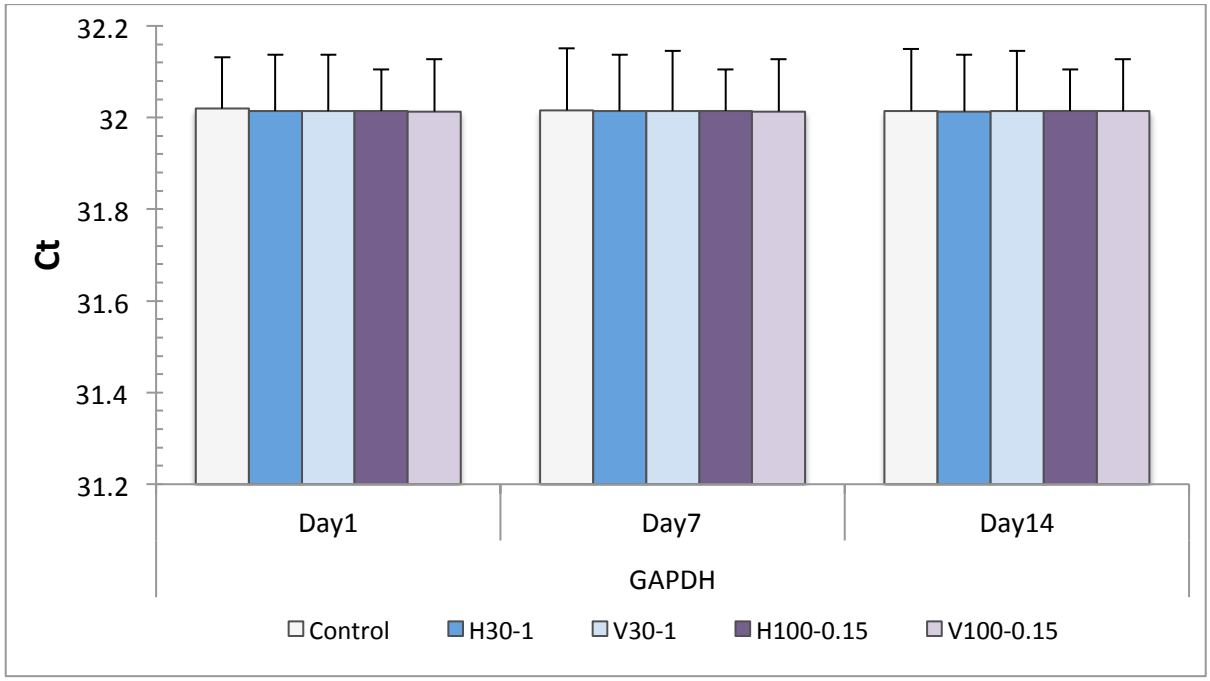

Figure A8: The scale of the **Figure** A4 was expaneded from 31.2-32.2. The GAPDH was the most abundant in all tested housekeeping genes. Over time, the level of GAPDH was stable. Additionally, the GAPDH expression level was not changed with the experimental condition. From the NormFinder, we found that the GAPDH was the most stable. Here, we chose the GAPDH to be our housekeeping gene for human stem cells.

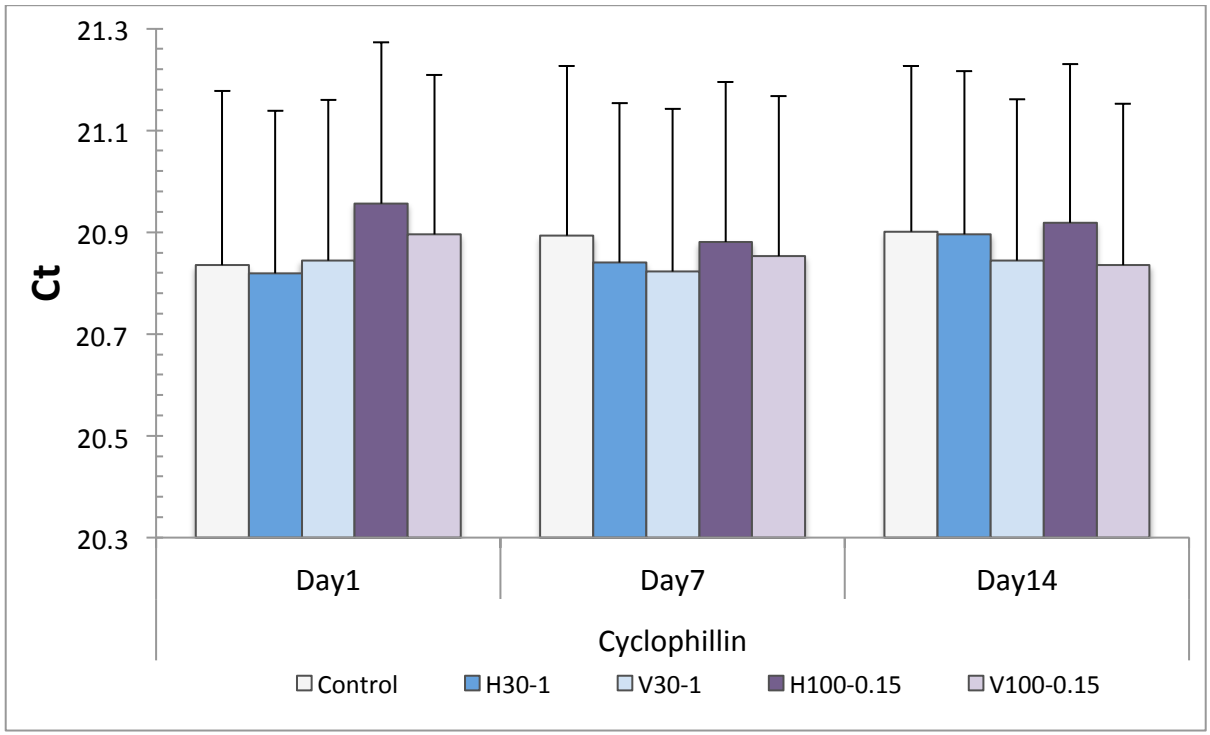

Figure A9: To see the details of the fluctuation, the scale of the **Figure** A4 was expaneded from 20.3-21.3. The cyclophillin (Cyp) was abundant, but changed with experimental conditions and fluctuated over time. With instability, we did not use the cyclophillin as a housekeeping gene in the PCR gene expression analysis.

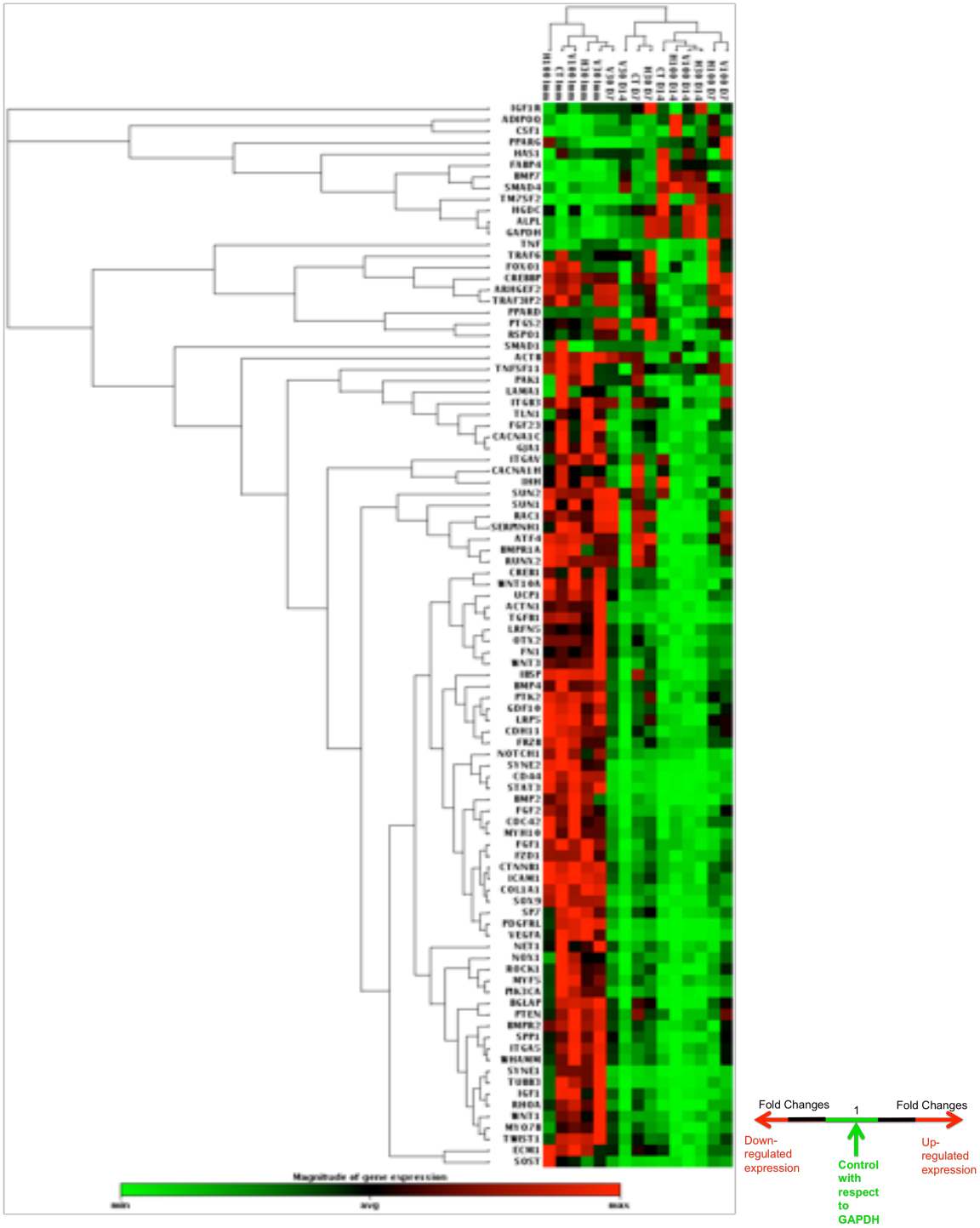

Figure A10: To achieve cluster analysis, we used SABioScience templates and modified it with the MatLab programming. Since the built-in program is (i) only limited for the

company's customized array and (ii) can only have one time point of the control, so we could not use the template directly. Our array was specifically modified to calculate several controls at the different time points of all the experimental groups. By adding in the gene name and its Ct value of each condition at each time point, we could visualize the magnitude of the gene expression of the entire gene array at all time points into one cluster diagram with at least >95% confidence ($p<0.05$) with respect to the GAPDH housekeeping gene at each time point. Qualitatively, the red color represented the maximal magnitude at the farthest away from the control values. Meaning that the fold changes could be in the highest or in the lowest level with respect to the control. On the other hand, the green color represented the minimal magnitude closer to the control in both higher and lower sides. The mixed color of red and green in between represented somewhere in between the maximum and minimum in the expression magnitude.

The data showed in general that the horizontal LIV provided a higher magnitude (brighter red color) in (i) the osteogenic differentiation (e.g. ALP, Runx2, BMPs, Wnts), (ii) nuclear activities such as the ribosomal energy biosynthesis and mitochondrial nucleotide activities (e.g. CREBBp, aRhGef2), (iii) cellular and nuclear structures such as (a) the outer membrane, integrins and cytokine (e.g. ECM1, FGFs, ITGs, CTNNb1, GJa1), (b) the adherent junction and intercellular filament interactions (e.g. CDH11), and (c) the cytoskeletal and nuclear filaments (e.g. ACTn1, Syne1, Syne2, Sun1, Sun2) when compared to the vertical LIV and non-LIV. The gene expression levels of the function related gene such as the osteogenic differentiation related genes (e.g ALP, Runx2, Wnt10α), and the structure related gene such as the outer filament adherent junction,

including cytoskeletal and nuclear filaments (e.g. CDH11, ACTn1 and Syne2) were the farthest away from the control under the LIV at H100Hz-0.15g.

During LIV, the rapid increase in Crebbp and αRhGef2 showed that the nucleus endured several nuclear activities and is in needs of bioenergy. The high demand of the bioenergy indicated a high nucleotide energy exchange from the ribosome and mitochondria. Additionally, across signal combinations, the LIV had no causes of inflammation in human stem cells as seen the green color in the inflammatory markers (e.g. TNF, Traf6, and Tm7sf2), and the balancing bioprocess genes (e.g. CSF-1 and TGFb1) across the signal combination. With increasing TGFβ1 but moderated CSF-1, the hBMSCs could lessen the ICAM1 down, in which activated the pro-healing phenotype of macrophages in the bone marrow niche. This relation could explain the LIV moved the bone marrow niche towards the healing cycle rather than the inflammatory defense.

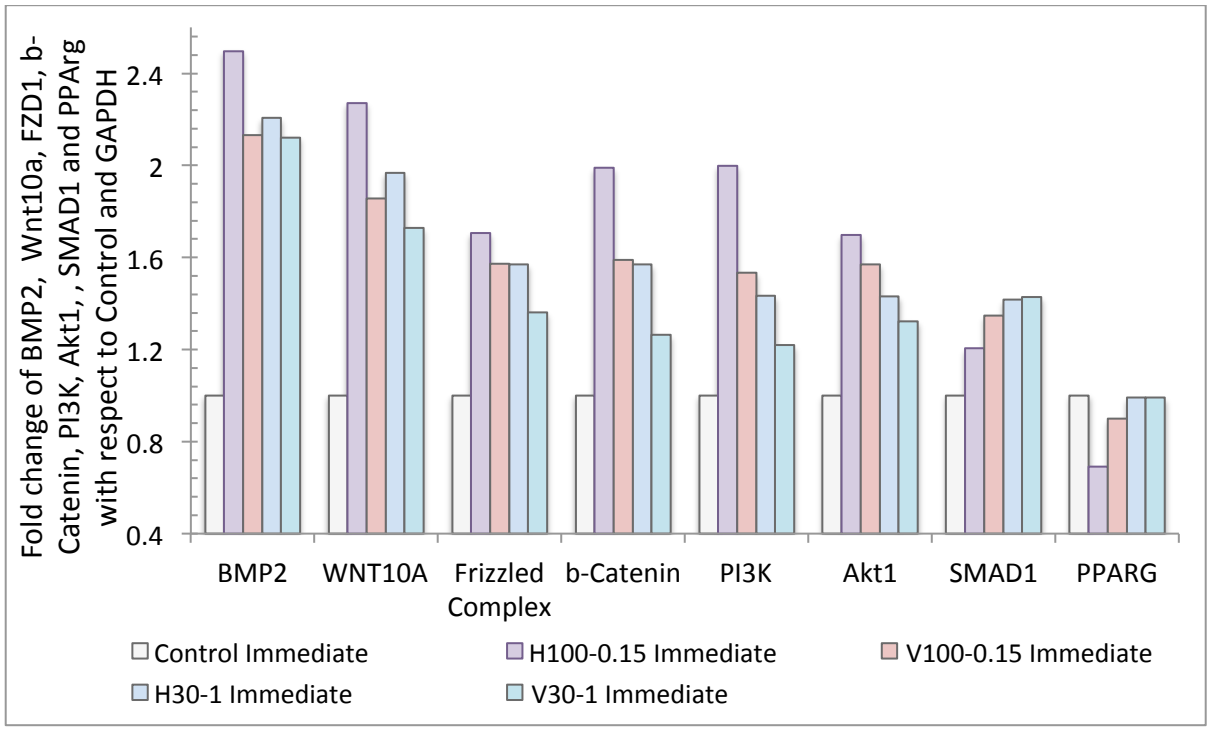

Figure A11: From the lowest fluid shear stress (0.04Pa at 100Hz-0.15g) to the highest fluid shear stress (0.94Pa at 30Hz-1g), the upregulated BMP2/Wnt10α showed to control the Frizzle complex. The PI3K and β-Catenin seemed to regulate the Akt to suppress Smad1 and PPARg (similar to Lowe et al. 2011).

Additionally, LIV of all signal combinations seemed to suppress adipogenesis (e.g. Adipoq, Fabp4, PPARg and PPARd). Their expression in all of the LIV groups was less than in the non-LIV control group. As time progressed, the suppression moved further down away from the control. The uncoupling related lipoproteins (i.e. UCP1) progressed down at the farthest away from the control as if the adipogenesis was suppressed right away after cells underwent the LIV. The adipogenesis suppression of LIV potentially derived from LIV suppressed Smad1, which is the direct downstream of

Bmp2 and Wnt10α/β-catenin, in turn inhibiting the c/EBPa to activate PPARg. If Bmp2 up-regulated Smad1 or Wnt10α activated Smad1 without β-catenin, the PPARg would be rapidly increased through c/EBPa. But the LIV activated Bmp2 and Wnt10α/β-catenin while down-regulated Smad1, consequently suppressing PPARg. Another word, both Bmp2, and Wnt10α/β-catenin balanced osteogenic differentiation with adipogenic differentiation in human bone marrow stem cells. With LIV, Bmp2 and Wnt10α/β-catenin suppressed Smad1 leading toward favorable osteoblastogenesis much more natural than moving toward adipogenesis.

Reference:

1. Lowe CE, O'Rahilly S, Rochford JJ. '*Adipogenesis at a glance*.' J Cell Sci. **2011**, 124: 2681-2686.

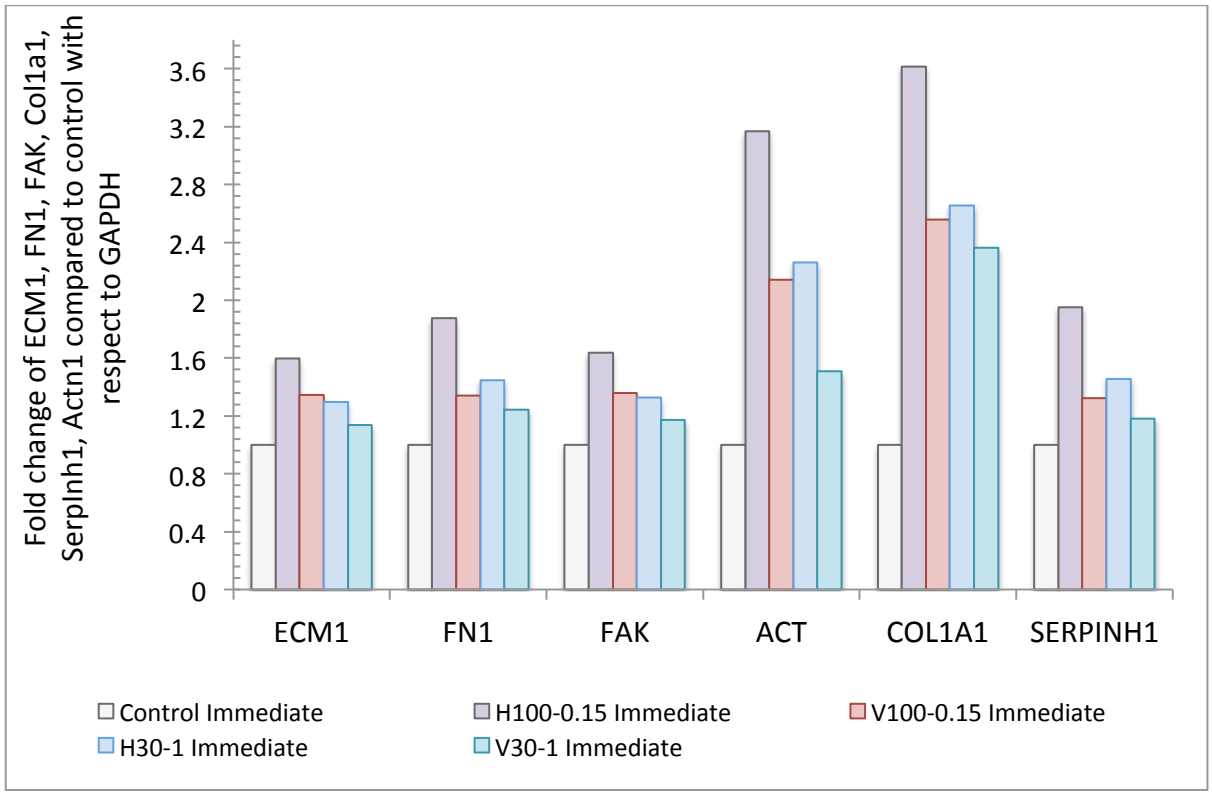

Figure A12: From the lowest fluid shear stress (0.04Pa at 100Hz-0.15g) to the highest fluid shear stress (0.94Pa at 30Hz-1g), the upregulated cytoskeleton (ACTn1) showed similar trends with collagen I (Col1a1) and collagen I binding protein (SERPINH1). Similarly, the vascular cell adhesion fibronectin (FN1) and its binding protein (LrFn5) including integrins (e.g. ITGαv, ITGα5) showed similar upregulation to the collagen I. These data could imply that the cytoskeletal orientation and remodeling could control the collagen I, including its proteins. The extracellular matrix (ECM1) and focal adhesion kinase (FAK) expressed very similar trend.

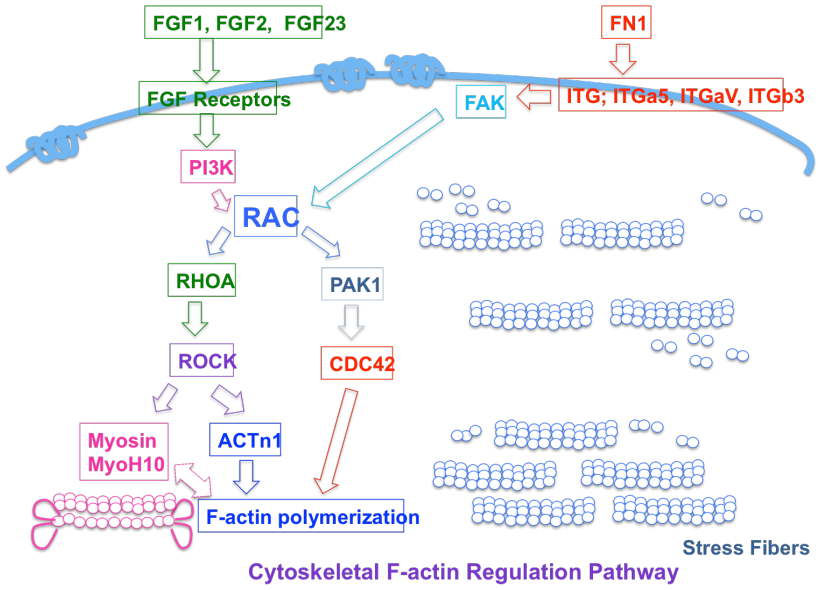

Figure A13: From the relation of the gene expression, our data could suggest that the cytoskeletal f-actin regulation pathway that was able to explain an increasing fold change in the gene expression in relation to (1) an increasing amount of the cytoskeleton from an increasing cytoskeletal polymerization and formation, and (2) the increasing cytoskeletal orientation from the more packed, more oriented fibers from the stress fiber. The elevated FGF1 and FGF2 (>1.5-2x) could activate PI3K, increasing Rac1, RhoA and Rock1 in the horizontal LIV more than in the vertical LIV (~1.2-1.7). During the LIV, the human stem cell could sense the LIV by upregulating the integrin and cytokine. The LIV activated the growth factor FGF2 that could directly stimulate the PI3K. The upregulated PI3K could stimulate Rac1 and RhoA/Rock1 to regulate the cytoskeletal formation (i) to be more fibers (increasing amounts of the cytoskeleton), and (ii) to form a longer fiber, including packed closer together (upregulated cytoskeletal gene).

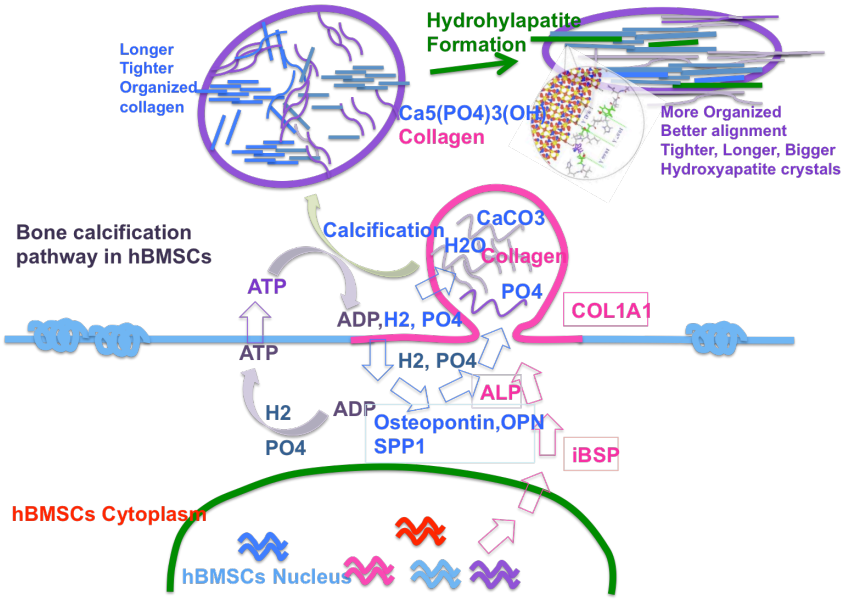

Figure A14: Our data showed that the ALP and Col1a1 increased (>2-3x) while the IBSP increased >2x across all signal combinations over time. From the relation of these gene expression levels, we modified the calcification pathway. Using our modified calcification pathway, we could explain the mechanism of the osteoblastic differentiation at the early stage where the upregulated alkaline phosphatase (ALP) elevated and caused an increasing calcification. Through the upregulated integrin-binding sialoprotein or bone sialoprotein (IBSP), the collagen I (Col1a1) and ALP could become upregulated. The IBSP could act as a nucleus of the forming hydroxyapatite along the collagen fibers within the extracellular matrix. Consequently, the upregulated IBSP could activate the use of ATP to release phosphates and hydrogen during the phosphorylation that could activate the upregulated osteopontin (Spp1). The elevation of the IBSP and Spp1 could activate the cells to calcify and increase collagen I formation as seen in the upregulating ALP and Col1a1.

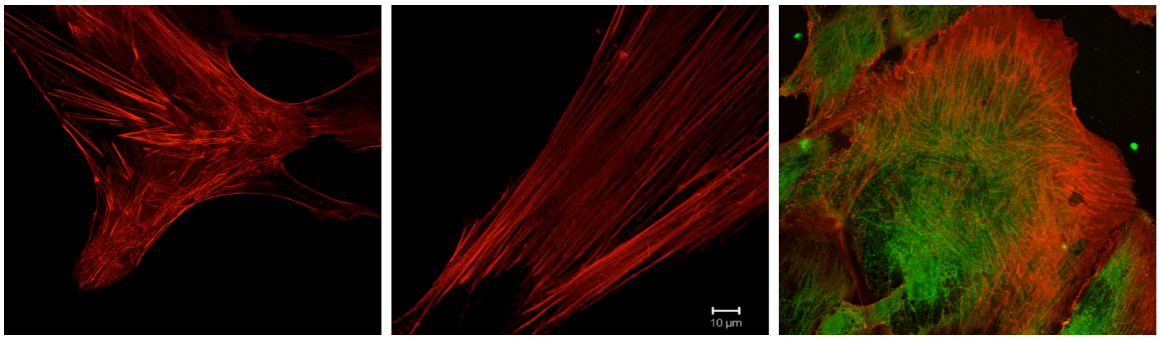

Figure A15: We used the two-photon confocal microscopy to observe the cytoskeletal orientation. During LIV, we marked the plate according to the LIV direction. The two-photon images were taken according to the vibration direction axis. The image showed that the cytoskeletal orientation of the horizontal LIV at 100-Hz-0.15 (the middle image) had a better orientation when compared to the non-LIV (the first image) and the vertical LIV (the far right). Using MatLab Image Processing, we quantified the % fiber orientation.

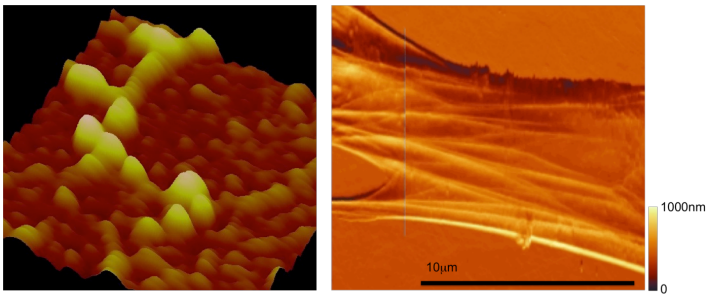

Figure A16: The atomic force microscopy (AFM) with the liquid mode was used to find the force-displacement. Before setting scanning parameters for the force-displacement, we first used the contact mode to observe the cytoskeletal morphology of the non-LIV (the image on the left). The cytoskeletal morphology of the hBMSCs under the LIV showed the cytoskeletal bundles of the more packed, longer fibers (the middle image).

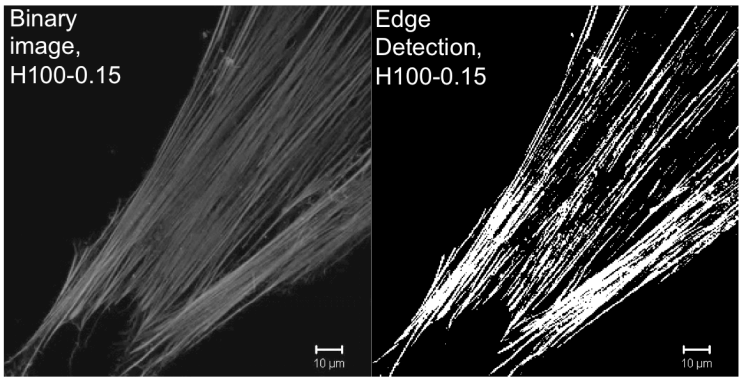

Figure A17: To calculate the %fiber orientation, first we transformed the two-photon images into the binary images using ImageJ before using the edge detection of the MatLab programming.

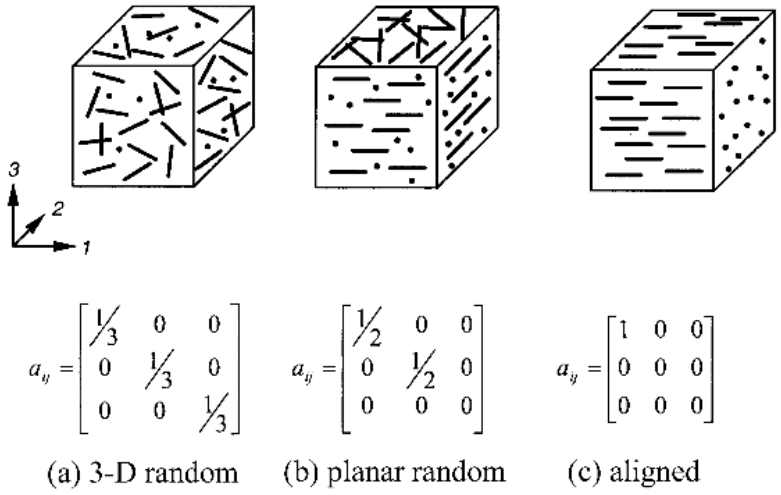

Figure A18: We calculated the fiber orientation by the tensor diffusion, where the fiber orientations in one or more directions could be set in a matrix such as an orthogonal matrix for the random alignment. With this assumption, the 3D matrix can be represented by the linear equation [Kolewe et al 2013].

Reference:

1. Kolewe M., Park H., Gray C., Ye X., Langer R., Freed L.E. '*3D Structural Patterns in Scalable, Elastomeric Scaffolds Guide Engineered Tissue Architecture*' Advanced Materials **2013**, 25 (32): 4459–4465 DOI: 10.1002/adma.201301016

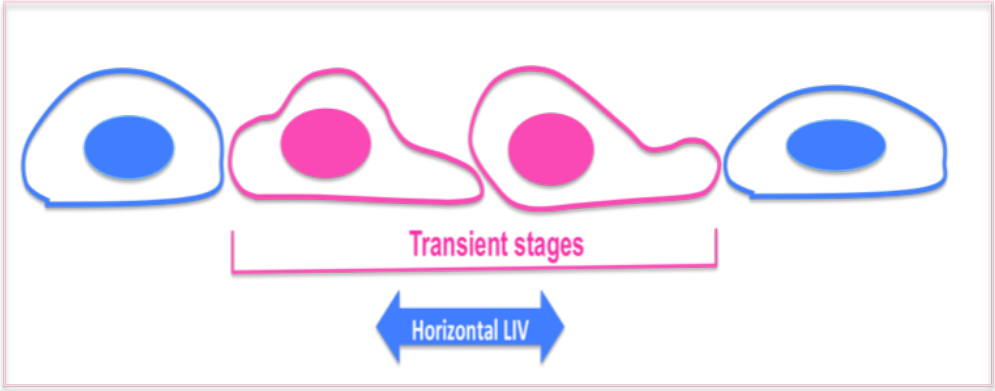

Figure A19: During the horizontal LIV, the human stem cells may stretch side-to-side and behaving as if they were under the tensile stretching. The model was assumed that the human stem cell was changed under the tensile force during the horizontal LIV.

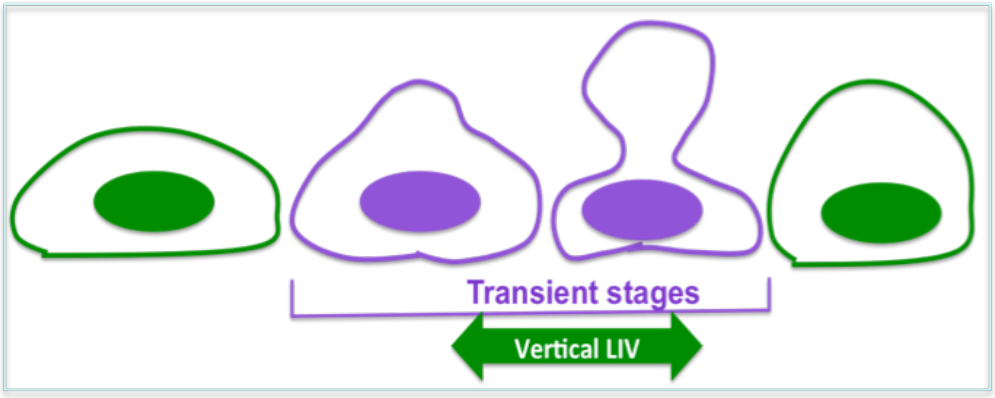

Figure A20: During vertical LIV, the human stem cells may bounce up and down and may behave as if they were under the compression force. The model was assumed that the human stem cell was changed under the compressive vertical LIV.

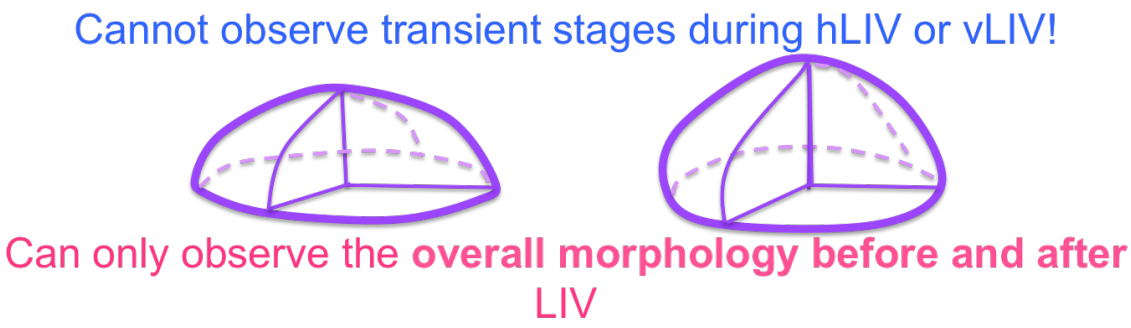

Figure A21: During LIV, the human stem cell could respond to the mechanical stimulation via changing the cell shape, morphology and the cellular and nuclear structure. The human stem cell may stretch side to side during the horizontal LIV or may bounce up and down during the vertical LIV. With all technology, we can only observe the overall change after the LIV.

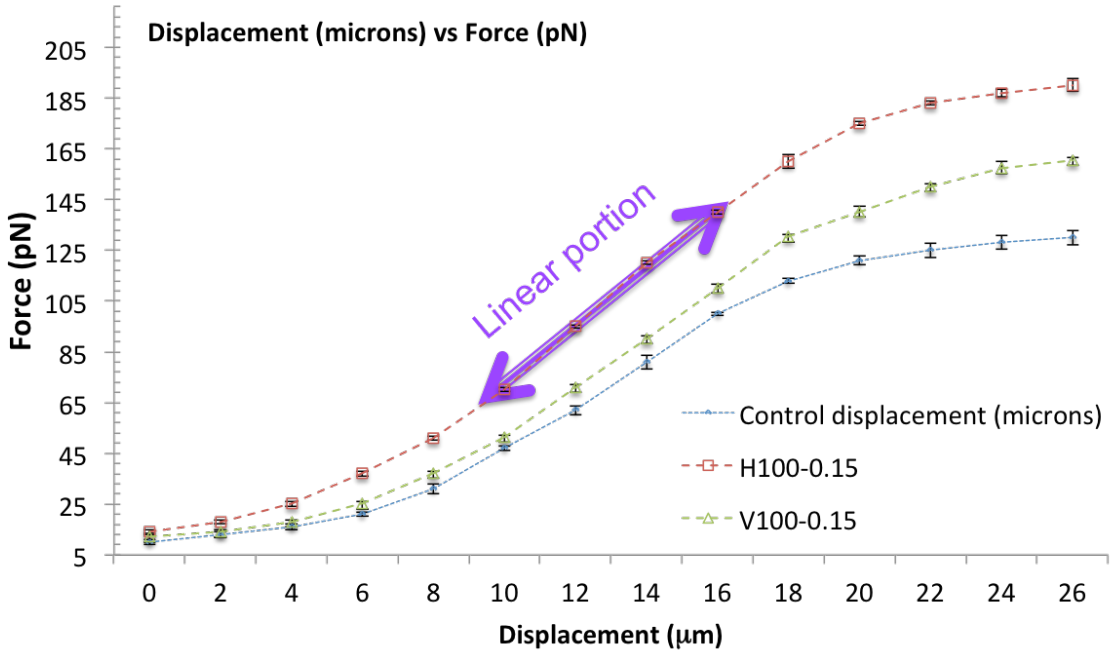

Figure A22: The relation of the force and displacement from the liquid AFM was plotted to estimate the relative modulus. The linear portion of the force-displacement is the relative modulus.

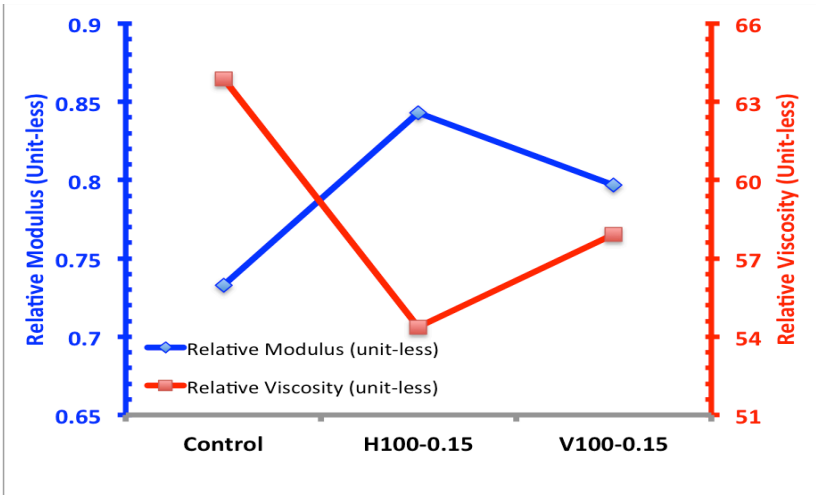

Figure A23: The relation of the force-displacement provided the relative modulus of the single cells. The relaxation time could be estimated by an injection of the same cell concentration through the flow cytometry. If the relaxation time relates directly to the duration of fluid flows from one point to another, with setting at the same 10,000 events, the time of each injection could be the relaxation time. From the relation of the relaxation (τ) and the viscoelasticity (η) as $\tau = \left[\frac{G' + G''}{G'G''}\right]\eta$. If the complex modulus can be assumed to be equal to the relative modulus from the AFM, therefore, the viscoelasticity is the ratio of the relaxation time to the relative modulus. From this relationship, we plotted the estimated relative modulus and the relative viscoelasticity. The hBMSCs under the horizontal LIV seemed to get stronger with less viscoelasticity than the vertical LIV and the non-LIV.

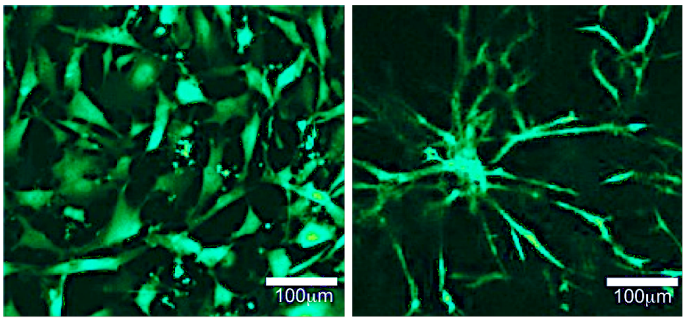

Figure A24: The fluorescent image of the hBMSCs cultured in vitro in 2D and 3D showed similar morphology and behaviors (both proliferation and osteogenic differentiation).

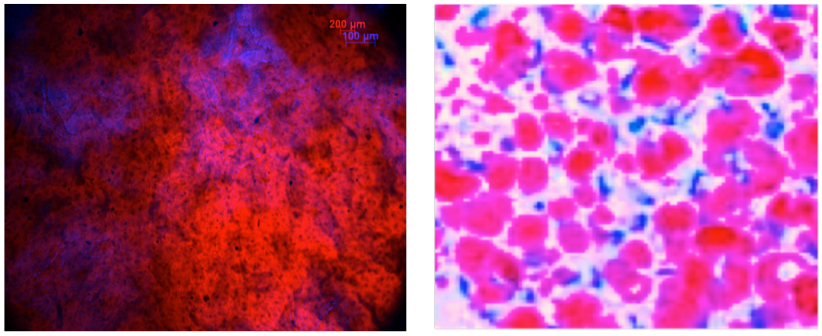

Figure A25: The Oil Red O assay of the hAMSCs after the adipogenic induction for 14 days without the LIV showed the most increased lipoprotein accumulation. (The red color represents the lipopeptide and the blue color represents the nucleus. The right image was modified by photoshop.)

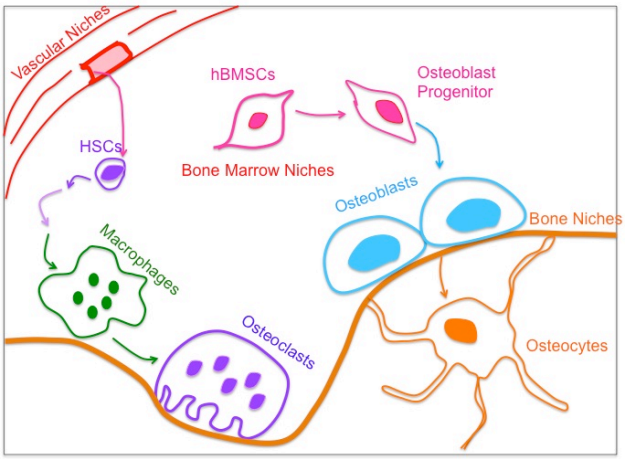

Figure A26: The relation of the bone niches and bone marrow niches with the vascular niches was from several articles [Baron et al 2013, Ehninger et al 2011, Wilson et al 2006, Yin et al 2006]. The model showed that the hBMSCs are related to the osteoblasts, osteocytes, osteoclasts, and macrophages, including HSCs. Therefore, controlling hBMSCs could influence these cells.

References:

1. Baron R, Kneissel M. '*Wnt signaling in bone homeostasis and disease: from human mutations to treatments'. Nature Medicine*.' **2013**, 19: 179–192. doi:10.1038/nm.3074.

2. Ehninger A, Trumpp A. '*The bone marrow stem cell niche grows up: mesenchymal stem cells and macrophages move in*.' J. Exp. Med. **2011**, 208 (3): 421-428.

3. Wilson A, Trumpp A, '*Bone-marrow haematopoietic stem-cell niches*.' Nature Reviews: Immunology. **2006**, 6: 93-106.

4. Yin T, Li L. '*The stem cells niches in bone*.' J. Clin. Invest. **2006**, 116: 1195–1201. doi:10.1172/JCI28568.

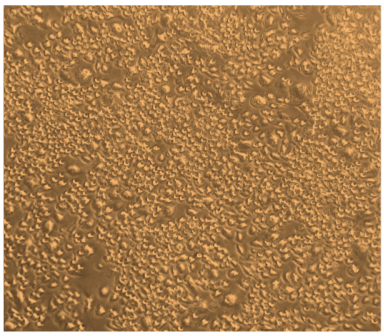

Macrophages under non-vibrated control
- There are some colonized pro-healing
- and also inflammatory

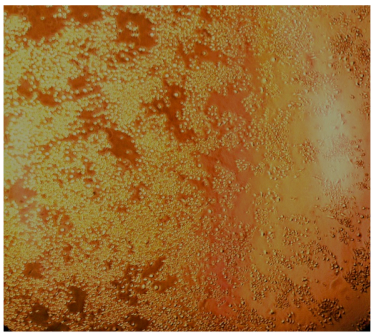

Macrophages under hLIV at H100Hz-0.15g
- Pro-healing macrophages colonize together

Figure A27: The fluorescent images showed that the macrophage was more colonized together under the LIV. The image supported the data on the increasing ratio of pro-healing : pro-inflammatory macrophages. These data suggested that the macrophages under the LIV had more pro-healing phenotypes than the non-LIV.

Appendix B

(Pending publication and/or patent)

B1: Enrichment Analysis of Gene Expression:

To understand what genes represent which functions and if at all they can be related to one another with 95% confidence, we used the enrichment analysis using NIH DAVID program. The enrichment analysis is considered genes by their gene name (not by their fold changes and/or Ct) as their functions using one or more known potential pathways. Then, these genes were statistically related to one another by their possibility in the known pathway. If they can relate to one another at a statistic confidence more than 95% ($p<0.05$), these genes are considered to be as functional genes in general. However, which pathway that these genes belong to depends on their expression and how we link them.

From the NIH, DAVID enrichment analysis, by putting in the gene name (without any Ct or fold change ($2^{-\Delta(\Delta Ct)}$) values), the analysis showed that all of our selective genes in our customized array were related to one another in some way at more than >95% confidence (or $p<0.05$). Therefore, we can have confidence that all data in our array can be related together as their functions with $p<0.05$.

In the **Table 3.1**, genes were related to one another and/or to the whole array. Additionally, they also involved with other genes in their functions with more than >95% confidence. For instance, there were at least 5 genes that positively could link directly into the osteogenic differentiation pathway with $p < 0.05$. The VEGF, for example, is a functional gene for angiogenesis, which is important to osteoblast bone cells in developing and surviving in the bone structure. During the osteogenic differentiation, the stem cell required several developing proteins (such as Bmps), the secreted growth factors (such as FGFs), which showed an upregulation in our array (with $p << 0.05$).

We related the structure related genes such as the cytoskeleton (e.g. ACT, ACTb, RhoA, Tal, Tubb, Whamm) and nuclear filaments-proteins complex (e.g. Nesprins (Syne1, 2), Suns, Lamins) with the osteogenic differentiation as a potential mechanotransduction pathway. The analysis showed that there were strong potentials of their involvement with one another for more than 95% confidence. Additionally, the function related genes involving the membrane and integrins (e.g. IBSP, ITGs), including nuclear energies and activities through transcription factors and regulations (e.g. Crebs, NADPH, PAK1) also supported our proposed pathway of the cytoskeletal and nuclear skeleton involving in the mechanotransduction ($p < 0.05$). Therefore, from the enrichment analysis, the 96 genes in our array were significantly related to one another in their functions and/or physical connection.

Note that we pooled the cDNA of samples from the dilution of 6 different RNA-extractions in each condition (not directly from the lysate). To ensure that the calculated fold changes of the pooled sample were significant ($p < 0.05$), we assumed that all samples were in utopic case, where there should be no biological variance, but only technical variance. Therefore, the standard deviation of the pooled sample would be 0.09 cycles^2 (or at standard deviation of 0.03 cycles). Each pooled samples were performed at triplicate measurements for each gene. Therefore, the standard error would be $\sqrt{\frac{0.09}{3}}$ or $\sqrt{0.03}$. By error propagation, the standard error of a mean difference (ΔCt) is calculated to be $\sqrt{0.03\times2}$ and the standard error of a mean difference of such differences ($\Delta(\Delta Ct)$) is $\sqrt{0.03\times2\times2}$ or $\sqrt{0.12}$ or 0.346 if the standard error were based on 4 degree of freedom (2*(3-1)). Therefore, 95% confidence interval of half width is t[0.025,4]*0.346 = 2.77*0.346 = 0.96 or roughly a 1 cycle. Therefore, with 3 replicates, the smallest fold changes that still remained 95% confidences should be in the range of 0.346 or

0.522 for 6 replicates. Therefore, the lowest fold changes in our data showed at least >95% confidence.